From bee venom to blood-brain barrier shuttles. Development of minimized apamin derivatives for brain delivery of antibodies and other cargoes

Benjamí Oller Salvia

ADVERTIMENT. La consulta d'aquesta tesi queda condicionada a l'acceptació de les següents condicions d'ús: La difusió d'aquesta tesi per mitjà del servei TDX (**www.tdx.cat**) i a través del Dipòsit Digital de la UB (**diposit.ub.edu**) ha estat autoritzada pels titulars dels drets de propietat intel·lectual únicament per a usos privats emmarcats en activitats d'investigació i docència. No s'autoritza la seva reproducció amb finalitats de lucre ni la seva difusió i posada a disposició des d'un lloc aliè al servei TDX ni al Dipòsit Digital de la UB. No s'autoritza la presentació del seu contingut en una finestra o marc aliè a TDX o al Dipòsit Digital de la UB (framing). Aquesta reserva de drets afecta tant al resum de presentació de la tesi com als seus continguts. En la utilització o cita de parts de la tesi és obligat indicar el nom de la persona autora.

ADVERTENCIA. La consulta de esta tesis queda condicionada a la aceptación de las siguientes condiciones de uso: La difusión de esta tesis por medio del servicio TDR (**www.tdx.cat**) y a través del Repositorio Digital de la UB (**diposit.ub.edu**) ha sido autorizada por los titulares de los derechos de propiedad intelectual únicamente para usos privados enmarcados en actividades de investigación y docencia. No se autoriza su reproducción con finalidades de lucro ni su difusión y puesta a disposición desde un sitio ajeno al servicio TDR o al Repositorio Digital de la UB. No se autoriza la presentación de su contenido en una ventana o marco ajeno a TDR o al Repositorio Digital de la UB (framing). Esta reserva de derechos afecta tanto al resumen de presentación de la tesis como a sus contenidos. En la utilización o cita de partes de la tesis es obligado indicar el nombre de la persona autora.

WARNING. On having consulted this thesis you're accepting the following use conditions: Spreading this thesis by the TDX (**www.tdx.cat**) service and by the UB Digital Repository (**diposit.ub.edu**) has been authorized by the titular of the intellectual property rights only for private uses placed in investigation and teaching activities. Reproduction with lucrative aims is not authorized nor its spreading and availability from a site foreign to the TDX service or to the UB Digital Repository. Introducing its content in a window or frame foreign to the TDX service or to the UB Digital Repository is not authorized (framing). Those rights affect to the presentation summary of the thesis as well as to its contents. In the using or citation of parts of the thesis it's obliged to indicate the name of the author.

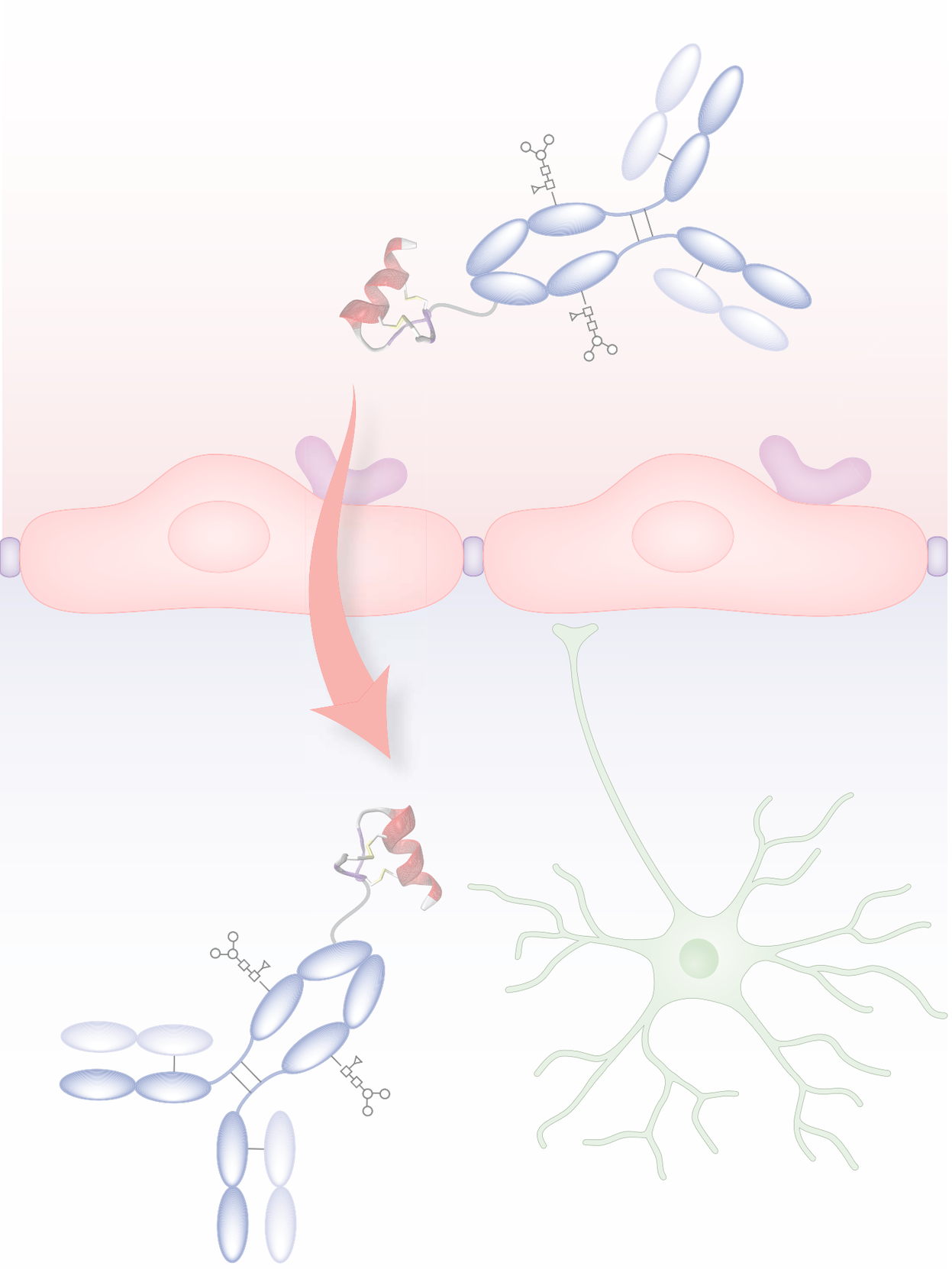

Benjamí Oller Salvia

Tesi doctoral

2015

From bee venom to blood-brain barrier shuttles. Development of minimized apamin derivatives for brain delivery of antibodies and other cargoes.

Benjamí Oller Salvia

Universitat de Barcelona

Universitat de Barcelona

IRB BARCELONA
INSTITUTE FOR RESEARCH IN BIOMEDICINE

Programa de doctorat de química orgànica

From bee venom to blood-brain barrier shuttles. Development of minimized apamin derivatives for brain delivery of antibodies and other cargoes.

Benjamí Oller Salvia

Tesi doctoral dirigida per:

Prof. Ernest Giralt Lledó

Universitat de Barcelona
Facultat de Química
Departament de Química Orgànica

Dra. Meritxell Teixidó Turà

IRB Barcelona
Programa de química
i farmacologia molecular

Barcelona, 2015.

Als meus pares, als meus avis i a la Irene.

Acknowledgements

Foremost, I would like to acknowledge my thesis directors Prof. Ernest Giralt and Dr. Meritxell Teixidó for their enthusiasm, guidance and encouragement. I am also deeply grateful to Dr. Macarena Sánchez, with whom I have worked side by side so many hours and who was always ready to lend a helping hand. I also acknowledge all the other people working in Prof. Giralt's laboratory and all my colleagues at IRB Barcelona, who provided a convivial atmosphere to enjoy working and learning. Especially, I would like to give prominence to the people that have contributed to some extent to the present work, namely Dr. Roger Prades, Dr. Bernat Guixer, Dr. Michael Goldflam, Sonia Ciudad, Pol Arranz, Cristina Díaz, Josep Garcia and Cristina Garcia. In this regard, I also acknowledge our collaborators and other scientists who have participated in some experiments, including Dr. Roger Gomis, Dr. Joan Seoane, Dr. Maria del Mar Inda, Josep Calderón, Marc Guiu and Nuno Vasconcelos. And how could I forget the two people that helped me discover IRB and Prof. Giralt's laboratory: Dr. Joan Serratosa and my longtime friend Sílvia Vilaprinyó.

During these years I had the chance to benefit from several research stages abroad, which have undoubtedly enriched the overall experience of my thesis. I would like to acknowledge all the supervisors and scientists that made it possible. First I would like to thank Prof. Kai Johnsson for allowing me to perform a 3-month research stage in his laboratory at EPFL; I would like to emphasize my gratefulness to the invaluable help of Dr. Grazvydas Lukinavicius and to all the other people in the laboratory for providing an outstanding working atmosphere. I would also like to acknowledge Prof. Dario Neri for making it possible to go to his laboratory at ETH. I could not forget the fruitful trainings by Emmanuel Sevin and Stéphane Nion in Prof. Romeo Cecchelli laboratory at Université d'Artois. Finally, I would like to thank Prof. Elazer Edelman and Prof. Mercedes Balcells, at MIT, with whom I first worked on BBB models.

Lastly, but not less important, I am at a loss for words to convey my infinite gratitude to my parents, grandparents and Irene for their limitless patience and unconditional support.

The present work was performed at IRB Barcelona with the financial support of "La Caixa"/IRB fellowship.

Unus pro omnibus, omnes pro uno.

(Tradition Swiss motto inspired on "Les trois mousquetaires" by Alexandre Dumas)

CONTENTS

ABBREVIATIONS

aa	amino acid
ABC	ATP-binding cassette
ACH	α-cyano-4-hydroxycinnamic acid
AcOH	acetic acid
AChR	acetylcholine receptor
ACLT	acrylate
Acm	acetamidomethyl
AD	Alzheimer's disease
ADC	antibody drug conjugate
ADCC	antibody-dependent cellular cytotoxicity
AMT	adsorptive-mediated transcytosis
Apo	apolipoprotein
APP	amyloid precursor protein
ATP	adenosine triphosphate
AUC	area under the curve
AuNP	gold nanoparticle
BBB	blood-brain barrier
BBBCM	cell-based BBB model
Boc	*tert*-butyloxycarbonyl
BCA	bicinchoninic acid assay
BSA	bovine serum albumin
Bv	bevacizumab
CBH	chlorobenzylhydrazyde
CD	circular dichroism
CDC	complement-dependent cytotoxicity
CDR	complementary determining region
CFluorescein	carboxyfluorescein
CNS	central nervous system
COSY	correlation spectroscopy
CPP	cell-penetrating peptide
CSF	cerebrospinal fluid
CTAB	cetyltrimetilammonium bromide
CuAAC	copper-catalysed azide-alkyne cycloaddition
Cx	cetuximab
DBU	1,8-diazabicyclo[5.4.0]undec-7-ene
DCM	dichloromethane
DHB	2,5-dihydroxybenzoic acid
DIEA	*N*,*N*-diisopropylethylamine
DIC	diisopropylcarbodimide
DLS	dynamic light scattering
DMAEMA	*N*,*N*-dimethylaminoethyl methacrylate

DMAP	4-(dimethylamino)pyridine
DMEM	Dulbecco's modified eagle medium
DMF	dimethylformamide
DMSO	dimethylsulfoxide
DNA	deoxyribonucleic acid
DOTA	1,4,7,10-tetraazacyclododecane-1,4,7,10-tetraacetic acid
DTNB	5,5′-dithiobis(2-nitrobenzoic acid)
DSPE	distearoylphosphatidylethanolamine
DTPA	diethylentriaminepentaacetic acid
DTT	D,L-dithiothreitol
EDC	*N*-(3-dimethylaminopropyl)-*N*'-ethylcarbodiimide hydrochloride
EDT	1,2-ethanedithiol
EDTA	ethylenediaminetetraacetic acid
EGF	endothelial growth factor
EGFR	endothelial growth factor receptor
ELISA	enzyme-linked immunosorbent assay
eq	equivalent
Fab	antigen-binding fragment
FcRn	neonatal Fc receptor
FDA	food and drug administration
FET	fish embrio toxicity
Fmoc	9-fluorenylmethoxycarbonyl
HBSS	Hanks balanced solution salt
hGDNF	human glial-derived neurotrophic factor
HEPES	4-(2-hydroxyethyl)piperazine-1-ethanesulfonic acid
HER	human epidermal growth factor
HIV	human immunodeficiency virus
HOAt	1-hydroxy-7-azabenzotriazole
HPLC	high performance liquid chromatography
HRP	horseradish peroxidase
HSQC	heteronuclear single quantum coherence spectroscopy
ICP	inducing-coupled plasma
Ig	immunoglobulin
ISA	imidazole-1-sulfonyl azide hdyrochloride
FPLC	fast protein liquid chromatography
GBM	glioblastoma multiforme
GFAP	glial fibrillary acidic protein
GFP	green fluorescent protein
GM1	monosialotetrahexosylganglioside
GSH	glutathione
IAMC	immobilized artificial membrane chromatography

ICP	inductively coupled plasma
IDUA	α-L-iduronidase
i.v.	intravenous
LC	liquid chromatography
LAT	large neutral amino acid transporter
LD50	lethal dose, 50 %
LDL	low-density lipoprotein
LDLR	low-density lipoprotein receptor
LRP	low-density lipoprotein receptor-related protein receptor
LY	Lucifer yellow
mAb	monoclonal antibody
MALDI	matrix-assisted laser desorption ionization
MeCN	acetonitrile
MeOH	methanol
MPS	mucopolysaccharidosis
MRI	magnetic resonance imaging
MS	mass spectrometry
MTT	3-(4,5-dimethylthiazol-2-yl)-2,5-diphenyltetrzolium bromide
MWCO	molecular weight cut-off
m/z	mass over charge
nAChR	nicotinic acetylcholine receptor
NaPi	sodium phosphate
NHS	*N*-hydroxysuccinimide
NIR	near infrared
NMR	nuclear magnetic resonance
NOE	nuclear Overhauser effect
NOESY	nuclear Overhauser effect spectroscopy
NP	nanoparticle
ObR	obesity-related leptin receptor
OECD	organization for economic co-operation and development
PAGE	polyacrylamide gel electrophoresis
PAMAM	polyamidoamine
PAMPA	parallel artificial membrane permeability assay
Papp	apparent permeability
PAR	peptide/antibody ratio
PBS	phosphate-buffered saline
PCL	polycaprolactone
PDA	photodiode array
PDB	Protein Data Bank
PEG	polyethylene glycol
PFA	paraformaldehyde

P-gp	P-glycoprotein
PK	pharmacokinetics
PDisp	phage display
PLA	polylactic acid
PLGA	poly(lactic-co-glycolic acid)
PLP	pyridoxal 5'-phosphate
PNGase	peptide N-glycosidase
PTD	protein transduction domain
PyBOP	1H-benzotriazol-1-yloxytris(pyrrolidino)phosphonium hexafluorophosphate
QDot	quantum dot
RAP	receptor-associated protein
RFP	red fluorescent protein
RH	Ringer HEPES
RMSD	root-mean-square deviation
RMT	receptor-mediated transcytosis
RNA	ribonucleic acid
ROI	region of interest
RP	reverse phase
RVG	rabies virus glycoprotein
RT	room temperature
RTU	ready-to-use
SATA	*N*-succinimidyl-*S*-acetyl thioacetate
SD	standard deviation
SDS	sodium dodecylsulfate
SEC	size exclusion chromatography
SEM	standard error of the mean
SiR	silicon rhodamine
SOD	superoxidase dismutase
SPECT	single photon emission computed tomography
SPPS	solid-phase peptide synthesis
SPR	surface plasmon resonance
SRhodamine	sulforhodamine B
STED	stimulated emission depletion
TBTU	*O*-(benzotriazole-1-yl)-1,1,3,3-tetramethyluronium tetrafluoroborate
*t*Bu	*tert*-butyl
TCA	trichloroacetic acid
TCEP	tris(2-carboxyethyl)posphine
THPTA	tris(3-hdyroxypropyltriazolylmenthyl)amine
TEA	triethylamine
TEER	transendothelial electrical resistance

TEM	transmission electron microscopy
TFA	trifluoroacetic acid
Tf	transferrin
TfR	transferrin receptor
TIS	triisopropylsilane
TJ	tight junction
TMB	3,3',5,5'-tetramethylbenzidine
TOCSY	total correlation spectroscopy
TOF	time-of-flight
t_R	retention time
Trt	trityl
UPLC	ultra high performance liquid chromatography
UV	ultraviolet
VEGF	vascular endothelial growth factor

Proteinogenic amino acids

A
Ala
L-Alanine

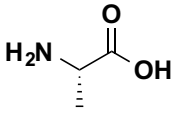

C
Cys
L-Cysteine

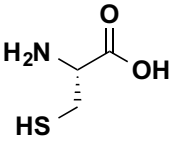

D
Asp
L-Aspartate

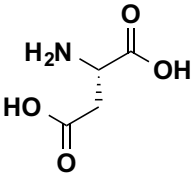

E
Glu
L-Glutamate

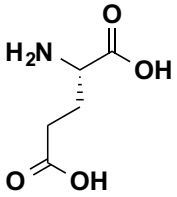

F
Phe
L-Phenylalanine

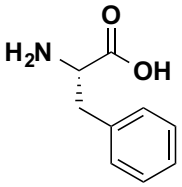

G
Gly
L-Glycine

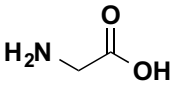

H
His
L-Histidine

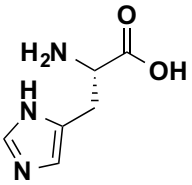

I
Ile
L-Isoleucine

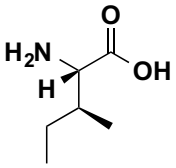

K
Lys
L-Lysine

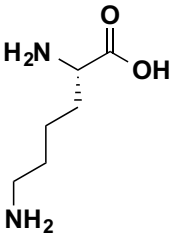

L
Leu
L-Leucine

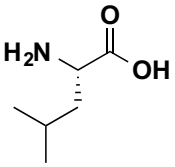

M
Met
L-Methionine

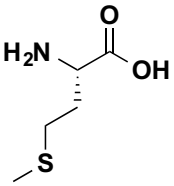

N
Asn
L-Asparagine

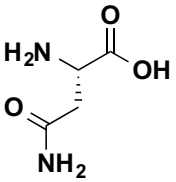

P
Pro
L-Proline

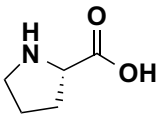

Q
Gln
L-Glutamine

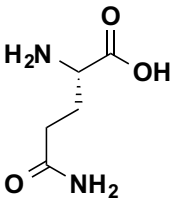

R
Arg
L-Arginine

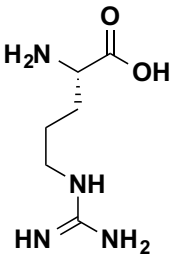

S
Ser
L-Serine

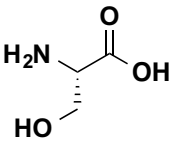

T
Thr
L-Threonine

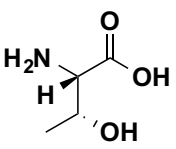

V
Val
L-Valine

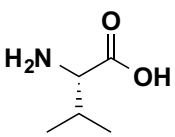

W
Trp
L-Tryptophan

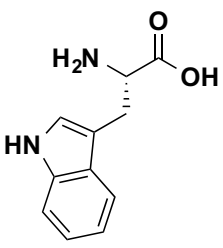

Y
Tyr
L-Tyrosine

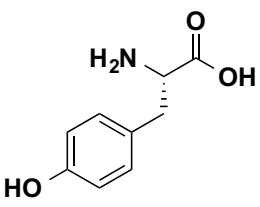

Protecting groups

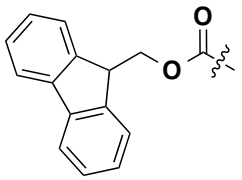

9-fluorenylmethoxycarbonyl
(Fmoc)

tert-butyl
(*t*Bu)

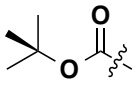

tert-butoxycarboyl
(Boc)

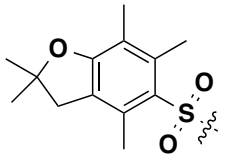

2,2,4,5,7-pentamethyl-
dihydrobenzofurane-5-sulfonyl
(Pbf)

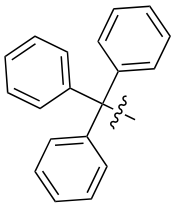

Trityl
(Trt)

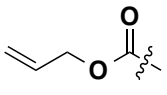

Allyloxycarbonyl
(Alloc)

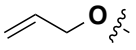

Allyl
(OAl)

Coupling reagents and additives

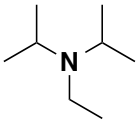

N,N-diisopropylethylamine
(DIEA)

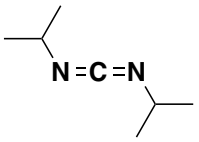

diisopropylcarbodiimide
(DIC)

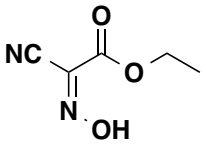

ethyl cyano-
glyoxylate-2-oxime
(Oxima)

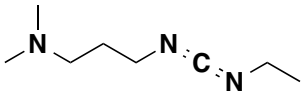

N-(3-
dimethylaminopropyl)
-*N*′-ethylcarbodiimide
(EDC)

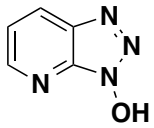

1-hydroxy-7-azabenzotriazole
(HOAt)

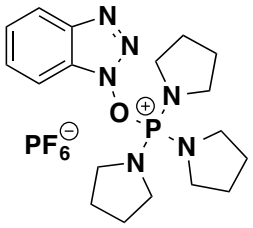

1H-benzotriazol-1-yloxytris
(pyrrolidino)phosphonium
hexafluorophosphate
(PyBOP)

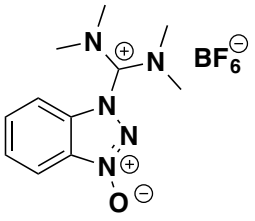

O-(benzotriazol-1-yl)-1,1,3,3-
tetramethyluronium
tetrafluoroborate
(TBTU)

Resins

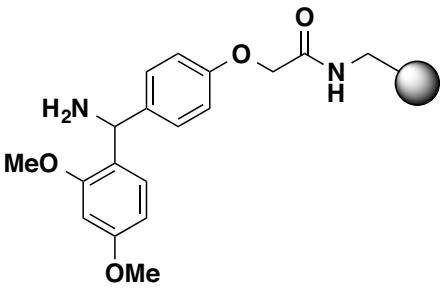

RinkAmide-Chemmatrix resin

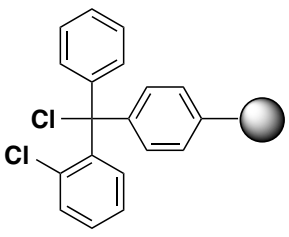

2-chlorotrityl resin

This introduction will give rise to the review article:

Oller-Salvia B.; Sánchez-Navarro M.; Giralt, E.; Teixidó, M. BBB-shuttle peptides as an emerging paradigm for brain delivery. *In preparation.*

INTRODUCTION

The growing prevalence of neurological disorders, mainly due to an ageing population, and also the increasing incidence of brain cancers make delivery to the brain a major unmet challenge in drug development.[1] Moreover, the lack of efficient treatments for most diseases affecting the central nervous system (CNS) generates high direct and indirect costs, which correspond to 1/4 of the burden of all diseases in Europe and high-income countries.[2] Therefore, improving CNS drugs would not only increase the well-being of an important part of the population but also considerably reduce the costs incurred by brain pathologies. However, most active compounds cannot reach their targets in therapeutically relevant amounts due to a formidable obstacle, namely the blood-brain barrier (BBB).[3]

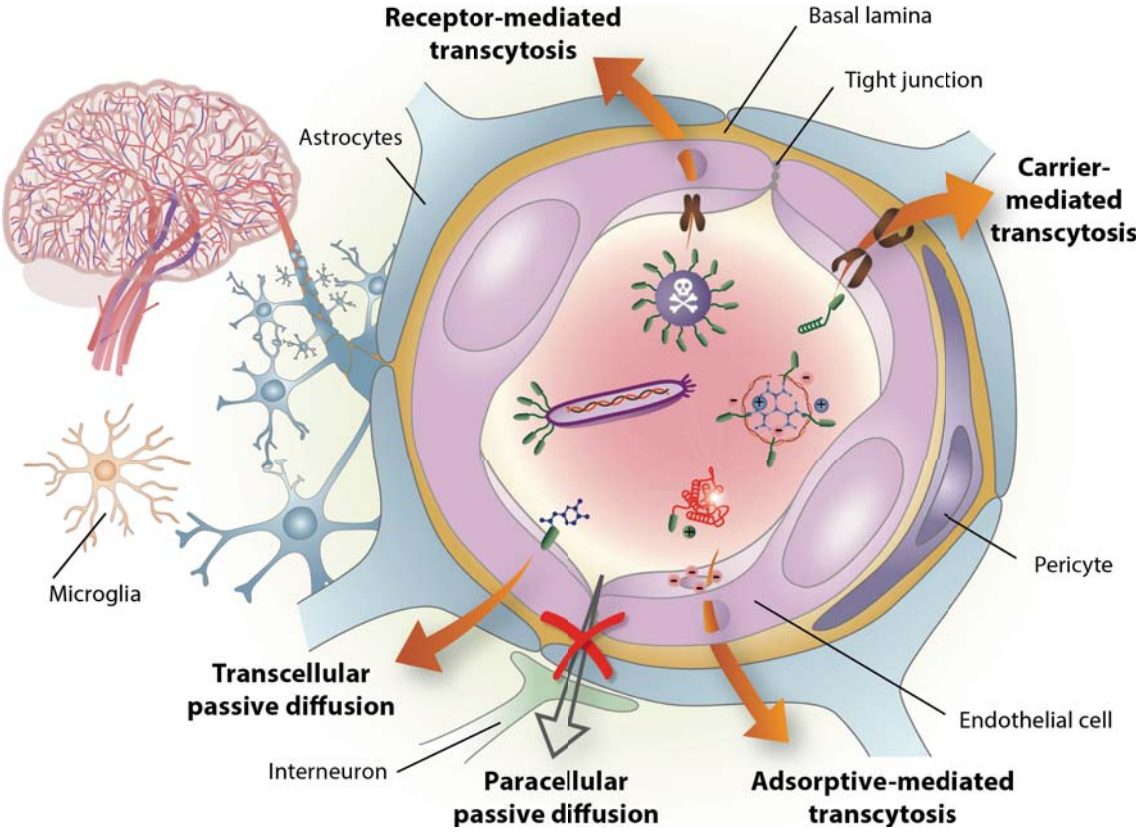

Figure 1. *Transcytosis of BBB-shuttle conjugates across the BBB. (Design: Benjamí Oller-Salvia. Drawing: Iris Joval)*

Although many ways to overcome the BBB have been proposed and some of them are currently applied, to date no general approach has a satisfactory efficiency-safety balance. At one end of the spectrum, direct drug administration into the brain has a high risk and is extremely local and, at the other end, modification of molecules to enhance their diffusion through the barrier is only applicable to some small drugs. Among the non-invasive approaches, BBB-shuttles (*Figure 1*) have proved their potential in preclinical research over the last two decades and hold great promise as many of them are in clinical trials. The BBB-shuttle concept includes Trojan horse

antibodies[4] and any other molecules capable of transporting a cargo into the brain parenchyma without affecting BBB integrity. Over the last five years, peptide shuttles have thrived because they provide an excellent opportunity to overcome some of the weaknesses presented by classical antibody and protein shuttles. Among the advantages of peptide vectors with respect to proteins are their lower production cost, ease of derivatization and characterization, and lower immunogenicity.

In this introduction, firstly we will give an overview of the BBB and brain delivery, secondly the techniques used to assess BBB permeability will be covered and finally we will review the state of the art of BBB-shuttle peptides. Based on this knowledge, we will explain how we developed a new shuttle from bee venom and also our work on enhancing the challenging transport of antibodies across the BBB.

The BBB: a resilient challenge for drug delivery to the brain

The BBB protects the CNS from injury and disease by tightly controlling the extracellular environment in neural tissues. This barrier, together with the blood-cerebrospinal fluid (CSF) barrier and ependyma, limit the access of noxious substances and pathogens but also the penetration of molecules for therapy and diagnosis. However, at the same time, the BBB is the main route of entry for nutrients into the brain. The capillary surface is 20 m^2, 1000-fold larger than the blood-CSF interface.[5] Moreover, the maximal cell-capillary distance is 20 μm, which can be permeated by small molecules in half a second through free diffusion.[6] Therefore, efficiently overcoming this barrier would be the best way to deliver substances to any part of the brain.[7]

The BBB is a physical, metabolic, and transport barrier formed mainly by endothelial cells on brain capillary walls. These cells differ from those in non-neural tissues because they form restrictive cell-to-cell connections called tight junctions (TJs). TJs are intricate nets of trans-membrane and cytoplasmic accessory proteins linked to the actin cytoskeleton that preclude paracellular passage. Furthermore, the brain endothelium does not display pores (fenestrae) and forms a continuous layer. These cells contain many cytosolic and extracellular-membrane enzymes, and transcellular passage of solutes is subjected to a particular regulation. Moreover, the brain endothelium has 100-fold lower vesicular transport than non-cerebral endothelium[4] and expresses many efflux pumps, such as the ATP-binding cassette (ABC) transporter P-glycoprotein (e.g. P-gp). The BBB also includes the basement membrane and the other cells from the neurovascular unit, which play a key role in conserving the brain endothelium phenotype and regulating its permeability. The main cell-types participating in these processes are astrocytes and pericytes but microglia, circulating leukocytes, and neurons are also involved.[6,7]

Although the brain parenchyma is protected by the highly regulated BBB, it is not completely insulated as it needs nutrients, ions and hormones to ensure normal function. Many small hydrophobic compounds (< 500 Da) cross the BBB by lipid-mediated passive diffusion, while polar molecules such as glucose, amino acids and also several peptides have specific transporters. Brain endothelial cells express a wide variety of carrier proteins most of which are polarized in their expression on the luminal and abluminal sides of the membrane. Certain macromolecules can cross the BBB by endocytotic mechanisms involving receptor-mediated transcytosis (RMT) and/or adsorptive-mediated transcytosis (AMT). The latter includes all vesicular transport mechanisms that do not involve protein receptors and it is favoured mainly by the positive charge of the molecule, which promotes its interaction with membrane phospholipids and the glycocalyx eventually inducing endocytosis. In the process of transcytosis, the vesicle formed circulates across the

cell, bypassing the degradation pathway, and eventually releases its content to the parenchyma by exocytosis. Regarding RMT, a few receptors have been well characterized, including those for insulin, low-density lipoproteins, leptin, and especially transferrin (Tf); however, many others have been reported and the list continues to grow.

Many pathologies involve BBB dysfunction, including Alzheimer's, Parkinson's and lysosomal diseases, as well as epilepsy and cancers, among others. This disfunction can range from minor and transient opening of the TJs to chronic breakdown and can involve changes in the transport systems.[7] However, these alterations are usually only significant in advanced stages of disease, when it is more difficult to treat, and in the most affected sites. For instance, in brain tumours, the BBB is disrupted in the core but not where infiltrating cells are found, which is one of the main causes of the low efficiency of current treatments.[8]

Brain delivery

Unfortunately, most direct and effective strategies for drug delivery into the brain that circumvent the challenge of crossing the BBB are invasive, involving the highest risk of brain damage or infection and requiring demanding set-ups. In addition, they provide only very localized delivery, which is an important pitfall, especially for macromolecules, which have slow diffusion.[9] Intra-cerebral or -arterial injections and convection-enhanced diffusion are among these techniques. Intraventricular and intrathecal administration routes are also invasive and give access only to the CSF, which is cleared every 4-5 h. However, the latter are effective for drugs with poor BBB penetration and whose receptors are near the interface between brain or spinal cord and CSF. This is why intrathecal injection is sometimes used to administer deep anaesthesia, chemotherapy, or to treat intense pain.[10,11]

Nasal delivery of therapeutic agents is currently studied as a way to bypass the BBB. Although it is believed that drugs move through the olfactory epithelium, the uptake mechanisms involved remain unclear. Moreover, small administration volumes and low efficiency to achieve a therapeutic concentration in target areas of the brain are still a concern in this method.[12]

Enhancing drug transport across the BBB would enable the use of non-invasive administration pathways such as intravenous, transdermal or oral routes. Moreover, it would allow an efficient distribution of the drug to all parts of the brain because of the rich vascularity of this organ. In order to overcome the BBB, many research efforts have focused on its temporal disruption by chemical or physical stimuli.[13] However, opening the barrier entails severe risks, including toxicity to cerebral cells induced by blood-borne substances, imbalance of ions and neurotransmitters, release of cytokines and chemokines and glial activation. BBB disruption has also been related to neuronal dysfunction, neuroinflammation and neurodegeneration.[14]

In view of the risks involved in invasive methods and the alteration of the BBB, much effort has been channelled into other approaches that improve transport across brain endothelial cells. The strategies for small molecules rely mostly on the modification of their physicochemical properties to improve penetration through passive diffusion, while for larger molecules the only viable way is to target an active mechanism.[4]

It is known that lipophilicity, pKa, molecular weight, topological polar surface area, and number of hydrogen bond donors and acceptors are the most relevant parameters for predicting the BBB permeability of small molecules through passive diffusion.[15] Therefore, using the appropriate algorithms and screening technologies, modification of a small drug in order to increase its brain permeability is challenging but often feasible.[16] However, these changes usually imply enhanced lipophilicity, which increases unspecific interaction with cell membranes and may result in off-

target effects.[17] Moreover, higher lipophilicity also entails a greater chance of the drug becoming a better substrate for an efflux pump.[7] This is why co-administration of inhibitors for these efflux transporters has proved efficient in many cases.[13] An approach to further enhance the concentration of lipophilic molecules inside the CNS is to trap them after passage through the BBB. This can be achieved by introducing a moiety, such as dihydropyridine, susceptible to modification in the CNS to become less BBB-permeable, generally by increasing charge through oxidation.[18]

Another strategy to increase the permeation of certain small molecules into the brain in a more selective way is to modify drugs so that they mimic endogenous substrates of transporters with high expression in brain capillary endothelial cells. Several amino acid drugs using this mechanism, such as gabapentin and melphalan, are currently used in clinics.[19]

A major limitation of these approaches is that the modification of an active molecule to increase its permeability or metabolic stability may result in a decrease in its potency. To address this issue, the prodrug strategy was developed, which consists in designing a stable derivative that is transformed into an active drug after reaching the target location. The most successful case is that of levodopa for the treatment of Parkinson's disease; this prodrug is actively transported across the BBB through the large neutral amino acid transporter (LAT1) and then decarboxylated into dopamine inside the brain.[19]

In spite of the plethora of modifications that have been investigated to improve the delivery of small molecules to the brain, no general method can be applied. Moreover, the efficiency of such techniques is limited, and they are not appropriate for large compounds, including the growing number of biological drugs. With respect to proteins, although cationization has long been known to increase their permeability across the BBB, it also enhances their uptake in peripheral organs and their toxicity.

In an attempt to provide a more general approach for drug delivery to the CNS, many efforts have focused on finding brain delivery vectors. Biological vectors such as viruses[8,20] and cells have been used to increase BBB permeability. However, generally viruses can access only when the BBB is immature or compromised;[21] moreover, control of viral replication and immunogenicity is an issue.[8] With regard to cells, they have low targeting and release efficiency and the high risk of cytotoxicity and even tumour formation require further research.[22]

The BBB-shuttle approach

Molecular vectors, dubbed BBB-shuttles,[23] aim to provide more versatile, selective and safer delivery systems. Some of these shuttles have been designed to undergo transport by passive diffusion and others target active mechanisms. The former can be applied only to drugs that do not significantly alter their physicochemical properties. Conversely, BBB-shuttles targeting RMT or AMT may allow the transport of larger cargoes, including proteins, oligonucleotides, nanoparticles (NPs) and even viruses. Therefore, BBB-shuttle-mediated brain delivery offers a strategy with a very general scope and the possibility of enhanced brain selectivity. This targeting approach, together with appropriate formulations, nanoparticulate delivery systems and devices, holds great promise for efficient and mild administration of CNS therapeutics.[24]

In fact, many terms have been used to refer to these molecules that enhance the brain permeation of other substances. Among them, highly generic expressions such as "brain delivery/transport vectors/vehicles/carriers" may describe targeting moieties but also to refer to nanocarrier systems. In addition, the terms "cell-penetrating peptides" or "chimeric peptides" have been used fur this purpose, while they designate families of peptides that have applications other than crossing the BBB. Regarding the concept of "Trojan horses", it includes only antibodies, proteins, and peptidomimetics that undergo transcytosis across brain capillary endothelial cells.[4] Given the increasing nature of molecules and mechanisms for drug delivery into the brain and the wide use of the expression "shuttle",[10,23,25-35] in this thesis we will use the term "BBB-shuttle".

The concept of BBB-shuttle was first implied in the fusion protein delivery strategy proposed by William M. Pardridge in 1986.[36] Despite the early beginning of this concept, its practical application evolved very slowly. The first successful attempts, also pioneered by Pardridge, used cationized albumin to deliver β-endorphin[37] and were followed by those of Frieden, who used an anti-Tf receptor (TfR) antibody to enhance the transport of methotrexate.[38] In the subsequent years and especially in the last decade, a plethora of new BBB-shuttles have appeared, some of which are currently in clinical trials.

Shuttles for the transport of small drugs rely mainly on passive diffusion and carrier-mediated uptake mechanisms. The latter involve small substrates of natural transporter systems, such as glucose, large neutral amino acids, and nucleosides, among others.[39] This mechanism is highly sensitive to the substrate because it requires a conformational rearrangement of the membrane protein in order to transport substances into the cell.[6] Therefore, an endogenous ligand or a very similar analogue must be used as a carrier. However, endogenous molecules used as shuttles

must compete with their blood-borne counterparts. This is why passive diffusion shuttles, in spite of their lower selectivity, may achieve higher transport rates.

With regard to larger cargoes, such as proteins and nanocarriers, they require vesicle-mediated mechanisms to permeate the BBB. Although such mechanisms are downregulated at the brain endothelium,[40] they have been shown to carry sufficient amounts of drugs and imaging agents to be relevant for therapy and diagnosis. Macropinocytosis and AMT allow the transport of substances without the need of a particular receptor. Moreover, the amounts of cargo transported by AMT is significantly larger than by RMT as the saturation of the former occurs at a concentration 3 orders of magnitude higher than the latter.[41] However, a remarkable disadvantage of AMT is that it is unspecific and generally results in an enhanced uptake in many other tissues, thereby increasing the risks of off-target effects. These issues explain why the quest for molecules interacting with receptors overexpressed in brain endothelium has received considerably more attention.[42,43]

Many authors have used the endogenous ligands of these receptors to deliver NPs across the BBB, including apolipoproteins (Apo) A, B and E, receptor-associated protein (RAP), transferrin (Tf), lactotransferrin, melanotransferrin (p97), and leptin. This strategy has also been indirectly applied to nanocarriers using polysorbate 80, which has been shown to recruit apolipoproteins.[44] However, all these ligands must compete with the blood-borne proteins, which can be above receptor saturation, as in the case of Tf. Competition lowers their efficiency of the shuttles and may alter the homeostasis of nutrient delivery. In order to overcome this drawback, many efforts have been devoted to developing antibodies that bind to the receptors of Tf and insulin. These Trojan horses tightly bind to an epitope of the receptor different to the region where natural substrate interacts and deliver a wide variety of cargoes.[3,4] However, the capacity of these high-affinity antibodies to reach the brain parenchyma is controversial.[40,45] In this regard, in the last 4 years, scientists from Genentech and Hoffman-La Roche have focused on demonstrating that lower-affinity antibodies or antibody fragments do efficiently transcytose across the BBB and can be released from the receptor.[25,45,46] In addition to antibodies, other non-endogenous proteins, such as wheat germ agglutinin[47] and a non-toxic mutant of diphteria toxin (CRM197),[48] have been applied to a lower extent.

Nevertheless, the production and characterization of biopharmaceutics, such as antibodies and other proteins, is challenging and expensive. Moreover, low immunogenicity is an issue. This is why research in this field in the last decade has focussed mainly on peptides, namely small proteins with up to 50 amino acid residues. These molecules can combine the low cost of small drugs with the high specificity of biologics.[49] They are easier to obtain and characterize than the latter and have very low immunogenicity. Moreover, they display medium to low

affinities, a property that is critical in the development of anti-TfR shuttles.[25] In addition, peptides are amenable to chemical synthesis, thus opening up the possibility of applying a wide range of non-natural modifications and of introducing a plethora of functional groups for conjugation to nanocarriers or site-specific modification of proteins. Although they have often been undervalued in pharmaceutical chemistry because of their low resistance to proteolytic degradation, their limitations can now be overcome by means of various techniques, such as the use of non-natural amino acids (including D-amino acids), *N*-methylation, and cyclization.

After this broad introduction, we will now give an overview of the main techniques used to assess brain penetration of BBB-shuttle-cargo constructs and then we will review the main achievements accomplished using BBB-shuttle peptides.

Assessing BBB penetration of shuttle-cargo constructs

Developing BBB-shuttle-cargo constructs and evaluating their transport across the BBB requires an integrated approach that includes many models and techniques. *In vivo* experiments provide a physiological model of the BBB and allow assessment of the pharmacokinetics (PK) and pharmacodynamics (PD). However, concerns regarding ethics and costs, together with complexity, make them inadequate for the first stages of development.[6] Moreover, results obtained in animals in BBB studies often do not translate into humans because of the difference in PK and in the expression amounts and intrinsic activities of transporters among others.[50,51] Therefore, *in vitro* assays, especially those incorporating human components such as cells or isolated receptors, are very valuable and a necessarily simplified platform for the screening of new compounds and mechanistic studies.

In vitro screening and mechanistic studies

Passive diffusion BBB models

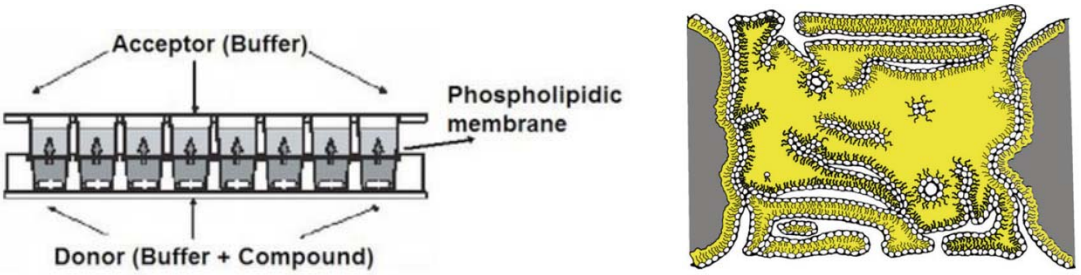

Figure 2. *A scheme of the PAMPA model (left) and a representation of the lipid multilayer (right).*

Passive diffusion models can be useful to assess improvements in the transport of small molecules using BBB-shuttle that cross the BBB uniquely through diffusion across the lipid membrane; thus, aberrant values are obtained if the compounds are substrates of influx or efflux pumps or if they have a non-negligible paracellular transport. Although many assays to estimate diffusion across the BBB membrane exist, ranging from immobilized artificial membrane chromatography (IAMC), liposome-buffer partition coefficient or film balance measurements method,[6] PAMPA is the reference test for this purpose (*Figure 2*).[15,52] This model consists of a multilayer of lipids on a membrane that separates two compartments. The compound to be assayed is placed in a donor compartment that is intensely stirred mimicking circulation through blood capillaries and the amount that has crossed into the acceptor compartment is measured after a certain time.

Cell-based BBB models

Cell-based BBB models offer a compromise between costs, throughput and predictive value. However, there is a wide variety of models available, and the

pharmaceutical industry has not adopted any of them as the "gold standard", thus indicating that none meets all the requirements.[53,54] In general terms, cell-based BBB models consist of a monolayer of cells seeded on a membrane that separates two compartments. In the classical transport assay, a solution containing the compound is incubated in the apical compartment, where the cells forming the monolayer are seeded, mimicking the molecule present in blood. At the end of the assay, the compound found in the compartment placed on the other side of the membrane (named basolateral) represents the amount that reaches the brain parenchyma. The tightness of the cell monolayer is usually assessed by the permeability of an easily detectable compound (e.g. Lucifer yellow, ^{14}C-sucrose) and/or by the transendothelial electrical resistance (TEER). Although the latter is faster, the former is more robust and comparison with the literature is more reliable.

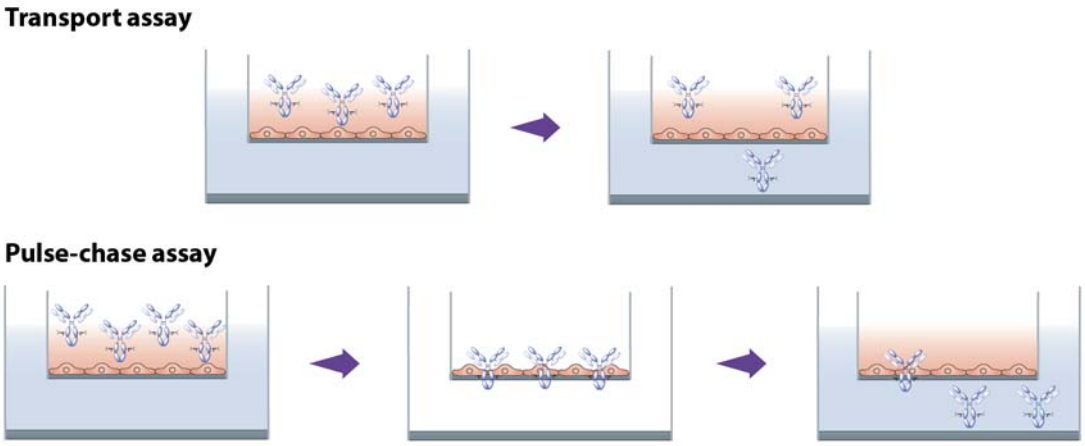

Figure 3. *Traditional transport assay and pulse-chase assay in cell-based BBB models.*

The first barrier models were set up with non-cerebral cells because they were more robust. However, more physiological models have been developed based on primary, immortalized and induced brain endothelial cells of distinct origin, ranging from bovine to human and including mouse, rat, porcine and monkey. They are generally set up in co-culture with other cells from the neurovascular unit, mainly glial cells but also pericytes and even neurons. Many of these models have been shown to comply with most characteristics of *in vivo* BBB, including paracellular transport restricted by TJ proteins and functional expression of many transporters, though often in different amounts with respect to *in vivo*.[55,56] Moreover, interspecies differences are also of major importance when active transport is studied.[50,51] Human cells are the best choice but the hCMEC/D3 line, which is the most widely used and characterized,[53,57] is considered to be excessively leaky.[25] Very recently, more robust and tighter models have been set up,[58,59] but they need further refinement and validation.[53]

Shear stress has an important effect on the regulation of growth and polarization of endothelial cells. Although dynamic models ranging from 2D cone plate

apparatus to 3D hollow fibres have been explored, their improved features do not appear to compensate for their higher complexity and lower throughput. These models may be more adequate for the study the effects of pathological conditions on endothelium.

Permeability values obtained in classical transport assays on static cell-based models of the BBB have shown good correlation with *in vivo* data for small molecules.[60] However, less comparative information is available for large molecules and NPs. Evaluating BBB-shuttle studies leads to the conclusion that although permeability values cannot be accurately predicted, large changes in permeability between BBB-shuttle-cargo constructs obtained in cell-based models often imply a significant difference in mice.[61-63] It is also worth mentioning that Angiopep-2, one of the most successful BBB-shuttles, was found in the bovine BBB cell-based model developed by Cellial Technologies.[64]

Data obtained with these models must be interpreted with care[53] as there are still some concerns about the non-negligible paracellular passage and about whether all the receptors that have not been compared are also functionally present in these models. As an alternative to traditional apical-to-basal transport assay and in order to minimize the paracellular contribution, some authors prefer pulse-chase experiments (*Figure 3*). The latter consist in incubating the compounds in the apical side to allow them to bind to the endothelial cell receptors and/or internalize, washing the cells and performing the transport assay with the compound that has remained bound or taken up by the cells.[25,65] Another limitation of these models is that they are usually performed in serum-free media or in buffers to preserve monolayer integrity. Although BSA has been used to mimic unspecific absorption, it is difficult to predict binding to other serum proteins, as reflected in the work by Markoutsa *et al.*[66]

Cell uptake – mechanistic studies

Cell uptake is not generally used to predict BBB permeability. However, it is a very valuable tool to gain a mechanistic insight into the transport using an easier setting. Primary endothelial cells are not commonly used because they lose their natural phenotype when isolated and require a reinduction of BBB properties in co-culture with other cells. Therefore, immortalized cell-lines are preferred for this purpose and currently the most common one is a mouse endothelialpolyoma cell-line from cerebral cortex, bEnd.3.[54]

The mechanistic study usually starts by determining whether the uptake is active or passive. For this purpose, internalization is measured at 37ºC and at a lower temperature (generally 4ºC), but also inhibitors of the respiratory chain such as sodium azide are used. Aiming to classify or assess the contribution of each type of

mechanism, inhibitors for macropinocytosis, clathrin- and caveolin-mediated endocytosis are used. In order determine whether a receptor is involved in endocytosis, competition experiments of the BBB-shuttle construct with an excess of the shuttle are performed. In order to verify or find the receptor involved, more specific competition experiments with endogenous substrates like Tf or α_2-macroglobulin (LRP1) are applied. Confocal fluorescence microscopy is often used to study the internalization and intracellular fate of the BBB-shuttle-cargo constructs. Colocalization with receptors (endogenous or transfected)[15,67] has been analysed and also with endosomes and lysosomes to study the recycling or degradation of the constructs.[25]

In vivo evaluation of BBB transport

In vivo testing not only implies the challenge of facing a completely physiological BBB but also involves many other pharmacokinetic factors such as protease degradation, liver modification, renal clearance, and interaction with serum proteins and cell membranes. This approach allows the measurement of the BBB-shuttle-construct PK and also its selectivity for the brain. Moreover, the therapeutic effect or diagnosis efficiency can be studied in the appropriate pathology model.[6]

With respect to the way to assess and report BBB transport, many parameters have been proposed: permeability surface area product (PS), which evaluates the rate in which components cross the BBB; total brain uptake, given by the ratio of total brain and plasma concentration under steady-state conditions (K_p) or its logarithm (log BB); and unbound partition coefficient ($K_{p,uu}$), among others.[6,15,68] Despite the higher correlation of free drug concentrations with efficacy, most BBB-shuttle studies focus on the extent of BBB penetration, as in most preclinical settings,[69] because it is easier to measure.

Regarding the animal model used, most studies in this field have been performed in mice because it has a good balance between cost, complexity, throughput and predictability can be achieved. Although insects such as locust, fly and zebra fish have been used to increase the throughput, these models are still not well characterized.[70] Moreover, mouse models are available for a wide variety of pathologies, thereby allowing the assessment of PD. Especially when using these models, BBB dysfunctions must be taken into accounts and integrity markers are required in order to study whether the peptide coating improves transport across the BBB or only has a targeting effect.

The administration route is of great relevance. Most studies involving BBB-shuttle development use systemic parenteral administration via tail vein injection. This route is the most direct way among clinical administration routes to evaluate BBB permeability as it bypasses the need for solute absorption and provides the

highest bioavailability in a short time.[71] However, in i.v. administration, the compounds are still exposed to degradation by serum proteases, adsorption on blood cells and molecules, absorption in tissues, and clearance. The only way to bypass all these physiological conditions and accurately measure permeation across the BBB is *in situ* brain perfusion. This technique consists in infusing the compound of interest in artificial blood, plasma or saline into a major vessel that leads directly to the brain by use of a perfusion pump.[72] However, this method of BBB permeability quantification is seldom used because of its low throughput and high complexity.[15]

A plethora of imaging and quantification techniques to study BBB-shuttle constructs *in vivo* are currently available. The selection will depend on many factors, mainly the target information, the nature of the compound and the sensitivity required but also cost, time and accessibility.

The decision on the analytical technique may imply the use of a label but care should be taken, as the measure may not reflect the PK of the compound but that of a metabolite.[73,74] Moreover, the label may severely alter the physichochemical properties of the cargo. However, in some cases, even if the cargo could be quantified on its own, labelling can be more practical, affordable or provide higher sensitivity. This last point is important to consider because concentration of the studied compound can affect the mechanism.[45]

The only techniques that allow assessing the integrity and/or functionality of the cargo after crossing the BBB are those that measure a property of the analyte itself. Among them, the gold standard in the pharmaceutical industry for small molecules is HPLC-MS.[75] For macromolecules ELISA is the most sensitive label-free method but is only indicative of functionality for high-affinity biomolecules such as antibodies, to which it has frequently been applied.[25,45,46] Luminescence or fluorescence have also been used if the cargo is or contains genetic material able to transfect a suitable protein, for instance GFP[76,77] or an enzyme (β galactosidase,[78-83] lysosomal enzymes,[84] luciferase[80,85-87]) capable of activating a chromogenic, fluorogenic or luminescent substrate. Flurophores such as FITC[88], Cy5.5®[89,90] and GFP[91,92] have also been used as mock cargoes or for imaging purposes. For nanoparticulate systems, some authors use fluorophores such as coumarin-6[93] or fluorescent drugs such as doxorubicin[94] as model payloads. In case of fluorescent labels, the compound may be analysed *ex-vivo* using a fluorometer[95] or HPLC coupled to a fluorescence or UV detector.[62,93,94,96] An alternative method to measure the relative amount of fluorophore in specific brain structures is flow cytometry.[76,88] Although the homogenization in this case is very mild to preserve cell integrity, exocytosis of the construct that has been internalized may occur. Exclusively for

nanoparticles containing metals or rare atoms, ICP-MS[63,97] is a very sensitive technique that has been also applied for quantification.

In vivo quantification

Intracerebral microdialysis is the gold standard technique for quantification of drugs in the brain. This approach allows measuring during long times the amount of unbound drug in the interstitial fluid, which is the one that may elicit a pharmacological effect, and following PK site-specifically and virtually online. However, the semi-permeable membrane used in the probes can only be crossed by small hydrophilic drugs and therefore cannot be applied to large protein, oligonucleotide or NP constructs. This is why only a few BBB-shuttle studies use this technique.[94,95,98]

Methods based on live-imaging allow a less accurate but generally more high-throughput estimation of kinetics. Among them, the most used nowadays by far is *in vivo* fluorescence imaging. However, tissues have high absorption in the UV and visible side of the spectrum and high scattering, which remarkably reduces sensitivity and resolution.[99] Therefore, this technique can be considered semi-quantitative and only identical regions of mice can be compared. Moreover, fluorescence depends on the environment, therefore behaving differently in distinct tissues and cell compartments. When aiming to deliver genes, luciferase can be included in the gene or used as a mock cargo. In this way, when luciferin is injected i.v., the site of expression of the gene is revealed.[100]

In comparison to fluorescence for bulk *in vivo* imaging, radioactive labelling offers a dramatically reduced background, especially in the brain, which has a considerable autofluorescence. Until now, in this field, gamma-ray isotope emitters such as ^{125}I have been used for Single Photon Emission Computed Tomography (micro-SPECT)[82] and positron emitting labels containing ^{18}F or ^{68}Ga have been incorporated to the BBB-shuttle-cargo constructs for Positron Emission Tomography (PET) combined with computed tomography.[101,102] A considerable inconvenient of PET is that radioisotopes must be incorporated immediately prior to imaging because of their short half-lives.[73]

With Magnetic Resonance Imaging (MRI) whole animal view with low background is possible and, in addition, offers higher resolution. This technique is frequently used to locate iron oxide NPs[103] or DTPA/DOTA-Ga^{3+} labelled constructs.[44,97,104-108] However, quantification is far more challenging.

Ex vivo quantification

Kinetics of brain permeation can also be studied ex-vivo but are more time-consuming and require a dramatically larger amount of animals. However, these

studies allow a more accurate quantification in the brain and other organs, providing more reliable figures about the selectivity for the brain.

An ideal quantification method would accurately measure the total amount of BBB-shuttle-cargo constructs with minimal processing of the sample. The technique that mostly approaches this description requires labelling with high intensity energy emitters such as ^{125}I and ^{131}I.[45,104,105,109,110] Quantitative autoradiography of brain slices can give an accurate though low-resolution picture of the distribution of the construct inside the brain.[104,107,109] For this purpose, also organ fluorescence quantification can be used, though only the organs of the same type can be compared.

Nevertheless, quantification of entire organs does do not allow the identification of the entities being quantified. Moreover, if the sample has high affinity for the capillaries, like in the case of anti-TfR antibodies, the amount could be considerably overestimated. This is why quantification of brain homogenates is relevant in assessing BBB permeation. After extracting the organs from the perfused animal and performing the homogenate under mild conditions, a capillary depletion protocol can be applied. This procedure consists in a density centrifugation based on a dextran solution that separates most of the vascular component from the rest of the tissue. However, it is important to take into account that separation is not complete and redistribution of the compound during the process may produce artefacts.[111] After homogenization and capillary depletion, if applied, most techniques require at least a further step of extraction or purification, which generally should be quantitative. Here, all techniques can be used, including those using low energy radioisotopes such as ^{3}H and ^{14}C β-emitters[94,107,112,113] or no labels.

Microscopy – in or out?

In order to localize BBB-shuttle-cargo constructs more precisely, we have to turn our attention to microscopy techniques. Despite the great value of the information they may provide, it is very important to take into account the possible artefacts that can be introduced during fixation, slicing and further processing of the sample.

Classical optical microscopy has been used to assess the presence and a rough localization of very robust enzymes that have coloured substrates such as HRP[47,114] and β-galactosidase,[80,82,88] which can be delivered as a cargo or transfected as a DNA sequence with *in situ* expression. However, results must be interpreted with care because of the possible interference of endogenous enzymes. Moreover, in order to assess whether the cargo has reached the parenchyma, more selective microscopy techniques are required. TEM is without any doubt the most reliable, sensitive and precise technique for metal nanocarriers, such as gold NPs,[63,115] as it can detect even single particles. However, for other constructs the technique of choice is

fluorescence microscopy. Furthermore, this approach allows to clearly locate the real boundaries of the brain parenchyma by staining the capillaries. Immunostainings can also reveal colocalization with certain cell types, such as neurons and glial cells.

Intravital two-photon confocal microscopy through a cranial window is the only technique that provides live visual evidence of BBB permeation. The most remarkable advantages of this technique are the possibility to study the blood-to-brain transport in real time and with minimal perturbation of the system. It must be taken into account that removing the organs from the animal triggers many processes such as autolysis that may significantly alter the sample. In order to minimize this, animals are usually perfused with PBS and then with PFA. Although this crosslinking process is efficient, it is not quantitative and the position of the molecules can be altered or they can even be washed out depending on the amount of exposed groups able to react with PFA.[116] Using this approach immunostainings cannot be applied; however, the capillaries can be stained with fluorescently labelled lectins or dextran, which in turn provides information about BBB integrity. However, an important drawback of this approach, like in all fluorescence microscopy, is the difficulty to obtain quantitative data.

Therapeutic effect

Ultimately, the aim of most studies is the increase the therapeutic effect of the cargo or the loaded drug. Measuring an improvement in the pharmacodynamics of the compound will imply a success in the delivery strategy. Some studies rely on the quantification of a biochemical indicator and others in behavioural or survival improvements. However, the results must be interpreted with care in regard to BBB permeation because the effect that has been achieved might be due to a peripheral effect or, less probably, to a mechanism that circumvents the BBB such as retrograde axonal transport. Moreover, it is important to take into account if the BBB preserves its integrity under the studied pathological conditions.

BBB-shuttle peptides classified according to the proposed transport mechanisms

After reviewing the main tools used to assess BBB passage, we will cover the current state of BBB-shuttle peptides going through the proposed transport mechanisms.

The field of peptide shuttles was pioneered in 1999 by Schwarze *et al.*[88], who demonstrated the capacity of a fragment from the HIV TAT protein to deliver *β*-galactosidase into the brain and other organs. After that, other peptide shuttles providing enhanced brain delivery but without organ selectivity appeared. However, it was not until the publication of Kumar *et al.*[76] in 2007 that a peptide was clearly shown to selectively transport cargoes into the brain. In the same period, the great potential of Angiopep-2 and glutathione as BBB-shuttles was unravelled, both of which are included in formulations that have recently entered Phase II clinical trials. In the last 5 years, owing to the rise of nanomaterials for drug delivery and also to the application of phage display screening technologies, over 30 BBB-shuttle peptides have been described.

The need for safer therapeutics has pushed research towards targeted strategies in an attempt to achieve Paul Ehrlich's "magic bullet". Although there is a wide variety of receptors present on the BBB, only those that show at least the following properties are attractive for brain delivery purposes: high expression in the luminal side of brain vasculature with respect to other tissues, capacity to mediate transcytosis and high turnover. Unfortunately, part of this informaiton is available only for only a few of these receptors. Moreover, although there is certain evidence that transcytosis is the main route for CNS delivery for most shuttles interacting with these transporters, contribution of other mechanisms cannot be excluded.[40]

Low-density lipoprotein receptors

Although the low-density lipoprotein receptor (LDLR) family includes over 7 members,[117] only the parent LDLR and the lipoprotein receptor-related proteins 1 (LRP1) and 2 (LRP2 or megalin) have been used for drug delivery to the CNS.[42] Of these, LRP1 is the only one that appears to be expressed in higher amounts in the brain with respect to other organs (though it can also be found in high amounts in the liver and the lung).[118] The endocytosis of the LDLR family of receptors has been intensely studied, and transcytosis has also been described.[119] This explains why LDLRs, in spite of the many roles as scavengers, transporters and signalling receptors, have attracted the attention of many researchers interested in brain delivery.[120] Moreover, LDLRs are also overexpressed in many tumours, which is an additional benefit when aiming malignant cells.[121] Peptides targeting this family of receptors are derived mainly from natural protein ligands of endogenous receptors, namely ApoB and ApoE and proteins with a Kunitz domain, but others were found by phage display.

Table 1. *Representative peptide BBB-shuttles and some relevant features.*

Peptide	Typical sequence	Proposed mechanism	Origin	Main cargoes	BBB passage evidence
diketo-piperazines	&(*N*-MePhe)-(*N*-MePhe)&	Passive diffusion	Serendipity	small drug	• PAMPA • BBBCM
***N*-methyl Phe**	(*N*-MePhe)$_n$-*NH$_2$*	Passive diffusion	Nat. pep. derived	small drug	• PAMPA • BBBCM
TAT (47-57)	YGRKKRRQRRR-*NH$_2$*	AMT	PTD	protein NP	• BBBCM • Capillary depletion • Fluorescence microscopy • TEM
D-penetratin	rqikiwfqnrrmkwkk-*NH$_2$*	AMT	PTD	small drug	• Capillary depletion
SynB3	RRLSYSRRRF-*NH$_2$*	AMT	PTD	small drug	• Capillary depletion
Angiopep-2	TFFYGGSRGKRNNFK TEEY-*OH*	LRP1	PTD derived	small drug DNA/RNA NP	• BBBCM • Capillary depletion • Fluorescence microscopy • TEM • Effect in glioma, epilepsy and Parkinson's mouse models
Angiopep2 *retroenantio*	yeektfnnrkgrsggyfft	LRP1	PTD derived	NP	-
ApoB (3371-3409)	SSVIDALQYKLEGTTR LTRKRGLKLATALSLS NKFVEGS	LRP2 LDLR	PTD	protein	• Capillary depletion • Effect in MPS 3a mouse model
ApoE (159-167)$_2$	(LRKLRKRLL)$_2$	LRP1 LRP2 LDLR	PTD	protein NP	• BBBCM • Capillary depletion • Fluorescence microscopy • Effect in MLD mouse model
Peptide-22	*Ac*-M&PRLRGC&-*NH$_2$*	LDLR	PDisp	NP	• BBBCM
B6	GHKAKGPRK	TfR1	PDisp	NP	• Effect in AD mouse model
T7	HAIYPRH-*NH$_2$*	TfR1	PDisp	RNA	-
THR	THRPPMWSPVWP-*NH$_2$*	TfR1	PDisp	RNA NP	• BBBCM • TEM
THR *retroenantio* (THRre)	pwvpswmpprht-*NH$_2$*	TfR1	PDisp derived	small drug NP	• BBBCM • Live fluorescence microscopy
CRT	C&RTIGPSVC&	TfR1	PDisp	Virus	• Capillary depletion
Glutathione (GSH)	*γ-L-glutamyl*-CG-*OH*	GSH transporter	Nat. pep.	NP	• Intracerebral microdyalisis • Effect in glioma and MS mouse models
Leptin30	YQQILTSMPSRNVIQIS NDLE-NLRDLLHVL	Leptin receptors	PTD	DNA	• Capillary depletion
g7	GFtGFLS(O-β-Glc)-*NH$_2$*	Unknown receptor	Nat. pep. derived	NP	• Fluorescence microscopy
cRGD	&RGDfK(linker)&	Integrins	Nat. pep. derived	NP	• Fluorescence microscopy
RVG29	YTIWMPENPRPGTPC DIFT-NSRGKRASNG-*OH*	NAchR	PTD	RNA/DNA NP	• Capillary depletion • BBBCM • Effect in viral enkephalitis and Parkinson's mouse models
RDP	KSVRTWNEIIPSKGCL RVGGRCHPHVNGGG (R_9)-*OH*	NAchR?	PTD	protein DNA	• Effect in stroke mouse model
G23	HLNILSTLWKYRC	GM1	PDisp	NP	• BBBCM • Fluorescence microscopy
TGN	TGNYKALHPHNG	Unknown (clathrin +caveolae)	PDisp	NP	• Fluorescence microscopy • Effect in glioma and AD mouse models

PTD: protein transduction domain, PDisp: phage display, Nat. pep.: natural petpide; BBBCM: cell-based BBB model; AD: Alzheimer's disease. Nomenclature for cyclic peptides is based on that suggested by Spengler *et al.*[122]

LRP1 appears to be the gateway for the main reference in the field of BBB-shuttle peptides, Angiopep-2. This shuttle has been used in over 50 original studies documented in the Web of Science. Angiopep-2 was identified by alignment of sequences of aprotinin with human proteins also having Kunitz domains (*Figure 4*).[64] This peptide was initially exploited to transport small molecules such as doxorubicin and etopside.[113] Its conjugate with paclitaxel (ANG1005 or GRN1005) is currently in phase II clinical trials for breast cancer with brain metastases and recurrent high-grade glioma (ClinicalTrials.gov ID: NCT02048059, NCT01967810, NCT0148053). Phase I clinical studies showed that ANG1005 was tolerated in patients with brain tumours;[123,124] hence, this shuttle does not appear to have major toxicity issues. There are also a few examples of Angiopep-2 applied to peptides and proteins; among the most notable achievements in this regard are the enhancement of the antinociceptive peptide neurotensin[125] and the increase in lifespan of HER2+ tumour-bearing mice achieved by a trastuzumab-Angiopep-2 conjugate.[126]

Angiopep-2 has been used to transport a wide variety of nanocarriers loaded with small molecules, proteins or genetic material into the CNS. These carriers include liposomes,[127,128] nanotubes[129] and NPs made of PEG-PCL[29,130-132] and PEG-PLGA,[110] PAMAM dendrimers,[104,105,133-135] poly-L-lysine dendrigrafts,[136] thermoresponsive hydrogels formed by DMAEMA and ACLT-PEG[96] and also gold.[137] The diameter of these constructs ranged from 7 to 180 nm and the ζ-potential from -3 to 17 mV, which further confirms the versatility of this shuttle. Moreover, the amount of peptides on the NP surface required for an efficient delivery is relatively low. Four peptides are considered optimal for 7-8 nm dendrons[133] and 53 peptides on the surface of a 90 nm NP were enough to provide an efficient delivery.[29] The increase in brain delivery for these constructs is between 1.6- and 2.6-fold in mice, as assessed mainly by *in vivo* and *ex vivo* fluorescence imaging and, to a lesser extent, by ^{125}I labelled NPs.

Most studies focus on the preparation and delivery of conjugates for the diagnosis[104,105,138] or the treatment[110,130] of brain tumours; in the second case a significant increase in survival with respect to the free drug or untargeted nanocarrier has often been reported.[129,131,134,137,139] Although in tumour models the BBB may be compromised, Angipep-2 has also been succesfully applied to others models, including meningoencephalitis[140,141], epilepsy[96] and Parkisnon's disesase.[136] Moreover, BBB peremation has been assessed in healthy mice and in a tight monolayer of brain endothelial cells.[96]

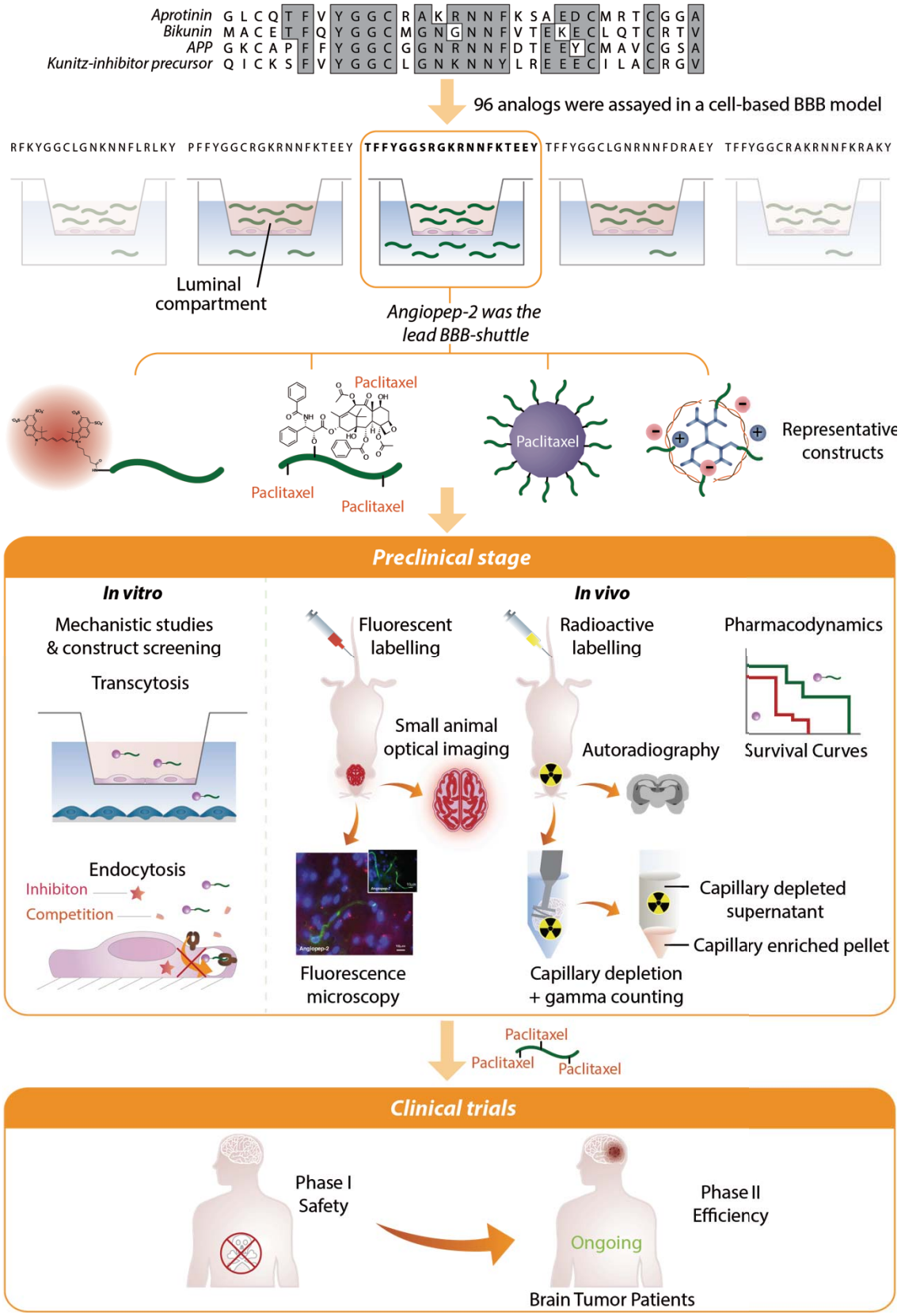

***Figure 4**. A scheme of Angiopep-2 discovery and validation process including the techniques used to assess its efficiency in delivering cargoes into the brain. (Design: Benjamí Oller-Salvia. Drawing: Iris Joval)*

In spite of its attractive features, Angiopep-2 can still be improved. This shuttle has the same weakness as most linear peptides made of L-amino acids, namely lability to proteases. In this regard, in a recent publication, a *retro-inverso* (or *retro-enantio*) version of this peptide was obtained and showed more efficient delivery of DSPE NPs into mouse brains.[142] The *retro-enantio* approach applied in this context consists in obtaining a protease-resistant peptide by changing the stereochemistry of all the amino acids (from L-aa to D-aa) but preserving the topochemical features inverting the order of the sequence. In this way, only the direction of the amide bond is reversed and the structure is often conserved. Moreover, D-amino acids may provide peptides with lower immunogenicity.[143]

Another family of BBB-shuttles interacting with the LDLRs are those derived from apolipoproteins. Although these proteins have been reported to bind other macromolecules for lysosomal degradation, they have also been extensively described to undergo transcytosis and to deliver cargoes into the brain.[92] Apolipoprotein B100 (ApoB) is the primary component of LDL and it interacts with LDLR and LRP2.[118] Although the binding domain of ApoB has proven capable of delivering some proteins into the brain parenchyma,[84,92] it was less effective than shuttles obtained from ApoE when applied to other proteins.[61,65] This difference may be due to the fact that the latter[144,145] bind to LRP1, as well as to LDLR and LRP2.

Peptides derived from the *N*-terminal domain of ApoE have been shown to interact with the LDLRs mainly by ionic interactions, especially in the presence of lipids.[146-148] Based on these studies, Wang *et al.*[65] compared the capacity of a variety of fragments to transport an enzyme into the brain parenchyma. In a very exhaustive study they used these ApoE fragments to target to the brain a lysosomal enzyme (IDUA) expressed as a fusion protein in the liver (*Figure 5*). They achieved up to a 3.6-fold increase in transport in a pulse-chase experiment using a cell-based BBB model and a 10 to 20-fold increase in capillary-depleted brain tissue *in vivo*. In addition, these authors provided fluorescence microscopy images indicating colocalization of the construct with neurons and astrocytes outside brain capillaries. Furthermore, by restoring 23 % of normal brain IDUA activity, they normalized brain glycosaminoglycan and *β*-hexosaminidase in MPS I mice.

One of the two peptides with the best performance found by Wang *et al.*[65] was the tandem dimer sequence ApoE(159-167)$_2$, which had better transport in a cell-based BBB model than the monomer.[149] This peptide coincided with the best-ranked BBB-shuttle in a very recent comparative study by Böckenhoff *et al.*[61] also using a lysosomal storage disease mouse model, namely metachromic leukodystrophy. In that study, ApoE(159-167)$_2$ did not provide the best results in endocytosis or in a porcine BBB cell-based model; however, it was the only peptide to increase brain delivery *in vivo* of arylsulfatase A when compared to Angiopep-2, ApoE(148-170),

and ApoB. Curiously, the uptake of this ApoE peptide-cargo conjugate was the same as in an ApoE knock-out mouse model, thereby indicating that the peptide does not compete with the endogenous protein.

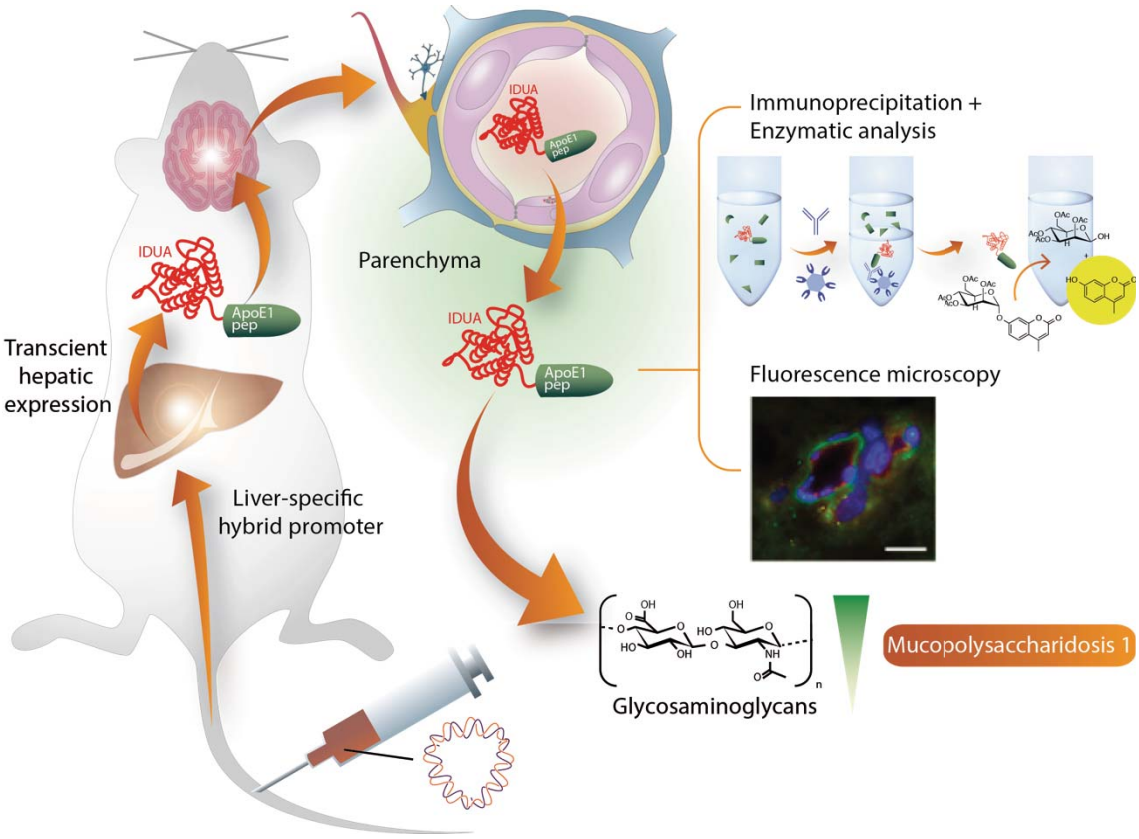

***Figure 5**. Brain delivery of enzymes fused to ApoE peptide and expressed in the liver.[65,92] (Design: Benjamí Oller-Salvia. Drawing: Iris Joval)*

It is also worth highlighting the work by Sarkar *et al.*,[82] who delivered large proteins (*β*-galactosidase, IgG and IgM) to the brain using a physical mixture with ApoE(151-170) in tandem with a 16-lysine sequence. However, in a more recent publication,[150] these authors showed that this peptide delivered the cargo mainly through a transient disruption of the BBB. Therefore, the ApoE peptide with this oligolysine sequence cannot be strictly considered a BBB-shuttle.

The only shuttle targeting a receptor from the LDLR family that does not derive from a natural protein is Peptide-22. The peptide was found by phage display biopanning directed to the extracellular domain of a human LDLR by Malcor *et al.*[30] In this seminal study, they demonstrated that Peptide-22 did not compete with endogenous LDL and reached the perivascular region in the spinal chord through a receptor-mediated mechanism. More recently, Jiang *et al.*[27] proved that this peptide also carries paclitaxel-loaded PLA-PEG NPs across the BBB *in vitro* and *in vivo,* increasing the surivival of mice bearing glioblastoma.

Transferrin receptor

Although two TfRs have been described, TfR2 has 25-fold lower affinity for Tf and is expressed mainly in the liver.[151] Therefore, the main gateway for BBB-shuttles is considered to be TfR1. TfR1 is the best characterized among BBB receptors and, together with LRP1, the one that has been most often used for brain targeting because of its high expression on the brain endothelium.[152] TfR1 overexpression is significantly higher than that of LRP1 (t-test, $p < 0.05$), both in humans,[50] and rodents.[153] In addition, the endocytosis of this receptor has been widely characterized and its transcytotic capacity is now widely accepted. Furthermore, TfR1 is also overexpressed in tumours.[42]

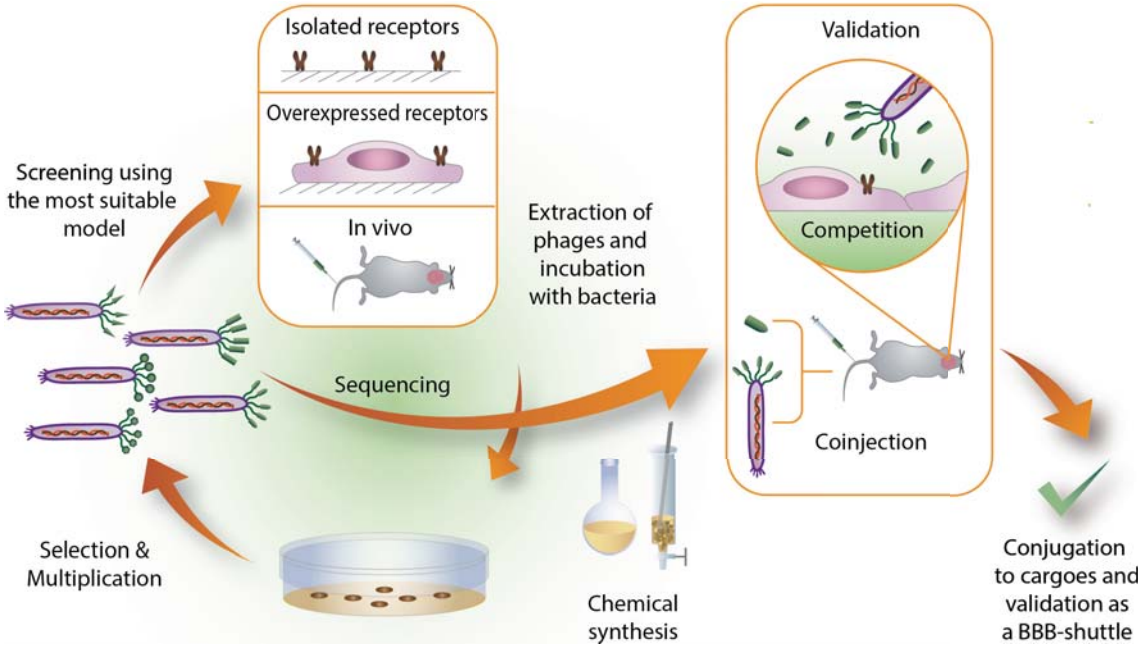

***Figure 6**. Phage display applied to the discovery of BBB-shuttles. (Design: Benjamí Oller-Salvia. Drawing: Iris Joval)*

At least four peptides have been shown to undergo transcytosis through this receptor. These were discovered by applying phage display biopanning in various ways (*Figure 6*): B6 was found from a nonamer library screened against the extracellular domain of human TfR,[154] THR and T7 were found to bind the human receptor expressed in chicken fibroblasts (chicken TfR does not bind human Tf),[67] and the CRT peptide was found to be selective for mouse brain *in vivo*.[101]

An important advantage of THR and T7 over B6 is that the former do not compete with Tf[67] while the latter does.[154,155] In our laboratory, Prades *et al.*[63] used THR to enhance the transport of gold NPs across a tight monolayer of bovine endothelial cells (1000-fold increase). Moreover, this shuttle also increased the passage *in vivo* of these NPs coated with a peptide capable of binding amyloid-β in order to disrupt aggregates upon irradiation. TEM micrographs confirmed the

presence of NPs in the parenchyma. THR in tandem with transportan and a myristoyl chain has also been shown to significantly increase the passage of siRNA across a monolayer of bEnd.3.[85] The sequence of this peptide has been shown to substantially influence uptake[67] and translocation,[85] supporting a receptor-mediated transport mechanism. Nevertheless, we have very recently reported that a *retro-enantio* version of THR (THRre) shows a significant enhancement of shuttling capacity, further proving the great potential of this approach (part of this work was derived from this thesis). Moreover, not only was THRre more efficient than the parent peptide in several *in vitro* and *in vivo* experiments, but it also transported quantum dots into the brain parenchyma as shown by two-photon intravital microscopy (*Figure 7*).[156]

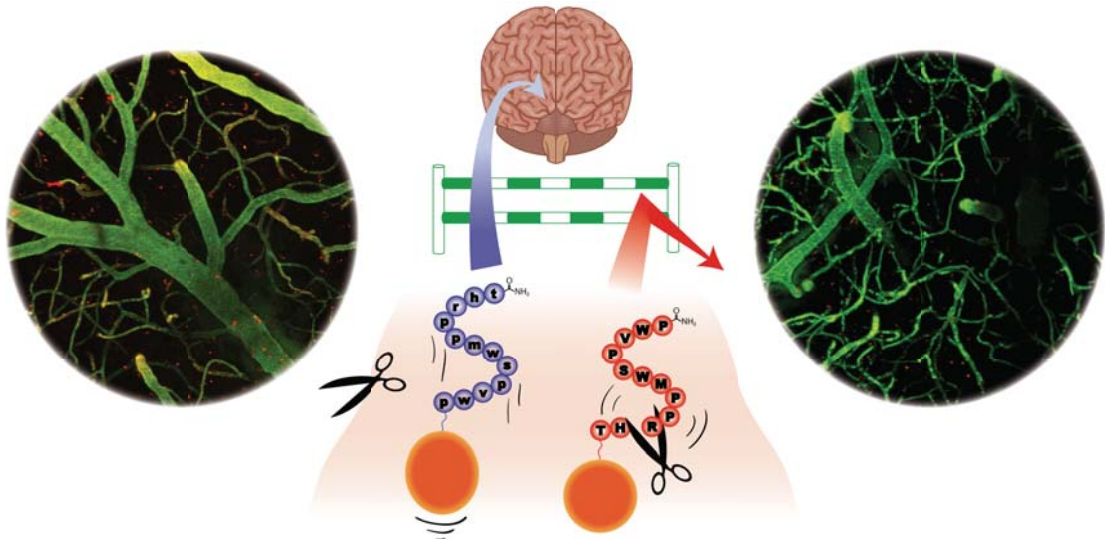

***Figure 7**. Protease-resistant THRre is able to transport quantum dots into the brain parenchyma. (Drawing by Benjamí Oller-Salvia. Graphical abstract from Prades et al. 2015 with some modifications)[156]*

Regarding T7, it has been used to significantly enhance gene and small molecule delivery into glioma bearing mice and even to increase their lifespan.[100,157] However, the enhancement in transport could be due to a mechanism other than the T7 interaction with TfR because this sequence has appeared in multiple panning experiments with unrelated targets.[158]

Another peptide transported through the TfR without competing with Tf is CRT. This shuttle was chosen from a phage display biopanning through intravenous injection (i.v.) in mice after observing its high accumulation in the brain and because it resembled a sequence fragment of Tf.[101] Surprisingly, instead of interacting directly with TfR, CRT was shown to mimic iron in Tf.

Nicotinic acetylcholine receptor

Nicotinic receptors are ligand-gated ion channels that are naturally regulated by the binding of neurotransmitter acetylcholine. At least 17 subtypes[159] of channels

have been identified and those containing an α7 domain account for most of the high affinity α-bungarotoxin binding sites.[160] Although receptors containing this domain are present in many tissues, it is also widely expressed in brain endothelium, which makes it an attractive target for BBB-shuttles. Despite data about the endocytotic or transcytotic capacity of nicotinic acetylcholine receptor (nAchR) is scarce, several peptide shuttles have been designed inspired in the rabies virus and snake venoms interacting with this receptor.

Studying the high brain tropism of the rabies virus, which is mediated by its glycoprotein (RVG), Kumar *et al.*[76] found a peptide with great capacity to transport siRNA into the CNS. After showing that this sequence could indeed reach the brain parenchyma, a tail with 9 arginines was incorporated to bind siRNA. As a proof of concept, this construct was first used to transport oligonucleotides into healthy mouse brains silencing GFP in GFP-transgenic mice as well as endogenous SOD1 in the CNS. As a final demonstration of its value, this delivery strategy was successfully applied to protect mice with JEV-induced encephalitis. The authors reasoned that its translocation could take place by RMT through interaction with the α7 subunit of the nAchR because this peptide specifically bound neurons and competed with α-bungarotoxin. The same group published another study providing further evidence that the nAchR was involved in the translocation of this BBB-shuttle. In the second study, RVG29 was found in cells that overexpress this receptor in normal mice, unlike a scrambled version of the sequence, and it was not detected in knockout animals devoid of this receptor.[161]

Results from other groups have confirmed the high potential of this sequence for gene delivery, using either the 9-Arg tail,[86,162] a polylysine dendrigraft,[163] polyethylenimine,[164,165] polyasparthydrazide[166] or PAMAM dendrimers[167] to bind the oligonucleotide chains, some of them exerting a therapeutic effect.[168] An alternative nanocarrier for gene delivery are targeted exosomes, which have been shown to be 5 times more efficient than (9-Arg)-RVG in knocking-down a protein *in vivo*.[169]

Recently, the scope of the RVG shuttle was widened to include the delivery of a protein, i.e. β-galactosidase, encapsulated in pluronic-chitosan NPs.[78] However, the delivery of proteins by fusion with the BBB-shuttle has been published only with longer sequences derived from RVG.[79-81] In spite of the excellent results obtained with RVG peptides, their long sequences (29-43 residues) may partly explain the lack of interest on the part of investors to take it into clinical trials.

In view of the remarkable achievements of RVG, Zhan *et al.*[170,171] took advantage of the high affinity of some snake neurotoxins for the nAchR to design two new BBB-shuttles. The native toxins have a "three-finger" structure, which is shaped by three loops forming a globular core, and the second loop is known to interact with nAchR. KC2S is a 20-mer containing one disulfide bond based on *Ophiophagus*

hannah toxin b, whereas ^{L}CDX is a 16-residue linear sequence from *Bungarus candidus* candotoxin. Both peptides increased NP accumulation in mouse brain and enhanced the survival of tumour-bearing mice. More recently, the same group has developed a *retro-enantio* analogue that retains the capacity to interact with the same receptor.[172] Although the affinity of this analogue is 5-fold lower than the original peptide, its transport capacity is enhanced because of its remarkably higher resistance to proteases in serum and in the lysosome. The authors postulate that the increased translocation of the ^{D}CDX is due to a saturation of the lysosomal compartments.

Leptin receptor

The neurotropism of the satiety-regulator hormone leptin has also drawn attention to its receptors in the field of BBB-shuttles. Moreover, this protein has been described to undergo transcytosis through the ObRa and ObRb receptors, which are present in brain microvasculature.[173] Drawn by evidence that leptin crosses the BBB, Barrett *et al.* identified several fragments that reached the parenchyma and that could be used as BBB-shuttles[174] and Liu *et al.*[87] used leptin30 to deliver a plasmid DNA complexed with a dendrigraft of polylysine in a very complete study.

Glutathione transporter

Together with Angiopep-2, glutathione (GSH) is the peptide shuttle that is most advanced in the route towards clinical application. PEGylated nanoliposomes targeted with GSH loaded with small drugs, known as G-Technology®, are currently in Phase I/IIa clinical trials for brain cancer and multiple sclerosis (ClinicalTrials.gov ID: NCT01386580, NCT01818713, NCT02048358). Data from several preclinical studies has recently been unravelled showing transport enhancements of up to 6.5-fold in mice.[17,94,98,175-177] Important features of this formulation are that it does not require the alteration of the drug, which is protected from degradation and clearance, and that it can be applied to a wide range of compounds, including biologics.[17,178] In all these studies, native GSH proved highly efficient; however, an improvement in its metabolic stability could lead to an even better delivery vector. More *et al.* showed that a peptidomimetic analogue with a urea scaffold was capable of efficiently transporting dopamine in an MDCK Transwell model.[179]

Despite the incontestable contribution of GSH to increasing the concentration of liposome-encapsulated molecules in the brain parenchyma, little is known about the targeting and/or translocation mechanism involved. Certainly many transporters mediate the influx and efflux of GSH and its endogenous conjugates;[180] in particular, the sodium-dependent GSH transporter has a preferential expression in the CNS[95] but further research is required to elucidate the putative transcytotic route.

Integrins

Although integrins are not selectively expressed in the brain microsvasculature, they have been extensively used for targeting to brain tumours and inflamed regions of the CNS.[181] Cyclic RGD (cRGD) and its analogue iRGD[182] are peptides derived from a sequence present in many proteins that recognise these receptors. Because integrin $\alpha_v\beta_3$ is overexpressed in neovasculature, cRGD has been extensively used to target NPs into gliomas[183-187] and it has been occasionally used together with CPPs such as TAT[184] and octaarginine.[185] Although only the tumour-targeting capacity of cRGD does not make it a BBB-shuttle, it has also been shown to indirectly mediate transcytosis across the BBB. Target integrins are also expressed on the surface of leukocytes, which are able to cross the intact BBB and are recruited into the brain in response to inflammation. Therefore, these cells can internalize NPs bearing the cRGD sequence[188-190] and transport them into inflamed regions of the brain, even when the BBB is still intact.[7,22]

Gangliosides

Protein receptors are not the only gateways to transcytosis. Gangliosides, which are amphipathic molecules consisting of a ceramide lipid moiety and a glycan chain, have also been reported to facilitate this intracellular traffic in polarized cells.[191-194] Therefore, targeting the exposed glycan emerges as an interesting strategy to achieve transport across cell barriers. Peptide G23 was found by *in vitro* phage display biopanning against trisialoganglioside G_{T1b} followed by elution with tetanus toxin C fragment.[195] Georgieva *et al.* reasoned that since caveolae are enriched in GM1 (a ganglioside structurally similar to G_{T1b}), G23 could be suitable as a BBB-shuttle.[196] In this study, the G23 sequence was shown to be 2-fold more effective in transporting polymersomes than a scrambled peptide in a cell-based BBB model.

Unclassified CNS-selective translocation mechanisms

Although many shuttles using the mechanisms described above have yielded outstanding results, none is yet used in clinical practice. This gap indicates that all pathways should still be considered and that new transport mechanisms need to be explored. Therefore it is extremely important not to neglect those sequences derived from phage display or natural sources that have shown interesting brain targeting capacity, regardless whether the translocation mechanism is still unclear.

At least two shuttles derived from opioid peptides have been used, Leu-enkephalin[102] and g7. Although the amphipathic structure and the strong interaction with cell membranes displayed by some peptides belonging to this family may suggest that they use adsorption-mediated mechanisms,[197] for g7 there is strong evidence indicating receptor-mediated brain delivery.[198] The *in vivo* capacity of this peptide to successfully deliver drug-loaded PEG-PLGA NPs has been reported in

many papers, which have recently been reviewed[199] and is currently still being investigated.[200-203] Further evidence of the therapeutic effect of this peptide upon intravenous injection would certainly encourage a more widespread use.

Bacteriophages (or simply phages) can be considered as one of the largest cargoes that can be transported into the brain parenchyma and are highly unlikely to cross by passive difffusion. Filamentous phages, which are the most commonly used, measure 6.5 nm in diameter and 930 nm in length and only display 5 copies of peptide per viral particle. These characteristics, together with the high number of sequences they are capable to display, may explain why this screening technique has been successfully applied *in vivo* to find peptides capable of translocating NPs. This is the case of TGN, which was discovered by Li *et al.*[204] and used to efficiently and selectively target PEG-PLGA NPs into the brain. The increase in brain penetration induced by this peptide is supported by several studies showing an enhanced therapeutic effect of a variety of drugs.[93,205,206]

Among the peptides that have not yet been applied to cargoes other than phages, the study with PepC7 is remarkably complete.[91] Also using a 7-mer phage library, Gumbleton *et al.*[207] described that the SxTSSTx and xxxSSTx motifs appeared to be relevant for brain accumulation. Van Rooy *et al.*[208] also reported two peptides found by phage display applied to *in situ* mouse brain perfusion and used them for the selective targeting of liposomes to the brain.[209]

Adsorptive-mediated transcytosis triggered by cationic peptides

BBB-shuttle peptides capable of triggering AMT mainly belong to the cell-penetrating peptide (CPP) family. This family includes all short amphipathic or cationic sequences with a high capacity to cross cell membranes without the need of a receptor and to transport cargoes with them.[210,211] Since the high internalization capacity of the transcription-transactivation protein of HIV-1 (TAT) was discovered,[212] other peptides displaying this property have been obtained from single protein transduction domains (PTDs) (e.g. SynB, penetratin and mastoparan), by merging several PTDs (e.g. transportan) or through biomimetic design (e.g. oligoarginine). While direct translocation into cells has been described for some CPPs, AMT appears to be the preferred pathway when carrying large cargoes.[41] Although it is well established that these peptides undergo endocytosis in many cell types, exocytosis from the endothelium of the entire BBB-shuttle constructs is more controversial than in RMT. In spite of this and regardless of the lower brain selectivity, many studies show that these peptides are able to mediate an efficient delivery of cargoes into the brain parenchyma.

TAT is the most used CPP for brain delivery because it was the first to be described as a BBB-shuttle and also because it has been shown to be safe in diverse

clinical trials.[213] This peptide has proven capable of increasing the brain concentration of a variety of proteins.[88,214-217] Although in some cases the constructs improve the therapeutic effect with respect to the non-targeted cargo,[218] no further evidence of reaching the parenchyma has been presented. Only the TAT-BcL-xL construct has been reported to colocalize with neurons and astrocytes in healthy mice.[219] By contrast, in more recent studies focused on TAT-coated NPs, many techniques have been applied to study BBB passage. One of the most notorious examples is the work by Rao *et al.*,[220] in which an 800-fold increase in ritonavir delivery two weeks after injection was achieved using PLA NPs. To perform this quantification, capillary depletion was applied and, despite the limited accuracy of this technique, an increase in the parenchyma/capillary ratio over time is irrefutable. As expected for the cell-penetrating ability of TAT, NPs coated with this peptide were efficiently internalized in capillary endothelial cells and were released during at least 14 days. Another proof that TAT is localized mainly in the capillaries is the image obtained using quantum dots coated with this peptide, which showed very bright fluorescence in the vasculature when compared to the parenchyma.[221] Hence, although TAT-coated NPs provide a sustained delivery of the drug into mouse brain, further studies should also explore the potential side effects caused by the long-term accumulation of these nanocarriers and their loads in endothelial cells.

It is also true that other nanocarriers coated with the same peptide appear to reach a peak in a relatively short time after injection (< 2h).[222-225] However, in these cases very little qualitative data is available regarding BBB penetration. Other studies using TAT-targeted doxorubicin provide evidence of enhanced lifespan[97,226] and tumour visualization[97] using chelated Gd^{3+} in mouse glioma models, which could partly be due to an impaired BBB.

The other main class of CPPs that have been exploited for brain delivery of a variety of small cargoes are pegelins (SynB1 and SynB3). They derive from the antimicrobial peptides protegrins. Although the natural peptides have been described to form pores in the lipid matrix of bacterial membranes, pegelins lack the disulfide bonds essential for pore formation.[227] These linear peptides have a high positive charge and can efficiently penetrate cells by an energy-dependent mechanism. However, unlike TAT, they have been applied only for brain delivery and, surprisingly, they do not cause a general unspecific uptake of small drugs such as doxorubicin in other organs.[228] SynB1 and its shorter analogue SynB3 have been shown to increase the therapeutic effect of other small molecules[229-231] and enhance the transport of gelatin-siloxane NPs.[232]

Penetratin was also one of the first CPPs used as a BBB-shuttle together with TAT and SynB1 for the transport of doxorubicin.[228] This CPP has also been used *in vivo* to

enhance transduction of anti-sense RNA[233] and morpholino oligonucleotides, [234] and also to enhance the transport of PEG-PLA NPs.[235]

Recent studies have shown that dual-targeted liposomes with either T7 and TAT or Tf combined with TAT, penetratin or mastoparan outperformed those with a single targeting moiety both *in vitro* and *in vivo*.[62,236] This strategy may provide a way to overcome possible capillary accumulation and take advantage of the penetrating capacity of CPPs by combining it with the higher selectivity of receptor ligands.

Passive diffusion

For small drugs, peptide shuttles targeting active mechanisms are usually unreasonably large and hinder the interaction of the molecule with its target. Instead, short peptides that enhance BBB transport of these cargoes through passive diffusion have been applied. In the seminal study by Chikhale *et al.*[237], hydrogen bonding and water desolvation were reported to have a better correlation with BBB permeability of peptides than logP. Based on this criterion, two families of BBB-shuttle peptides, diketopiperazines[35] and *N*-methylphenylalanines,[32-34] were developed in our laboratory. They were evaluated and optimized using a parallel artificial membrane permeability assay (PAMPA), the gold standard BBB model for passive diffusion used in the pharmaceutical industry.[15,52] These compounds undermined the long-standing belief that peptides were not able to cross the BBB in significant amounts and could transport a variety of small molecules. More recently, we have applied diketopiperazines in combination with a redox chemical delivery system to enhance the transport of prolyl oligopeptidase inhibitors across PAMPA and a cell-based model.[238]

Despite the achievements described above, the applicability of passive diffusion peptide BBB-shuttles is limited by solubility issues and the non-negligible impact of the cargo on the efficiency of the shuttle and vice versa. On the side of the BBB transport capacity, this problem can be overcome by fine-tuning the peptide for each particular cargo, including hydrophobicity, hydrogen bond donors/acceptors, length of sequence and also other factors such as flexibility, halogenation and stereochemsitry.[32] In order to decrease the effect of the construct on the activity of the molecule, linkers that can be cleaved inside the brain parenchyma could be incorporated. However, further work in this direction is required to extend the use of these shuttles.

Outlook and opportunities

Undoubtedly the BBB remains a formidable obstacle, and yet since William M. Pardridge described the Trojan horse concept in 1986, the field of drug delivery to the brain has made a remarkable progress. In the last few years, a plethora of new BBB-shuttle peptides and also improved antibody fragments have emerged and hold great promise to overcome the limitations of the first generation of large shuttles. Peptides are more economical, easier to characterize and to link to nanocarriers or proteins and have lower immunogenicity. Furthermore, many do not compete with the endogenous substrate and do not stay bound to the receptor as it happens with some antibodies.

BBB-shuttle peptides have so far provided promising results in terms of brain delivery and also in therapy. These shuttles range from those transported through LRP1, such as Angiopep-2 and ApoE fragments, to others that use less exploited routes like RVG29, glutathione or TGN. Peptide alternatives to the classical anti-TfR antibodies, such as THR and CRT, have also proven capable of translocating challenging cargoes. However, most studies have focussed on NPs loaded with small molecules and DNA, while there is a growing need to improve brain delivery of therapeutic proteins such as antibodies to treat brain cancers.

Moreover, despite the important achievements described, new shuttles with higher transport capacity and selectivity are required. Therefore, exploiting combinatorial approaches like phage display and natural sources of peptides reaching the CNS offers an excellent opportunity to explore the multitude of incipiently characterized or still unknown pathways that may allow enhanced delivery.

Certainly one of the limitations of most peptide shuttles is their low metabolic stability. We, among others, have recently shown that increasing the protease-resistance of these constructs can lead to a significant enhancement in brain delivery. The new generation of peptide shuttles should therefore aim to enhance transport efficiency by increasing metabolic stability and also by improving selectivity for the brain through new and more efficient transcytotic pathways.

OBJECTIVES

1) The first goal of this thesis was to find a new peptide shuttle with high resistance to serum proteases and capable of transporting large cargoes such as proteins and NPs across the BBB.

In order to accomplish the first objective, the following secondary aims were established:

1. To study whether new non-toxic and intrinsically protease-resistant BBB-shuttle peptides can be derived from venoms.

2. To minimize the length and the complexity of the peptide found in order to make it more synthetically accessible while preserving protease-resistance.

3. To assess the immunogenicity and toxicity of the most promising analogues with respect to the native peptide.

4. To verify that the shuttle candidate is able to carry large cargoes across a cell-based BBB model.

5. To study whether the shuttle is capable of delivering a cargo *in vivo*.

2) The second goal of this thesis was the application of BBB-shuttles to increase the transport of antibodies as challenging and therapeutically relevant cargoes for the treatment of glioblastoma.

The following secondary aims were proposed to reach the second objective:

1. To set up suitable methods for the conjugation of BBB-shuttle peptides to antibodies.

2. To assess the stability of the linkage in serum.

3. To verify that the antibody remains functional upon the conjugation of BBB-shuttles.

4. To study the permeability of antibody-shuttle constructs in a cell-based BBB model.

RESULTS
AND DISCUSSION

This chapter is partly based on the following articles and patent:

Oller-Salvia, B.; Sánchez-Navarro, M.; Ciudad, S.; Guiu, S.; Arranz-Gibert, P.; Garcia, C.; Gomis, R.; Cecchelli, R.; Garcia, J.; Giralt, E.; Teixidó, M. MiniAp-4: a venom-inspired peptidomimetic for brain delivery. *In preparation.*

Prades, R.; Oller-Salvia, B.; Schwarzmaier, M. S.; Selva, J.; Moros, M.; Balbi, M.; Grazú, V.; de la Fuente, J. M.; Egea, G.; Plesnila, N.; Teixidó, M.; Giralt, E. Jumping hurdles: revisiting the retro-enantio approach to obtain a peptdie able to overcome the blood-brain barrier. *Angewandte Chemie International Edition.* **2015**, *54*, 3967-3972.

E. Giralt; M. Teixidó; B. Oller. Actively transported and protease-resistant peptides as BBB shuttles and shuttle-cargo constructs. WO 2015/001015 A1. Universitat de Barcelona & IRB Barcelona.

Oller-Salvia, B.; Teixidó, M.; Giralt, E. From venoms to BBB shuttles. Synthesis and blood-brain barrier transport assessment of apamin and a non-toxic analog. *Biopolymers-Peptide Science.* **2013**, *100*, 675-686. (Front cover picture)

Mini-apamins
as new BBB-shuttles

Venoms have evolved to attain high affinity and selectivity for a wide range of biological targets. However, this potential remained almost unexploited until the recent miniaturization of bioassays and the development of high-throughput techniques, which have boosted the number of studies in this field and renewed interest in these products in drug discovery programs.[239]

One of the most relevant properties of many venoms is their effect on the CNS. However, most of these substances reach the brain through the bloodstream subsequent to inflammation of the BBB, which facilitates unspecific paracellular diffusion. To date, only a small number of known venom components are suspected to penetrate the BBB without disrupting brain endothelium.[240] However, it is estimated that there are several hundred thousand constituents, including many neurotoxic molecules, about which little is yet known.[241] Moreover, many of these compounds are disulfide-rich peptides with high resistance to proteases. Hence, studying the venoms that have been reported to affect the CNS appears as a novel and promising approach to find new BBB-shuttles.

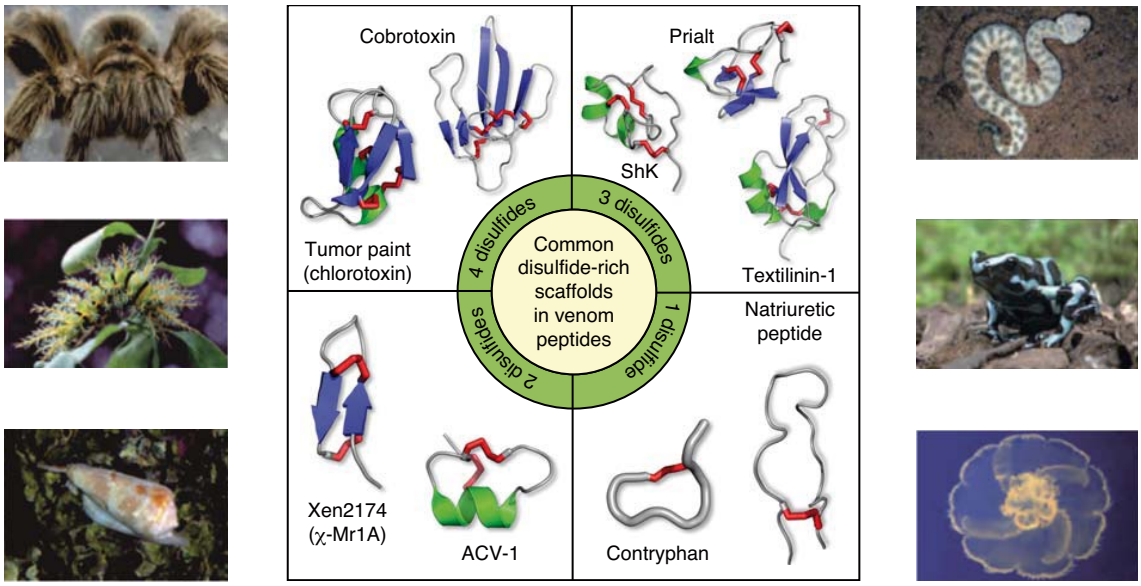

Figure 8. *Representative cysteine-rich peptides in venoms classified by the number of disulfide bridges and surrounded by diverse poisonous animals. (Modified from King et al. 2011)*[239]

Many peptidic animal toxins have been detected in the brain but very few in such amounts that would allow their use as therapeutics or BBB-shuttles.[240] Among the ones claimed to cross the BBB substantially are two peptides derived from 3-finger snake toxins, candoxin and *Ophiophagus hannah* toxin b,[170,171] chlorotoxin[242] and apamin (*Figure 9*).[243] Chlorotoxin and peptides from 3-finger toxins have been described to increase intracranial delivery of micelles into mice bearing brain tumours but it is not known if they are able to cross an intact BBB.[108,170,171,244] For apamin, data about BBB passage was also not conclusive. However, we decided to

focus on the latter because it was smaller than the other toxins (18 vs 36, 66 and 73 residues) and had not yet been used as a shuttle when our project was started.

Apamin accounts for 2 % of bee (*Apis mellifera)* venom dry weight[245] and was one of the first K^+ channel blockers to be described. Hence, it has long been used for their identification. It has high affinity for the small conductance Ca^{2+} -dependent K^+ channel KCa2.2 and binds more weakly to KCa2.1 and KCa2.3 of many species. These channels are mostly expressed in neuronal cells but KCa2.2 and KCa2.3 are also found in other tissues including vasculature.[246] Although biodistribution studies have been performed on mice, the permeability of BBB to apamin is controversial. While the accumulation of this peptide in the brain and spinal cord after intravenous injection has been demonstrated,[243] the selectivity for these organs is not well established[247] and there is no data on whether this peptide is able to cross the endothelium or just remains bound to it.

Although apamin, at low doses, has been described to be neuroprotective and to delay neuronal ageing through interaction with ion channels,[248] the therapeutic window is very narrow. In higher amounts it causes convulsions and its LD_{50} in mice is 2.5 μmol/kg when injected intravenously.[249] The neurotoxic effect of this peptide is clearly an undesirable characteristic for drug delivery purposes, thus its sequence should be altered. Some structure-function studies based on the modification of the natural peptide or the synthesis of analogues have shown that the residues responsible for toxicity are mainly Arg13 and Arg14 and Gln17.[247,249,250] Among the non-toxic analogues obtained, the one that is most similar to the original peptide was described by Cosand and Merrifield and bears two ornithine residues instead of arginines.[249] The slight shortening of these positively-charged side chains proved sufficient to reduce harmful effects below detectable limits. From now on, this analogue will be referred to as ApOO.

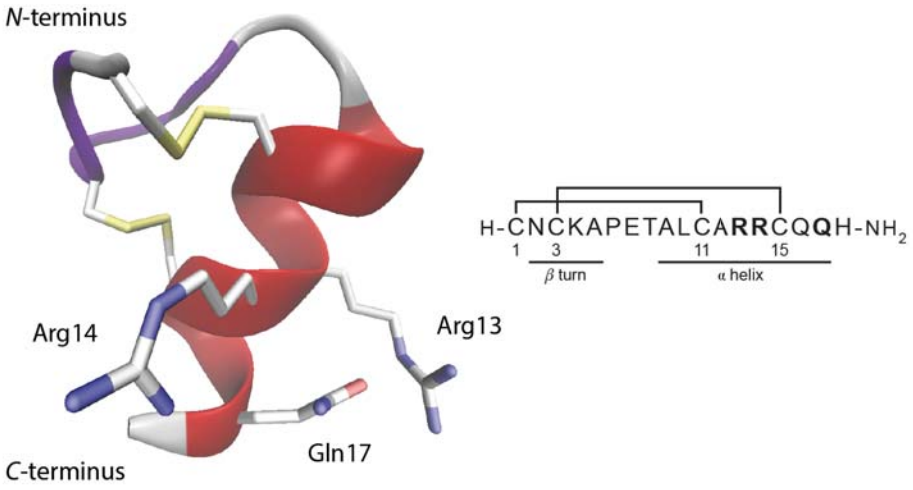

Figure 9. *A 3D representation of apamin highlighting Arg13, Arg14, and Gln17 and its sequence. This model is based on X-ray coordinates from PDB ID: 3IUX for a structural analogue of apamin.*

However, the interest of apamin lies not only in its biological activity but also in its characteristic structure. The shape of this peptide is defined by a β-turn at the *N*-terminus and an α-helix, which are tightly held together by two disulfide bridges. This feature has drawn the attention of numerous researchers, who have used apamin as a model for studies on disulfide bond formation,[251-256] NMR techniques[257-259] and peptide synthesis.[260,261] Furthermore, this compact structure confers very high stability in a wide range of pH values and temperatures.[254,262] Owing to these properties, apamin has been exploited as a structural template of an α-helix in at least three studies. Brazil and coworkers exchanged some of the residues on the helix for the sequence of interest to study the recognition of chaperons,[262] Weston and collaborators took advantage of this scaffold to obtain a highly resistant miniature protein with oxaloacetate decarboxylase activity,[263] while Li *et al.* designed p53 peptide activators based on this structure.[264]

In this chapter we will first show that apamin and a non-toxic analogue appear to be transported by an active mechanism in a bovine cell-based BBB model; we thus proposed that they could be used as BBB-shuttles.[265] One year after we published these results, Wu *et al.*[77] proved that the native apamin was indeed able to target streptavidin and a polymeric micelle to the brain and spinal cord in mice. They showed that when conjugated to large nanocarriers the toxicity of apamin was decreased to a level that allowed the delivery of therapeutic amounts of drug. Meanwhile we had chosen a different approach, which was to develop simplified analogues. Our target was not only to reduce toxicity regardless of the cargo but also immunogenicity because apamin had been described to be a very good immunogen *per se*,[266,267] which could be a problem for repeated administration of the targeted therapeutic. We also envisaged reducing the length and the structural complexity of these analogues while retaining protease-resistance and BBB-transport capacity. From now on we will refer to these peptides as mini-apamins (MiniAps).

Considerations on the cell-based BBB models used

In this thesis we were mainly interested in optimizing and studying BBB-shuttle peptides that are able to delivery large cargoes selectively to the brain. Therefore, we needed a model that allowed a reasonable throughput and that was also suitable for studying active transport. We found that cell-based BBB models satisfied these two criteria to a reasonable extent and, thus, used them as the main tools for screening.

We initially used a kit commercialized by Cellial Technologies® based on a monolayer of bovine endothelial cells seeded on Transwell® inserts and treated with astrocyte conditioned medium. This model, being recently developed in Prof. Roméo Cecchelli's laboratory, which has extensive expertise in the field,[60] was relatively high throughput (24-well plates) and required only 4 days of culture. Moreover, the permeability of a variety of compounds had a reasonable correlation with *in vivo* data ($R^2 = 0.8$).[268] In order to become familiarized with its handling, I stayed in Cellial's headquarters in Lens (France) for a short training. Unfortunately, this company stopped its activity in November 2012 and we had to look for an alternative.

Before using the model from Cellial Technologies®, Dr. Roger Prades, during his thesis, set up a more complex BBB-model based on a co-culture of bovine brain endothelial cells and rat astrocytes in our laboratory. The protocol was based on the one developed by Dr. Peter J. Gaillard and Prof. Alabertus G. de Boer.[269] Although in our hands this model was considerably less robust and more labour-intensive than Cellial's, it had also been shown to express functional receptors and had a higher TEER (> 120 $\Omega \cdot cm^2$). Thus, in order to continue our screening we decided to go back to this model. Setting it up again took several months because of diverse circumstances such as high batch-to-batch variability in primary bovine endothelial cells and the discontinued production of the Lonza's endothelial cell growth medium. Fortunately, Dr. Roger Prades and Dr. Bernat Guixer's help, together with the experience I had acquired at MIT working on BBB-models, were very valuable to obtain eventually excellent TEER values (> 150 $\Omega \cdot cm^2$) and Lucifer yellow permeability.

Despite managing to set up the bovine cell-based model again in the laboratory, we still had problems of reproducibility for compounds with active transport mechanisms. Therefore, we contacted Prof. Roméo Cecchelli in order to use another model that they had very recently developed based on human endothelial cells developed from induced-pluripotent stem cells.[59] This opportunity looked extremely promising to study actively transported shuttles because we would not have to be concerned about interspecies differences of receptors. Moreover, this model had a remarkable correlation with *in vivo* data, was extremely robust and required significantly less time than the bovine one (*Figure 10*). Therefore, I went back to

Lens for a 1-week training on its handling. Taking advantage of the change of model we also introduced shaking, which has a significant effect on permeability of hydrophobic compounds because it minimizes the thickness of the aqueous boundary layer (or unstirred water layer) on the cell surface.[270] In this regard, it was very important to find an orbital shaker that did not heat up excessively during the 2-h assay and use insulators under the plates in order to keep temperature between 37 and 38ºC. Moreover, the radius of the orbit was also important for the shaking, as it had to be similar to that of the inserts to be effective.

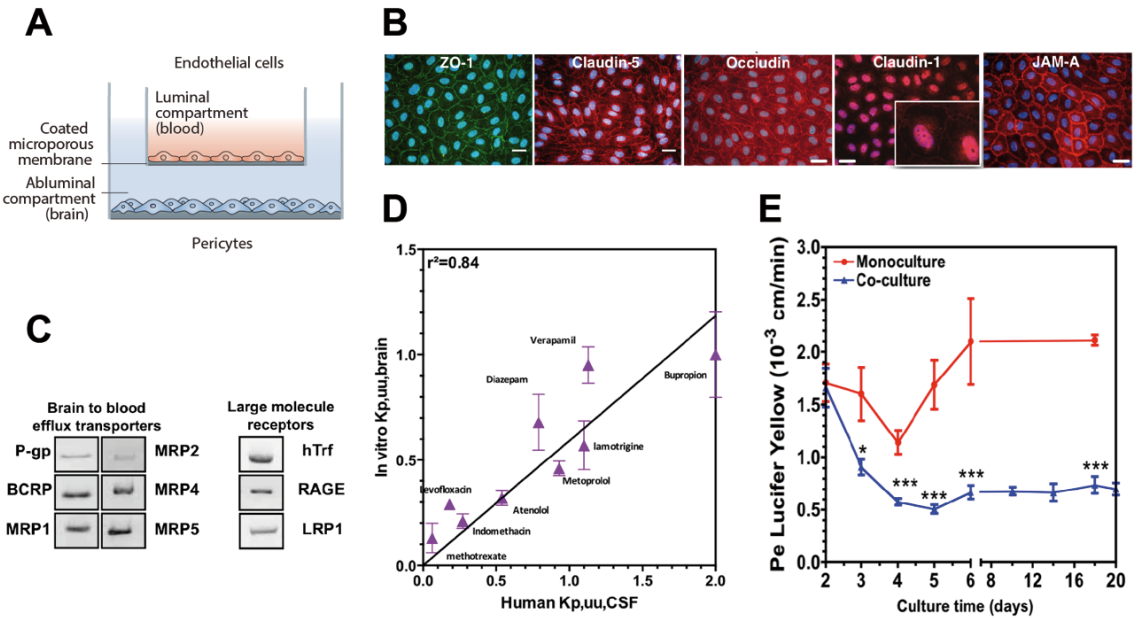

Figure 10. *Main features of the human model developed in Prof. Cecchelli's laboratory A) Scheme of the model B) Immunostaining of the most relevant proteins forming TJ. C) Western blot showing the presence of several relevant receptors. D) Correlation with in vivo data E) Relevance of the co-culture to achieve low and stable LY permeability. (Modified from Cecchelli et al. 2007 [60] and Cecchelli et al. 2014 [59])*

In order to maintain certain coherence, the models were introduced at key points during the shuttle development process and some peptides were evaluated in more than one set-up as a control. Because comparisons of absolute permeability values between models may be misleading, we will express most results in permeability ratios, such as analogues with respect to the parent peptide or cargo-BBB-shuttle constructs with respect to the naked cargo.

Exploring the suitability of non-toxic derivatives of apamin as BBB-shuttles

Synthesis and characterization of apamin and a less toxic analogue

In order to study the BBB transport of apamin, we first synthesized this peptide using Fmoc/*t*Bu solid-phase peptide synthesis followed by cyclization in solution. Three possible disulfide bond pairings can be obtained upon full oxidation of a peptide with four cysteines, namely *beads*, *globule* and *ribbon* (*Figure 11*).[253,255]

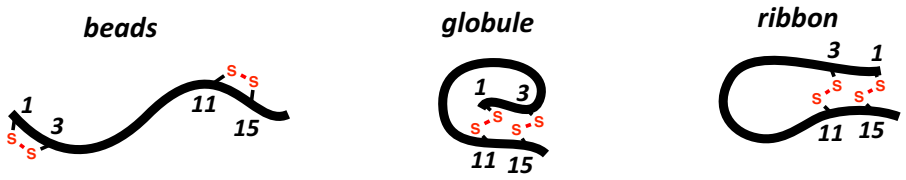

Figure 11. *The 3 possible disulfide bond regioisomers that can be formed upon oxidation of 4 cysteines.*

Although it is usually assumed that the major isomer of apamin generated under the described oxidation conditions is the *globule* one, the disulfide bond connectivity was verified by co-elution with a natural standard and by NMR. Dr. Michael Goldflam acquired the spectra in a 600 MHz NMR machine and later I performed the assignment.

The high similarity of the chemical shifts obtained in the TOCSY experiment with those reported by Fiori *et al.* indicated that the desired isomer had been obtained. Only α protons of Asn2 and Glu7 were slightly downfield. These protons are the most sensitive to pH in this structure as shown by Glushka *et al.*[259]. According to the data provided in their study, the shift we observed showed that the real pH in our experiment was closer to 3 than to 2.5 used by Fiori and coworkers, whose publication we used as a reference. Furthermore, stronger evidence of the disulfide bond connectivity was provided by the through-space couplings between the α proton in Cys3 and the α and β protons of Cys15 in a NOESY experiment (*Figure 12*).

The ApOO analogue was first synthesized like apamin with all cysteine residues protected by trityl groups, which were later removed during the cleavage using TFA; therefore, cyclization was performed in a single step in buffered aqueous solution. Cosand and Merrifield alleged to have obtained this peptide under similar conditions with the same folding as apamin because it acquired a very similar toxicity after guanidination of the ornithine residues. To further prove their assertion, we synthesized the same analogue using a two-step regioselective oxidative cyclization based on the acetamidomethyl group (*Figure 13*).

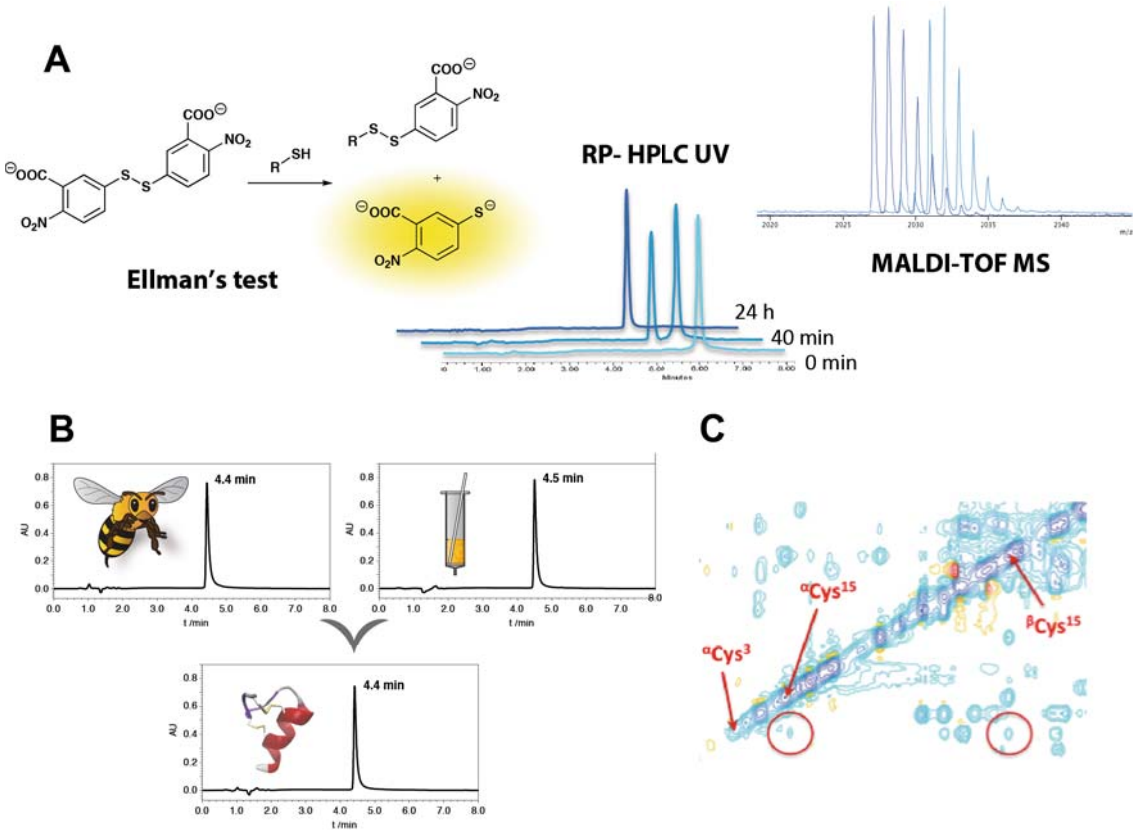

Figure 12. *The folding of apamin. A) Monitoring the cyclization using Ellman's reagent, RP-HPLC and MALDI-TOF MS. B) Coelution of the synthesized peptide with a natural standard. Chromatograms were obtained in an 8-min linear gradient from 5 to 20 % of MeCN with (0.036 % TFA) in H_2O (0.045 % TFA). C) NOESY spectrum in which the through-space couplings between cysteines are highlighted.*

ApOO was also obtained with Cys1 and Cys11 protected by the acetamidomethyl (Acm) group at a 25-μmol scale. As this protecting group is orthogonal to cleavage with TFA, the sequence was amenable to cyclization in two steps, the first in buffered aqueous solution and the second by removal of the Acm groups with iodine in an acidic medium. Acm removal under these conditions minimizes scrambling of the preformed disulfide bridges,[271] thereby allowing the regioselective formation of the second disulfide bond.

The products of both syntheses co-eluted in an 8-min linear gradient from 5 to 15 % of MeCN (0.036 % TFA) in H_2O (0.045 % TFA), indicating that the isomers obtained were indeed the same. The confirmation of the correspondence between apamin and ApOO disulfide bond pairings implies that the difference in toxicity and any other biological activity can be attributed only to the distinct properties of ornithine and arginine side chains.

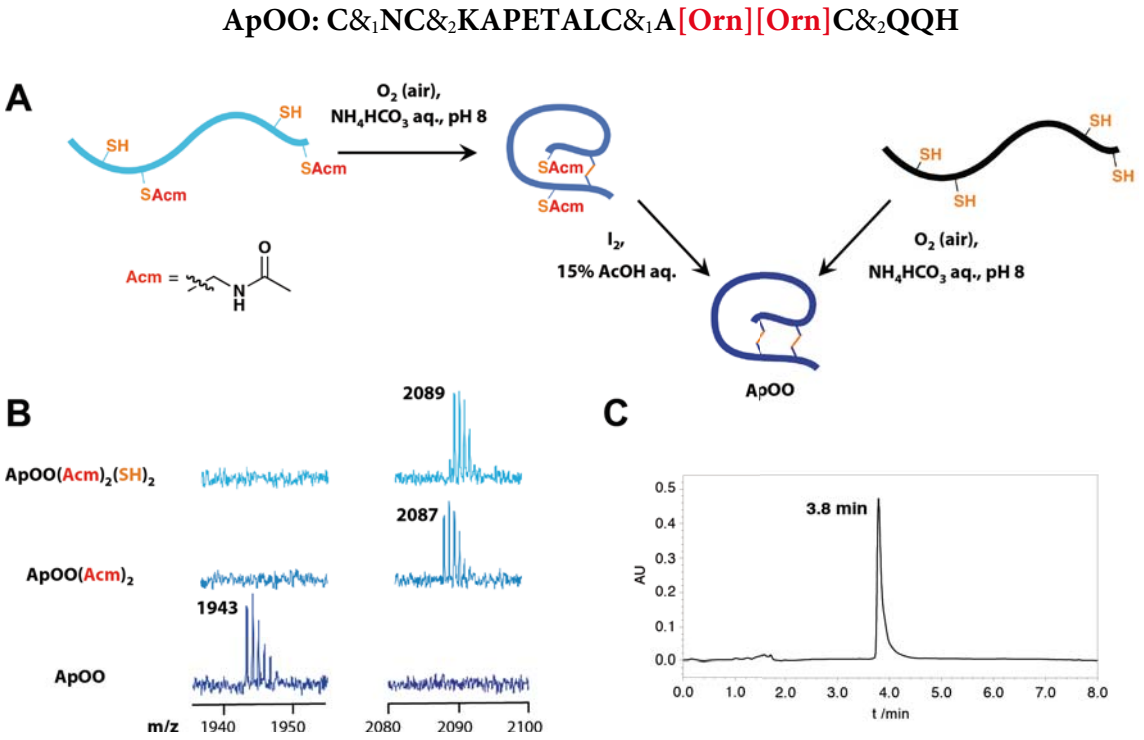

Figure 13. *Synthesis of ApOO A) Scheme of regioselective vs. free disulfide bridge formation. B) MALDI-TOF MS of intermediates. C) Coelution of peptides synthesized using both syntheses. The chromatogram was obtained in an 8-min linear gradient from 5 to 15 % of MeCN (0.036 % TFA) in H_2O (0.045 % TFA).*

Assessment of the permeability of apamin and ApOO in BBB models

It had been reported that the natural peptide and this analogue differ greatly in toxicity. However, the effect of the sequence alteration on the capacity of these peptides to cross the BBB had not yet been assessed. It was thus unknown whether the decrease in toxicity of ApOO was due to a lower affinity for the K^+ channel or because of its inability to reach the brain. In order to address this issue, we first compared the permeability of apamin and ApOO in a cell-based BBB model.

The cell-based BBB model

The BBB-model used for this initial study was the one commercialized by Cellial Technologies®. The permeability in the BBB cell-based model was calculated integrating the peaks at 220 nm obtained in the chromatograms from the HPLC-UV and using *Equation 1*. Apparent permeability (P_{app}) values are preferred to transport percentages because they express the amount of compound that has reached the acceptor compartment per unit of time and area, corrected by the concentration initially introduced in the donor filter. Thus, only when values are obtained under the same conditions transport is proportional to Papp. In addition to the quantification, the presence and the integrity of the peptides in all acceptor wells were confirmed by MALDI-TOF MS.

$$P_{app} = \frac{d\,Q_A(t)}{d\,t} \cdot \frac{1}{A} \cdot \frac{V_D}{Q_D(t_0)} \qquad \textbf{Equation 1}$$

where P_{app} is obtained in cm/s, t is the length of the assay in seconds, A is the area of the membrane in cm, V_D is the volume in the donor well, $Q_A(t)$ is the amount of compound at time t in the acceptor wells, $Q_D(t_0)$ is the amount of compound at the beginning of the experiment in the donor wells.

Surprisingly, this first assay in the BBB cell-based model revealed that the permeability of apamin ($1.7 \pm 0.1 \cdot 10^{-6}$ cm/s) was very similar to that of ApOO ($1.6 \pm 0.2 \cdot 10^{-6}$ cm/s). Therefore, the replacement of arginine residues by ornithines decreased the toxicity but did not alter the transport. This result indicates that the residues most relevant for toxicity are not involved in the transcytosis of apamin across the BBB, which was the first step to produce non-toxic BBB-shuttles.

In addition, the permeability values obtained were promising as they were of the same order of magnitude as other BBB-shuttles previously reported. Prades *et al.* described a peptide shuttle with a permeability of $3.9 \pm 1.2 \cdot 10^{-6}$ cm/s able to carry another peptide and even gold NPs.[63] Aprotinin, on which Angiopep vectors were based, also has a similar transport ($4.4 \cdot 10^{-6}$ cm/s) in Cellial's model. Moreover, the permeability of apamin and ApOO is superior to that of Tf ($9.5 \cdot 10^{-8}$ cm/s), which is the endogenous ligand for one of the receptors with highest overexpression in brain capillary endothelial cells.[272]

A P_{app} of $1.7 \cdot 10^{-6}$ cm/s corresponds to a transport of 2.2 % in this assay conditions, i.e. 2.2 % of the compound initially introduced in the donor compartment was in the acceptor compartment at the end of the experiment (*Table 2*). Maximal transport of any compound at equilibrium would correspond to 80 % of the initial amount because the acceptor compartment volume is 4 times larger than that of the donor. Transport is always lower than this maximal value even in the absence of cells because of the presence of the coated polycarbonate filter. This filter and its coating are generally assumed to mimic the basal lamina surrounding the capillary, which also has a certain barrier effect. However, because the composition of the coating (in this case collagen type IV) and the basal lamina is not the same, it is also interesting to quantify its effect on transport without cells, especially for very hydrophobic compounds. Although apamin and ApOO are very hydrophilic we also measured this value to verify that the translocation was essentially limited by endothelial cells. As expected, we obtained a very high transport through the filter alone (40-43 %), which indicates that it did not contribute significantly in decreasing the passage of peptides and therefore endothelial permeability (P_e) was essentially the same as P_{app}.

Table 2. *Permeability of apamin and ApOO in the bovine cell-based BBB model. Data represent mean values ± SEM (n = 3).*

	apamin	**ApOO**
P_{app} ($\cdot 10^{-6}$), cm/s	1.7 ± 0.1	1.6 ± 0.2
P_e ($\cdot 10^{-6}$), cm/s	1.8 ± 0.1	1.7 ± 0.2
Transport, %	2.2 ± 0.1	2.1 ± 0.2

Regarding the mass balance for the filters without cells, the peptides present in the donor and acceptor wells accounted for over 99 % of the amount assayed. Hence, no peptide was adsorbed on the polycarbonate membrane coated with matrix proteins. The same calculation for the plate with cells showed that there had been no accumulation inside the cells or on their membranes and that no degradation had taken place.

It should be noted that the highest permeability value for the internal control (Lucifer yellow) in wells containing peptides was $7.7 \pm 0.6 \cdot 10^{-6}$ cm/s; the result being similar to the wells containing only this control ($6.6 \pm 0.4 \cdot 10^{-6}$ cm/s) and lower than the threshold value associated with BBB leakage ($17 \cdot 10^{-6}$ cm/s).[268] Therefore, apamin had no effect on the tight junctions between endothelial cells.

The BBB-PAMPA model

We aimed to find BBB-shuttles capable of carrying large cargoes, which implied translocation using vesicular mechanisms. Already the relatively high molecular weight of these peptides (2 kDa), their high solubility in water (> 10 mM) and the slightly positive charge at physiological pH (+ 2-3) made an active vesicular transport mechanism more likely than passive diffusion. However, in order to have some experimental evidence we assayed them in PAMPA.

Apamin and ApOO were assayed at a 400 μM concentration and they were not detected by HPLC-UV in any acceptor well. The solutions of acceptor wells were also analysed by MALDI-TOF MS, which revealed the presence of barely detectable amounts of apamin in one replicate. The difference in concentration of peptides in the donor wells at time 0 and after 4 h was below 1 % for both peptides, indicating that they were not retained in the membrane. Propranolol was used as a positive control and had an average permeability ($2.0 \pm 0.4 \cdot 10^{-5}$ cm/s) near the reported values ($1.6 \pm 0.4 \cdot 10^{-5}$ cm/s),[33-35] which ensured the correct functioning of the assay. These results confirmed that the main transport mechanism of these peptides was not passive diffusion.

The Caco-2 model

There are many peptides capable of translocating cargoes across cell membranes and even the BBB. However, only a few achieve some degree of selectivity for the brain without increasing uptake in other tissues. In order to have a first hint of whether apamin and ApOO were selectively translocated across brain endothelial cells, Dr. Roger Prades assayed them among other compounds in a 96-well Caco-2 epithelial cell-based model.

It is noteworthy that apamin and ApOO were not detected by HPLC-UV (220 nm) in acceptor wells. Detection limit of this technique in our hands indicated that apparent permeability should be lower than 10^{-7} cm/s. Using MALDI-TOF MS, no peak corresponding to the peptides was detected either. Despite the Caco-2 model has a higher TEER (trans-endothelial/epithelial electrical resistance) than the BBB cell-based model, if we assume the contribution of the transcellular pathway to be negligible, this result suggests that transcytosis is more favoured in brain endothelium than in epithelial cells.

Serum stability of apamin and ApOO

One of the main reasons we chose venoms as a source of shuttles was that they contained many protease-resistant peptides that could eventually outperform the labile shuttles currently available. In this sense, apamin had a globular structure tightly bound by two disulfide bridges that should provide a long endurance in serum by analogy to other cysteine-rich peptides. However, the exact lifetime had to be studied because, to our knowledge, the stability of this peptide to proteases had not yet been determined.

Therefore, we incubated apamin and ApOO with 90 % human serum at 37 ºC for 24 h and aliquots were taken at different time-points. Proteins were immediately precipitated with methanol (in which the peptides were fully soluble) and subsequently centrifuged. The supernatant was analysed by HPLC-UV (220 nm) and MALDI-TOF MS.

Remarkably, no degradation was appreciated at any time for neither of the two peptides. Moreover, the amount present in the sample, as determined by HPLC-UV, remained constant throughout the 24-hour incubation (***Figure 14***). The half-life obtained for THR (30 ± 5 min), an L-amino acid peptide used as a control, corresponded to that previously reported (30 min),[63] thereby proving that the serum was active and the assay conditions were appropriate. The peaks present in the initial chromatograms (0 h) that did not correspond to the main peptides were the same in all cases, thus they were attributable to non-precipitated impurities from the serum. These impurities appeared smaller in the control-peptide chromatograms because the absorption at 220 nm of THR is higher than that of apamin.

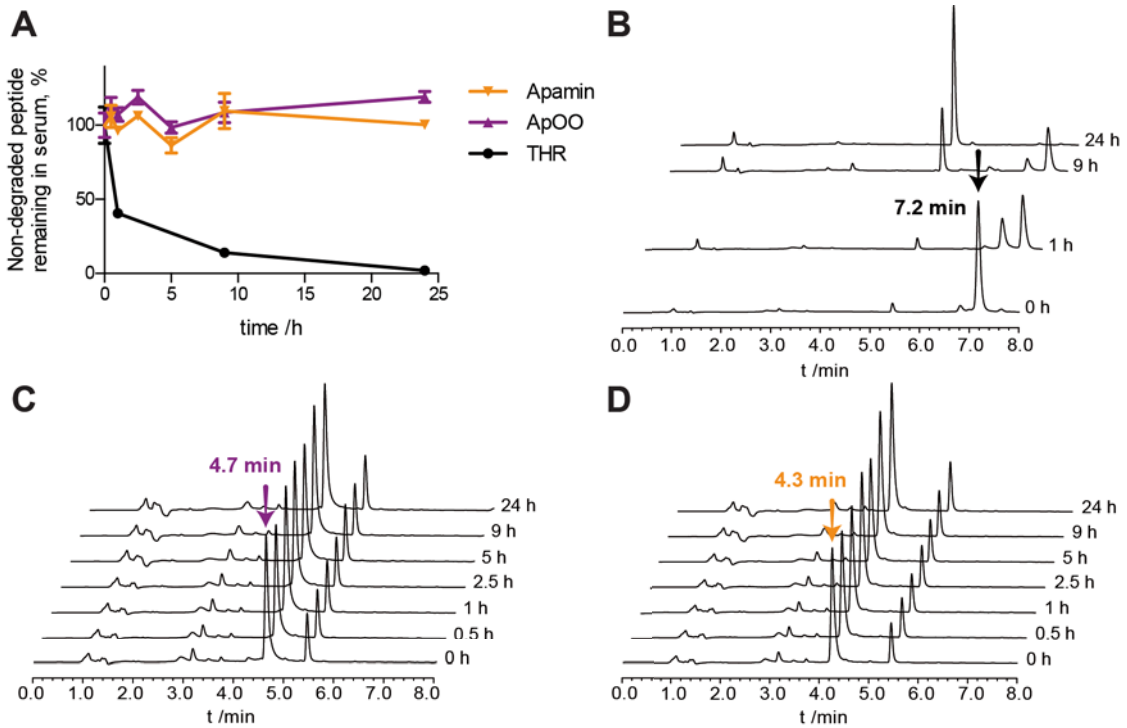

Figure 14. *Stability of apamin, ApOO, and control peptide in human serum. (A) Evolution of relative peptide concentration over time. Data represent mean values ± SEM (n = 3). Chromatograms at different time points are shown for (B) apamin, (C) ApOO, and (D) control peptide. All peptides were analyzed in an 8-min linear gradient from 0 to 40% of MeCN (0.036% TFA) in H_2O (0.045% TFA). The peaks corresponding to each peptide at time 0 h are marked with an arrow.*

Such high biostability was surprising for a peptide containing only natural amino acids even taking into account its cyclic nature. Unlike most of the shuttles currently available, including the CDX peptide from 3-finger snake venom, apamin and its analogue do not require the use of D-amino acids to achieve a half-life in serum over 24 h. The peptides here studied thus rival more highly knotted peptides such as chlorotoxin[273] and even cyclotides.[274] Moreover, an important advantage of apamin derivatives as potential BBB-shuttles is the relatively reduced length of their sequences and the presence of only 2 disulfide bridges instead of the 3 or 4 that characterize the aforementioned peptides.

Apamin non-toxic derivatives as BBB-shuttle candidates

The similar permeability obtained for apamin and ApOO in the BBB cell-based model implies that non-toxic analogues should be considered as BBB-shuttle candidates (*Figure 15*). Moreover, the values obtained are comparable to other potent shuttles described in the literature. Regarding the BBB translocation mechanism of these peptides, it is most probably due to an active mechanism given their high hydrophilicity and the undetectable passage in a model for passive-diffusion (PAMPA). In addition, their negligible permeability in a non-neural cell barrier model, together with their relatively overall charge (+ 2-3) that is

significantly lower than CPPs used for brain delivery (+ 5-8), make receptor-mediated transcytosis the most likely option. This hypothesis is in line with the work by Strong and coworkers, who observed that apamin could undergo endocytosis in liver cells and also provided evidence suggesting it was receptor-mediated.[275] Active translocation across the BBB with some degree of selectivity renders these molecules excellent BBB-shuttles candidates because they will very probably be able to carry large cargoes across this barrier. In addition, high resistance to serum proteases may increase their potency with respect to current BBB-shuttles *in vivo*.

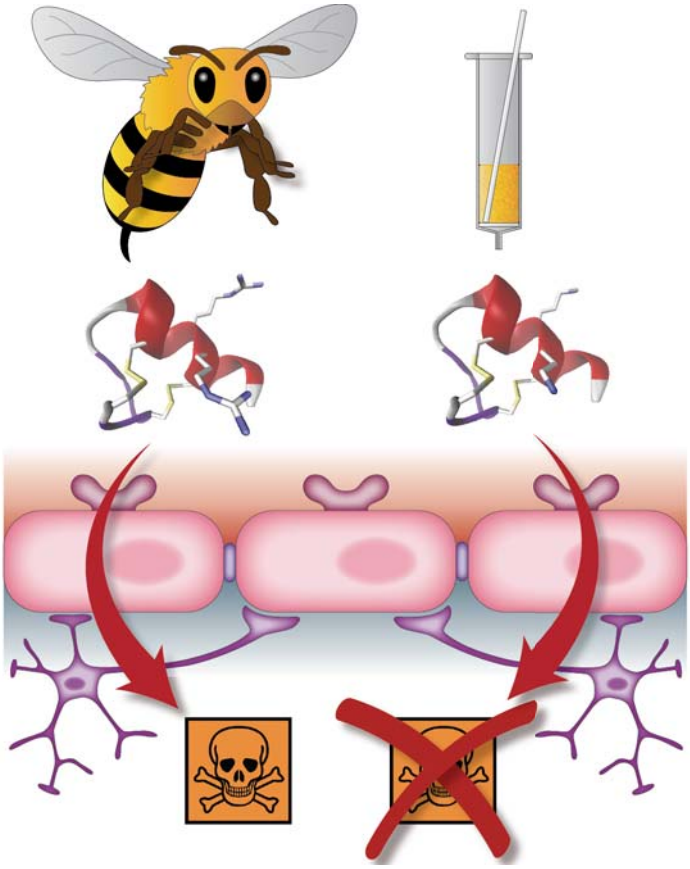

Figure 15. *Decrease in toxicity in apamin derivatives is not due to a minor transport across the BBB. (Selected as cover picture of Biopolymers.* ***2013****, 100)*

Development of new apamin analogues for brain delivery

MiniAp-1 as a proof of concept for the capacity of apamin derivatives to actively cross the BBB and to transport small cargoes.

After showing that non-toxic apamin analogues were interesting BBB-shuttle candidates, we aimed to explore if their structure could be further dissected to obtain more accessible and less immunogenic analogues. Therefore, we prepared a new derivative without the main residues implied in toxicity (MiniAp-1). Glutamines were removed and arginines were switched to alanines in order to avoid the positive charges without perturbing the α-helical folding.

Permeability across the BBB of MiniAp-1

MiniAp-1 and apamin were assayed in a cell-based BBB model of bovine endothelial cells in co-culture with rat astrocytes. The permeability of MiniAp-1 was surprisingly 60 % higher than that of the native peptide. Lucifer yellow was used as an integrity marker in all the assays and its permeability was always below the threshold established for a similar model.[268] Moreover, this internal control was not significantly different between the groups that were compared.

MiniAp-1 was sensibly more hydrophobic than apamin according to the hydrophilicity values calculated as suggested by Hopp and Woods:[276] 0.2 for MiniAp-1 and -0.2 for apamin (scale goes from -3.4 to 3.0). Therefore, in order to check if the increase in permeability was due to this change, the two peptides were assayed in PAMPA and none of them was detected by HPLC-UV to cross the lipid barrier despite the high concentration used (400 μM).

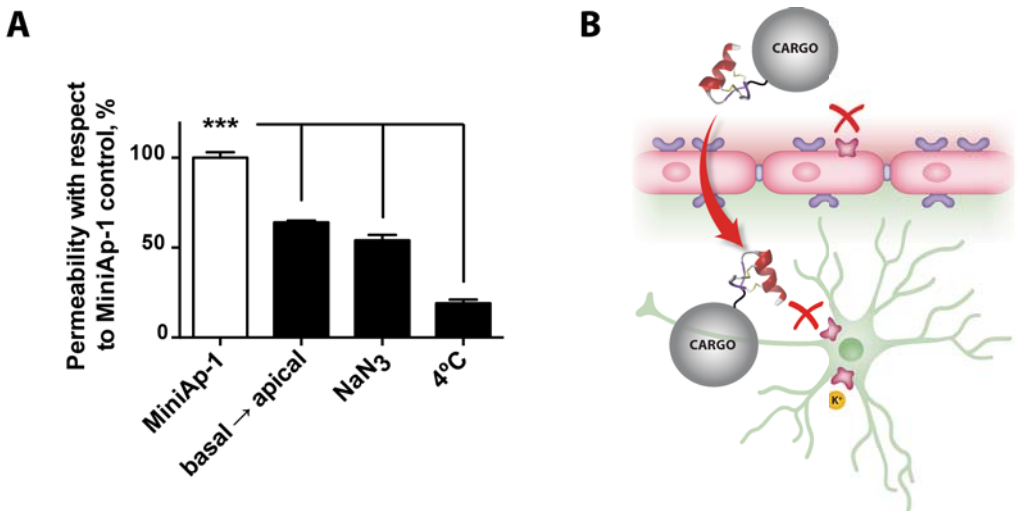

Figure 16. *Active transport of MiniAp-1. A) Effect of reverse transport, sodium azide and low temperature on the apparent permeability of MiniAp-1 in a bovine cell-based BBB model. Data represent mean values ± SEM (n = 3). *** P < 0.001 (t-test). B) Representation of the hypothesis that apamin non-toxic analogues do not interact with the potassium channel but are able to transport cargoes across the BBB through an active mechanism.*

Active transport of MiniAp-1 was verified by significant inhibition ($p < 0.001$) of transcytosis by temperature and using sodium azide (*Figure 16*). Moreover, its P_{app} was significantly higher from the apical side of the well to the basolateral than viceversa ($p < 0.001$), which indicated that the transport was polarized and that this peptide was not likely to be a substrate of an efflux transporter. Moreover, its permeability in a Caco-2 intestinal model was below the detection limit of this technique as described for apamin,[265] indicating a certain selectivity for brain endothelial cells as observed for apamin.

A possible hypothesis for the enhanced active transport is based on the lower affinity of MiniAp-1 for the ion channel that apamin blocks, which is also present in endothelium.[246] The weaker binding to the channel, would allow a higher amount of this peptide to interact with the putative receptor that mediates apamin endocytosis[275] and transcytosis[265] (in addition to providing a toxicity decrease) (*Figure 16*).

Transport of small cargoes

In order to check the capacity of MiniAp-1 to transport small cargoes, it was conjugated to levodopa, carboxyfluorescein (CFluorescein) and sulforhodamine B (SRhodamineB) through the *N*-terminus and to an amyloid *β*-sheet breaker peptide[277] through the *C*-terminus (*Figure 17*). MiniAp-1 was able to translocate these molecules in the cell-based BBB model without any significant decrease in permeability, further suggesting that apamin analogues were good BBB-shuttle candidates.

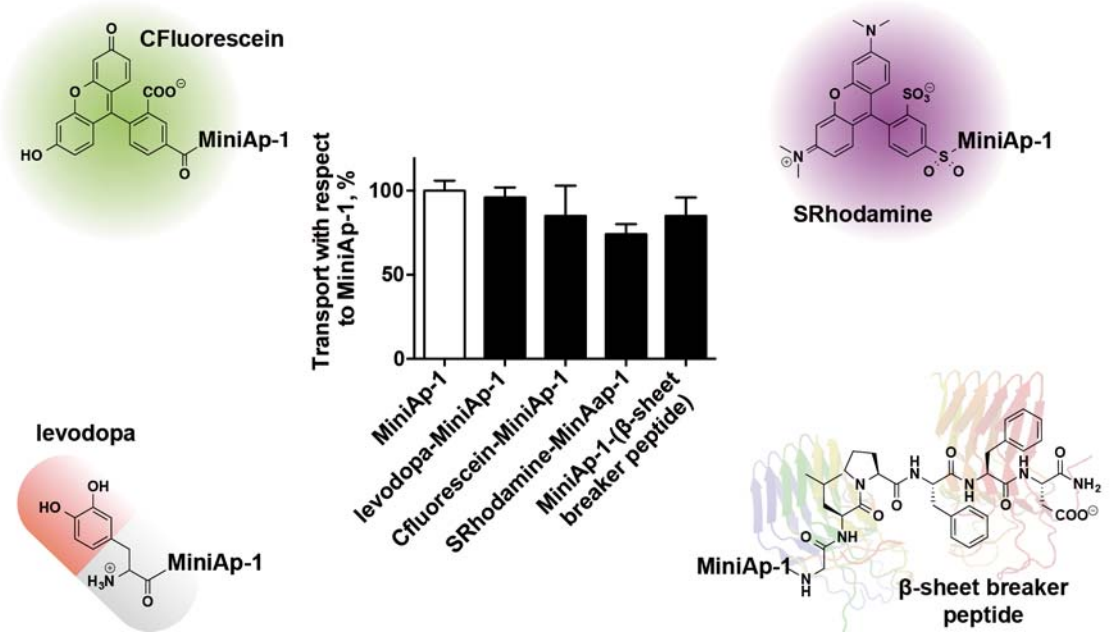

Figure 17. *Effect of the conjugation of small cargoes to MiniAp-1 permeability in the bovine cell-based BBB model. Data represent mean ± SEM (n = 3).*

Acute toxicity and teratogenicity assessment in zebra fish embryos

At this stage and taking into account that MiniAp-1 was a hit in our quest for shuttles, we looked for an affordable test to evaluate its toxicity and that could also be applied to several analogues that we intended to prepare. The noxious effect of apamin arises from the blockade of KCa2 channels but this compound does not appear to be cytotoxic to isolated neuronal cells.[247] Moreover, we had not detected any effect on the integrity of endothelial cell TJs in the 2-h transport assays. Therefore, a more complex model was required.

Zebrafish (*Danio rerio*) embryo appeared to be a suitable organism for this study because we aimed to minimize ethical issues, as well as to decrease the large peptide amounts and high costs of working with mice or other mammals. Working with embryos up to 5 days does not require a permission from ethics committee because they are not free feeding, thus the use of this model is consistent with the 3Rs rule (replacement, reduction and refinement) of animal experiments.[278] Although important differences in the exposure and pharmacokinetics may account for the low correlation between zebrafish and mammals of certain compounds,[279] this model has been shown to be useful to analyse drug toxicity in early drug discovery stages.[278,280,281] Moreover, fish embryos are a good alternative to adult fish for these tests although they are also sensitive to teratogenic substances.[282] Embryos allow a higher throughput and also they are static and transparent, enabling a simple and rapid inspection of internal organs. In addition, substances below 3 kDa easily permeate them, thus administration can be performed through absorption from the medium. Furthermore, apamin has been described to cause a 3-fold increase in the duration of neuronal periodic depolarizations in zebra fish. This effect was observed at 100 nM concentrations in the water.[283] Therefore, we expected that higher concentrations would lead to observable toxicity.

Experiments were performed by NeuronBio (Granada) following OECD guidelines for the fish embryo acute toxicity (FET) test.[284] Briefly, this test consisted in incubating zebrafish eggs, previously fertilized *in vitro*, with solutions containing the substances under study in a 24-well plate. After 24 and 48 h, eggs are visualized under a microscope to determine a variety of parameters ranging from malformations to heart rhythm and movement.

Apamin, ApOO and MiniAp-1 were assayed in this experiment at concentrations ranging from 2 to 50 μM. Surpisingly, no sign of toxicity was found for any of them, whereas parameters obtained from a positive control consisting of 3,4-dichloronaniline were in the expected range. Therefore, in the concentrations used, this model did not provide any information on whether the modifications on ApOO and MiniAp-1 decreased the toxicity of apamin. However, the lack of toxicity of MiniAp-1 also indicated that the modifications made did not confer any additional

acute toxicity or teratogenicity. Although we might have obtained some response at higher doses, an excessive amount of peptide was required (> 40 mg). Therefore, we decided to obtain additional analogues and test the most promising ones in mice.

Development of smaller shuttles with good protease-resistance and improved transport across the BBB.

MiniAp-1 was already more appealing as a BBB-shuttle than apamin because it was more permeable and was two residues shorter. Nevertheless, this analogue still presented a synthetic challenge for an extended use as a shuttle and for a potential large-scale production. Therefore, we took the risk to waive the bicyclic structure of the native peptide and synthesized simplified analogues based on the loop between Cys3 and Cys11: the linear sequence (MiniAp-2) and two monocyclic versions (MiniAp-3 and -4). MiniAp-3 was obtained by forming a disulfide bond between the *N*- and *C*-terminal cysteines, whereas MiniAp-4 was cyclized through a lactam bridge by exchanging the cysteine residues by diaminopropinate and aspartate residues (*Figure 18*).

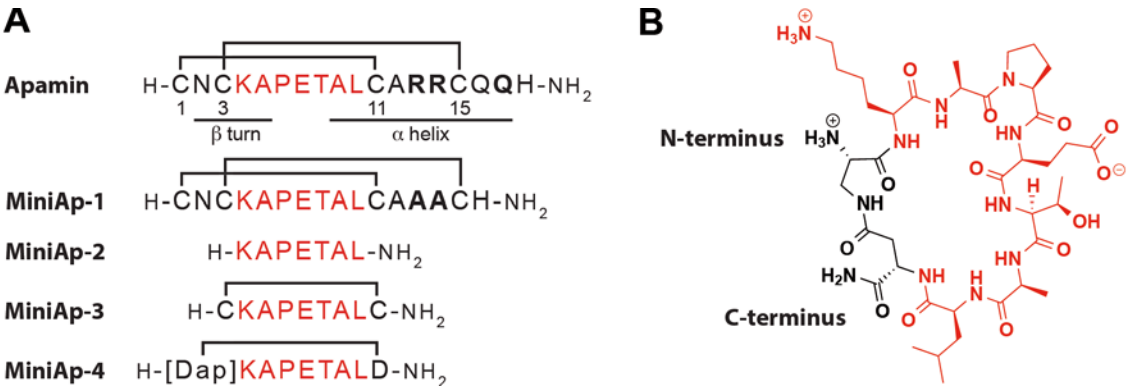

Figure 18. *Mini-apamin shuttle candidates. A) Sequences represented with one-letter code. B) Molecular structure of MiniAp-4.*

Cell-based model

Mini-apamins were assayed in the bovine cell-based BBB model. The disulfide analogue (MiniAp-3) had the same permeability as MiniAp-1 and that of the linear version (MiniAp-2) dropped to the level of the native peptide. Most surprisingly, the transport of the lactam derivative was 3-fold higher than that of apamin (*Figure 19*). In an attempt to find an explanation for these differences in permeability we studied the structure of the peptides by circular dichrosim and NMR and we evaluated their stability to serum proteases.

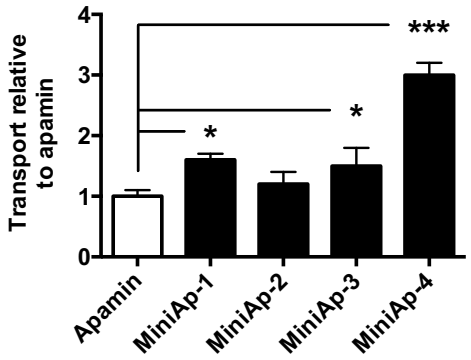

Figure 19. *Relative transport of mini-apamins in the bovine cell-based BBB model with respect to apamin. Data represent mean values ± SEM (n = 3). * P < 0.05, ** P < 0.01 (t-test).*

NMR and circular dichroism

The NMR study was performed by Sonia Ciudad under the supervision of Dr. Jesús Garcia. I acquired the circular dichroism spectra and we worked together for the interpretation of all the data.

Both circular dichroism and NMR spectra of all analogues were acquired under the same conditions as a previous study of wild type apamin.[255] The CD spectra of MiniAp-1 was practically identical to the one of apamin, displaying similar elipticity and a negative maximum at 208-209 nm indicating a predominance of an α-helical structure (*Figure 20*).

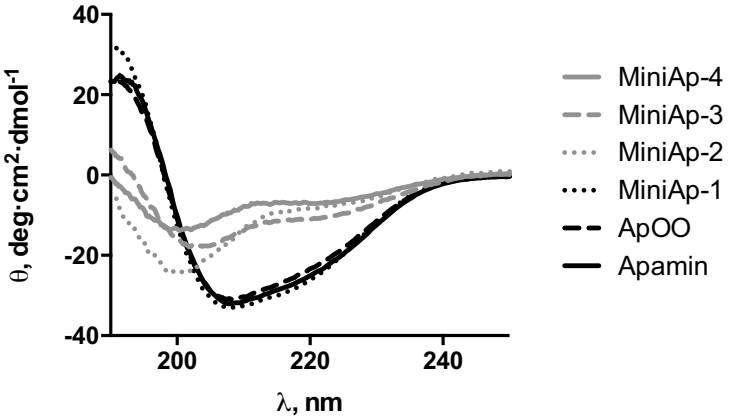

Figure 20. *Circular dichorism spectra of mini-apamins. Data represent the mean of 3 measurements.*

In the ^{1}H-NMR spectrum we detected two sets of signals with 90 % and 10 % relative populations corresponding to the *trans* and *cis* rotamers of the Ala5-Pro6 bond respectively. The *trans* conformer was confirmed to be the major species, as previously described for apamin and it was characterized by studying H_{α} and $^{13}C_{\alpha}$ secondary chemical shifts, temperature coefficients of NH amide protons and NOEs. The ^{1}H and ^{13}C chemical shifts and the NOE pattern, together with temperature coefficients and $^{3}J_{\alpha N}$ coupling constants, indicated that the conformation adopted by MiniAp-1 in solution was very similar to that described for the native peptide.

In order to obtain a three-dimensional structure of MiniAp-1, they performed a simulated annealing calculation including distance and dihedral angle constraints (described in the Material and methods section). *Figure 21* represents an overlay of the ten structures with lowest energy resulting from the calculation. The main features of MiniAp-1 structure are the same as those of apamin, i.e. an *N*-terminal loop (residues 1-8) and a *C*-terminal α-helix,[285] with a RMSD value of 0.72 Å for the backbone superposition of both structures. Only the loop orientation is slightly different and the *C*-terminal residue is less defined in MiniAp-1.

A

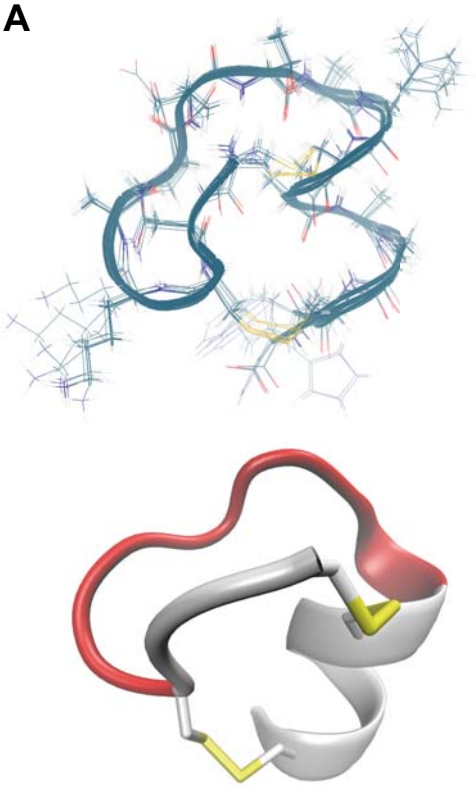

B

Restraints	
NOE	
Sequential ($\|i-j\| = 1$)	21
Medium range ($1 < \|i-j\| \leq 4$)	25
Long range ($\|i-j\| > 4$)	6
Dihedral angle restraints	
ϕ	8
ψ	8
Ramachandran Analysis	
Most favoured regions	12 (92.3%)
Additional allowed regions	1 (7.7%)
Generously allowed regions	0 (0%)
Disallowed regions	0 (0%)

Figure 21. *NMR structure of MiniAp-1. A) Top panel: Ensemble of the best 10 structures of MiniAp-1. RMSD values of 0.24 and 1.31 Å were calculated for the backbone and heavy atom superimposition respectively. Bottom panel: cartoon representation of MiniAp-1. The loop, on which MiniAps-2, -3 and -4 are based, is highlighted in red and the disulfide bonds are shown in yellow. B) Structural statistics for MiniAp-1. (Modelling performed by Dr. Jesús García)*

The CD spectrum of linear analogue MiniAp-2 was indicative of a random coil conformation. In agreement with this observation, MiniAp-2 did not show any evidence of α-helical formation by NMR. Notably, the NMR spectra of both MiniAp-3 and MiniAp-4 showed equally populated *cis* and *trans* conformers. The close resemblance of H_α and C_α chemical shifts, $^3J_{\alpha N}$ coupling constants and NH temperature coefficients between the *trans* conformers of both peptides on one side and between the *cis* conformers on the other side, suggested that the backbone conformation adopted by the two monocyclic peptides is very similar. The above-mentioned NMR parameters and the absence of non-sequential NOEs did not suggest a defined secondary structure for either the *cis* or the *trans* conformers of

both monocyclic derivatives. These results were also consistent with the CD spectra obtained for these analogues, which were very similar to that of the MiniAp-2.

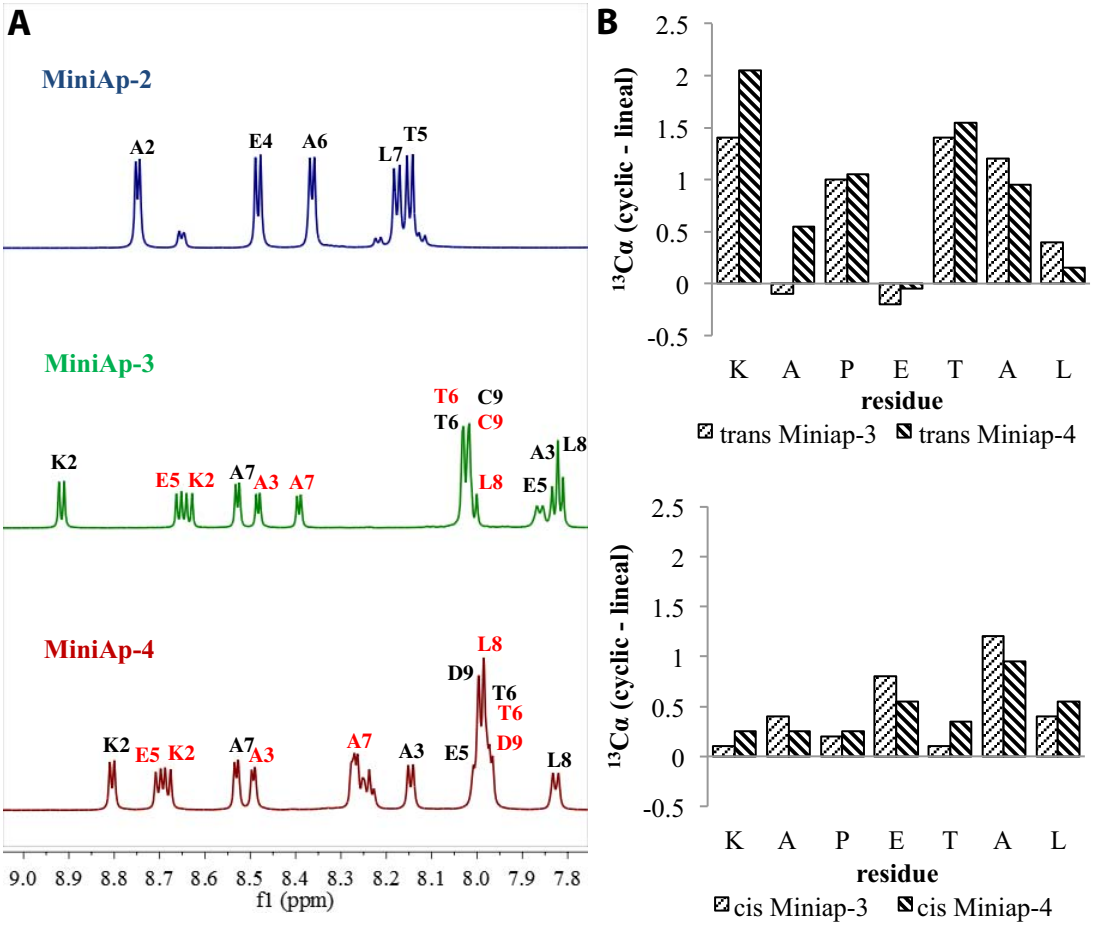

Figure 22. *Comparison of chemical proton and carbon chemical shifts in monocyclic and linear mini-apamines. A) Amide region of the ^{1}H-NMR spectra of MiniAp-2, MiniAp-3 and MiniAp-4. Amide resonances for the trans (black) or cis (red) conformers are labeled. B) Comparison of ^{13}Cα chemical shift values between MiniAp-2 and the trans (top) and cis (bottom) conformers of MiniAp-3 and MiniAp-4. (Figure made by Sonia Ciudad)*

However, when compared to the linear peptide, the *trans* conformers of both monocyclic derivatives showed significantly larger amide chemical shift dispersion (*Figure 22*), suggesting less conformational flexibility. Significant differences in $^{13}C_{\alpha}$ chemical shifts were also observed between each conformer of both monocyclic derivatives and the linear MiniAp-2 peptide, further suggesting that cyclization constrains the peptide (*Figure 22*). This lower flexibility together with the change in conformational preferences induced by the non-native cyclization in MiniAp-3 and -4 are most probably related to the permeability differences with respect to the bicyclic and the linear derivatives.

Serum stability

NMR revealed many differences between the bicyclic, the monocyclic and the linear analogues that could account for the variations in permeability. However,

MiniAp-3 and -4 were conformationally very similar and we made the hypothesis that the higher transport of the latter might be related to its higher resistance to proteases.

The stability in 90% human serum was evaluated for 24 h (*Figure 23*). It was qualitatively assessed by MALDI-TOF MS and quantitatively by HPLC-UV. The linear analogue was degraded with a half-life of 5-10 min, starting by the cleavage at the *C*-terminal lysine, Pro3, Asp4 or Thr5. By contrast, the disulfide derivative (MiniAp-3) showed remarkably improved stability, with a half-life up to 2.8 h but the lactam analogue (MiniAp-4) was even more stable as over 80% of intact peptide remained after 24 h. This surprisingly higher stability of MiniAp-4 was probably due to the fact that the lactam bond could not be reduced unlike the disulfide bridge, which could be opened to form conjugates with other molecules bearing free thiols such as cysteine, glutathione or albumin. This difference in the metabolic stability of the bond used for cyclization could certainly account for the higher permeability of MiniAp-4 with respect to MiniAp-3. Regarding MiniAp-1, it showed no degradation throughout the assay probably due to its bicyclic and tight structure as we had shown for apamin.

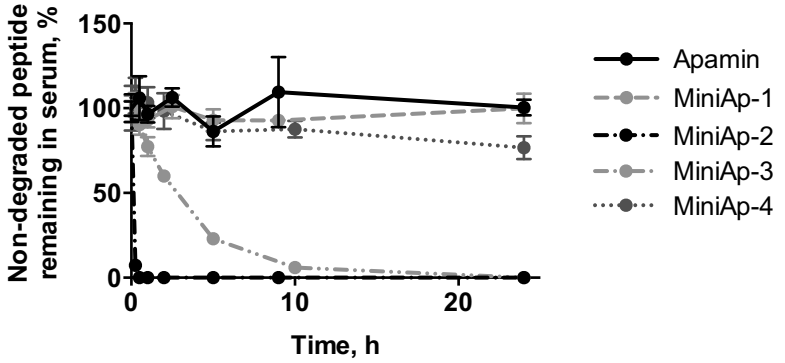

Figure 23. *Stability of mini-apamines in human serum at 37°C. Data represent mean values ± SD (n = 3).*

Cell viability assay

Although we had already concluded that the specific toxicity of apamin was difficult to assess in cell-based assays, we verified that none of the analogues had a clear cytotoxic effect. In order to assess viability we used the MTT reagent (3-(4,5-dimethylthiazol-2-yl(-2,5-diphenyltetrazolium)). This was the first metabolic dye used for this purpose and still has wide application because it is metabolized by most cell types and provides robust results. The MTT assay relies on the conversion of tetrazolium, which is a yellow water-soluble salt, into insoluble blue formazan crystals by reduction (*Figure 24*). This conversion takes place mainly in the cytoplasm but also in mitochondria and cell membrane.[286]

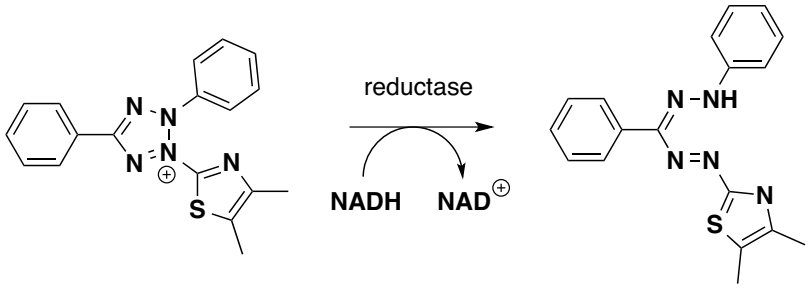

Figure 24. *Reduction of the tetrazolium salt MTT to formazan.*

With this test we confirmed that none of the analogues remarkably altered viability (*Figure 25*), as in all cases over 80 % of cells were alive after a 24-h incubation even at very high concentrations (500 μM). The only significant differences with respect to the non-treated cells were found for MiniAp-1 and MiniAp-2 at 500 μM in HeLa cells and MiniAp-1 at 200 μM in bEnd.3 ($p < 0.05$, t-test). However, there was no trend that indicated a clear decrease of viability with concentration in any case.

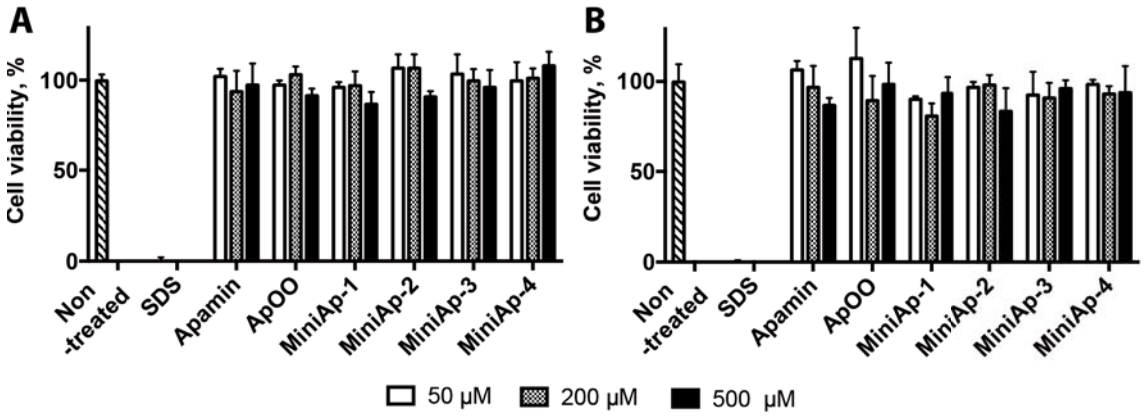

Figure 25. *Influence of mini-apamins in cell viability assessed by an MTT assay. A) HeLa B) bEnd.3.*

Acute toxicity in mice

The next step we faced was *in vivo* evaluation of toxicity and immunogenicity. Therefore, we needed to minimize the compounds to be tested. Results from the permeability and serum stability assays clearly indicated that the most promising candidates were MiniAp-4, which had the highest BBB transport in the cell-based BBB model, followed by MiniAp-1, which was the most protease-resistant. This experiment was performed together with Pol Arranz in the animal facility of Hospital Clínic de Barcelona.

In order to reduce the number of mice to a minimum we only assayed MiniAp-1 and MiniAp-4 at a single dose in a concentration near the solubility limit of the first peptide in water. This amount (1200 nmol) corresponded to 24 times the LD50 of apamin. The native peptide was also assayed as a positive control with a dose

corresponding to the LD50 and another control group was administered only the vehicle (PBS).

All peptides were injected via tail vein (n = 6) and animals were observed at different times for a period of 24 h. All mice that were administered apamin had convulsions, which disappeared after 10-30 min except for 2 of them that died in less than 5 min after injection. All mice injected with MiniAp-1 and MiniAp-4 behaved like the control group and none showed any envenomation symptoms. This result indicates that the LD50 for acute toxicity of the two assayed analogues was well over 24-fold the one of apamin.

Immunogenicity

Apamin has been described to be immunogenic *per se*.[266] Therefore, reducing the capacity of this sequence to elicit an immunogenic response was essential to prove the value of these compounds as BBB-shuttles for treatments requiring repeated administration. This is why an immunogenicity study was commissioned to AntibodyBCN.

A

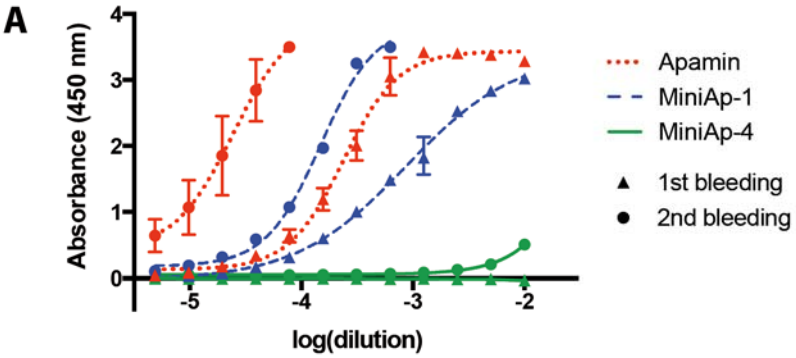

B

	Apamin	MiniAp-1	MiniAp-4
1st bleeding	3.6 ± 0.1	3.0 ± 0.1	<< 2
2nd bleeding	4.6 ± 0.2	3.8 ± 0.1	< 2

Figure 26. *Antibody titration after the 1st bleeding (4 doses, triangles) and the 2nd bleeding (7 doses, dots). A) Absorbance in the ELISA plate plotted against the logarithm of the serum dilution. Data represent mean values ± SD (n = 4 for apamin and MiniAp-4; n = 2 for MiniAp-1 in the first bleeding and n = 1 in the second). Fitting was performed using a sigmoidal dose-response model. B) Antibody titer reported as –log(IC50).*

During the 12-week experiment, doses of MiniAp-1, MiniAp-4 and apamin were administered each other week. Apamin was administered in 25-μg doses to avoid toxicity and it was confirmed to be remarkably immunogenic. MiniAp-1 and MiniAp-4 were injected at double the concentration because mice appeared not to be affected after the 1st or 2nd immunization. However, although MiniAp-1 generated between 4- and 6-fold fewer antibodies than apamin, at this concentration it appeared to be remarkably virulent, as 3 mice died throughout the study (*Figure 26*).

Conversely, MiniAp-4 had no visible effect on the animals. Moreover, no antibodies could be detected after the 4th immunization and the antibody titer at half-response at the end of the study was at least 400-fold lower than that of apamin. The outcome of the experiment clearly indicated that MiniAp-4 was safer than MiniAp-1 and, hence, that it was the lead BBB-shuttle among the synthetized analogues.

Confirmation of MiniAp-4 as a lead shuttle

Transport capacity and endocytosis mechanism

At this point, we switched to the more relevant but lower throughput (12 vs 24-well plate format) BBB-model using induced human endothelial cells. In this new model MiniAp-4 had a very similar permeability to the one obtained in the bovine model, suggesting that the mechanism of transport was also present in human cells. As this nonapeptide was remarkably shorter than MiniAp-1 (9 vs 16 residues), we first evaluated if the *N*-terminus could still be modified with small molecules such as CFluorescein and levodopa without affecting its transport. In this case the fluorophore was coupled using a glycine spacer and the permeability assay in the cell-based model showed that the transport was not dramatically affected in any of the two cases, though the decrease was more pronounced that in MiniAp-1.

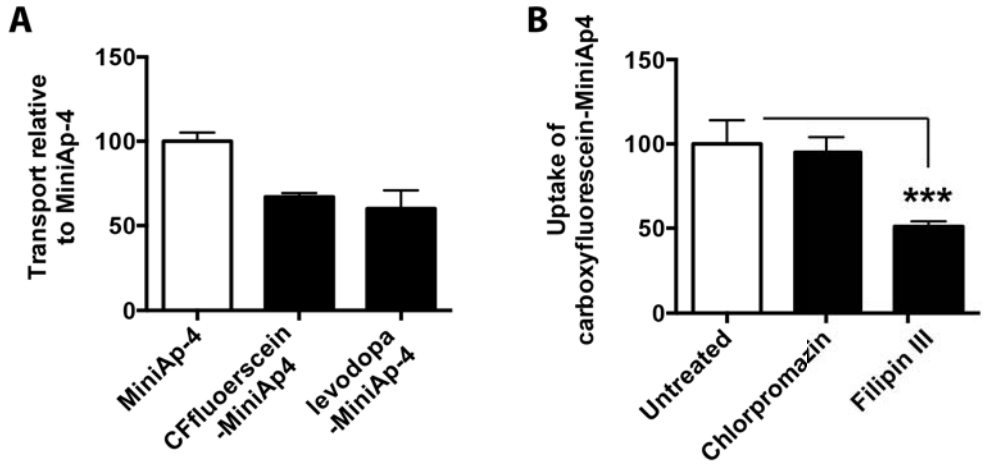

Figure 27. *Influence of small cargoes and inhibitors to the transport of MiniAp-4. A) Transport of small cargoes across a human cell-based model of the BBB. B) Effect of selective inhibitors on the uptake of CFluorescein-MiniAp4 analysed by FACS. *** P < 0.001 (t-test).*

We then studied the internalization of the CFluorescein-MiniAp-4 construct in bEnd.3 cells using selective inhibitors of endocytotic pathways that had been used in this cell-line.[29] Uptake was significantly reduced by filipin III (t-test, $p < 0.001$) but not chlorpromazin. The former has been described to selectively inhibit caveolae-mediated endocytosis without altering clathrin-mediated pathways, whereas the latter prominently affects clathrin-dependent internalization. This result indicated that, firstly, the transport of this peptide was at least partially due to an endocytotic mechanism and, secondly, that this mechanism was mediated by caveolae rather than clathrin. Caveolae-mediated endocytosis is compatible with the transport of large cargoes because they undergo transcytosis in the BBB[287] and have an appropriate vesicle size to accommodate large cargoes (50-80 nm).[288]

Challenging MiniAp-4 to transport large cargoes

Conjugation to quantum dots

We conjugated MiniAp-4 to quantum dots (QDot605) because they are large cargoes (15 nm) that could eventually be monitored *in vivo*. Moreover, they have previously been used in our laboratory to prove THRre capacity to carry NPs into the brain parenchyma using 2-photon life microscopy.[156] For this previous study, Dr. Roger Prades set up a conjugation method based on the direct modification of QDot-COOH carboxylates by activation with the water-soluble carbodiimide (1-ethyl-3-(3-dimethylaminopropyl)carbodiimide, EDC) followed by reaction with the *N*-terminus of the peptide. In order to pursue the study of THRre and apply this approach to other peptide shuttles, I started working on the optimization and characterization of the peptide-quantum dot linkage with this peptide before applying it to MiniAp-4.

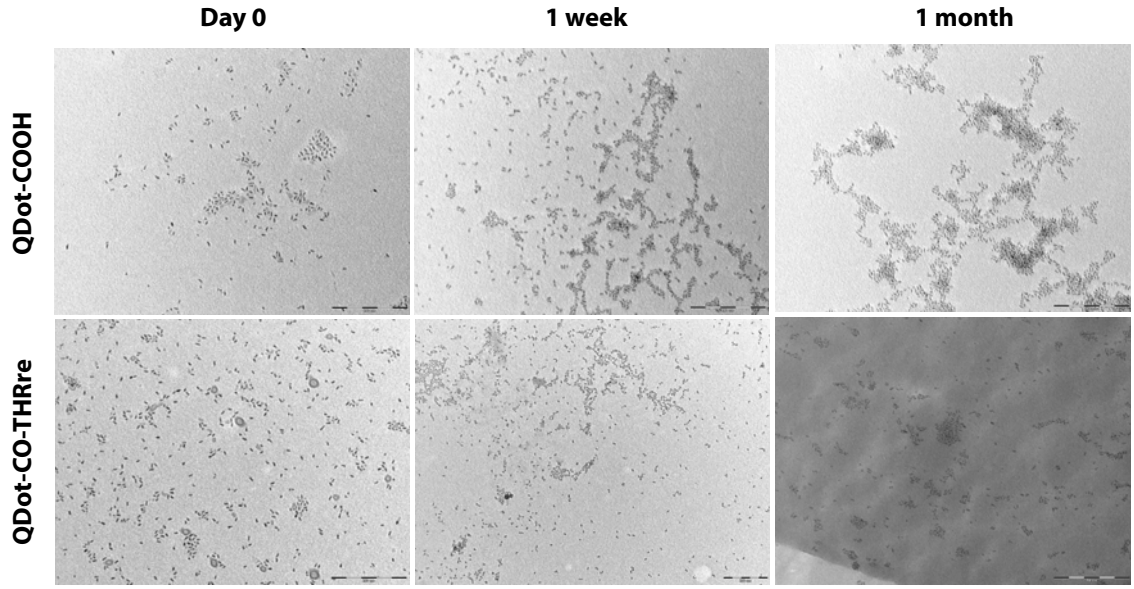

Figure 28. *TEM micrographies showing aggregation of QDot-COOH in water at different times. Scalebars represent 200 nm.*

In a preliminary study we inspected visually the stability of QDot605-COOH modified with 110 THRre molecules per NP in MilliQ water, 20 mM borate buffer (pH 7.4), 20 mM phosphate buffer (pH 7.4), Ringer HEPES and phosphate buffer saline (PBS). We observed that these quantum dots immediately precipitated when they were mixed with PBS 1:1. In Ringer HEPES there was no precipitation in the first few hours and in 20 mM phosphate buffer they were stable for several days. In water they lasted up to 1 month until precipitation was observed and, after this time, no solid was yet visible in 20 mM borate buffer. However, when we analysed the samples from different days using TEM, aggregation was already visible after 1 week in water (*Figure 28*). In addition, unreacted peptide could not be completely removed from the solution because gel filtration with PD-10 or NAP-5 columns did

not provide enough resolution and dialysis using 8 kDa MWCO membranes proved ineffective even after 3 days. Moreover, these NPs could not be submitted to more than one cycle of centrifugal filtration without remarkable precipitation. Therefore, we decided to set up a more robust conjugation method based on commercial pegylated quantum dots (QDot605-PEG-NH_2) following a protocol established by Cai and coworkers.[289]

This conjugation strategy was based on the modification of quantum dot amines with a linker containing an *N*-hydroxisuccinimide activated ester and a maleimide moiety (*Figure 29*). A peptide bearing a cysteine could then be linked to the maleimide through a Michael addition. This approach would enable the use of peptides with more than one amine, like MiniAp-4, as thiols react 1000-times faster than amines at pH 7.0.[290] Using this approach we incorporated 120 THRre peptide molecules on QDot-PEG-NH_2, as assessed by amino acid analysis after thorough buffer exchange, which is almost the same amount obtained with the QDot-COOH.

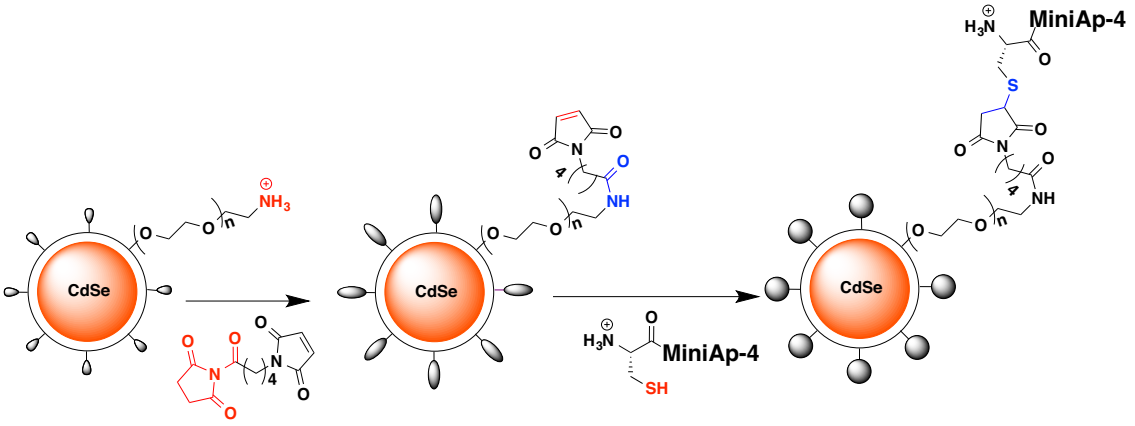

Figure 29. *Modification of quantum dots with MiniAp-4*

The coupling of PEGylated QDots with the peptide was already performed in PBS. Hence, we only analysed the stability of QDots in this buffer and we could not see any precipitation even after 2 months. Besides, there was no sign of aggregation when we examined TEM micrographs of this preparation even in a sample that had been submitted to 4 centrifugal filtrations after gel filtration to completely remove unreacted peptide (*Figure 30*).

After setting up the conjugation with THRre, quantum dots were functionalized with MiniAp-4. Upon amino acid analysis of the sample and quantification of QDots by UV absorption, we calculated an incorporation of 50 molecules of MiniAp-4 per NP.

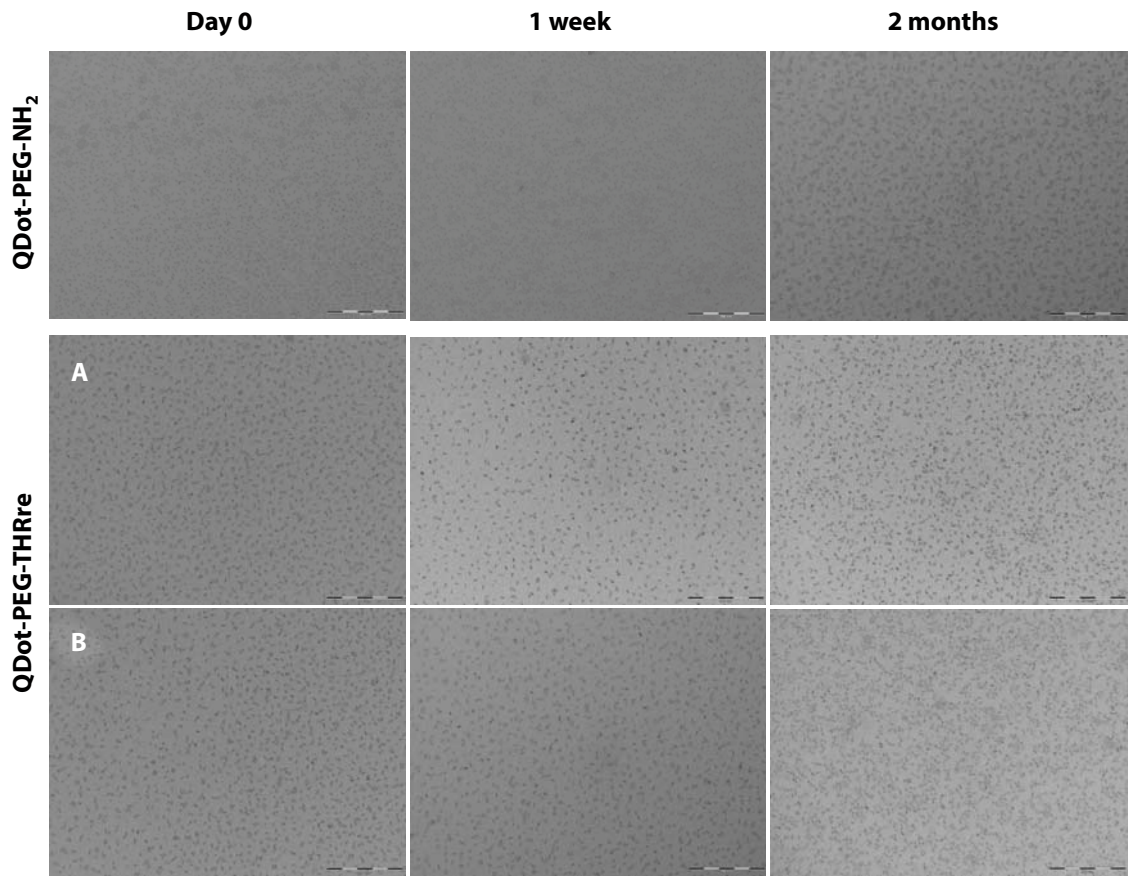

Figure 30. *TEM micrographies showing the stability of QDot-PEG-NH_2. No difference could be appreciated in QDot modified with THRre before (row A) or after (row B) centrifugal fitlration. Scalebars represent 200 nm.*

Synthesis and conjugation of gold NPs

12 nm gold NPs (AuNPs) have a very low permeability across the BBB and are thus a challenging cargo to drive across this barrier.[63] We synthesized AuNPs by reduction of chlorauric acid ($HAuCl_4$) using sodium citrate. After the synthesis, we coated them by ligand exchange with MiniAp-4 bearing a cysteine at the *N*-terminus (*Figure 31*). After washing an aliquot of the conjugated NPs with 1% TFA to remove any adsorbed peptide that could have remained, we digested the sample in hydrochloric acid for 3 days and submitted the sample to amino acid analysis. The NPs were quantified spectrophotometrically based on an extinction coefficient reported for AuNPs with the same diameter and synthesized following the same protocol.[291] With this procedure, the number of peptides obtained per NPs was approximately 900, which indicated that essentially all the surface of the NP is covered by MiniAp-4.[291]

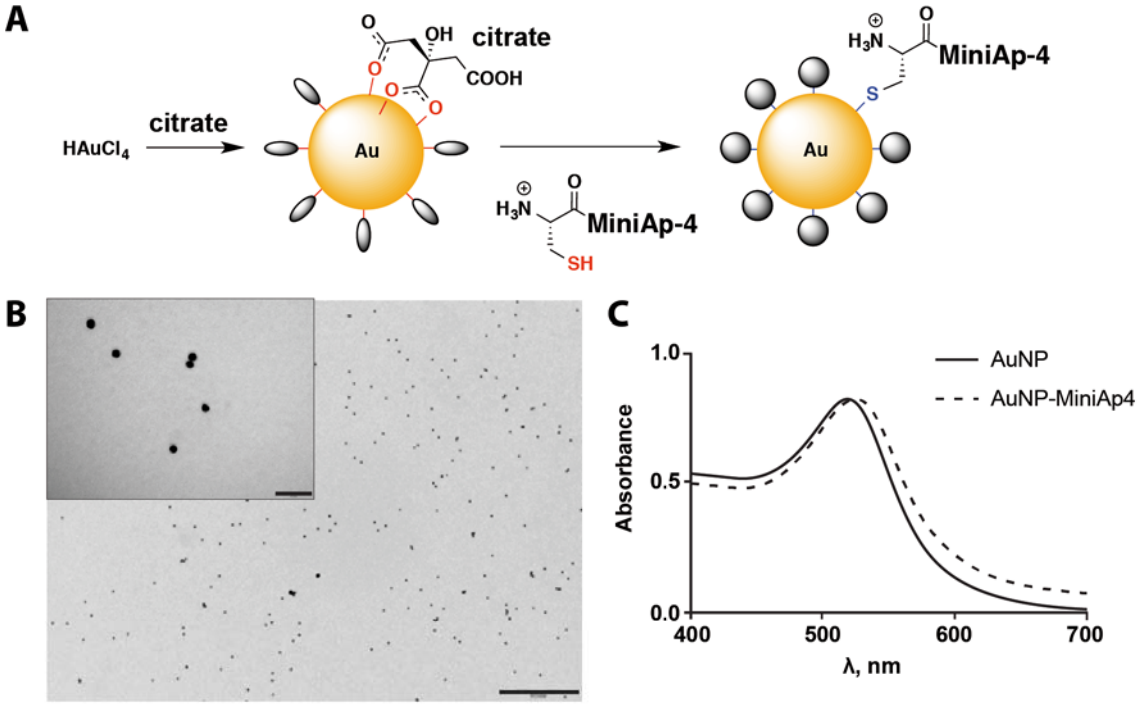

Figure 31. *Synthesized and conjugated AuNPs. A) Synthesis and conjugation scheme. B) TEM micrographies. Scale bars: 500 nm in the low magnificaiton image and 50 nm in the zoomed image. C) Absorption spectra.*

Conjugation to GFP

We next aimed to test the capacity of MiniAp-4 to transport large cargoes, namely proteins and NPs. We chose GFP as a model medium-sized (28 kDa) and slightly acidic protein (pI = 6.2), both of which render it a challenging cargo for brain delivery.[7] The protein was first derivatized with 2-iminothiolane to generate reactive thiols on its surface, which were then linked to MiniAp-4 bearing a maleimide at the *N*-terminus (*Figure 32*). The reaction (performed by Dr. Macarena Sánchez) yielded an average of 0.9 peptides/protein as estimated by the relative intensity of the peaks corresponding to each species in the mass spectrum. We also applied the reaction under the same conditions to a larger peptide (Angiopep-2) that could be resolved by SDS-PAGE, which provides a more robust quantification. The peptide/protein ratio was 1.6 by electrophoresis and 1.2 by MS, suggesting that the ratio for MiniAp-4 was higher than 0.9.

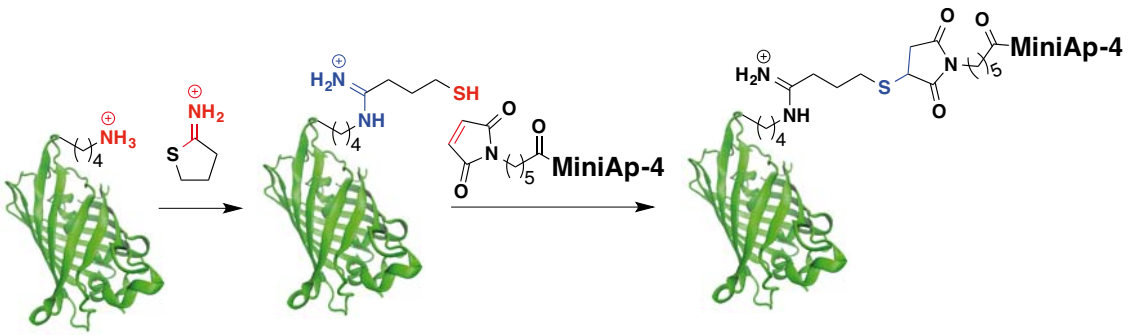

Figure 32. *Conjugation of MiniAp-4 to GFP.*

Evaluation of the cargoes in the cell-based BBB model

With the conjugates in hand, we tested the ability of MiniAp-4 to transport these large cargoes in the human cell-based BBB model. QDots and AuNPs were assayed at very low concentrations (30 and 5 nM respectively) based on reported data[63,156] and preliminary toxicity tests we performed on this model. In order to detect the amount present in the acceptor, which was expected to be below 0.5 %, we used ICP-MS at the Agència de Salut Pública de Barcelona under the supervision of Josep Calderón. For AuNPs we quantified the only stable isotope of gold, ^{197}Au. With regard to QDots 605, we had several possibilities as they are made of the semiconductor compound CdSe. Among the various isotopes of cadmium and selenium, we quantified the one that has the least common isobaric interferences, namely ^{111}Cd, despite its relatively low isotopic abundance (12.8 %).[292] Initially we digested QDots with *aqua regia*, as it had been previously described[156] but we obtained a high background coming from the digestion tubes. Thus, we switched to infusing the intact nanoparticles and we interpolated the signal in a standard line prepared with the same QDots used in the assay instead of Cd^{2+}. Concerning the quantification of GFP, we initially intended to take profit from its inherent fluorescence. However, because of the small amount of protein available we used ^{125}I labelling to obtain more accurate data (for further details see the antibody labelling description in the BBB permeability evaluation section of next chapter).

Remarkably, MiniAp-4 was capable of increasing the transport of all three cargoes in the cell-based model (*Figure 33*). The permeability was increased 2.4-fold in the case of GFP and 2.0-fold QDot605. These results are similar to those obtained under similar conditions for proteins and NPs linked to other peptide BBB-shuttles. However, most of these reference shuttles are remarkably larger and are susceptible to protease degradation such as Angiopep-2,[96] gH625[28] and ApoE(141-149)$_2$;[61] these differences can be highly relevant for a potential large-scale production and *in vivo* brain delivery, respectively.

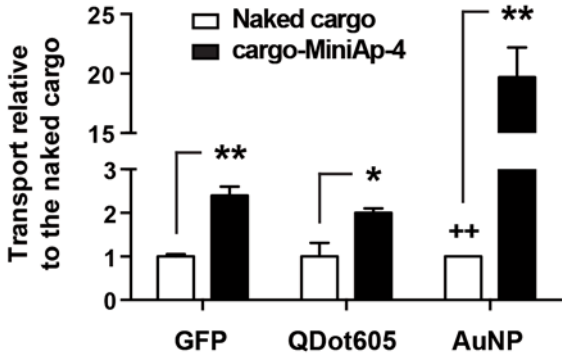

Figure 33. *Increase in the transport of large cargoes by MiniAp-4 in a human cell-based BBB model. ++ represents the quantification limit of the technique. Data represent mean values ± SEM (n = 3). *P < 0.05, **P < 0.01 (t-test).*

For AuNPs the rise was even more outstanding, over 20-fold (the transport of AuNPs alone could not be detected). The higher transport of AuNPs with respect to QDot605 could be explained by the larger number of shuttle peptides on the surface but also because the citrate-coated AuNPs are less stable and may form aggregates, which are less permeable. Further characterization of the NPs in the assay medium is required to address this point.

Validation of MiniAp-4 as a BBB-shuttle *in vivo*

Choice of cargoes and analytical techniques

After showing the ability of MiniAp-4 to transport a variety of compounds in a human BBB model, we aimed to demonstrate that this peptide was indeed capable of delivering a cargo *in vivo*. This part of the project was carried out with the help of Marc Guiu, who injected the compounds via tail vein into the animals, performed the necropsies and imaged the whole-animal fluorescence. Nuno Vasconcelos also contributed to transcardially perfuse mice and harvest the brains.

The first goal was to get an idea of the PK of the compound in the brain. After that, taking into account the time in which concentration was highest, we intended to compare the biodistribution of the constructs after perfusion and extraction of several organs. Eventually we also expected to quantify the compounds in a more accurate way using HPLC-fluorescence after brain homogenization and capillary depletion. Finally, using fluorescence microscopy we aimed to assess whether the compound had reached the brain parenchyma. Ideally the same compound should be used for all experiments because changing the fluorophore might imply a significant alteration of PK.

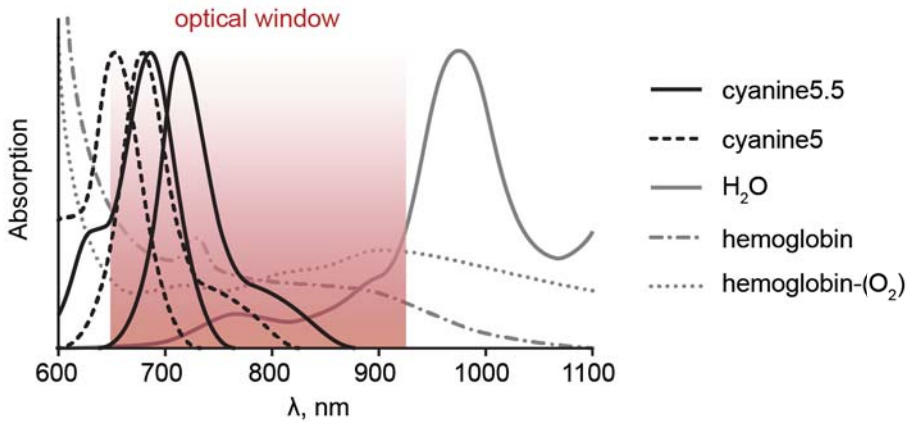

Figure 34. *Optical window for in vivo fluorescence imaging. (Adapted from Phan et al. 2010)*[293] *Excitation and emission spectra of the two fluorophores used in this section are shown in black.*

In order to minimize the number of animals used, we performed the measurement at different time-points on the same mice using whole animal fluorescence. Therefore, we needed a fluorophore absorbing above 600-650 nm to minimize tissue and blood absorption and reduce scattering. Regarding emission, it

should be lower than 900-1000 nm to minimize absorption from water and lipids (*Figure 34*).[99,294] After that, in order to precisely locate the compound outside the capillaries we needed high-resolution 3D imaging and therefore we turned to confocal microscopy.

The most red-shifted beams at the IRB microscopy facility were at 633 and 639 nm and no white laser was available. Taking this limitation into account, the most suitable far-red fluorophore was cyanine-5 (*Figure 35*). This molecule has excitation and emission maxima at 646 nm and 662 nm respectively. Moreover, it has a reasonable brightness taking into account that its low quantum yield (Φ = 0.2) is compensated by a high extinction coefficient (250000 $cm^{-1}M^{-1}$). However, the filter sets in the equipment available at the PCB to monitor whole-animal fluorescence (IVIS-200 Spectrum) did not match the spectra of this dye completely. For the IVIS, the best-suited fluorophore was cyanine-5.5, which had excitation and emission maxima at 673 nm and 707 nm, respectively, and a brightness similar to cyanine.5 (ε = 2090000 $cm^{-1}M^{-1}$, Φ = 0.2). In addition, a derivative of this compound (Cy5.5®) has been used to study the integrity of the BBB and also to prove the capacity of Angiopep-2 to reach the brain parenchyma.[90,295] Hence, we prepared the peptide shuttles with both labels to find out which one was most appropriate.

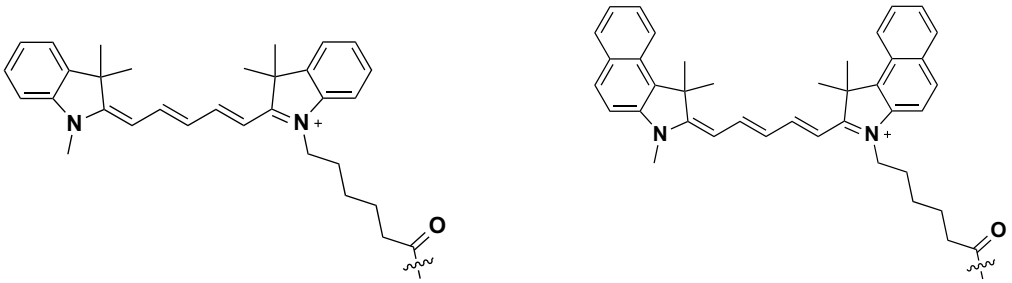

Figure 35. *Structure of cyanine-5 (left) and cyanine-5.5 (right).*

Test with Zyentia peptide

As a first cargo we chose a peptide that inhibits amyloid-β aggregation, which had been developed in our laboratory in collaboration with Zyentia S.M.E. (we will thus refer to it as "Zyentia peptide").[296] We linked this peptide to the *N*-terminus of MiniAp-4 and also of THR and THRre; the latter were used as control BBB-shuttles. The cargo-BBB-shuttle constructs were prepared by sequential coupling of each residue on resin. At the *N*-terminus of the peptides we added an hexynoic acid to link the label through cupper-catalyzed azide-alkyne 1,3-dipolar cycloaddition (CuAAC). We initially used a triazole linkage because it provides a higher physiological stability,[297] especially in small molecules, than other widely used conjugation methods such as those based on thiol-maleimide.[298]

In a preliminary test we injected THRre conjugate to FVB mice and measured the fluorescence after 30 min. In this experiment we obtained a strong signal that

outlined the shape of the brain with the cyanine-5.5 derivative. Starting from a dose reported in previous studies using similar labels (40 nmol),[90,295] we adjusted the amount to 4 nmol in order to obtain a non-saturated signal. Conversely the signal for cyanine-5 at the same concentration was more than 10-fold lower, barely distinguishable from the background. Therefore, we decided to use the cyanine-5.5 conjugates and keep those with cyanine-5 in case the signal was not strong enough in confocal microscopy.

After the initial test, we assayed all the peptides in CD-1 mice. The first observation was that, in this mice strain, we did not obtain the same outline of the brain but a less defined signal. Moreover, in these animals an important degree of fluorescence was also observed on the upper part of the back, probably coming from accumulation in the lungs. It is difficult to explain the differences observed between the FVB and CD-1 strains without a more in-depth study because, *a priori*, the main difference is that the former is inbred while the latter is outbred, which results in higher genetic diversity.

To our surprise, when we analysed the results from this experiment with CD-1 mice, we found out that the cargo only bearing the fluorophore was more permeable than the constructs containing the BBB-shuttle peptides (*Figure 36*). This could probably be explained by the high hydrophobicity of the Zyentia peptide, which was further enhanced by the label. Therefore, for this cargo (i.e. cyanine5.5-Zyentia_speptide), passive diffusion probably had a much higher contribution than transcytosis mediated by any of the shuttles.

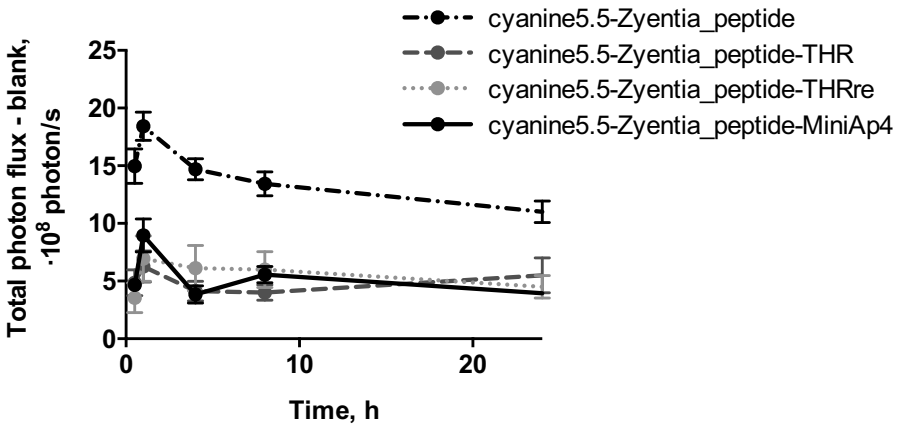

Figure 36. *Fluorescence measured in the brain area in vivo for cyanine5.5-Zyentia_peptide-BBB_shuttle conjugates. Data represent mean values ± SEM (n = 4).*

Study of cyanine-5.5 as a model cargo for brain delivery

As the Zyentia peptide appeared to accumulate in the brain on its own, we decided to use the fluorophore alone as a model cargo. Therefore we prepared the conjugates, this time using thiol-maleimide chemistry because of the reagents available and the time constraints. Cyanine-5.5 was bound to THR, THRre, apamin

and also to cysteamine as a control. The latter bears a free amine that mimics the positive net charge of the peptides and additionally provides a reactive group to fix the fluorophore with paraformaldehyde for microscopy.

After injecting the compound into mice, MiniAp-4 displayed a surprising 4.3-fold increase in brain concentration of cyanine-5.5 calculated as the area under the curve (AUC) (Figure 6A and B). The maximum accumulation was reached 1 h after administration and the concentration of the targeted fluorophore was significantly higher throughout the 24-h assay (t-test, $p < 0.01$). This prolonged effect could be due partly to the high stability of the peptide to serum proteases.

The increase in the AUC with respect to the control fluorophore provided by THRre was 2.0. This poor performance with respect to MiniAp-4 could be explained by a possible interaction between the cargo and the aromatic residues of THRre peptide, decreasing the affinity of this shuttle for the TfR. The same explanation could be applied to THR, which shows a very similar brain accumulation as the cysteamine-derivatized fluorophore. The reduced transport efficiency of THR compared to the *retro-enantio* version (THRre) could be explained by the higher resistance to proteases of the latter. This result is in line with the arguments supporting the higher efficiency of more protease-resistant peptides as BBB-shuttles.

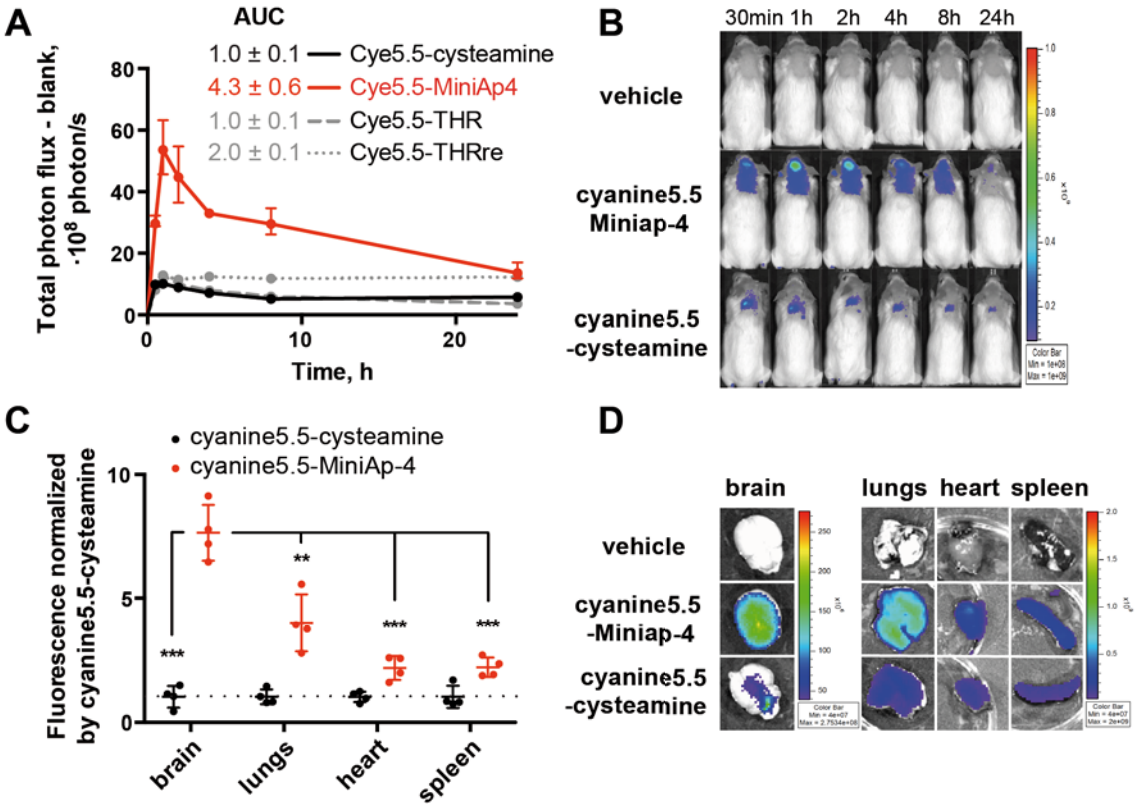

Figure 37. *In vivo evaluation of cyanine5.5-MiniAp4. A) Fluorescence measured in the brain area in vivo. Numerical values are given for the area under the curve. B) Mice imaged in the IVIS chamber. C) Relative fluorescence intensity of various organs ex vivo after perfusion. D) Representative organs imaged in the IVIS chamber. All data represent mean values ± SEM (n = 4). **P < 0.01, ***P < 0.001 (t-test).*

In order to verify the results, we harvested the organs at a single time point and imaged them using IVIS. The time chosen for MiniAp-4 was 1, while for THR and THRre we switched to 4 h because difference between these two peptides appeared to be higher. Two groups were injected the cyanine5.5-cysteamine conjugates, one for each time-point, whereas we only injected one control group with the vehicle.

Compounds were administered under the same conditions as the previous experiment and, after 1 or 4 h, mice were deeply anesthetized, imaged in the IVIS chamber and perfused with PBS for 5 min. This perfusion was performed to remove the labelled molecules remaining in blood and those that were possibly adsorbed on brain capillary walls. The organs were immediately excised and fluorescence was quantified in the IVIS chamber. The increase in brain transport of MiniAp-4 *in vivo* could be confirmed and we observed it was even higher after perfusion with PBS (7.6- vs 6.7- fold) (*Figure 37*). Most importantly, the MiniAp-4 conjugate had a remarkable selectivity for the brain, as the increase in other organs was significantly lower (t-test, $p < 0.01$), especially in heart and spleen (t-test, $p < 0.001$). The signal in liver and kidneys saturated the CCD camera in both the targeted and non-targeted fluorophore and thus could not be quantified. For THR and THRre we confirmed that they were not able to significantly increase the transport of this cargo in the brain or any other organ.

Finally, in order to assess whether the cyanine5.5-MiniAp-4 construct could indeed reach the brain parenchyma we administered this compound to a new set of mice for microscopy imaging. One hour after injecting the compounds, animals were perfused with PBS and PFA to fix the tissues and the molecules. Cyanine5.5 could be well excited by the 639 nm laser as there was a clear difference between the control groups and the brains containing the targeted fluorophore. The MiniAp-4 conjugate colocalized with capillaries but was also found in the brain parenchyma in the form of aggregates. By contrast, the cysteamine conjugate could not be detected in the brain using the same settings (*Figure 38*). The cyanine5.5-MiniAp4 aggregates were shown to colocalize with neurons immunostained with NeuN and only to small extent with GFAP glial marker. A similar neuronal colocalization, which is of great interest in many neurodegenerative diseases, has been shown with other protease-labile BBB-shuttles[65,89,92] but not yet for any protease-resistant vector.

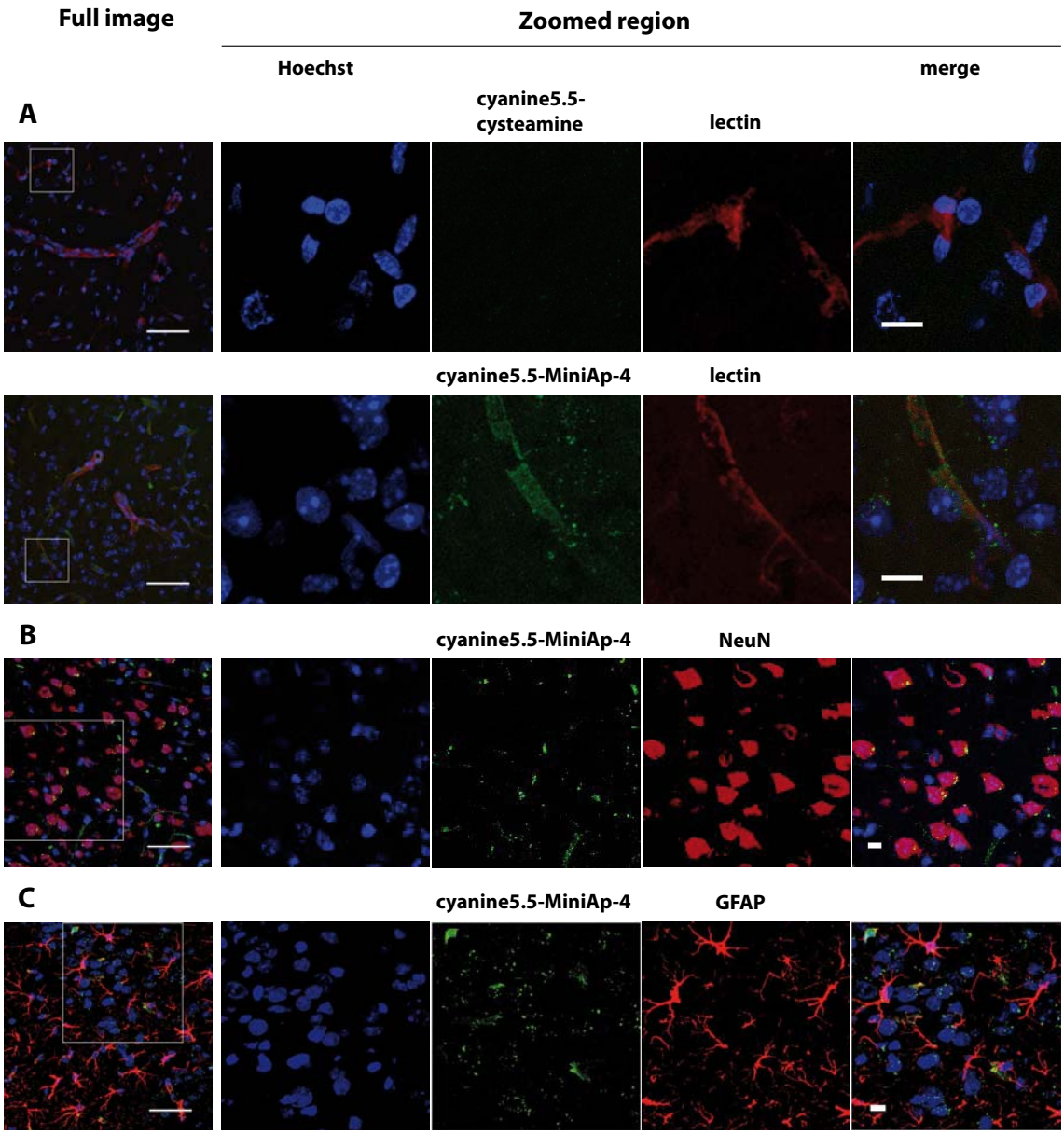

Figure 38. *Representative confocal microscopy images of brain slices. Scalebar is 50 μm on the full images and 10 μm in the zoomed regions. In all images cell nuclei are shown in blue and cyanine5.5 conjugates in green. A) Cyanine5.5-MiniAp-4 is found in the capillaries (in red) and in the brain parenchyma, whereas cyanine5.5-cysteamine is not observed in either. B) Cyanine5.5-MiniAp-4 is observed in neurons (in red). C) This cargo-BBB-shuttle construct is rarely observed in astrocytes (in red).*

Summary and perspectives of mini-apamins as new BBB-shuttles

In summary, we have shown that minimized cyclic derivatives of apamin have a higher transport than the native peptide across endothelial cells and preserve a notable resistance to serum proteases. Moreover, they are able to efficiently transport a variety of cargoes across the BBB in bovine and human cell-based models. MiniAp-4 BBB-shuttle is capable of delivering a cargo into the brain of mice with remarkable selectivity. Furthermore, this peptide has lower toxicity and is practically immunosilent compared to apamin.

Currently, further internalization and transcytosis experiments are being conducted to study the mechanism of the most promising member of the mini-apamin family, MiniAp-4. We have synthesized scrambled sequences to be used as a control for binding, competition and saturation assays. However, finding the putative receptor for this family of shuttles will be challenging and more potent approaches involving photocrosslinking and chemoproteomics will be required.[299]

MiniAp-4 may be regarded as a proof of concept of venoms as a new source of protease-resistant BBB-shuttles. However, even more efficient vectors might be present among the uncountable number of venom components still unknown. We have started exploring other venoms such as that of the Brazilian spider *Phoneutria nigriventer*. A preliminary experiment in which we have assayed the fractioned venom in the cell-based BBB model, appears to indicate that several substances are indeed able to cross the BBB without affecting the integrity of the barrier. Next step will be to repeat the assay with higher amounts venom and thoroughly analyse the acceptor compartments in order to identify the permeable peptides. However, the concentration of many components is extremely low and is further decreased after crossing the endothelial cell monolayer. Therefore, mass spectrometry equipment with high sensitivity and high resolution power such as LC-Orbitrap shall be used in combination with the available information on the spider proteome and transcriptome.[239]

In the next chapter, we will describe how we applied MiniAp-1, MiniAp-4 and other shuttles to the transport of a challenging therapeutic cargo: monoclonal antibodies for the treatment of brain tumours.

Toward antibody transport across the BBB

Monoclonal antibodies (mAbs) are currently used to treat a variety of diseases and numerous therapies based on these macromolecules are in clinical trials.[300] Their capacity to target large epitopes, the high affinities they display for their targets and their long circulation half-life are very appealing features that complement those of small drugs. However, they also present some important pitfalls. Issues such as a challenging large-scale production, a complex characterization and the need for humanization to minimize immunogenicity can now be overcome. Conversely, other drawbacks like slow diffusion into tissues and low permeability across biological barriers are still of major concern. Therefore, the BBB is one of the main hurdles for these large therapeutics. Furthermore, nowadays it is widely accepted that not only there is no solid evidence of an influx transporter for antibodies on the BBB but also that there are receptors in the parenchymal side that mediate their efflux towards blood.[301,302]

Antibodies have shown to be highly efficient for cancer therapy in peripheral organs but have very little effect on brain.[303] In particular, many efforts have been devoted to developing efficient cures for glioblastoma multiforme (GBM), which is the most prevalent (50 % in the US) and aggressive type of glioma. Gliomas arise from glial cells (astrocytes, oligodendricytes, ependymal cells) and are the most common among brain tumours (80 % in the US).[304] Median survival of GBM patients is 15 months, which shows the low efficiency of current therapies.[305] The main reasons for such low efficiency of anticancer drugs is attributed to their inability to cross the BBB together with tumour complexity and heterogenity.[306] As in most solid tumours, angiogenesis results in an abnormal growth of the vasculature, which forms a more permeable BBB often named blood-tumour barrier.[307] However, GBM is highly invasive and the BBB is still intact where infiltrating cells are found,[308] which results in a relapse of the tumour even after surgical resection and application of current treatments.

Our working hypothesis was that conjugating BBB-shuttles to mAbs we would enhance the effect of the latter on the peripheral part of the tumour, which would improve tumour control and minimize relapse. This approach has recently yielded promising results in a preclinical study with an antibody (trastuzumab) targeted with Angiopep-2 for the treatment of breast cancer metastases in the brain.[126]

The only immunoglobuline that has been approved for the treatment of GBM is Avastin®,[309] whose generic name is bevacizumab (Bv). Binding of Bv to the vascular endothelial growth factor A (VEGF-A) prevents its interaction with the corresponding receptor (*Figure 39*) and ultimately inhibits angiogenesis. As a result, growth of the tumour is controlled because of the lack of nutrients and oxygen.[310] Another antibody that is being studied to treat GBM is Erbitux® (or cetuximab, Cx), which has been approved for the treatment of colorectal cancer and squamous cell

carcinoma (a type of skin cancer).[311] Cx binds to epidermal growth factor receptor (EGFR),[312] which plays a key role in tumour proliferation and is overexpressed in 50 % of patients suffering from GBM. Although this antibody seemed promising for the treatment of brain tumours, phase II clinical trials recently revealed that it provided no benefit over existing therapies.[313] This lack of efficiency is attributed mainly to the incapacity of Cx to cross the BBB or the brain-tumour barrier and reach the EGFR expressed in cancer cells.

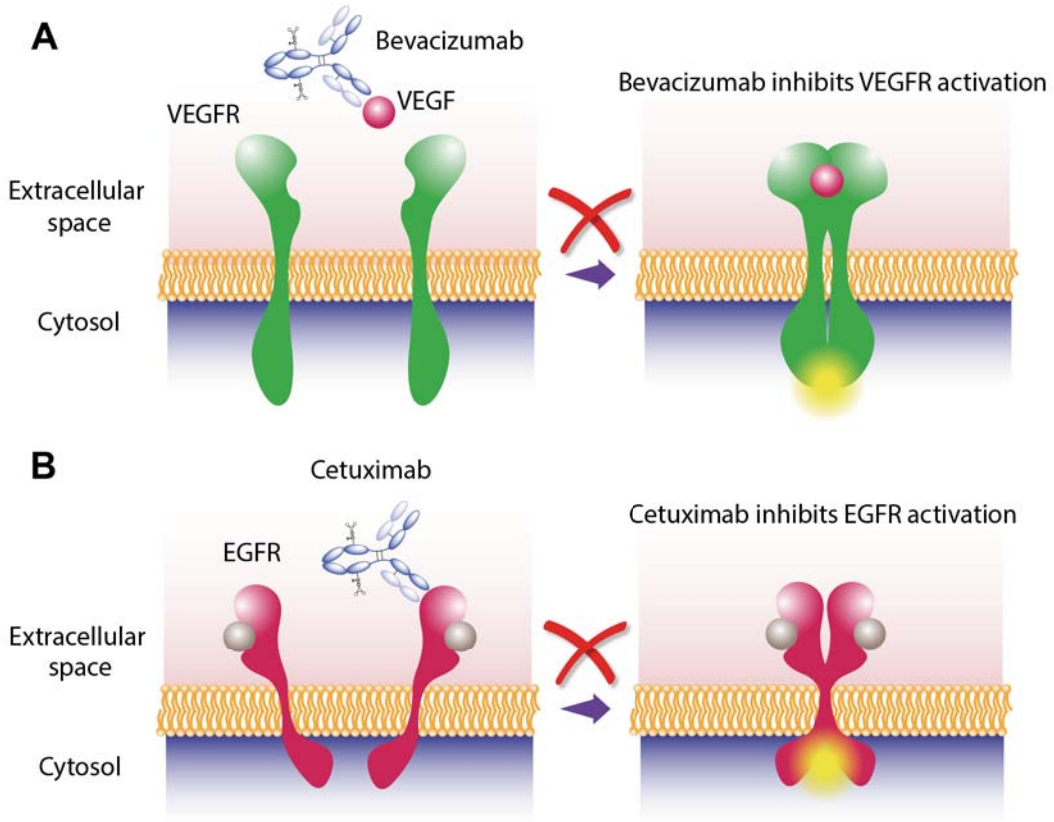

Figure 39. *Schematic mode of action of selected antibodies A) Bv B) Cx.*

Although this project was designed to include other antibodies for the treatment of GBM, we initially focussed our attention on Bv because it was the only one approved for this indication and we could obtain it in large amounts. Therefore, the conjugation techniques were chosen with the broadest applicability but taking into account especially the sequence and structure of Bv. However, this antibody started to be called into question after the withdrawal by FDA of its indication for breast cancer in November 2011. Confidence in Bv is decreasing due to the resistance to anti-angiogenic agents and to the pseudo-responses arising from a lower signal of MRI contrast agents; a drop in this signal indicates a reduction of the vasculature that apparently does not always correlate with the size of the tumour.[314] Due to the aforementioned reasons, despite all conjugation methods were set up with Bv, BBB permeability assessment focussed mainly on Cx conjugates.

Regarding the choice of BBB-shuttles to improve the transport of mAbs, we started using THRre because, at the beginning of this thesis, it was the most advanced BBB-shuttle developed in our laboratory (by Dr. Roger Prades).[156] Moreover, this shuttle targets the TfR, which is highly overexpressed in tumour cells in addition to endothelial cells. After setting up the conjugation strategies, we added a control peptide for THRre, which is the *retro-enantio* version of a reported scrambled sequence of THR.[67] We also added a 19-atom PEG spacer to THRre aiming to facilitate interaction with TfR. In order to compare the permeability of THRre with other reference shuttles we prepared conjugates with Angiopep-2, TAT, ApoE(159-170)$_2$ and RVG29. Finally, as soon as mini-apamins were validated with smaller cargoes, we also incorporated them to screening. In order to minimize the number of conjugates prepared, we only compared the diverse linkage methods using THRre and prepared the rest of shuttles using the most suitable technology.

After obtaining the constructs, we evaluated the stability of the thiol-maleimide linkage in serum and assessed the effect of the conjugated shuttles on the antibody affinity for its target. Finally, we studied the constructs in the human cell-based BBB model, which required setting up an appropriate detection procedure.

This chapter is based on an ongoing project in collaboration with Prof. Joan Seoane at the Vall d'Hebron Institute of Oncology (VHIO), initially financed by the competitive call Prova't (Generalitat de Catalunya). The contribution of our laboratory focussed on the design, synthesis and characterization of antibody-BBB-shuttle constructs, as well as on the evaluation of their permeability in cell-based BBB models. The final therapeutic effect of the selected mAb-BBB-shuttle conjugates is currently being evaluated in Prof. Seoane's laboratory using an orthotopic glioblastoma model positive for EGFR. In this project I worked together with Dr. Macarena Sánchez-Navarro, who joined our laboratory a few months after I had started working on it. Her experience in protein modification was of great help to set up some of the antibody conjugation techniques and for the characterization.

Exploring antibody-BBB-shuttle conjugation techniques

The only precedent on antibody-BBB-shuttle conjugates is the work with Angiopep-2, which was partly included in the patent of the peptide but has not been published until January 2015, while the thesis was being writen.[126] Therefore, at the beginning of the present thesis, to our knowledge, there was no information available about the effect of the number and the situation of shuttles on antibody transport. However, in the last decade, many protein conjugation techniques have been developed and in the last 4-5 years these techniques have acquired especial relevance in the field of antibody drug conjugates (ADCs). [315,316] ADCs follow the opposite scheme to mAb-BBB-shuttle constructs, because the mAb acts as the targeting moiety, aiming at cancer cells, and the cargo is a cytotoxic molecule. In spite of this, the conjugation technologies used to incorporate the toxic payloads can also be applied to peptide shuttles.

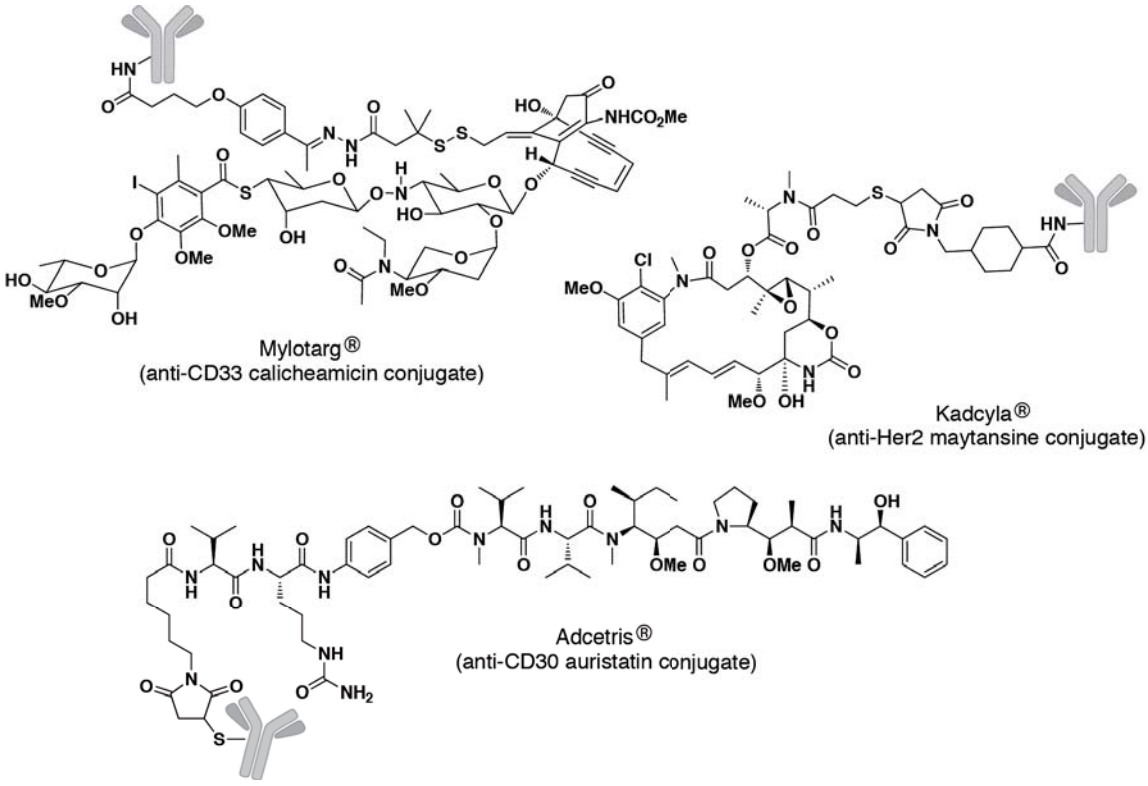

Figure 40. *Structures of representative ADCs (Modified from Perez et al. 2014).*[315]

The first ADC was approved by the FDA in 2000 (Mylotarg®) but many doubts were cast on its therapeutic benefit because of its side effects, which eventually led to its withdrawal in 2010 (*Figure 40*). However, since then 2 new ADCs have been commercialized (Adcetris® and Kadcyla®) and 30 more are in clinical trials.[317] Most ADCs bear tubulin polymerization inhibitors or DNA-acting cytotoxics. These molecules are generally conjugated either through a stable (thiol-maleimide

thioether) or a cleavable (hydrazine, disulfide or valine-citrulline) bond at the lysine or cysteine residues of the mAbs.[318]

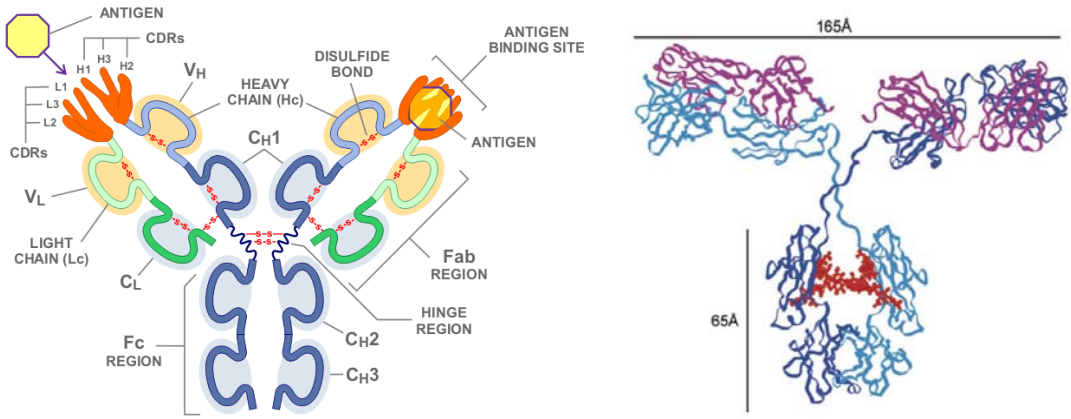

Figure 41. *Structure of an IgG. Left) Main parts of an IgG1 (From http://www.novimmune.com/science/antibodies.html. 29/12/2014). Right) Cartoon based on a crystal structure (From Arnold et al. 2007).*[319]

The antibodies used in this thesis, Bv and Cx, belong to the immunoglobulin G (IgG) class or isotype. IgGs are formed by four polypeptide chains, which are held together by noncovalent interactions and linked through disulfide bonds, and two or more small oligosacharides. The two longer protein chains (called heavy chains, ≈ 50 kDa), which are identical, interact at one end and then branch to stick separately to the two shorter chains (named light chains, ≈ 25 kDa), which are also identical between them (*Figure 41*). The branching point is called the hinge region, which separates the basal fragment (Fc from crystalizable fragment) and the antigen binding fragments (Fab). Each Fab has an antigen binding site or paratope, formed by several polypeptide loops called the complementary-determining regions (CDRs). The domains that contain CDRs are the ones with highest variability (thus called variable) and the rest are named constant because they are more conserved in IgGs of the same species.

An IgG has an average of 80 lysines[320] and most of them are on the surface because of their positive charge at physiological pH. More than half may be accessible for conjugation,[320] thus yielding heterogeneous mixtures of species bearing a different number of payloads in distinct positions (*Figure 42*). In spite of this, modification of lysines is used in many ADCs both in clinics and under development because high batch-to-batch reproducibility can be achieved when conjugation conditions are strictly controlled.[316] Moreover, these residues are very rare in IgG CDRs, thus efficiency of the antibody is not severely affected upon conjugation.[321] The optimal number of toxic molecules per antibody has been determined to be 3.5-4; higher ratios have a strong effect on the stability and the PK of ADCs, given mainly to the high hydrophobicity of the payloads.[322]

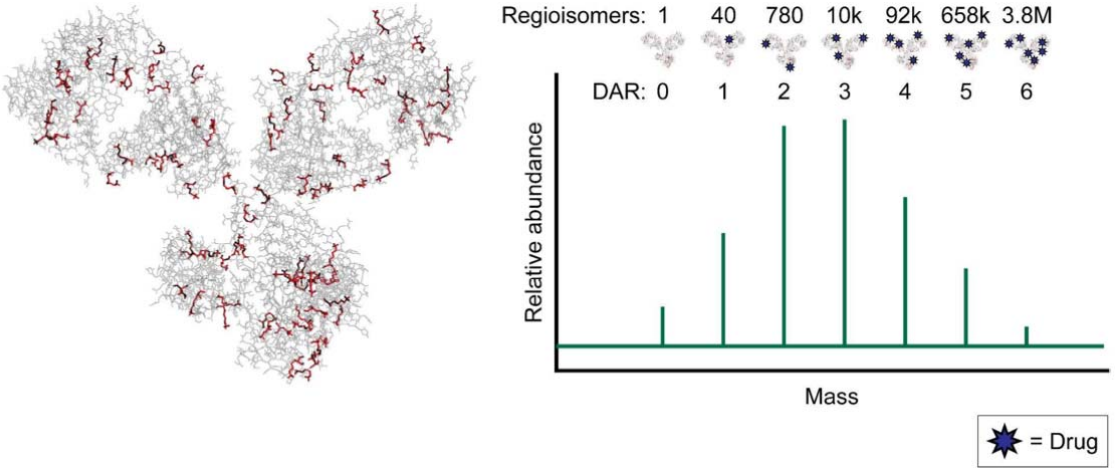

Figure 42. *Exposed lysines (highlighted in red) and theoretical product distributions (assuming 40 reactive residues) for a human IgG1. The increasing number of regioisomers for each drug antibody ratio (DAR) reflects an increase in constitutional heterogeneity. (From Agarwal et al. 2014)*[323]

A more selective conjugation technique also used in clinical practice and in advanced trials is the modification of endogenous cystines. Most commercial antibodies (such as Bv and Cx) belong to the IgG1 subclass, which has 16 disulfides, 8 of which can be reduced without affecting the integrity of the antibody.[324] The most accessible disulfides to reducing reagents are those in the hinge region and those linking the light and heavy chains,[325] all of which are far away from the CDRs. Although mixtures of 0, 2, 4, 6 or 8 peptides are also obtained in this way, they contain a lower diversity of regiosiomers.

Another classical conjugation site that is far away from the paratope or antigen-binding region, is the glycan chains. Human IgGs have a conserved glycosylation site at Asn297 in the C_H2 domain,[323] though 10-15 % of them can also be glycosylated on the variable regions.[326] However, glycan modification presents two major handicaps that have so far deterred investment of the large pharmaceutical industry. The first inherent drawback is that glycosylation is a heterogeneous posttranslational modification. The second pitfall is that it plays a key role in secondary immune functions. These effector functions such as antibody-dependent cellular cytotoxicity (ADCC) and complement-dependent cytotoxicity (CDC) can be beneficial by providing additional antitumor activity (*Figure 43*).[327] However, ADCC and CD could also decrease tumour localization, prevent internalization and lead to off-target toxicity.[328] This inconvenience may be overcome by the recent development of more site-selective strategies, often using enzymatic modifications. Thus, the possibility of regioselective modification, together with the increasingly potent analytical tools, makes this approach a competitive alternative to other traditional conjugation strategies.

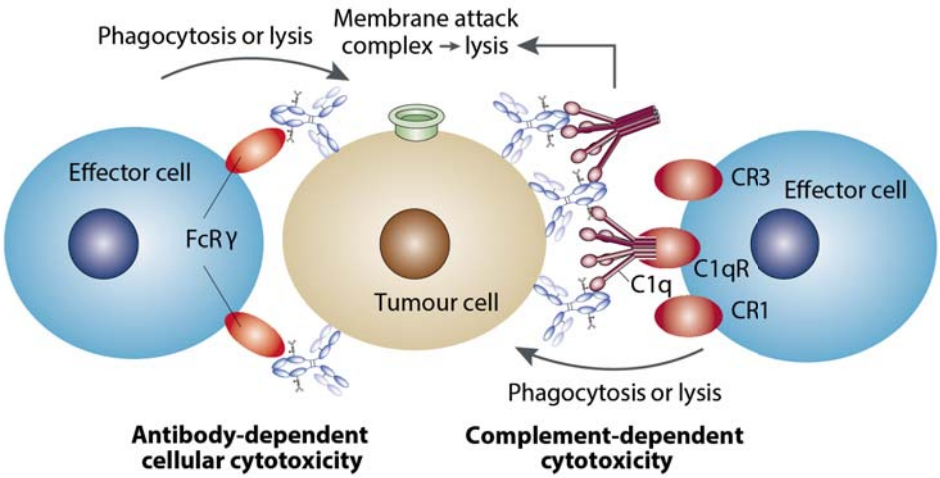

Figure 43. *IgG1 may direct the killing of tumor cells by ADCC or CDC. ADCC is triggred by an interaction between the Fc region of an IgG and the Fcγ receptors on immune effector cells such as neutrophils, macrophages and natural killer cells. CDC requires the recruitment of the complement component C1q by the IgG, which triggers a proteolytic cascade or, alternatively, C1q can bind to complement receptors on effector cells. (Modified from Carter et al. 2001)*[329]

Many efforts in academia have been devoted to improving site-selectivity. However, precise location of the drugs is not a guarantee for better performance of the ADC. An illustrative case is the development of a strategy to link 4 drugs per antibody molecule precisely at certain interchain cysteines by mutating other reactive points to serines.[330] The company that developed this method finally did not exploit it because the therapeutic effect did not outperform that of the heterogeneous mixture. Nonetheless, the control and versatility of site-selective strategies, have already shown some relevant improvements. Most of the new approaches rely on protein engineering to place a residue or a sequence that provide reactive points at selected places.[316] The most widely used technique is the insertion of cysteines. Genentech recently showed that placing a cysteine at the right spot may induce higher *in vivo* stability and induce higher potency than hetereogeneous mixtures of more highly conjugated ADCs.[331] However, it has to be taken into account that this technique requires additional manufacturing steps because IgGs are generated as mixed disulfides in cell culture and they require partial reduction and reoxidation.

An alternative site-selective approach that has shown great potential is the introduction of a noncanonical or unnatural amino acid, such as *p*-acetylphenylalanine, *p*-azidomethylphenylalanine or selenocysteine for bioorthogonal ligation.[332,333] This technique was introduced by Peter G. Schultz and there are some recent examples that show good *in vitro* and *in vivo* antitumor activity, as well as favourable PK.[323]

Other strategies rely on enzyme-assisted ligation using peptide tags. The enzymes that have been used for this purpose are sortase, transglutaminase and formyl-

glycine-generating enzyme. The latter recognizes a CXPXR sequence and converts a cysteine residue to formylglycine,[334,335] which can react with nucleophiles. Transglutaminase does not recognize native glutamines but can form an amide bond between a primary amine and glutamines inserted recombinantly on strategic sites.[336,337] And sortase catalyzes hydrolysis of the threonine-glycine bond in a LPXTG motif to form a new amide between the *C*-terminus of threonine and an *N*-terminal glycine.[338,339] A similar strategy consists in applying expressed protein ligation, which makes use of intein fusion to modify the heavy-chain *C*-termini.[340]

Finally, the only fully chemical approach with theoretical broad application that allows the conjugation of peptides on localized sites on antibodies is the modification of *N*-termini through exchange of the *N*-terminal amine for a ketone.[341] Although the *N*-termini are near the paratope, some antibodies have been reported to remain functional.[342]

In this project we wanted to use commercial antibodies. Therefore, we excluded all the site-selective strategies relying on recombinant modifications. Regarding enzyme-based conjugations to antibodies, most of them have been published in the last 4 years, thus we could not contemplate them at the beginning of the thesis. Therefore, we decided to set up the *N*-terminal linkage as a site-specific approach together with the three major conjugation strategies that use only chemical means, i.e. modification of lysines, interchain cysteines and oligosaccharide chains. Our final goal was to obtain information about the transport across the BBB of a variety of conjugates; hence, we performed only optimized the most critical steps of the conjugations.

Conjugation to *N*-termini

Selective direct modification of the *N*-termini is theoretically possible taking advantage of the lower pKa of *N*-terminal amines with respect to lysine side chains (6.7-7.1 vs 9.3-9.5). However, in practice, this difference does not provide high selectivity and it is difficult to apply to large proteins like antibodies because the number of lysine residues is 20-fold higher than that of *N*-terminal amines. By contrast, inside cells, transformation of the α-amine into amino acids takes place very selectively in a process named transamination. This reaction consists in an amine transfer from amino acids to α-ketoglutarate catalyzed by transaminases. Inspired by this natural reaction Snell,[343] Cennamo[344] and Dixon[345] showed that the *N*-terminus of a peptide could be transformed into a reactive carbonyl group in a highly selective way using metal catalysts. More recently, Matthew B. Francis and collaborators optimized the reaction conditions to apply this reaction to proteins, using pyridoxal phosphate (PLP) as a nitrogen acceptor, which is the natural cofactor of transaminases (*Figure 44*).[346]

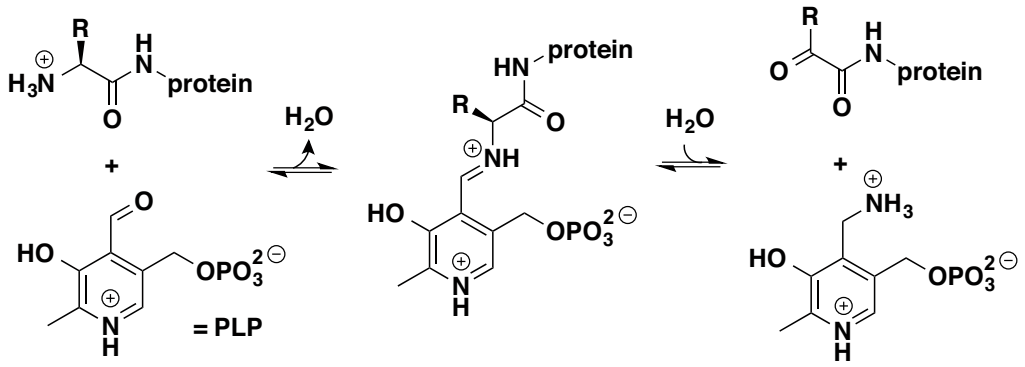

Figure 44. *Scheme of transamination mediated by PLP.*

Generating a reactive ketone group at the *N*-terminus of a peptide paves the way to nucleophilic addition. Although amines can be used for this purpose, they require a high pH to have a free electron pair and the resulting imine must be reduced because otherwise it is readily hydrolysed. Conversely, other nucleophiles such as hydrazines, hydrazides and oximes react at physiological pH or even under slightly acidic conditions due to their low pKa and do not require reduction.

Although hydrazine has been often used in protein conjugation to form hydrazone bonds, these are only stable for several hours under physiological conditions. In fact, withdrawal of the ADC Mylotrag® from the market was due to toxicity related to the instability of this linker.[347] Therefore, Francis and co-workers used alkoxyamine reagents to form oxime bonds, which are stable for several days at 37 ºC and pH 7.[348] Moreover, this ligation was already applied to antibodies without drastically perturbing their affinity.[342] Hence, we decided to start with this approach.

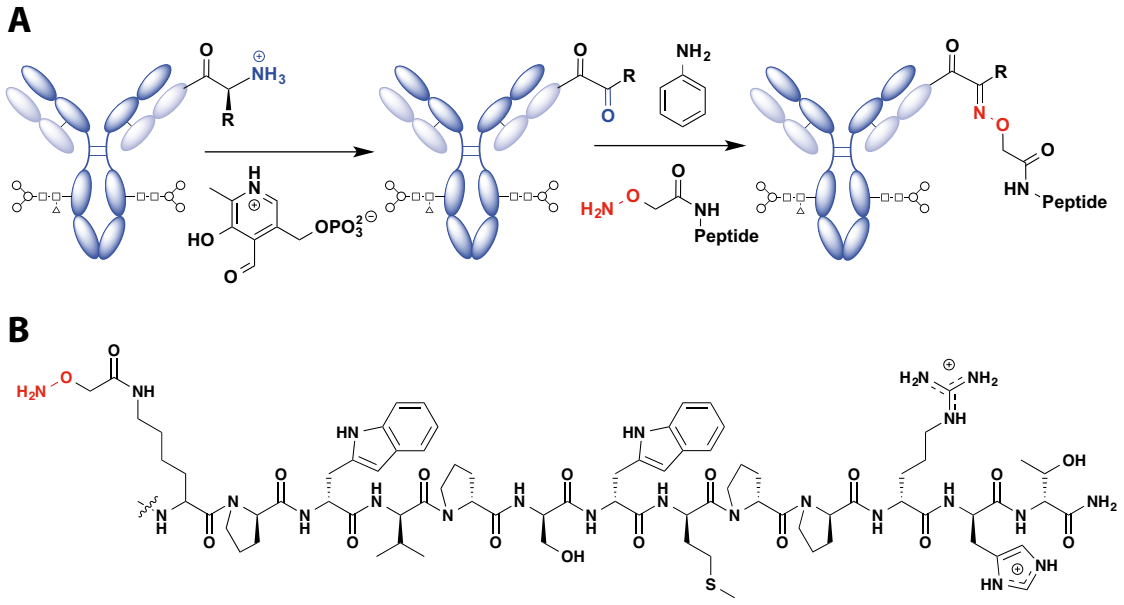

Figure 45. *Linkage of a peptide to an antibody through the N-termini. A) Scheme of the reaction. B) THRre with an alkoxyamine group incorporated through a lysine modified with aminooxiacetic acid; the N-terminus of this peptide was modified with glycine, CFluorescein or rhodamine B.*

Transamination is highly dependent on the *N*-terminal residue. Fortunately, Bv displays glutamates and aspartates, which had high conversions in the model peptides used by Francis and collaborators (*Figure 46*).

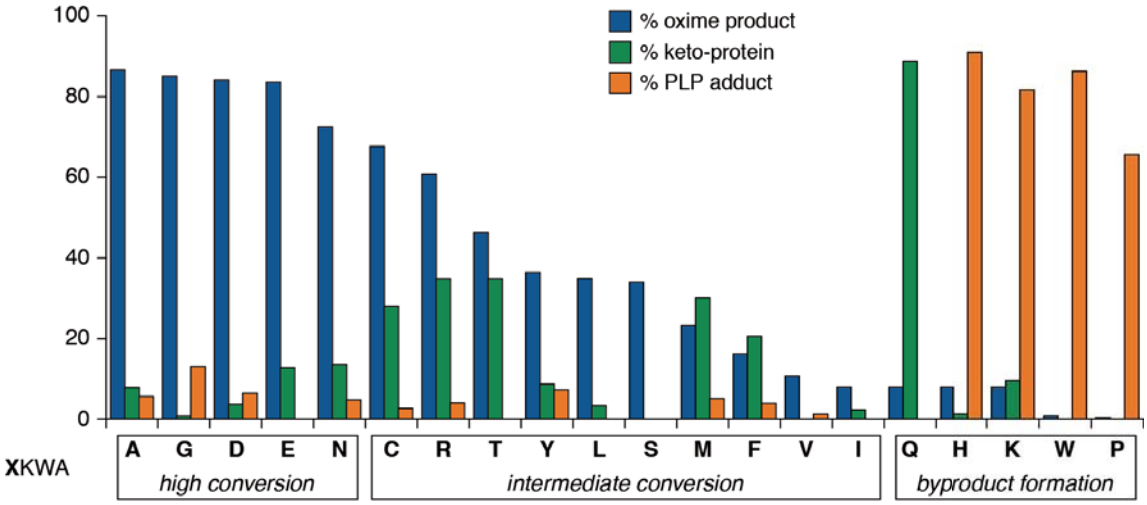

Figure 46. *Effect of the N-terminal amino acid on the reactivity toward PLP-mediated transamination. Studies were performed on tetrapeptide XKWA, where X is any of the twenty proteinogenic amino acids. The products include the benzyloxime product (blue), the non-conjugated transaminated species (green) and various species resulting from covalent PLP addition to the N-terminus (orange). (From Witus et al. 2010)*[341]

Before starting the conjugation, we estimated the distance between the antigen and the *N*-termini on a crystal structure of Bv Fab fragments bound to VEGF (*Figure 47*). The narrowest space between the *N*-terminal residues and the antigen was ≈ 0.9 nm. This value was slightly higher than the hydrodynamic radius estimated for THRre, 0.6 nm, which indicated that the shuttle might not affect the antibody-antigen interaction. The peptide radius was calculated using a general relationship for proteins with no shape restriction (r, nm = $0.24 \cdot N^{0.392}$, where N is number of residues).[349,350]

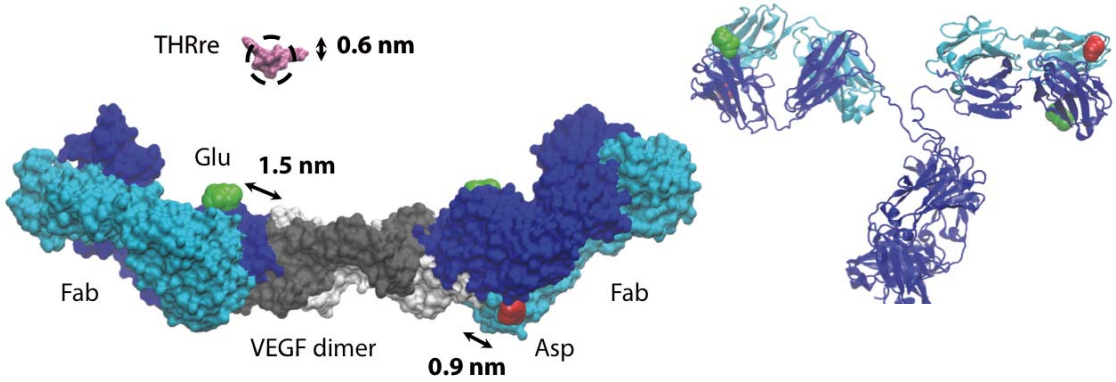

Figure 47. *(Top left) Structure of THRre obtained uisng the PEP-FOLD server. (Bottom left) Crystal structure (PDB: 1BJ1) of two Fab fragments of Bv binding VEGF, which is an antiparallel homodimer linked by two disulfide bonds. N-terminal glutamate (heavy chain) and asparatate (light chain) residues are depicted in green and red respectively. Distances from the N-terminal residues of Bv and the nearest residues from VEGF are shown. (Right) Crystal structure of an IgG (PDB: 1IGT).*

Alcohols may react with pyridoxal phosphate to form acetals and should be avoided in this reaction.[341] Therefore, we purified Bv because the commercial formulation contains trehalose as an excipient (175 mM, 1000 equivalents with respect to IgG). We first tried size exclusion chromatography using PD-10 (Sephadex® G-25) columns, which did not provide enough resolution (*Figure 48*). Conversely, we determined that 5-6 centrifugal filtration-washing steps left a concentration of trehalose similar to that of the antibody. This amount was not likely to interfere in the reaction because of the high excess of pyridoxal phosphate used (approximately 10000 equivalents with respect to the IgG).

With the purified Bv in hand, we assayed the transamination reaction followed by the coupling of the peptide under the conditions described by Scheck and Francis.[342] As an analytical tool to study the progress of the reaction we initially used MALDI-TOF MS. Although low resolution is obtained at this high mass range, this technique was easily accessible and has been used to assess modification of ADCs.[351] α-cyano-4-hydroxycinnamic acid (ACH) matrix provided the best compromise in terms of resolution between the whole antibody and the reduced chains, whereas 2,5-dihydroxybenzoic acid (DHB) matrix showed slightly higher resolution only for the light chain.

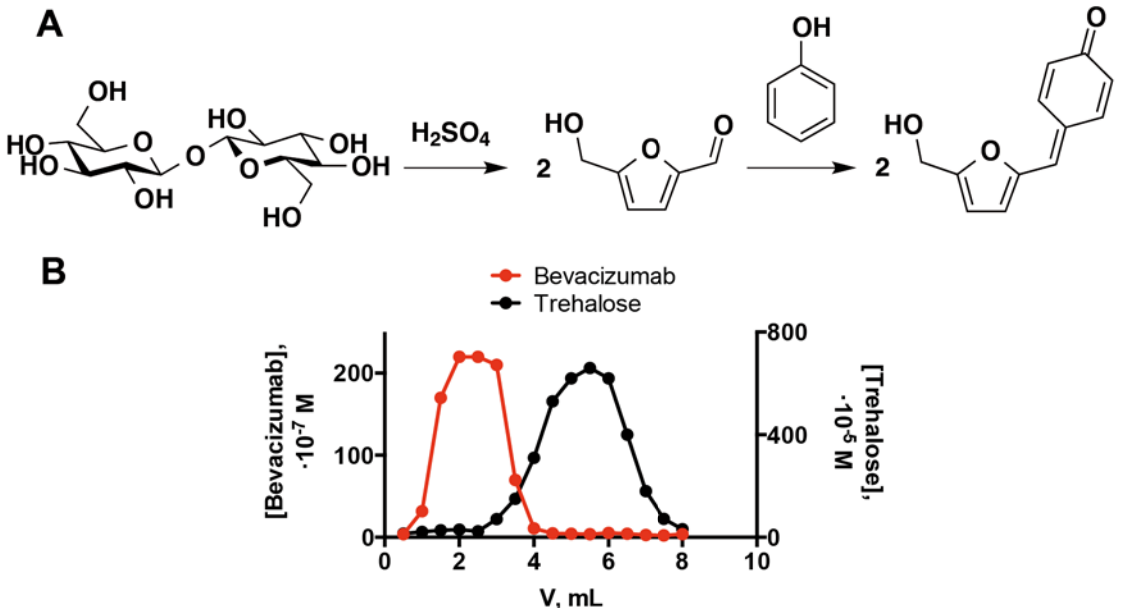

Figure 48. *Separation and quantification of trehalose contained in commercial Bv A) Proposed mechanism for trehaolse reaction with phenol in sulfuric acid based on the one described for 2-methyl-1-naphthol and rhamnose B) Elution from a NAP-5 column providing insuficient resolution.*[352]

In the first reaction attempt we did not see any mass shift in the mass spectrum. Thus, we explored a set of conditions for the transamination, combining two temperatures (37ºC and 55ºC) with two concentrations of PLP (10 and 100 mM) and two concentrations of peptide (0.5 and 2 mM). In all cases the antibody concentration was kept below 130 μM to prevent aggregation but as high as possible

in order to maximize effective collisions between the reactants and the macromolecule, which has a very slow motion. Unfortunately, none of the assayed conditions yielded a significant alteration of the MALDI-TOF spectrum. Hence, we decided to use a smaller protein to optimize the reaction.

As a test protein we selected myoglobin, which was the one used by Francis and collaborators to show the applicability of this approach.[346] Myoglobin is affordable and has a glycine at the *N*-terminus, which yields an aldehyde upon transamination instead of the less reactive ketone obtained with other residues. Moreover, the relatively low molecular weight of this protein (17 kDa) makes it easy to be analysed by MALDI-TOF-MS and LC-MS.

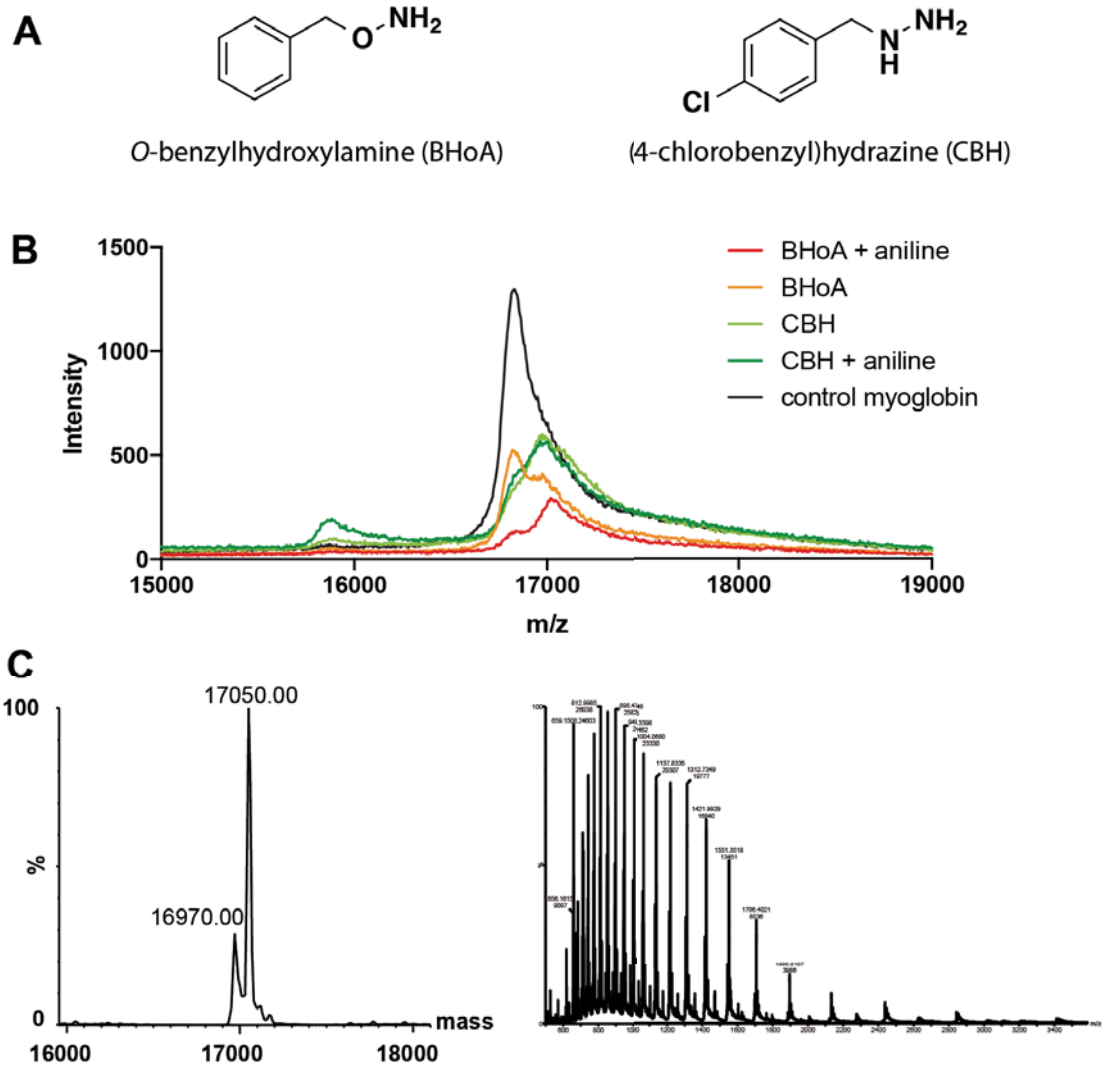

Figure 49. *Conjugation of small molecules to myoglobin N-terminus A) Structures of benzylhydrazine and O-benzylhydroxylamine B) MALDI-TOF MS of myoglobin (My) coupled to BHoA C) LC-MS spectra of My linked to BHoA.*

Initially, we conjugated chlorobenzylhydrazyde (CBH), a small hydrazide-containing molecule, to the transaminated protein. After 8 h, using 1 mM of CBH in phosphate buffer pH 6.5, we observed a high degree of conversion (*Figure 49*). By

contrast, when we tried *O*-benzylhydroxylamine (BHoA), a small alkoxyamine, under the same conditions the reaction did not take place even after 24 h. Thus, we added 1 mM aniline, which has been described to be an excellent nucleophyllic catalyst for this reaction by Dawson *et al.*[353] Thereby we could se an 82 % conversion after 24 h, as estimated by LC-MS assuming the incorporation of this small molecule did not affect ionization of the protein.

Once the reaction conditions were set up with small molecules, we conjugated THRre with an alkoxyamine group at the *C*-terminus using the same conditions that had worked for the *O*-benzylhydroxylamine. The extent of the conjugation for the peptide was very similar to the one obtained for the small molecule, 83 %. This conversion was quantified, after thorough purification, by Edman sequencing (*Figure 50*) in the Proteomics unit at the Barcelona Science Park in order to have a more accurate value than using MS.

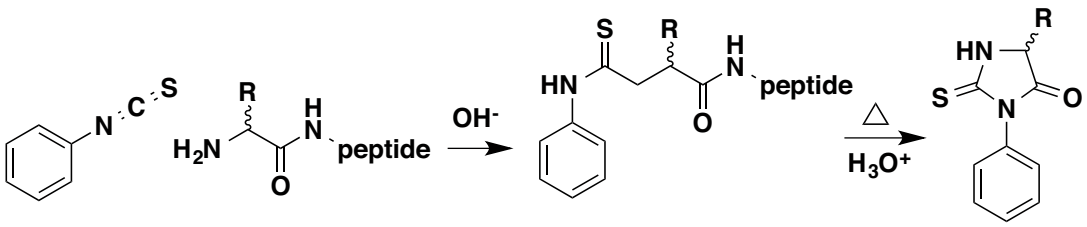

Figure 50. *Scheme of Edman sequencing.*

Taking into account the important effect of aniline on the reaction, we tested the conjugation on Bv. After many attempts to use MALDI-TOF to study the linkage of small molecules and peptides, we reached the conclusion that the instrument we were using did not provide enough resolution to clearly detect the expected shifts in m/z. Apparent increases in mass were often due to a lower antibody concentration, a change of buffer or the presence of residual reagents. Aiming to enhance resolution, we deglycosylated Bv with PNGase. Although the decrease in m/z (≈ 3100 amu) was close to the molecular weight of oligosaccharide chains (≈ 2400 amu), we observed no improvement in resolution (*Figure 51*).

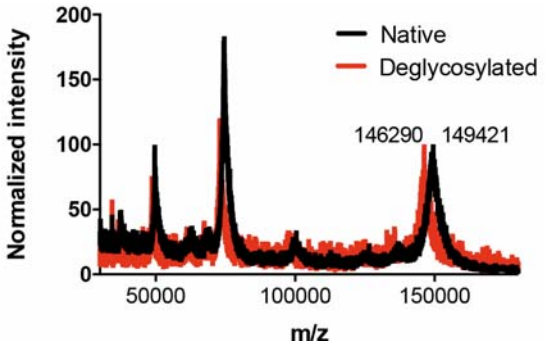

Figure 51. *MALDI-TOF spectra of intact (blue) and deglycosylated (red) Bv.*

As soon as we realized that we were not able to obtain reliable data using MALDI-TOF, we started analysing our constructs by SDS-PAGE systematically. Because

resolution was also limited in this technique, especially for the heavy chain, we initially used fluorescent labelling to increase the molecular weight of peptides and to distinguish the modified chains from the unmodified ones. We prepared both rhodamine B and CFluorescein THRre derivatives. However, rhodamineB-labelled peptides caused aggregation and partial precipitation of the antibody, probably because of their higher hydrophobicity. Moreover, the signal was very week for this fluorophore because the available gel readers lacked appropriate excitation filters. Hence, we used mainly the peptides labelled with CFluorescein.

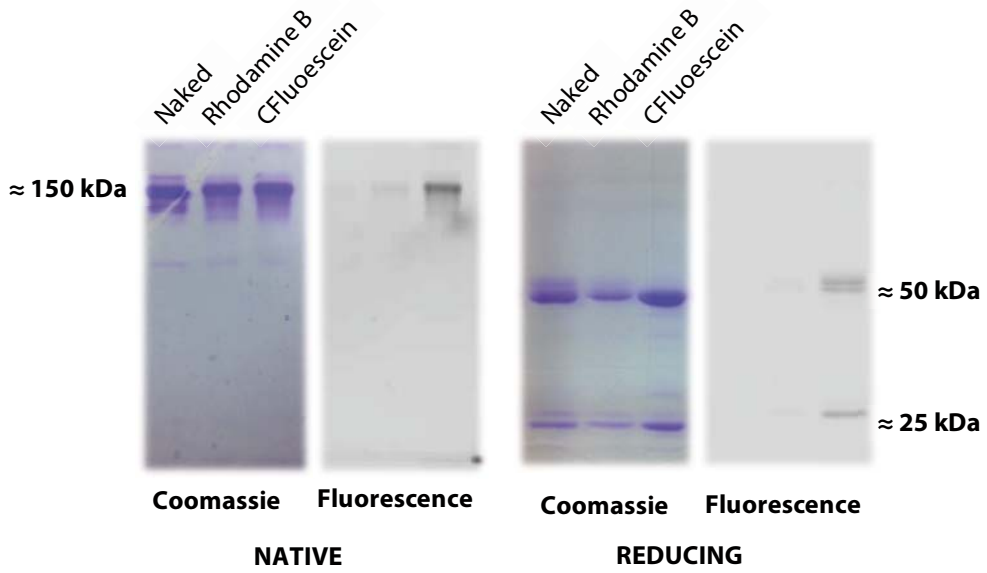

Figure 52. *N-terminal conjugation of fluorescently labelled peptides. Gel electrophoresis of native and fully reduced conjugates.*

Using labelled peptides we observed that some degree of transamination took place in 48-72 h at 37 ºC and 10 mM PLP, which was remarkably longer than the time suggested by Francis. We increase ten-fold the concentration of PLP. However, this resulted into covalent binding of the cofactor to the antibody, which turned yellow. Regarding the conjugation step, it was faster but also required 12-24 h at RT, as previously reported,[341] using 67 μM Bv, 1 mM peptide and 10 mM aniline.

Table 3. *N-terminal modification of Bv with CFluorescein and rhodamine B derivatives of alkoxyamine-THRre.*

	CFluorescein	Rhodamine B
heavy chain modification, %	40	28
light chain modification, %	24	21
peptides/antibody	1.3	0.7

Densitometric analysis of the SDS-PAGE gel stained with coomassie brilliant blue (*Figure 52*) showed that the conjugation of the CFluorescein-labelled peptide was more efficient than the reaction with the rhodamineB-peptide (*Table 3*); the difference was probably due to the aggregation caused by the latter. Although both

N-termini were expected to have a similar reactivity, the glutamate in the heavy chain reacted to a higher extent than the aspartate on the light one. The different reactivity could be due to the lower steric hindrance of the first considering their position in the crystal structure (*Figure 47*).

After this first successful reaction, we linked the unlabelled THRre. Although resolution was lower because of its reduced molecular weight, we could estimate an approximate peptide/antibody ratio (PAR) equal to 1. This value is probably more reliable than the 0.4 obtained by mass spectrometry, which can be affected by a poorer ionization of the conjugate because of the higher hydrophobicity induced by the peptide (*Figure 53*).

The distinct PARs of the naked peptide with respect to the labelled versions can be attributed partly to the different position of the alkoxyamine group. The reactive moiety was at the *N*-terminus in the label-free version instead of the *C*-terminus as in the CFluorescein and rhodamine B peptides. We switched the position, firstly, in order to facilitate the synthesis of the peptides with other functional groups and, secondly, because of the low yield obtained in synthesis of the *C*-terminal aminnooxy peptides. For the preparation of the labelled derivatives we used NovaTag hydroxylamine resin, which, in our hands, provided final yields below 1 %. Conversely, incorporation of the functional group at the *N*-terminus using a lysine with an aminooxyacetic acid moiety linked to the side-chain provided an amount of peptide 10-fold larger.

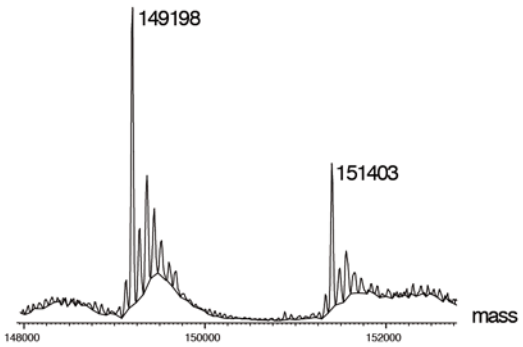

Figure 53. *Mass spectrum of Bv conjugated to the non-labelled alkoxyamino-(CFluorescien)THRre. Expected mass of the conjugate with one peptide is 151247.*

The promising results obtained with Bv encouraged us to apply the reaction to Cx. However, the conjugation to this antibody was considerably less efficient, as the PAR we estimated by densitometry analysis was lower than 0.3. The poor conversion can be explained by the presence of glutamine at the *N*-termini of the heavy chains, which yields a less reactive ketone upon transamination.[341] Because we were already using very long reaction times, high reagent concentrations and relatively high temperature, this result led us to focus our efforts on the other conjugation strategies.

Conjugation to oligosaccharide chains

The glycosylation of antibodies is a heterogeneous post-translational modification. Thus, a variety of *N*-linked biantennary complex glycan structures can be found on serum-derived IgGs. The core heptasaccharide containing *N*-acetylglucosamine (GlcNAc) and mannose can be modified with fucose and GlcNac, while the antennae may contain galactose and sialic acid. All these glycans have vicinal diols that can be oxidatively cleaved with periodate to generate aldehydes, which may in turn be modified with nucleophilic reagents. This method was pioneered by O'Shannesy and coworkers in 1984, thus aldehydes are considered the first bioorthogonal functional groups.[323] Since then, many authors have shown that the oxidized and conjugated antibodies did not have decreased affinity compared to unconjugated antibodies. However, heterogeneous populations of conjugates are obtained and oxidation of methionine residues by such procedure has been reported.

Recently, Neri and coworkers showed that this reaction could be performed in milder conditions and provide a certain degree of site-selectivity taking advantage of the singularity of fucose.[354] This monosaccharide is present in the glycan chains of most antibody molecules expressed in CHO cells and this cell-line is used to produce many therapeutic antibodies such as Bv. Fucose has a *cys*-glycol, which readily forms a reactive intermediate with periodate that generates a carboxylic acid and an aldehyde (*Figure 54*). The reaction is selective when a low periodate concentration is applied at reduced temperature and pH. In order to get familiarized with this reaction and mainly learn about antibody handling, I performed a one-week stay in Prof. Dario Neri's laboratory at the beginning of my thesis.

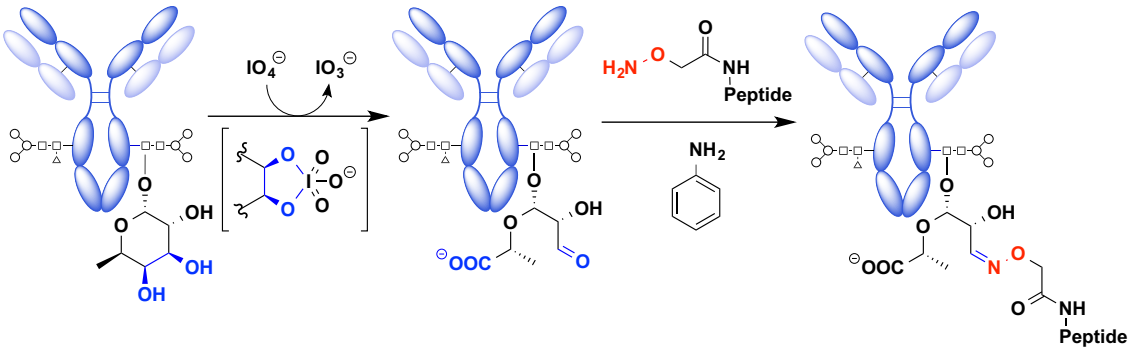

Figure 54. *Selective oxidation of fucose using sodium periodate and conjugation of the generated aldehyde.*

Attracted by the selectivity of Neri's approach, we applied this reaction to link THRre and Angiopep-2 to Bv. Although we obtained a mixture of conjugates, in both cases the most abundant species was indeed an IgG with 2 peptides. Curiously in the case of THRre the peaks in the deconvoluted mass spectrum were distributed in a bell shape, while for Angipep-2 there was no appreciable amount of IgG without a peptide or with a single incorporation (*Figure 55*). Because Angiopep-2 is 800 amu

larger than THRre, the conjugation in this case was also clearly appreciated by gel electrophoresis. Densitometry analysis confirmed that the most abundant species for Bv with Angiopep-2 was the one with a single peptide in each heavy chain.

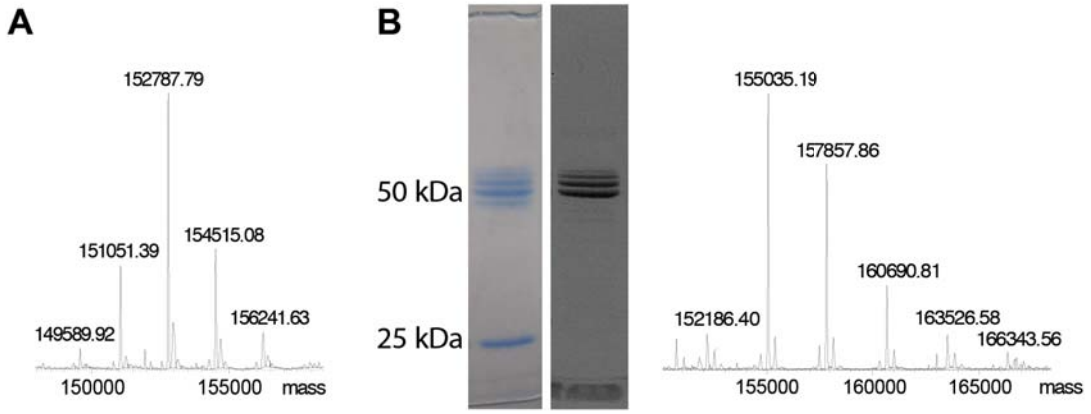

Figure 55. *Characterization of Bv conjugation through the glycans. A) Mass spectrum of the CFluorescein-THRre conjugate. B) SDS-PAGE with coomassie staining (left), fluorescence visualization (right) and mass spectrum of the CFluorescein-Angiopep-2 conjugate.*

Although this technique produced satisfactory Bv conjugates and proved to be robust, we decided not to apply it to Cx for two reasons. The first one is the growing concern of the modification of IgG Fc polysaccharides on effector functions.[355] This alteration might be due to the presence of the peptide or a side-reaction of the oxidation. A very recent example of the latter is the study by Zhou and co-workers.[356] These authors enzymatically incorporated sialic acid, which is the monosaccharide with the most accessible glycol, into an IgG and linked to it 1.3-1.9 peptides per antibody using periodate oxidation. Although the reaction conditions were extremely mild, two methionines were also oxidized, which led to o a lower affinity of the ADC for the neonanatal receptor (FcRn) and a shorter half-live *in vivo*. The second reason why we did not apply the oligosaccharide modification to Cx was because of the complex glycosylation pattern of this antibody, which has two additional glycosylation sites in each chain, other than Asn299, located near the paratope (Asn88 and Asn41).[357]

Conjugation to interchain cisteines

Modification of interchain disulfides is among the most widely used techniques to obtain ADCs because it is robust and ensures a distant position with respect to the paratopes. Although, this modification has been reported not to alter stability, antibodies with more than 4 drugs linked to interchain disulfide bond undergo more rapid clearance and have higher toxicity.[324] Although BBB-shuttles are more hydrophilic than drugs used in ADCs, we decided to use the most standard average payload/IgG ratio, namely 3-4.

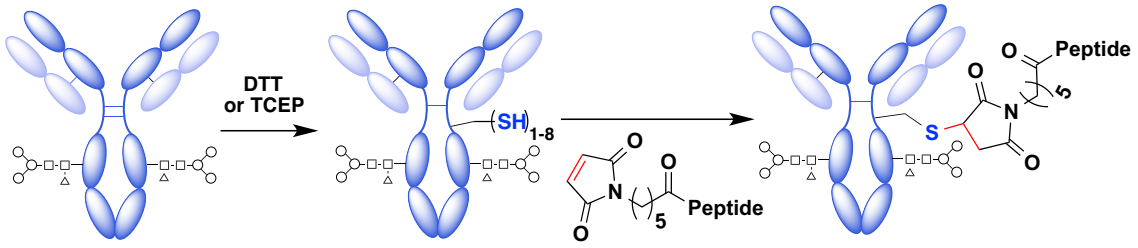

Figure 56. *BBB-shuttle conjugation through partial reduction of interchain disulfides.*

Two main reducing agents have been described to perform the partial reduction in ADCs, DTT and TCEP. Although TCEP is a milder reductant and does not require purification before conjugation to the peptide, in our hands the reaction with DTT was more robust. We explored different ratios of DTT and found that 3 equivalents, which could reduce up to 3 disulfide bridges, effectively provided 3.5 thiols per IgG (*Table 4*). The amount of thiols was quantified using Ellman's reagent. We also attempted to fully reduce the antibody and then partially reoxidize it as the disulfides that link the light to the heavy chains have been reported to reform first, which should lead to a more homogeneous product.[325] However, in our hands this procedure generated a higher and less reproducible amount of free thiols.

Table 4. *Free thiol groups generated upon reduction with DTT and TCEP.*

Reducing agent/eq.	equivalents	Free SH
TCEP	4	4.2
DTT	3	3.5
DTT	3.7	4.9
DTT	6.5	5.9
DTT (+ reoxidation)	150	20

After partial reduction, we conjugated Bv and Cx to THRre and Angipep-2 to Bv and Cx. We estimated a PAR of 3.5-4 for both antibodies from the reducing SDS-PAGE. Focussing on the analysis of Bv (*Figure 57*), for the two shuttles we detected 0 to 3 molecules on heavy chain, with an average of 1.4. Regarding the light chain, we observed two bands corresponding to 0 and 1 peptide, with a mean value of 0.4 for THRre and 0.6 for Angipep-2. A different batch of conjugates was analysed by non-reducing SDS-PAGE, which showed that all six covalent fragments with different molecular weight that could be generated upon partial reduction were present in the mixture. However, resolution of the gel only allowed to show that some of them had been modified with the peptides.

The high degree of conjugation to the light chain was also detected by MALDI-TOF MS (*Figure 57*). In addition, we confirmed the presence of a covalent fragment corresponding to the half-antibody containing two peptides by LC-MS using water/acetonitrile as a denaturing eluent. At this point we decided to forego the use

of unlabelled peptides for characterization because they did not provide any additional information.

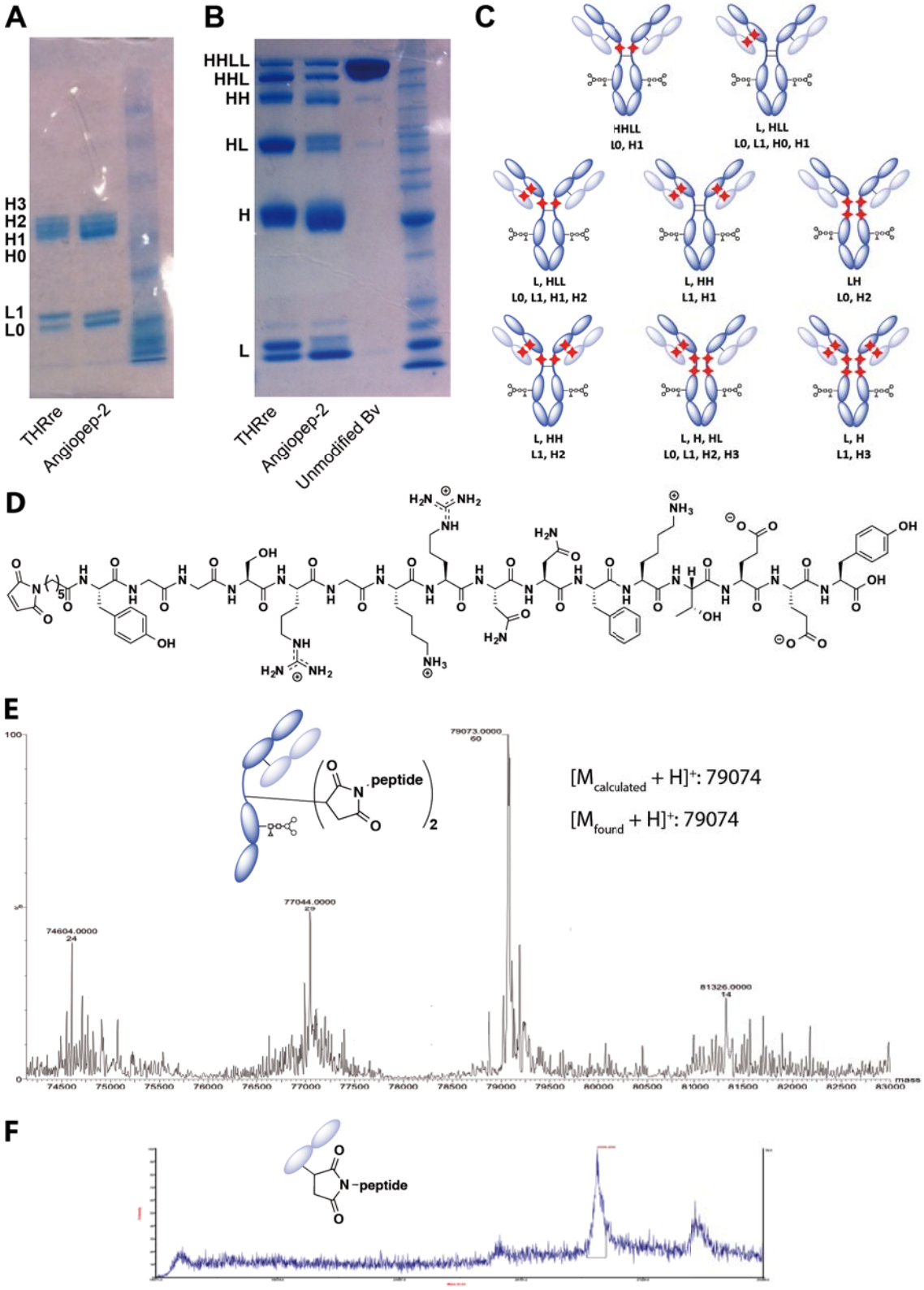

Figure 57. *Chracterization of Bv conjugated through cysteines. SDS-PAGE: A) after full reduction B) without adding DTT C) Potential species generated after partial reduction. (From Sun et al. 2005)*[325] *D-F) Characterization of Angiopep-2 conjugate. D) Structure of the peptide. E) LC-ESI-TOF MS spectrum F) MALDI-TOF MS spectrum of the light chain.*

We attempted without success to separate the species that we observed in the non-reducing SDS-PAGE through a variety of techniques that have been applied to characterize ADCs.[325,358] However, it is important to highlight that BBB-shuttle peptides are remarkably less hydrophobic than drugs used in ADCs, which severely affect the physicochemical properties on which some separation techniques rely.

In reversed-phase HPLC, using a large-pore column for proteins, we could partly resolve the naked light chain from the one conjugated to one molecule of THRre or ApoE(159-167)$_2$. The higher hydrophobicity of the former with respect to the light chain resulted into an increase in retention time (t_R), whereas the highly polar ApoE peptide decreased the t_R (*Figure 58*). By contrast, none of the shuttles exerted a significant effect on the elution of the heavy chain. We also tried hydrophobic interaction-HPLC (HIC), which is based on the interaction of the folded protein with a solid support functionalized to a low extent with a hydrophobic group, such as phenyl; in this technique, the elution is performed with an aqueous buffer, for instance ammonium sulfate, the concentration of which is decreased over time. Unfortunately, the BBB-shuttles did not provide a change in hydrophobicity large enough to resolve the different species. Finally, we attempted the separation by capillary electrophoresis, which relies on the same principle as SDS-PAGE but is used for a more accurate quantification. In this case, although the peaks of commercial standards were as sharp as expected, the species coming from Cx conjugation were not well resolved (*Figure 58*).

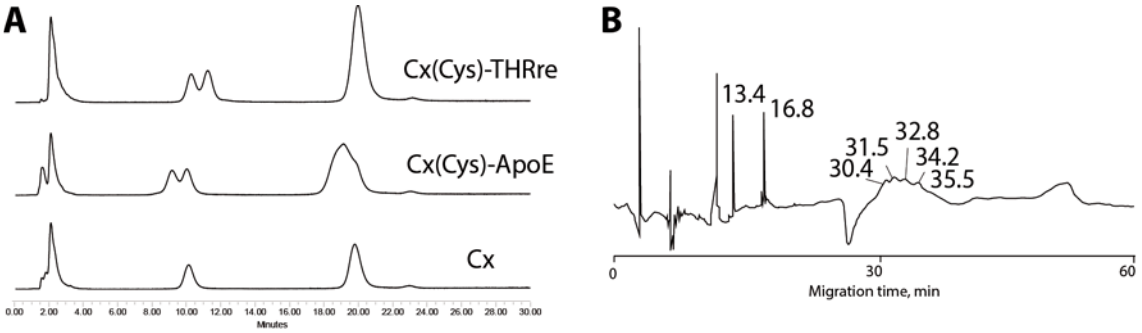

Figure 58. *Alternative techniques used to attempt antibody characterization. A) Reverse-phase HPLC of Cx and two conjugates modified through the cysteines. The light chain elutes at 10 min and the heavy chain at 20 min. B) Capillary electrophoresis trace of Cx with THRre linked to the cysteines. Migration times are given in minutes.*

FPLC using different size-exclusion columns was also insufficient to separate the conjugated species. However, this technique confirmed that the integrity of the antibody is preserved (in PBS) upon partial reduction and conjugation (*Figure 59*). Conversely, when the antibody was fully reduced, the elution volume of the heavy chain was slightly shifted with respect to the whole antibody and the light chain could be clearly resolved.

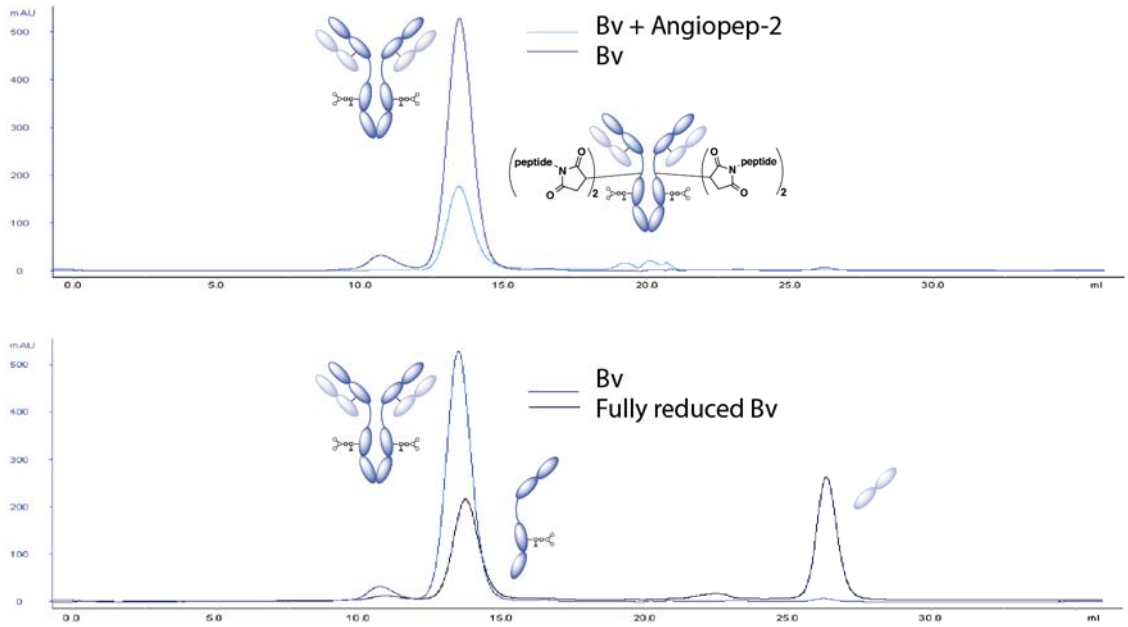

Figure 59. *FPLC chromatograms of Bv conjugated to Angiopep-2 and fully reduced Bv acquired using a Superdex 200 10/30 column and phosphate buffer 50 mM pH with 150 mM NaCl.*

Despite the difficulty in characterizing the species present in the crude, the partial reduction approach was the only one that allowed a robust and relatively site-selective modification of Cx. Therefore, we decided to apply this method to prepare the library of Cx-BBB-shuttle conjugates.

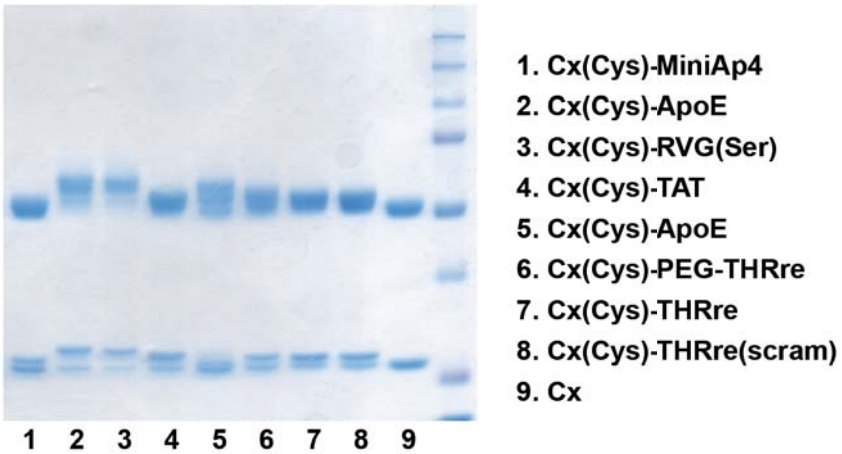

Figure 60. *SDS-PAGE with Cx conjugates prepared by partial reduction (Cx(Cys)) in addition to the one with Angiopep-2.*

After setting up the reaction with THRre and Angiopep-2, we prepared the Cx conjugates with MiniAp-4, TAT and ApoE. However, RVG contains a cysteine and, therefore, we had to change this residue to prevent cyclization; in the new peptide, RVG(Ser), we replaced the cysteine by a serine as it had been done in Angiopep-2. We also linked Cx to THRre scrambled and PEG-THRre (*Figure 60*). For most conjugates we could detect the light chain and the covalently-linked half-IgG with one and two peptides, respectively, by LC-MS (*Table 7* in *Product characterization*).

After preparing the library, we aimed to set up the conjugation on lysines in order to compare the efficiency of BBB-shuttles having higher availability for their receptor. In addition, we would also use alkyne-azide cycloaddition on derivatized lysines to conjugate cysteine-bearing peptides such as RVG and MiniAp-1 avoiding other thiols and maleimide.

Conjugation to lysines: thiol-maleimide and CuAAC

Several strategies have been applied to modify the ε amine of lysines on antibodies. The most direct one is the formation of an amide bond under basic conditions using an *N*-hydroxysuccinimide-ester-activated payload; this strategy was used to generate the ADC Mylotrag®.[315] However, activated esters are readily hydrolyzed in water and thus a large excess is required. This is why lysines are often derivatized with more reactive and unexpensive linkers that allow incorporating the valuable molecule more efficiently. The most common reaction used to link the payload after derivatization of the antibody is the thiol-maleimide Michael addition.

In the ADC Kadcyla®, lysines are first functionalized with a heterobifunctional spacer bearing an activated ester and a maleimide; the former is directly coupled to lysines whereas the latter is then reacted with a thiol-bearing drug. However, if a high concentration of load is used, dimerization of the drug by disulfide formation may occur. Conversely, if the IgG is derivatized with the thiol, it is less likely to interact with other antibodies because of their slow motion and low concentration. Hence, this approach is also very common in antibody modification and is the one we selected to conjugate our peptide shuttles.

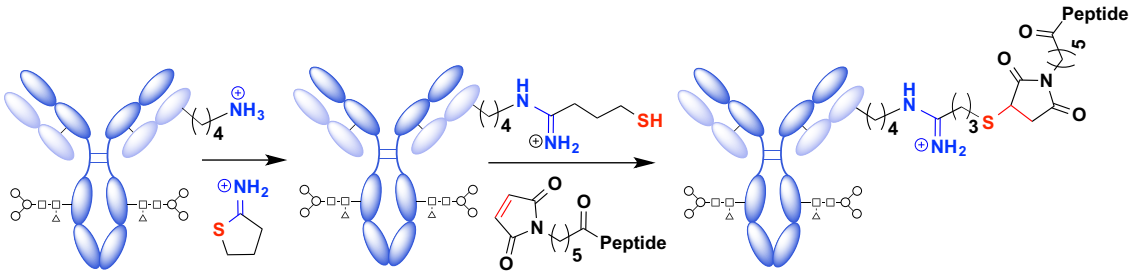

Figure 61. *BBB-shuttle conjugation through partial reduction of the antibody.*

Two main reagents have been used to incorporate thiols on lysines for protein modification:[359] *N*-succinimidyl-*S*-acetyl thioacetate (SATA) and 2-iminothiolane (Traut's reagent). The former has the advantage of providing a stable intermediate but the disadvantage of requiring an additional step to deprotect the thiol, which is in the form of thioacetate. Derivatization with small molecules and thiol-maleimide reactions are fast (< 2 h) and usually there is no need to store the functionalized antibody. In addition, purification of intermediate is using gel filtration is also straightforward. Furthermore, 2-iminothiolane has the additional advantage of

preserving the positive charge of lysine on the imidamide bond formed. For these reasons, we chose Traut's reagent instead of SATA.

In order to set up the reaction, we explored a series of antibody/2-iminothiolane/peptide ratios. We determined that using more than 50 eq of linker and 25 eq of peptide not only did not provide further conjugation (*Figure 62*) but also caused aggregation and precipitation.

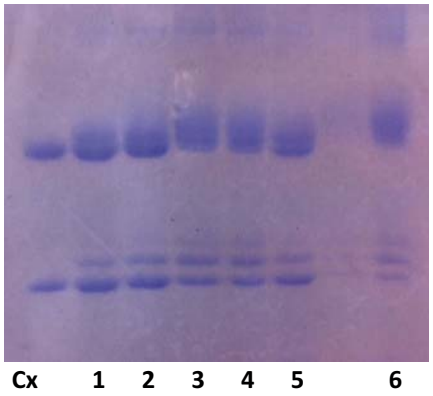

Entry	2-iminothiolane, eq	peptide, eq
1	20	15
2	20	20
3	**50**	**25**
4	50	50
5	80	40
6	80	80

Figure 62. *Optimization of reagent ratio for lysine modification of Cx.*

Although resolution for the heavy chain in the gel was limited (*Figure 63*), a PAR of 6-8 could be estimated in the case of Angipep-2 linked to Bv. It was clearly visible that the light chain had from 0 to 3 peptide molecules with an average of 1 and the heavy chain appeared to have 0 to 5-6 with an average of 2-3. For THRre the resolution was poorer and the PAR appeared to be slightly lower, between 4 and 7. Similar results were obtained for Cx, though lower resolution was obtained probably because the glycan content was higher and more heterogeneous.

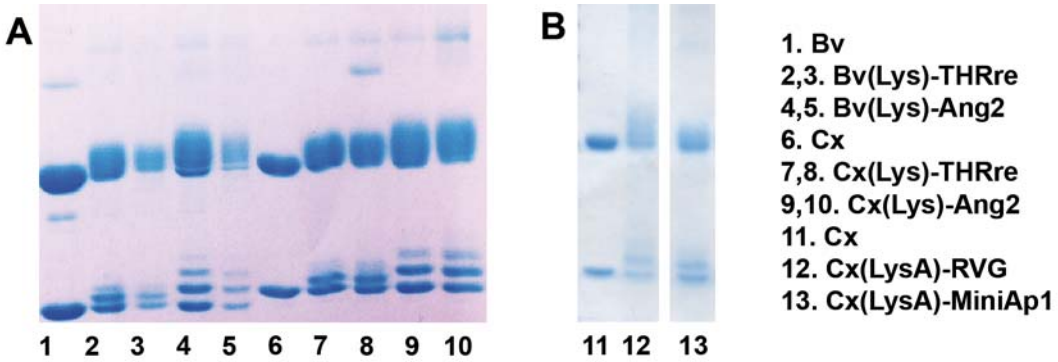

Figure 63. *SDS-PAGE of BBB-shuttles conjugates on antibody lysines A) Bv and Cx conjugates with THRre and Angiopep-2. B) Conjugates prepared using CuAAC. Conjugation through lysines is abbreviated as (Lys) when using 2-iminothiolane and as (LysA) when CuAAC was applied.*

For the peptides that contained cysteines, we performed the ligation using CuAAC (*Figure 64*). Imidazole-1-sulfonyl azide hdyrochloride (ISA·HCl) was used to transfer the azide functionality on antibody lysines. The water-soluble tris-(3-

hdyroxypropyltriazolylmenthyl)amine (THPTA) ligand was used to stabilize Cu^{+} coming from the *in situ* reduction of Cu^{2+} by sodium ascorbate.

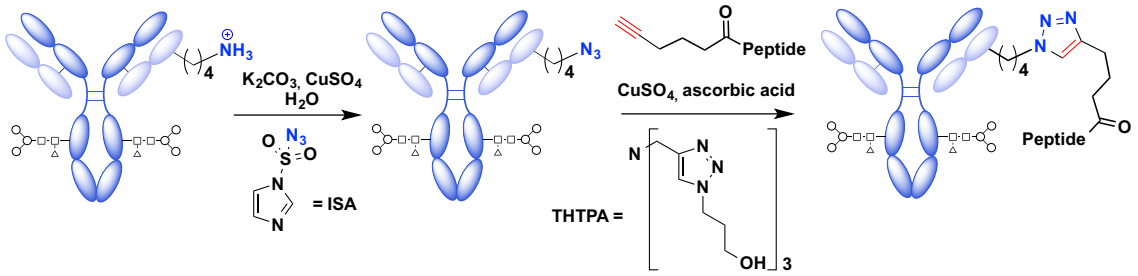

Figure 64. *Conjugation of peptides using CuAAC.*

Overview on the conjugation techniques that have been set up

To summarize, we have successfully set up 4 methods to link BBB-shuttle peptides to Bv. However, modification of *N*-termini could not be efficiently applied to Cx because of the low reactivity of terminal glutamines on the light chain. Glycan modification was also not used on Cx because of its complex glycosylation pattern and because of the risk to interfere in antibody effector functions.

For the modification of Cx and the generation of the BBB-shuttle conjugate library we applied thiol-maleimide chemistry to link the shuttles to interchain cysteines. Only those peptides bearing a cysteine that could react with the maleimide, were conjugated using CuAAC on antibody lysines. Maleimide-THRre was also linked to the lysines derivatized with 2-iminiothiolane in order to compare the effect of the location on the BBB-shuttle efficiency.

Table 5. *Summary of conjugations set up with THRre and Angiopep-2.*

		THRre		Angiopep-2	
Conjugation site	**Abbreviation**	**Bv**	**Cx**	**Bv**	**Cx**
N-termini	(Nterm)	1	0.3	-	-
Glycan	(Glyc)	2	-	2	-
Int. cysteines	(Cys)	4	3-4	4	3-4
Lysines (2-iminoth.)	(Lys)	4-7	4-7	6-8	6-8

Thiol-maleimide bond serum stability assessment

Although the thioether bond formed through thiol-maleimide ligation is stable *in vitro*, scientists from Genentech have recently shown that thiol exchange may occur *in vivo* under certain conditions (*Figure 65*).[298] Albumin, free cysteine and glutathione present in blood may displace the molecule linked to the maleimide at exposed sites in less than 24 h. By contrast, less exposed conjugates may remain almost intact for over 96 h in circulation. Full protection from thiol exchange was observed when the maleimide was hydrolysed in a region with net positive charge.

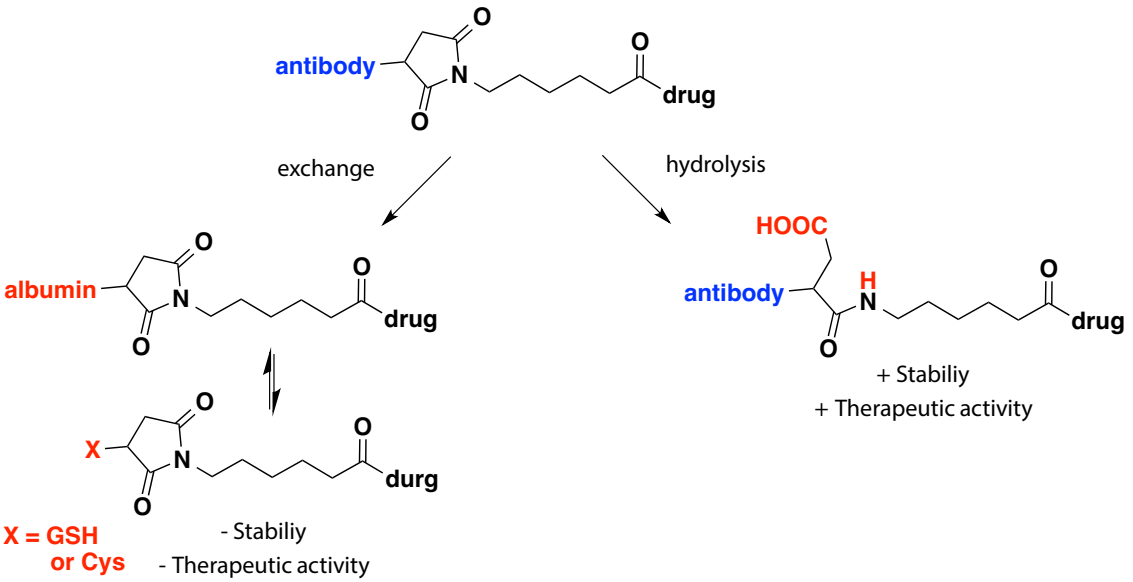

Figure 65. *Stability of thioether bond depending on the environment of the maleimide linker. (Modified from Shen et al. 2012)*[298]

Before exploring the stability of thiol-maleimide conjugates obtained from cysteine and lysine modification, we verified that the thiol in albumin could react with the maleimide linked to the peptides. For this purpose, we incubated THRre and Angiopep-2 labelled using CFluorescein with human serum albumin for 2 h at 37 ºC. In this experiment we verified that a protein-peptide conjugate was formed.

Then, we incubated the antibody-peptide conjugates in serum for 24 h. Although we used fluorescently labelled peptides to produce the conjugates for this study, fluorescence was completely masked in SDS-PAGE by the high amount of albumin present in the serum. Therefore, we resorted to magnetic beads coated with protein A to isolate the antibodies and monitor their stability. After 24 h, the intensity of the labelled chains had not visibly decreased, neither the one modified through cysteines nor the one conjugated through lysines (*Figure 66*). Therefore, we concluded that the tioether that bound the peptide to the antibody was stable in this time-scale.

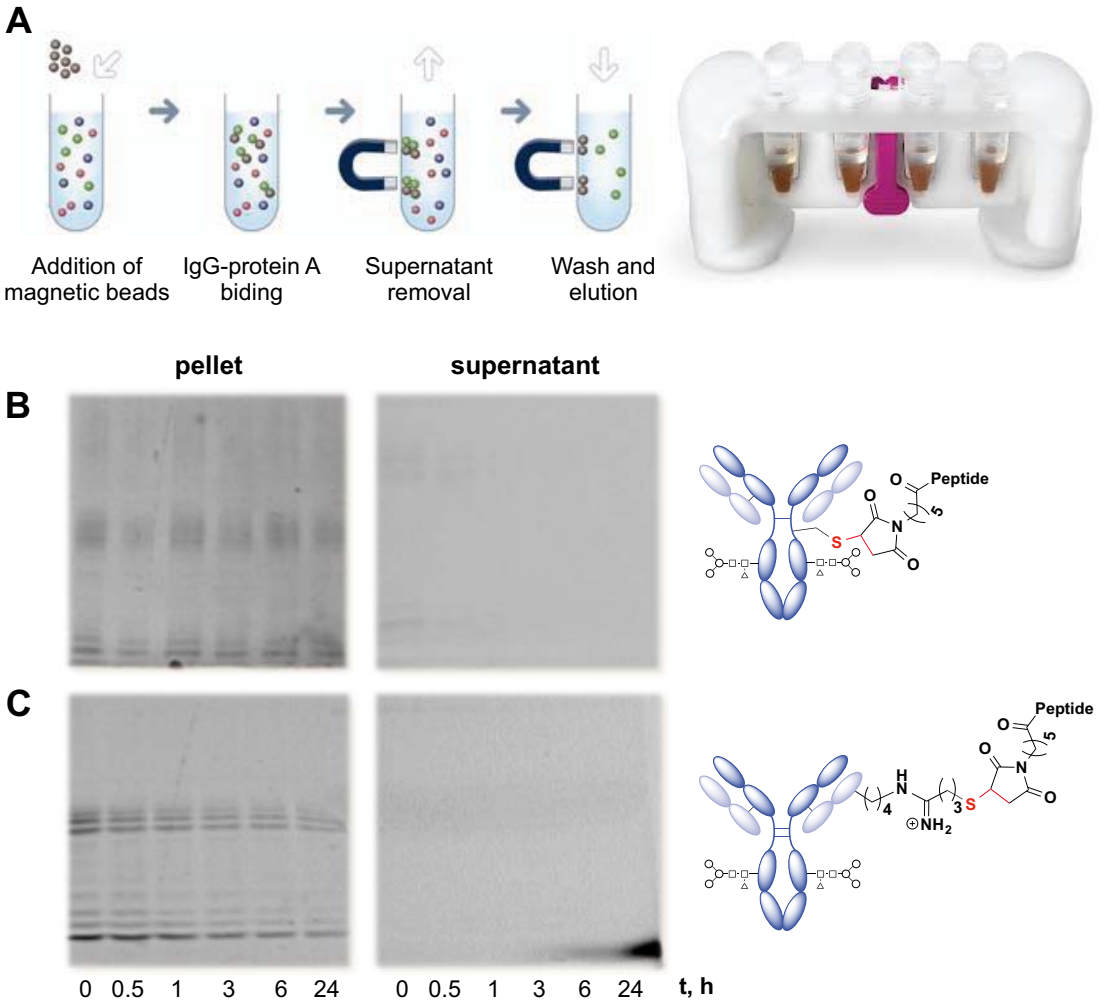

Figure 66. *Thioether bond stability assessment A) Scheme of the purification process. B) SDS-PAGE fluorescence in the pellet (t_0-t_{24h}) and the supernatant (s_0-s_{24h}) of Cx modified through cysteines. C) SDS-PAGE fluorescence of Cx modified through lysines.*

Assessment of the affinity of antibody conjugates for their antigens

In ADCs, the drug is usually inactive when conjugated to the antibody, thus cleavable spacers are generally used to release it. These linkers can be sensitive to either pH (e.g. hydrazines), glutathione (e.g. disulfide bonds) or specific proteases (e.g. valine-citruline for cathepsin B).[316] In our case, the drug is the antibody, which is 50-100 times larger than BBB-shuttles. Therefore, it should be possible to avoid its inactivation by locating the peptides pertinently. In spite of this, it is necessary to verify that the antibody is able to bind its antigen, not only because the peptides could be near the paratope but also because side-reactions from the conjugation may modify other residues on the IgG or even alter its structure.

Bevacizumab

Although surface plasmon resonance (SPR) or competitive ELISA are the most common techniques to estimate antibody affinity, ELISA dose-response curves use lower amounts of antigen and can also provide a rough estimation of antibody affinity at low epitope densities.[360] Therefore we set up an indirect ELISA based on a protocol described by Sinapis *et al.* for Bv (*Figure 67*).[361] Briefly, we coated an ELISA plate with the antigen (VEGF) and incubated the modified antibody after blocking. As a detection antibody we used an anti-human Fab conjugated to horse-radish peroxidase (HRP) and applied turbo TMB as a chromogenic substrate.

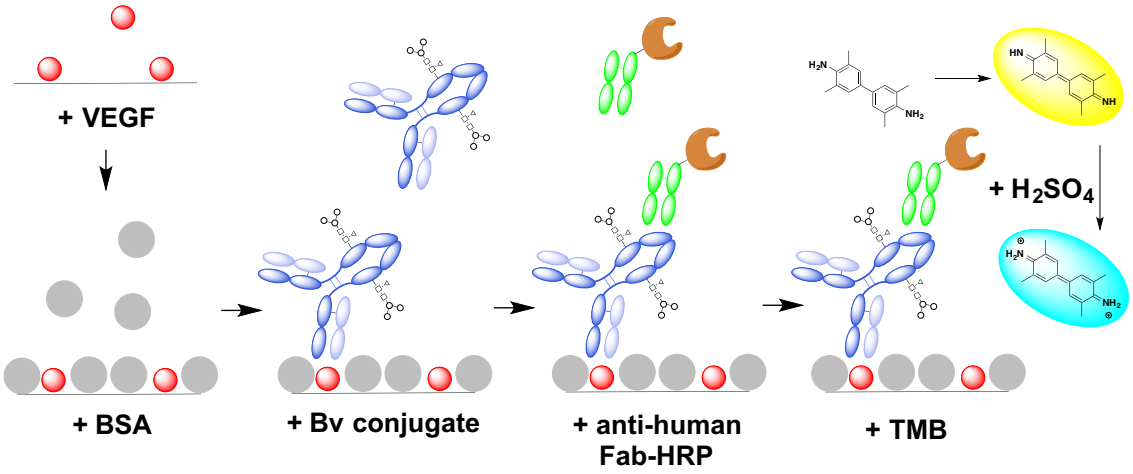

***Figure 67**. Indirect ELISA for the quantificaiton of Bv.*

We performed this affinity assay with THRre and Angiopep-2 conjugates (*Figure 68*). The results we obtained showed that, modification of lysines, cysteines and glycans had little effect on binding (< 25 %). Moreover, it should be noted that this measurement involves a second recognition process, in which the antibody is bound by an anti-human Fab. Hence, the slight decreases in affinity observed could also be due to an effect of this additional recognition process. However, modification of the

N-termini, which should not interfere in the binding of the Fab, did affect Bv affinity for VEGF up to 40%. This result is most likely due to the proximity of peptides to the paratope. The higher impact of Angiopep-2 with respect to THRre when conjugated to the *N*-termini, might be related to its longer sequence (19 vs 12 residues).

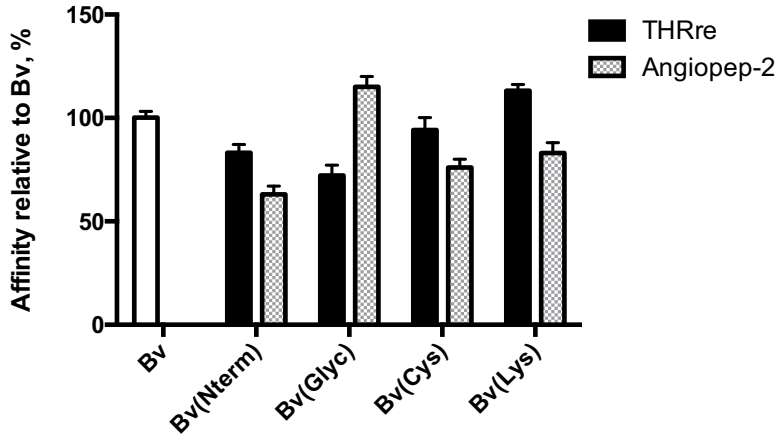

Figure 68. *Slopes of indirect ELISA as an indirect indicator for the affinity of Bv conjugates for VEGF. Data represent mean values ± SEM (n = 3).*

Cetuximab

In the case of Cx, we did not manage to set up a robust ELISA that required a reasonable amount of EGFR, thus we looked for an alternative assay. We also tried not very successfully to study this interaction by SPR. Fortunately, our collaborators at VHIO had a cell line that overexpressed EGFR and they set up an assay to qualitatively assess the Cx-EGFR binding (*Figure 69*).

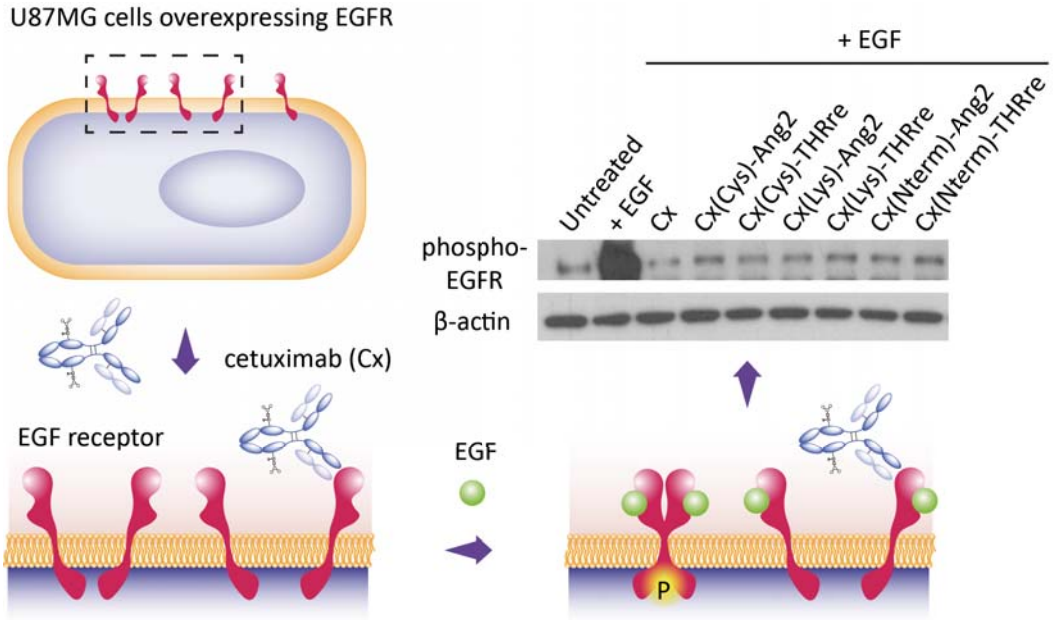

Figure 69. *Functional assay to assesss Cx inhibitory activity and Western blot showing the phosphorilation of EGFR after incubation with Cx-shuttle conjugates. β-actin was used as a control for protein load.*

The experiment, which was performed by Dr. Maria del Mar Inda at VHIO, consisted in preincubating the cells with Cx followed by stimulating EGFR dimerization with its ligand (EGF). Such dimerization was visualized through detection of the phosphorylated receptor in a western blot (*Figure 69*). In this assay, we observed that all conjugates clearly inhibited the phosphorylation of the receptor with respect to control cells, which had only been stimulated with EGF. Comparing the intensity of the bands in the western blot, no large differences were observed between Cx and any of the conjugates. Although this test is less accurate than ELISA or SPR, we could conclude that all the conjugates retained a high degree of inhibitory activity. Hence, affinity for their antigen did not appear to be substantially affected.

BBB permeability evaluation

High antibody conjugate concentration – ELISA

Once we knew that BBB-shuttle-antibody conjugates were functional, we tested them in the BBB cell-based model. Initially we assayed Bv conjugates with THRre and Angiopep-2 in the bovine model at a concentration similar to that present in blood (50-200 μg/mL) when therapeutic doses are administrated.[362] However, we did not observe any significant increase in the transport of the conjugates with respect to the naked antibody, partly due to the high variability. We repeated the test using Bv with peptides conjugated at different positions and obtained the same highly variable results (*Figure 70*). In spite of this, the transport of Bv(Cys)-THRre and Bv(Cys)-Angiopep2 was reproducibly over 20 % higher than the naked antibody. Also Angiopep-2 conjugated to the lysines appeared to increase permeability. Conversely, the same shuttles located at other sites of the antibody appeared to decrease translocation down to 50 %.

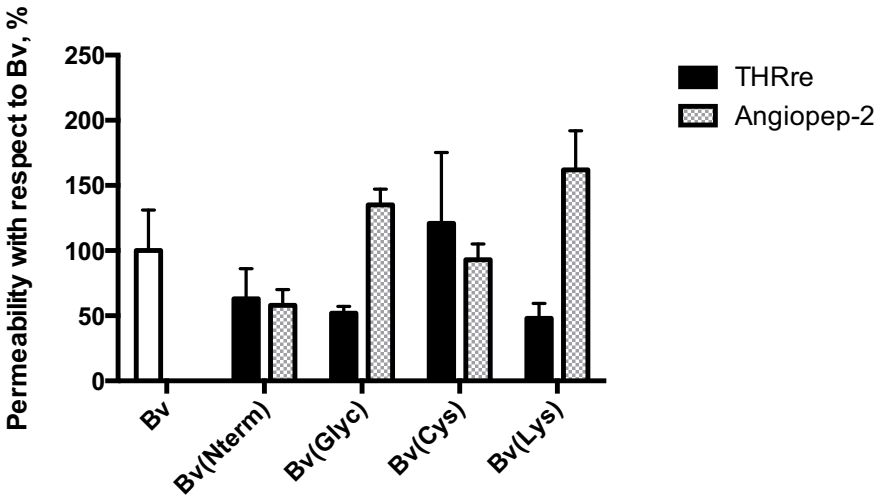

Figure 70. *Relative permeability of Bv conjugates assayed at 1.3 μM in the bovine cell-based BBB model. Bv showed a* $P_{app} = 3.8 \pm 1.1 \cdot 10^{-7}$ *cm/s. Data represent mean values ± SEM (n = 4).*

The low reproducibility between replicates might be due to the concentration present in acceptor wells being near to the quantification limit of this ELISA. Aiming to increase precision, we tried to set up a more sensitive indirect ELISA test based an anti-human Fab modified with alkaline phosphatase coupled to an amplification system from Invitrogen.[361] Amplification was provided by the enzymatic pair diaphorase/alcohol dehydrogenase; the former produced coloured formazan by oxidizing NADH resulting from alkalyne phosphatase dephosphorilation, while dehydrogenase reduced NAD^+ back to NADH. Despite the higher sensitivity of this test, we were not able to decrease variability, which suggested that the high deviation was due to the transport assay in the bovine cell-based BBB model. Therefore, we

decided to move to the human model as soon as it was available. At this point, we also switched to the most promising antibody, Cx.

Results from the first assay in the human model were even more discouraging than those from the bovine model, as transport of all Cx conjugates was lower than that of the naked antibody. In view of the unexpected outcome of the experiment, we verified that the concentrations we had measured with nanodrop and all of them were within an acceptable ± 15 % range; these differences between conjugates were due to the significant absorption of THRre at 280 nm because of its two tryptophans. In addition, by measuring the amount of antibody remaining in the donor wells, we calculated that mass balance was always above 80 %, which indicated that the conjugates were stable in Ringer HEPES and were not degraded or adhered to cells appreciably during the assay.

Regarding ELISA quantification, we prepared a different standard line for each conjugate to interpolate the readings from acceptor wells. In this regard, the response of all conjugates was similar, which was in agreement with the affinity study. However, it has been reported that quantification of ADCs using this technique may lead to artefactual results due to differential binding of the conjugates depending on the PAR and the location of peptides.[363] This effect might be enhanced by a potential enrichment of the populations bearing a higher number of BBB-shuttles in acceptor wells, as they are expected to cross the cell monolayer more efficiently.

Another factor that could induce the lower permeability observed is that the high concentration of Cx-shuttle conjugates saturated cell receptors, TfR in the case of THRre and LRP1 for Angiopep-2. In this scenario, other transport mechanisms such as unspecific fluid phase transcytosis and paracellular diffusion would have a higher contribution to permeability in the cell-based model. This hypothesis was the main one considered by our collaborators in Lens. Therefore, in the following assays we decreased IgG concentration 100-fold, which made us move to radioactive labelling. This detection method would also avoid the effect of heterogeneous populations of conjugates that could affect transport results calculated using ELISA.

Low antibody conjugate concentration – radioactive labelling

In order to label antibody-BBB-shuttle conjugates, we found that ^{125}I was the most suitable radiotracer because of its high sensitivity and stability.[364] Moreover, it has a half-life of 60 days, which is an acceptable compromise between minimal decay during the assay and waste management. In addition, the radiolysis[365] produced by this γ-emitter is considered negligible if the assay is performed short after labelling. Tyrosine iodination is a very common method to introduce this tracer because iodine is incorporated directly by generating iodine(I) chloride from sodium iodide

with a mild oxidant; this mixed halogen species readily undergoes electrophilic substitution at the positions adjacent to the hydroxyl group. The reaction is usually performed at pH 7 to make it selective for tyrosines because hystidines may also be iodinated at pH 8-9. However, if the paratope of the antibody contains tyrosines, iodine may be incorporated to a small molecule that can be coupled to other amino acid side chains. The most common alternative is the Bolton-Hunter reagent, which contains a phenol ring that is labelled with iodine and also an active ester to be reacted with antibody amines.

For the transport assay we were concerned about the effect of iodination on peptides and not on the antibody binding to its receptor. Therefore, we chose direct tyrosine modification because most BBB-shuttles we intended to use contained lysines whereas only RVG29 and Angiopep-2 contained tyrosines. Moreover, tyrosine was not critical for the transport of the Angipep-2 because this peptide had been found through screening of a library iodinated on this residue.

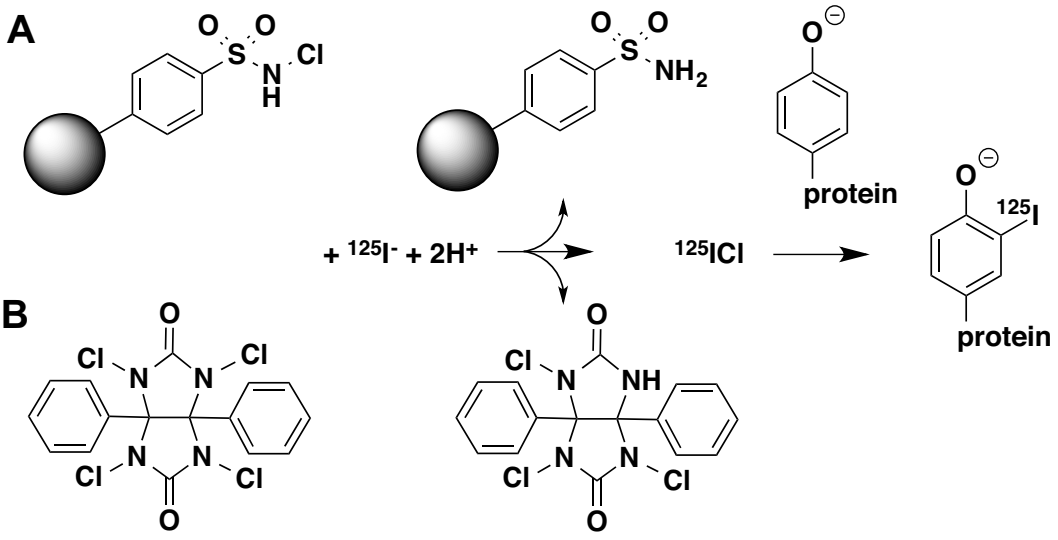

Figure 71. *Iodination of tyrosine with A) chloramine-T on Iodobeads® and B) iodogen reagents.*

As an oxidizing reagent we initially used Iodogen® tubes (*Figure 71*). These tubes have the bottom coated with 1,3,4,6-tetrachloro-3*α*,6*α*-diphenylglycouril, which is not soluble in water and thus provides protein surface modification and minimizes oxidative damage. However, a small portion of the reagent may be detached from the tube walls and extracting the solution may not stop the reaction completely. Therefore, quenching with tyrosine is recommended. To avoid this step and minimize costs we switched to Iodobeads® when we had to perform assays with a higher number of conjugates. These beads are made of polystyrene with covalently-linked *N*-chlorobenzenesulfonamide, which also allows a milder oxidation with respect to the water soluble version (Chloramine-T). In all cases, after the labelling, the conjugates were purified by gel filtration using PD-10 or NAP-5 columns.

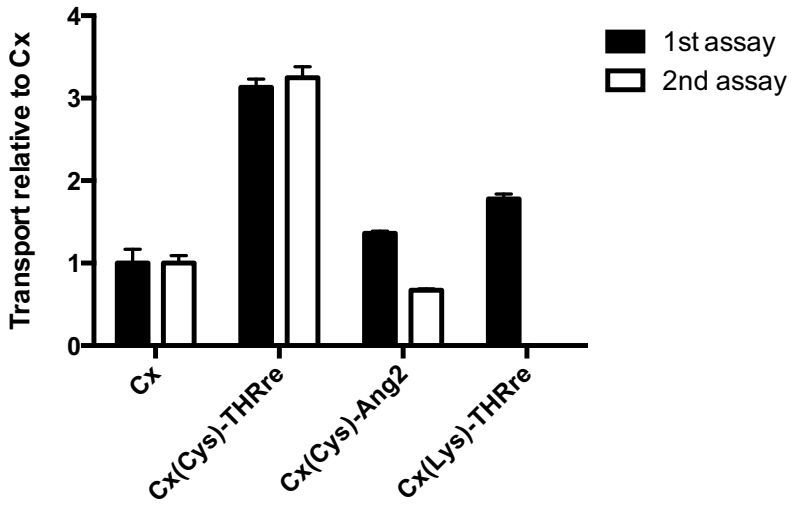

Figure 72. *Permeability results for 2 assays of Cx conjugates at 25 nM in the human cell-based BBB model. Data represent mean values ± SEM (n = 4)*

In contrast to previous experiments, in the first transport assay using radioactive labelling we obtained a significant increase for the three conjugates we tested (*Figure 72*). More precisely, THRre linked to interchain cysteine residues provided up to a 3-fold enhancement in transport with respect to unmodified Cx. By contrast, the same peptide linked through lysines only increased transport 1.8-fold and Angiopep-2 was not significantly different from Cx. The permeability obtained for Cx ($5.2 \pm 0.9 \cdot 10^{-7}$ cm/s) was comparable to the one we had previously obtained using ELISA at higher concentrations ($2.5 \pm 0.6 \cdot 10^{-7}$ cm/s) and also similar to the value our collaborators had obtained for a different antibody ($3.0 \pm 0.5 \cdot 10^{-7}$ cm/s).

Because results for the conjugates were so different from those obtained until now at higher concentrations measured using ELISA, we tried to verify that they were not due to the presence of tyrosine remaining from the labelling reaction. We first envisaged precipitating the protein with trichloroacetic acid (TCA) but we observed that precipitation was incomplete and variable at the low concentrations present in acceptor wells. Hence, we repeated the labelling under the same conditions but without using radioactivity ("cold" experiment) and collected the eluent of the NAP-5 column in the same fractions we had used for the experiment (*Figure 73*). Upon analysis of the fractions using HPLC-UV, we observed that this purification method had enough resolution to provide at least one fraction with neither antibody nor tyrosine.

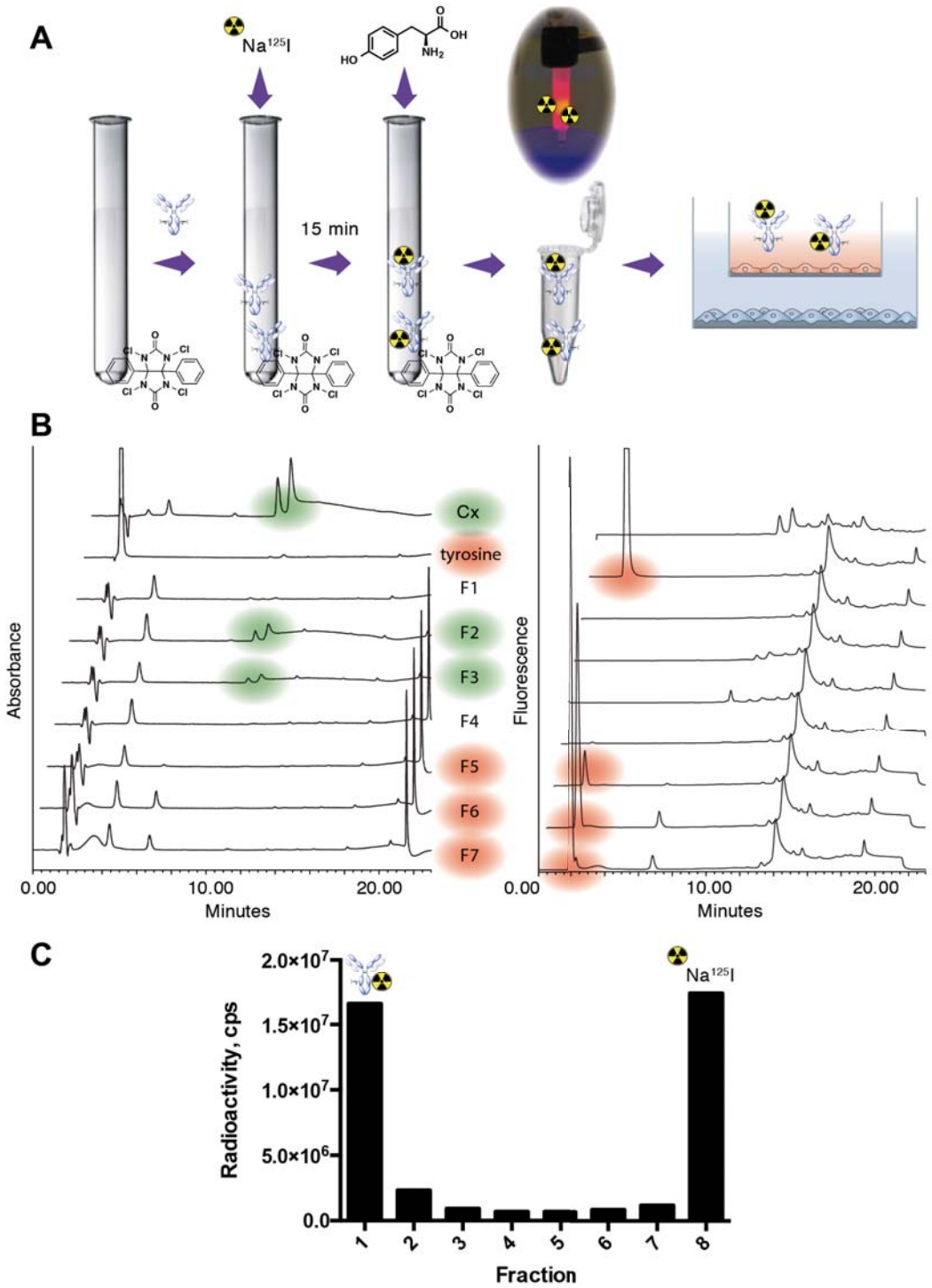

Figure 73. *Labelling and separation of tyrosine and/or $Na^{125}I$. A) Scheme of the labelling process using Iodogen® tubes. B) Separation of antibody from tyrosine after labelling with non-radioactive NaI using Iodogen® tubes. C) Separation of ^{125}I-labelled antibody (F1) from unreacted iodine (F8) after labelling with Iodobeads® (no quenching with tyrosine).*

When we repeated the assay with all the library of Cx conjugates, we obtained comparable values and a very similar trend between them (*Figure 72*). This time we performed the iodination using Iodobeads® and collected several fractions from each purification to verify that the labelled antibody was clearly separated from unreacted iodine.

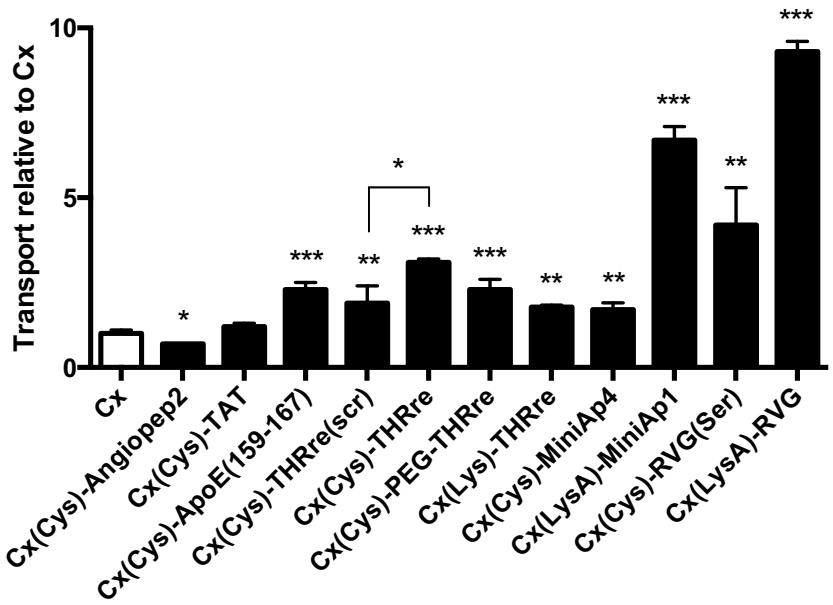

Figure 74. *Permeability of Cx-BBB-shuttle conjugates in the human cell-based BBB mode with respect to Cx. All data represent mean values ± SEM (n = 4). * P < 0.05, **P < 0.01, ***P < 0.001 (t-test).*

This experiment confirmed that the permeability of Cx could indeed be increased using BBB-shuttles (*Figure 74*). We tested mainly conjugates modified through interchain cysteines. However, we also included two constructs bearing RVG and MiniAp-1 modified through lysines using CuAAC, because the shuttles contained cysteines and could not be synthesized with a maleimide group. Although peptides used in both conjugation methods were not identical, we could observe a clear trend: the shuttles linked to lysines through the triazole were more efficient than the ones linked to cysteines through thiol-maleimide chemistry, especially comparing MiniAp-1 vs MiniAp-4 and RVG vs RVG(Ser). The difference in transport could be due to the higher accessibility of the BBB-shuttles placed on lysines to the putative membrane receptor, as these residues are naturally more exposed than the cysteines due to its charged state (*Figure 75*).

Nevertheless, the position of the peptide alone did account for the whole increase in permeability because we had previously observed that THRre anchored to lysines through the 2-iminothiolane linker was less efficient than the same peptide bound to cysteines (*Figure 72*). Moreover, the conjugate modified through the lysines using thiol-maleimide chemistry contained the highest number of shuttles, thus this did not appear to be a limiting factor. Therefore, the most reasonable hypothesis is that the triazole linker plays a key role in the orientation of the peptide. Another possibility is that copper traces remaining from the reaction affect the translocation; however, the tightness of the monolayer, according to the permeability of the internal standard (Lucifer yellow), was not altered. Yet an alternative explanation would be that an excessive capping of lysines, due to diazotransfer, had increased the

hydrophobicity of the conjugates altering their permeability. In any event, to assess the exact contribution of the linker to the transport, THRre and MiniAp-4 have been conjugated using the three methods and will be soon assayed. Also a control conjugate with L-homopropargylglycine will be prepared to assess the effect of a small molecule that is not expected to act as a shuttle.

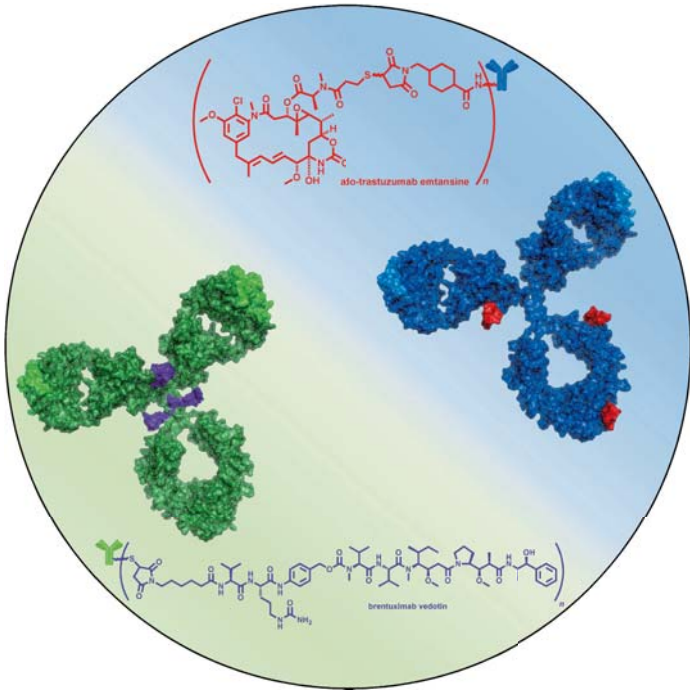

Figure 75. *Representative antibody conjugates modified through cysteines and lysines. (From Chari et al. 2014)*[316]

In the transport experiment, we observed that the two apamin derivatives we had assayed (MiniAp-1 and MiniAp-4) were both capable of improving the transport of antibodies. However, the increase relative to each other did not follow the same trend as the permeability of peptides alone or that of their conjugates with small cargoes. MiniAp-1 linked through lysines using CuAAC enhanced the transport of Cx 7-fold, while MiniAp-4 linked to cysteines provided only a 1.7-fold increase. We have prepared MiniAp-4 conjugated as MiniAp-1 to confirm whether this difference is only due to the linkage and conjugation site or also to the distinct capacity to transport IgGs of each mini-apamin.

This assay also confirmed that THRre was able to enhance the transport of Cx up to 3-fold. Moreover, the increase was significantly higher than that of a scrambled version of this peptide, in line with the expected RMT mechanism. However, the significant permeability improvement provided by THRre(scram) suggests that THRre is also partly transported through AMT. This hypothesis is fully compatible with the net positive charge and amphiphilic character of the sequence. In addition, we assayed THRre with a PEG-based spacer aiming to enhance the accessibility of the peptide to TfR. However, we did not observe any impact of this linker on the

transport. This observation suggests that increasing the hydrophilicity of the shuttle impacts negatively on its transport capacity, further indicating that AMT has a non-negligible contribution in the transport mediated by this peptide.

Among all the shuttles assayed, RVG29 linked through a triazole linker to lysines was the most efficient in transporting Cx. In the same line, RVG29(Ser) was the best performing peptide linked through cysteines. Another reference shuttle, described to undergo RMT, ApoE(159-167)$_2$ also provided a 2.2-fold increase. Conversely, TAT peptide did not enhance the transport of Cx significantly; the low efficiency of this shuttle could be due to its CPP nature, which mediates internalization but not necessarily transcytosis.

Interestingly, Angiopep-2, which has been reported to enhance the transport of trastuzumab across the BBB, did not work with Cx. Therefore, we decided to study the permeability of this peptide alone in the model and observed that it was degraded during the assay. In a MALDI-TOF spectrum we could see the main fragment resulting from its proteolysis in acceptor wells (*Figure 76*). Probably the location of the linker on Angiopep-2, which is not specified in the publication,[126] is highly relevant to enhance its stability. In addition, although trastuzumab and Cx have a very similar pI (8.5), the first is a humanized antibody (i.e. only the CDRs are non-human) while the latter is chimeric (i.e. the variable domains are preserved from the original species). This difference among others, such as the antibody glycosylation pattern, may also play a role in the transport efficiency of Angiopep-2.

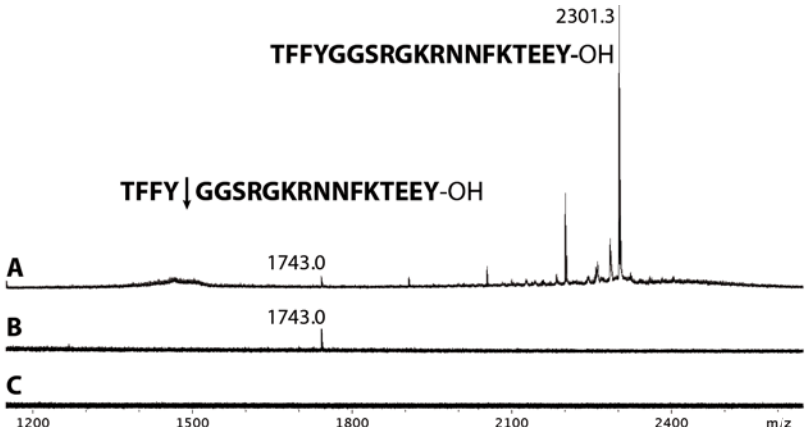

Figure 76. *Degradation fragment of Angiopep-2 present in the donor (A) and acceptor (B) wells after the transport assay. A well containing only Lucifer yellow (C) as a control.*

In order to confirm these trends minimizing paracellular contribution to permeability, we tried to perform a pulse-chase experiment. In this assay we incubated radiolabelled antibodies at a high concentration (1.7 μM) on the apical side for 30 min. Then we washed cells 3 times and measured the peptide concentration in both compartments after one hour. Results from this experiment had an extremely high variability due to the low amounts of compounds detected and it should be repeated optimizing the conditions. However, TAT and ApoE(159-

$167)_2$ were present in both the apical and the basal compartments in a concentration two orders of magnitude higher than the rest of peptide shuttles. The higher release into both compartments is a clear indicator of their cell-penetrating capacity, which suggests that ApoE peptide might not undergo transcytosis exclusively by RMT but also through AMT like TAT. This behaviour could be expected by the high net positive charge of the former. However, it is surprising that these two peptides perform so differently in the classical transport assays, not only carrying Cx in our case but also transporting other proteins, such an ASA in the study by Böckenhof and co-workers.[61]

Additionally, the improved permeability of Cx for some of the peptides could also be due partly to a decreased binding to the Fc efflux transproter. Competition experiments with the naked antibody should be performed in order to measure the extent to which this interaction is modified in each conjugate.

Summary and perspectives of BBB-shuttle antibody conjugates

In this chapter we have shown that a variety of BBB-shuttles are capable of increasing the transport of a monoclonal antibody across a tight monolayer of human endothelial cells mimicking the BBB. We have described how we set up a variety of conjugation strategies to link the BBB-shuttles to the antibodies and concluded that partial reduction of cysteines provided the best compromise between efficiency, robustness and site-selectivity in the case of Cx. However, the highest increase in permeability was observed for RVG and MiniAp-1 linked to the antibody lysines using CuAAC. Although the higher exposure of lysines may contribute to the permeability enhancement, THRre linked to these residues using thiol-maleimide chemistry was less efficient than conjugated to cysteines. Therefore, in order to discriminate the contribution of the linkage from that of the location or the peptide, several conjugates bearing the same peptides conjugated using the different methods will be tested. Also the integrity of the antibodies will be analysed after the assay combining refined TCA precipitation, gel electrophoresis and size-exclusion (using NAP-5 columns) to verify that the radioactivity measured in acceptor wells correspond to the intact antibodies. Competition and inhibition experiments are also envisaged in order to verify the mechanisms used for the transport of BBB-shuttle-antibody conjugates.

In addition to the *in vitro* work performed in our laboratory, we are also preparing mg-scale amounts of conjugates to test them *in vivo*. We expect that mini-apamines and THRre will outperform the other shuttles in these assays due to their high protease-resistance. The aim of the *in vivo* studies will be to assess the capacity to cross the intact BBB in healthy mice of the antibody conjugates and also to test the therapeutic effect in animals bearing orthotropic tumours at VHIO. Moreover, we also intend to perform immunostainings to assess whether the BBB-shuttle-modified antibodies provide an enhanced distrubtion, reaching the currently untreatable invasive cells.

CONCLUSIONS

Conclusions on the first objective, which was finding a new protease-resistant BBB-shuttle:

1. Apamin, a cysteine-rich peptide found in bee venom, and less toxic analogues can cross a tight monolayer of bovine endothelial cells through an active mechanism with a similar permeability. Therefore, the residues involved in toxicity are not required for BBB transport making apamin derivatives, without these residues, safer BBB-shuttle candidates.
2. The native peptide and the bicyclic derivatives have a high resistance to serum proteases, which is partly preserved in monocyclic analogues based on the non-helical moiety of apamin and completely lost in the linear version. In MiniAp-4, the lactam bridge used to cyclize it is key to its high protease-resistance, with a half-life in human serum over 24 h, and also to its increased transport, which was 3-fold that of apamin.
3. Apamin was confirmed to be highly immunogenic. The removal of arginines and glutamines in MiniAp-1 leads to reduced immunogenicity, while total suppression of the helical moiety in MiniAp-4 produces a practically immunosilent shuttle, generating at least 400-fold less antibodies. Moreover, neither derivative shows any envenomation symptoms after a single dose 24-fold times the LD50 of the native peptide (1.2 μmol/kg).
4. MiniAp-4 significantly increases the transport of green fluorescent protein, quantum dots and gold nanoparticles in a human cell-based BBB model, thus demonstrating its value as a BBB-shuttle *in vitro*.
5. MiniAp-4 enhances brain delivery of cyanine-5.5. When accumulation is highest, 1 h after injection, the increase is 7.6-fold with respect to the same fluorophore conjugated to cysteamine as measured after blood perfusion. In addition, this shuttle displays a remarkable selectivity for the brain because the increase in its accumulation in other organs is only between 2- and 4-fold. Furthermore, the construct is detected by fluorescence microscopy beyond brain endothelium, mainly inside neurons, proving its capacity to cross the BBB.

Conclusions on the second objective, which was increasing the transport of antibodies across the BBB:

1. Four conjugation techniques have been set up in order to link BBB-shuttles to antibodies for the treatment of glioblastoma using THRre and bevacizumab. However, in cetuximab, the *N*-terminal ligation has very low efficiency and the complex glycosylation pattern of this IgG make modification of polysaccharide chains impractical. Lysine and interchain cysteine modification have been successfully applied to both antibodies. However, the latter generates more

defined species than the former, making it the technique of choice to prepare a small library of conjugates with cetuximab and a variety of BBB-shuttles.

2. The thioether bond obtained upon thiol-maleimide linkage of Angiopep-2 on cysteines or lysines from cetuximab is stable for over 24 h in human serum.
3. The only conjugates of bevacizumab that display significantly lower affinity for VEGF than the non-modified antibody are the ones with *N*-terminal shuttles. Regarding cetuximab conjugates, all are able to inhibit the phosphorylation of EGFR to a similar extent in cells overexpressing this receptor.
4. Cetuximab conjugates bearing MiniAp-1, MiniAp-4, THRre, ApoE, RVG(Ser) and RVG have significantly higher permeability than the naked antibody in a human cell-based BBB model. Conversely, Angiopep-2 and TAT do not increase its transport in our assay conditions. Linkage of shuttles to lysines using copper-catalyzed azide-alkyne cycloaddition appear to provide a higher permeability increase compared to partially-reduced interchain cysteines. Although this observation can be partly explained by a higher accessibility of the shuttles to their receptor, further research is required to clarify this point.

EXPERIMENTAL SECTION

Materials and methods

Solvents and reagents

All the reagents employed were purchased to Sigma-Aldrich unless otherwise specified. Other providers for the most common reagents used are included in the following table:

Commercial supplier	Reagents and solvents
Applied GL Biochem Shangai	1-hydroxy-7-azabenzotriazole (HOAt)
Cell applications	bovine brain endothelial cells
Charles river	wistar rats
Corning Costar	transwells bovine model (0.33 cm^2; pore size 0.4 μm) transwells human model (1.13 cm^2, pore size 0.4 μm) 12-well and 24-well cell culture-treated plates, BD matrigel growth factor reduced matrix, 100mm diameter Petri Dish
Biochrom A.G.	Gentamycin 10 mg/mL, trypsin-EDTA
Innoprot	Endothelial cells medium (ECM)
Jescuder	NaOH
KaliChemie	trifluoroacetic acid (TFA)
Lonza	culture medium
Merck	molecular sieves 4Å, cupper sulfate ($CuSO_4$)
Millipore	polyvinylidine difluoride (PVDF) filters 0.45 μm
Novabiochem	benzotriazol-1-yl-oxytripyrrolidinophosphonium hexafluorophosphate (PyBOP), *N*-hydroxisuccinimide (NHS), hydroxylamine Novatag™ resin
Pierce	Pierce(R) iodination beads
Scharlau	dichloromethane (DCM), dimethylformamide (DMF), MeOH, tert-butylmethylether
SDS	acetone, MeCN, toluene
Thermo Scintific	Slide-A-Lyzer MINI dialysis device floats
GE-Healthcare	NAP-5 desalting columns, PD-10 desalting columns
Iris Biotech	All amino acids except otherwise specified, TBTU
Acros Organics	sulforhodamine b sulfonyl chloride
PCAS BioMatrix Inc.	ChemMatrix® resin

Peptide synthesis and characterization

All peptides were synthesized using Fmoc/*t*Bu solid phase peptide synthesis (SPPS) manually or using an automated microwave synthesizer. Syntheses were performed in a 250 μmol-scale and L-amino acids were used. Peptide elongation and other manipulations were done in 20 mL polypropylene syringes with a polypropylene porous disk. Solvents and soluble reagents were removed by suction. Washings between synthetic steps were done with DMF (5 x 30 s) and DCM (5 x 30 s) using 10 mL of solvent/g resin each time. During couplings the mixture was allowed to react with intermittent manual stirring.

Protected amino acids used were the following unless otherwize specified: Fmoc-Ala-OH, Fmoc-Cys(Trt)-OH, Fmoc-Asp(*t*Bu)-OH, Fmoc-Glu(*t*Bu)-OH, Fmoc-Phe-OH, Fmoc-Gly-OH, Fmoc-His(Trt)-OH, Fmoc-Ile-OH, Fmoc-Lys(Boc)-OH, Fmoc-Leu-OH, Fmoc-Met-OH, Fmoc-Asn(Trt)-OH, Fmoc-Pro-OH, Fmoc-Gln(Trt)-OH, Fmoc-Arg(Pbf)-OH, Fmoc-Ser(*t*Bu)-OH, Fmoc-Thr(*t*Bu)-OH, Fmoc-Val-OH, Fmoc-Tyr(*t*Bu)-OH, Fmoc-Trp(Boc)-OH

Solid-phase peptide synthesis

Tests to assess coupling completion

Colorimetric tests were used in the manual syntheses after each deprotection to verify Fmoc removal and after each coupling to know if the new protected amino acid had been successfully coupled. These tests are based on the detection of primary and/or secondary amino groups.

Kaiser or ninhydrin test

Ninhydrin test[366] detects primary amino groups as the ninhydrin chromophore is generated through a Shiff-base intermediate. In this assay, several dried but DCM solvated *beads* of resin were transferred into a glass tube. Subsequently, 6 drops of solution A and 2 of solution B were added and heated at 110ºC for 3 min. A deep blue or purple solution indicated the presence of free primary amines (positive test), whereas a yellow or pale pink/orange colour indicated the absence of amines.

Solution A was prepared by adding 40 g of phenol to 10 mL of ethanol and heated until they were dissolved. Another solution of 65 mg of KCN in 100 mL of water was prepared and mixed with 100 mL of pyridine (freshly distilled over ninhydrin). Both solutions were stirred for 45 min with 4 g of Amberlite MB-3 resin and finally filtered and mixed. Solution B was prepared by dissolving 205 mg of ninhydrin n 50 mL of ethanol. This solution had to be protected from the light.

De Clercq or p-nitrophenyl ester disperse red I test

De Clercq test[2] is a very sensitive qualitative assay to detect the presence of secondary amine groups such as the one on a proline. This test was performed by transferring a few beads of resin into a glass tube, in which 10 drops of the reagent were added. The mixture was heated at 70ºC for 8 min. The resin beads were then washed with MeOH (3 x 30 s), DMF (3 x 30 s) and DCM (30 s). Transparent or pink resin beads indicated the absence of free secondary amines (negative test), while red indicated a positive test. The De Clercq reagent was prepared by mixture of commercial *Disperse Red I* and ethyl diazoacetate, followed by saponification and condensation with *p*-nitrophenol using $POCl_3$. The product was purified by crystallization.

Initial conditioning of the resin

All peptides with an *N*-terminal amide were synthesized on ChemMatrix® resin with a substitution of 0.4-0.6 mmol/g.

Treatment	Reagents
Wash	MeOH (5 x 30 s)
Wash	DMF (5 x 30 s)
Wash	DCM (5 x 30 s)
Wash	1 % TFA in DCM (2 x 10 min)
Wash	DCM (5 x 30 s)
Wash	DMF (5 x 30 s)
Wash	DCM (5 x 30 s)
Wash	5 % DIEA in DCM (2 x 10 min)
Wash	DCM (5 x 30 s)
Wash	DMF (5 x 30 s)
Wash	DCM (5 x 30 s)
Linker coupling	4 eq Fmoc-Rinkamide-OH, 4 eq DIC, 4 eq OximaPure®, DCM/DMF 1:1 (2 h)
Wash	DCM (5 x 30 s)
Wash	DMF (5 x 30 s)

All peptides with an *N*-terminal carboxylate were synthesized on 2-chlorotrityl chloride resin.

Treatment	Reagents
Wash	DCM (5 x 30 s)
Wash	DMF (5 x 30 s)
Wash	DCM (5 x 30 s)
Coupling	1.2 eq Fmoc-Aa-OH, 1.2 eq DIC, 1.2

	eq OximaPure®, DCM/DMF 1:1 (2h)
Capping	MeOH (1 mL/g resin), 15 min
Wash	DCM (5 x 30 s)
Wash	DMF (5 x 30 s)
Wash	DCM (5 x 30 s)

Fmoc group removal

The Fmoc group was removed before each coupling by treating the resin with 20 % piperidine in DMF (10 mL/g resion, 1 x 1 min and 2 x 10 min). To remove the Fmoc group from Fmoc-L-Pro-OH, an additional treatment with DBU, toluene, piperidine and DMF (5:5:20:70) was performed (1 x 1 min and 2 x 5 min). After deprotection, the resin was washed with DMF (5 x 30 s), DCM (5 x 30 s) and again with DMF (5 x 30 s).

Quantification of resin loading capacity

In order to measure the loading capacity of a resin, after coupling the first amino acid, piperidine washes were collected and measured by UV spectroscopy. Loading was calculated using equation 2:

$$X = \frac{A \cdot V}{\varepsilon \cdot m \cdot b} \qquad \textbf{Equation 2}$$

where X is the loading of the resin, A is Fmoc absorbance at 301 nm, V is the volume of solvent, ε is the molar extinction coefficient of Fmoc at 301 nm (7800 $M^{-1}cm^{-1}$)[367], m is the mass of the resin in g and b is the optical path in cm.

Chain elongation in automated microwave synthesis

A CEM Discover™ microwave peptide synthesizer was used. Drain washings were performed with DMF (4 x 7mL) with nitrogen gas agitation.

Fmoc deprotection was carried out in two stages using 20 % piperidine in DMF (7.0 mL). In the first stage microwave heating was employed for 30 s at 35 W and a temperature of 33 ºC, while in the second one the temperature was raised to 75 ºC with 40 W power during 3 min. Nitrogen gas agitation was used during the heating.

The same protected amino acids as for the manual synthesis were used. Five equivalents of 0.2 M solutions of Fmoc-AA-OH in DMF were added with TBTU (5 eq., 0.5 M in DMF) and DIEA (5 eq., 2.0 M in DMF). The mixtures were stirred by means of N_2 bubbling in DMF (7 mL) for 5 min at 27 W and 75ºC, except for cysteines, which were coupled at 50ºC. In this automated synthesis only arginines were recoupled. After completion of the automatic synthesis following the final Fmoc-deprotection cycle, the peptidyl-resin was washed twice with 10 mL of DCM before being removed from the reactor.

Chain elongation in manual synthesis

Method 1 was used as a default for all Fmoc-Aa-OH and linker couplings. If the first coupling was not complete, a second coupling was performed. When the recoupling was unsuccessful, another coupling was performed using method 2 for primary amines or method 3 for secondary amines (proline and *N*-Methylated amino acids). Method 3 was also used to couple rhodamine B and CFluorescein.

Method 1 - DIC

Treatment	**Reagents**
Wash	DCM (5 x 30 s)
Coupling	4 eq Fmoc-Aa-OH, 4 eq DIC, 4 eq OximaPure®, DCM/DMF 1:1 (15 min)
Wash	DCM (5 x 30 s)
Wash	DMF (5 x 30 s)
Wash	DCM (5 x 30 s)

Method 2 - HATU

Treatment	**Reagents**
Wash	DMF (5 x 30 s)
Coupling	4 eq Fmoc-Aa-OH, 3.5 eq HATU, 8 eq DIEA, DMF (30 min)
Wash	DMF (5 x 30 s)
Wash	DCM (5 x 30 s)
Wash	DMF (5 x 30 s)

Method 3 – PyBOP/HOAt

Treatment	**Reagents**
Wash	DMF (5 x 30 s)
Coupling	4 eq Fmoc-Aa-OH, 4 eq PyBOP, 12 eq HOAt, 12 eq DIEA, DMF (1 h)
Wash	DMF (5 x 30 s)
Wash	DCM (5 x 30 s)
Wash	DMF (5 x 30 s)

Sulfonilation

Sulforhodamine B (lissamine rhodamine) sulfonyl chloride (2 eq) was coupled to the *N*-terminus of the peptide in DMF with DIEA (10 eq) for 16 h at 50 °C.

Synthesis of maleimide derivatives bearing a fluorophore

The peptides were synthesized by Fmoc/*t*Bu solid-phase peptide synthesis using regular protected amino-acids and Fmoc-L-Lys(Alloc)-OH. After coupling the fluorophore, Allyl and Alloc were removed using tetrakis(triphenylphosphine)-palladium(0) (0.2 eq) and phenylsilane (20 eq) in DCM. Four treatments of 20 min were performed and deprotection was assessed by cleavage of a small amount of resin and MALDI-TOF MS. Finally 6-maleimidohexanoic acid was coupled to the free amine of the lysine.

MiniAp-4 cyclization

MiniAp-4 was synthesized by Fmoc/*t*Bu solid-phase peptide synthesis using regular protected amino-acids and Fmoc-L-Asp(OAll)-OH and Fmoc-L-Dap(Alloc)-OH. Before deprotecting N-terminal diaminopropyl Fmoc, Allyl and Alloc were removed using tetrakis(triphenylphosphine)palladium(0) (0.2 eq) and phenylsilane (20 eq) in DCM. Four treatments of 20 min were performed and deprotection was assessed by cleavage of a small amount of resin and MALDI-TOF MS. Cyclization was achieved with DIC (4 eq) and Oxima Pure (4 eq) and monitored through the Kaiser test. Subsequently, the Fmoc group of diaminopropionyl residue was removed and either a reactive moiety was coupled (maleimide or cysteine) or the peptide was directly cleaved.

Cleavage and deprotection of side chains

Peptides were cleaved with concomitant removal of the side-chain protecting groups, using TFA, H_2O and TIS (92.5:5:2.5). When cysteines were present in the sequence the following cocktail was used instead: TFA, EDT, H_2O and TIS (94:2.5:2.5:1).

Work-up

After cleavage of the peptides, the solvent was evaporated applying a current of N_2. The residue was washed 3 times by suspension in *tert*-butyl methyl ether and subsequent centrifugation. After that, the cleaved peptides were dissolved in H_2O/MeCN (1:1) with 0.1 % TFA and freeze-dried.

Disulfide bridge formation in solution

Ellman test

This test allows the determination of free thiols in solution or in a polymer that is compatible with aqueous medium. The reagent was prepared on the day of the assay by dissolving 40 mg of 5,5′-dithiobis(2-nitrobenzoic acid) (DTNB) in 10 mL of phosphate buffer (0.1 M) at pH 7 and kept in a sealed vial under nitrogen

atmosphere. 0.5 mL of the crude, initially containing 0.1-0.2 μmol of free thiols, were diluted with 0.9 mL of phosphate buffer (0.1 M pH 8) and mixed with 100 μL of DTNB solution. A blank was prepared with the same volume of DTNB dissolved in 1.5 mL. The solutions were allowed to react for 15 min. After this time, the absorbance at 410 nm was measured in a 1 cm optical pathway cell. The initial molar concentration (C) of free thiols was calculated using Lamber-Beer's law, i.e. $C = 3 \cdot (A_{sample} - A_{blank})/13650$.

Free thiol cyclization conditions

Oxidation of apamin derivatives was performed at 20 ºC, with intense stirring under air oxygen during 24 h. Reaction were followed by Ellman test and HPLC. A 1 L round-bottom container with a large aperture was used to allow a better oxygenation and 10-15 mg of the peptide were dissolved in 300-500 mL of an ammonium bicarbonate buffer (pH 8.0). High dilution (10-20 μM) was required to minimize the formation of intermolecular disulfide bonds. After 24 h, the buffer was acidified with acetic acid or TFA to pH 3-4 and lyophilized.

ApOO(Acm)$_2$ cyclization conditions

After performing oxidation of the two free thiols under air oxygen as described, the peptide (1 mg/mL) was dissolved in 15 % AcOH in water under a blanket of N_2. 4 equivalents of iodine (5 mM in methanol) were added to the solution and it was left to react overnight under N_2. The crude was analysed at 0.5, 2 and 12 h by HPLC-UV and deprotection was only quantitative in the last time-point. No iodination of His was observed by MALDI-TOF MS.

Conjugation to azide -cyanine5 and -cyanine5.5

Peptides were obtained by manual Fmoc/*t*Bu solid-phase peptide synthesis as described previously, and 5-hexynoic acid was coupled at the *N*-termini in solid phase. After that, peptides were cleaved and purified. Two solutions were prepared prior to the reaction, the first one containing 25 mM ascorbate solution in aqueous TEA/AcOH (2 M, pH 7) and the second one mixing $CuSO_4$ (200 mM in water) and THPTA (200 mM in DMSO) 1:1. Conjugation to cyanine5/5.5-azide (Lumiprobe) was performed in aqueous buffer with DMSO. The alkyne-peptide (1.2 μmol) was disolved in 100 μL of DMSO and mixed with Cyanine5.5-maleimide (16 μmol, 16 μL DMSO), ascorbic acid (120 μL of 25 mM stock) and Cu-THPTA (3 μmol, 30 μL). The mixture was allowed to react for 30 min and purified by reverse-phase HPLC.

Conjugation to maleimide-cyanine5.5

Peptides were obtained by manual Fmoc/*t*Bu solid-phase peptide synthesis as described previously, and Fmoc-Cys(Trt)-OH was coupled at the *N*-termini in solid

phase. After that, peptides were cleaved and purified. Conjugation to cyanine5.5-maleimide (Lumiprobe) was performed in aqueous buffer. The cysteine- peptide (0.6 μmol, 60 μL water) was mixed with Cyanine5.5-maleimide (9 μmol, 9 μL DMSO) and triethylamine (pH 7-8). The mixture was allowed to react for 30 min and purified by reverse-phase HPLC.

Purification

Crudes were dissolved in H_2O/MeCN (keeping MeCN to a minimum), filtered through a 0.45 μm filter and purified by semi-preparative RP-HPLC. Fractions corresponding to the peak of interest were analysed by HPLC, pooled and lyophilized. The peptides were purified in a Waters system with a 2545 binary gradient module, a 2767 manager collector and a 2998 photodiode array detector with MassLynx 4.1 software. The column used was a Sunfire C_{18} (150 x 10 mm x 3.5 µm, 100 Å, Waters), solvents MeCN (0.1 % TFA) and H_2O (0.1 % TFA), flow rate: 6.6 mL/min. Purity was checked by reverse-phase HPLC.

Identification

MALDI-TOF MS

The determination of the molecular weight of all synthesized peptides and the tandem mass analyses were performed using a MALDI-TOF/TOF Applied Biosystem 4700. 1 μL of peptide solution (0.5-2 mg/mL) mixed with 1 μL of α-cyano-4-hydroxycinnamic acid (ACH) matrix were seeded on the MALDI plate and air-dried. The matrix was prepared as follows: a 10 mg/mL solution of ACH was prepared in MeCN/H_2O 1:1 (v/v) containing 0.1 % TFA.

HPLC-ESI MS

For some peptides chromatograms and spectra were obtained on a Waters system Alliance 2695, photodiode dectector Waters 2998, ESI-MS model Micromass ZQ and Masslynx 4.1 software (Waters). Column Sunfire C_{18} (100 x 2.1 mm x 3.5 µm, 100 Å, Waters), solvents MeCN (0.07 % formic acid) and H_2O (0.1 % formic acid), flow rate 1 mL/min.

LTQ-FT MS

Some of the peptides were analysed using a high resolution mass spectrometer to obtain their exact mass. Samples were dissolved in 200 μL of H_2O:MeCN and diluted in H_2O:MeCN 1% formic acid for MS analysis. The analysis was performed in a LTQ-FT Ultra (Thermo Scientific) and the sample was introduced by automated nanoelectrospray. A NanoMate (Advion BioSciences, Ithaca, NY, USA) infused the samples through the ESI Chip, which consists of 400 nozzles in a 20 x 20 array. Spray

voltage was 1.7 kV and delivery pressure was 0.3 psi. MS conditions were: NanoESI, positive ionization, capillary temperature 200 ºC, tube lens 119V, ion spray voltage 2 kV and m/z 100-2000 amu.

Purity assessment

UPLC

UPLC chromatograms were obtained on an Acquity high class (PDA eλ detector, sample manager FNT and Quaternary solvent manager) using a column Acquity BEH C_{18} (50 x 2 mm x 1.7 μm). The flow rate was 0.61 mL/min using MeCN (0.036 % TFA) and H_2O (0.045 % TFA). 2-min linear gradients were used in all cases.

HPLC – analytical scale

HPLC chromatograms were obtained on a Waters Alliance 2695 with an automatic injector and a photodiode array detector 2998 Waters (Waters, Milford, MA) using a Sunfire C_{18} column (100 x 4.6 mm x 5 μm, 100 Å, Waters) and software EmpowerPro 2. The flow rate was 1 mL/min using MeCN (0.036 % TFA) and H_2O (0.045 % TFA). 8 min linear gradients (G) were used in all cases.

Quantification by amino acid analysis

The content and ratio of amino acids present in a peptide sample were determined by ion exchange chromatographic analysis after acid hydrolysis. The hydrolysis is performed with 6M HCl at 110ºC for 16h. After that time, the sample was evaporated to dryness at reduced pressure. The residue was dissolved in 20 mM aqueous HCl, derivatized using the AccQ-Tag protocol from Waters, which uses 6-aminoquinolyl-*N*-hydroxysuccinimidyl carbamate as a derivatization reagent, and finally analyzed by ion exchange HPLC.

Structural analysis

Circular dichroism

Circular dichroism spectra were recorded using a Jasco 810 UV-Vis spectropolarimeterdic, equipped with a CDF 426S/426L peltier. Spectra were obtained between 190 and 250 nm, with a time response of 2 s, a scanning speed of 20 nm/min and a step resolution of 0.2 nm. Molar ellipticiy values were calculated from experimental ellipticity (in mdeg) using equation 3:

$$\theta = \frac{\theta_{exp}}{b \cdot C \cdot n} \qquad \textbf{Equation 3}$$

where θ is molar ellipticity in mdeg·cm^2·dmol^{-1}, θ_{exp} is measured ellipticity in mdeg, b is the optical path in cm, C is peptide concentration in M and n is the number of residues in the peptide.

Nuclear magnetic resonance

NMR experiments were carried out on a Bruker Avance III 600 MHz spectrometer equipped with a TCI cryoprobe. Samples were prepared by dissolving peptides in 90 % H_2O /10 % D_2O at 3-4 mM and pH was adjusted to 2-3. Chemical shifts were referenced to internal sodium-3-(trimethylsilyl)propanesulfonate (DSS). Suppression of the water signal was achieved by excitation sculpting.[368] Residue specific assignments were obtained from 2D total correlated spectroscopy (TOCSY)[369] and correlation spectroscopy (COSY)[370] experiments, while 2D nuclear Overhauser effect spectroscopy (NOESY)[371] permitted sequence specific assignments. ^{13}C resonances were assigned from 2D ^{1}H-^{13}C HSQC spectra. All experiments were performed at 298 K except NOESY spectra that were acquired at 278 K. Amide proton temperature coefficients were determined from a series of one-dimensional spectra acquired between 278 and 308 K. The TOCSY and NOESY mixing times were 70 and 250 ms, respectively.

Structures for MiniAp-1 were generated by the standard simulated annealing protocol implemented in the CNS software.[372] Only the distance restraints from inter-residue NOEs were used for the calculation. NOEs were classified as strong, medium and weak (upper limits for structure calculation were set as 2.5 Å, 3.5 Å and 4.5 Å, respectively). The necessary pseudoatom corrections were applied for non-stereospecifically assigned protons at prochiral centers and for the methyl group of aliphatic side chains. The Φ and Ψ backbone torsion angle restraints included in the calculation were derived from experimental ^{1}H, ^{13}C and ^{15}N chemical shifts using the PREDITOR server.[373] 80 structures were generated and 10 were selected based on lowest overall energy and on the basis of no violations of NOE or dihedral angle constraints larger than 0.2 Å and 5º, respectively. PROCHECK[374] was used to generate Ramachandram plot statistics of the final structures.

Stability in human serum

Peptides at a final concentration of 500 μM were dissolved in HBSS and incubated at 37 ºC in the presence of 90 % human serum during 24 h. The 50 μL aliquots were extracted at different incubation times and treated with 200 μL of MeOH to precipitate serum proteins. After 30 min centrifugation at 4ºC, the supernatant was filtered and analyzed by RP-HPLC to calculate the percentage of intact peptide in the sample.

Protein conjugation and characterization

GFP conjugation to MiniAp-4

A solution of GFP (Millipore) (0.5 mg/mL) in sodium phosphate buffer (NaPi) (50 mM, pH 8, EDTA, 1 mM) was treated with 2-iminothiolane (10 eq, 2 mg/mL in ddH_2O) during 1 h at RT. The excess of reagent was removed by SEC (NAP-5, for volumes up to 0.5 mL, PDmiditrap for volumes up to 1 mL or PD10 for volumes up to 2.5 mL, GE Healthcare). The columns were previously equilibrated with reaction buffer following manufacturer instructions. Alkylation of the activated protein was performed by addition of 6 eq of selected maleimido peptide at RT for 1h. The resulting protein was purified by SEC and stored at 4ºC in PBS.

Antibody and myoglobin modification through the *N*-termini

25 μL of cargo solution ($3.3 \cdot 10^{-9}$ mol) was diluted with 75 μL of phosphate buffer 25 mM pH 6.5. Pyridoxal 5'-phosphate (PLP) (298 eq, $1.0 \cdot 10^{-7}$ mol, $2.5 \cdot 10^{-5}$ g) was dissolved in 100 μL of phosphate buffer 25 mM and the pH was made up to 6.5 with 1 M HCl. The cargo solution was mixed with the PLP solution and incubated at 20 ºC for 48 h. Excess of small molecules were separated by SEC (NAP-5) from the derivatized cargo using NaPi 25 mM pH 6.2. The cargo was concentrated to 100 μL using a Vivaspin 500 with 50 kDa MWCO and washed twice with NaPi 25 mM pH 6.2. The BBB shuttle peptide bearing an aminooxy moiety (60 eq, $2.0 \cdot 10^{-7}$ mol) was dissolved in 50 μL of NaPi 25 mM and the pH was made up to 6.2 with 1 M aqueous HCl. The transaminated cargo from the NAP-5 column were mixed with the peptide solution and with 50 μL of a $4 \cdot 10^{-3}$ M solution of aniline (60 eq, $2.0 \cdot 10^{-7}$ mol, $1.9 \cdot 10^{-5}$ g); the mixture was left to react for 48 h. Excess reagents was removed using a NAP-5 size-exclusion column with phosphate buffer 25 mM pH 6.2.

Antibody modification through the glycans

25 μL of cargo solution ($3.3 \cdot 10^{-9}$ mol) was diluted with 75 μL of acetate buffer 50 mM pH 5 and mixed with 10 μL of 0.1 M $NaIO_4$ in water (54 eq, $1.0 \cdot 10^{-6}$ mol, $2.1 \cdot 10^{-4}$ g). The mixture was left to react preserved from light for 2h at 4ºC. A NAP-5 size exclusion column was used to separate the excess small molecules from the derivatized cargo using phosphate buffer 50 mM pH 6.2. The BBB shuttle peptide bearing an aminooxy moiety (60 eq, $2.0 \cdot 10^{-7}$ mol) was dissolved in 50 μL of phosphate buffer 25 mM and the pH was made up to 6.2 with 1 M aqueous HCl. The transaminated cargo from the NAP-5 column were mixed with the peptide solution and with 50 μL of a $4 \cdot 10^{-3}$ M solution of aniline (60 eq, $2.0 \cdot 10^{-7}$ mol, $1.9 \cdot 10^{-5}$ g); the mixture was left to react for 48 h. Excess reagents were removed using a NAP-5 column with phosphate buffer 25 mM pH 6.2.

Antibody modification through interchain disulfides

Free thiols were generated on the antibody by one of the following methods:

Method 1 - Limited disulfide reduction with DTT

The cargo solution was diluted (2 mg/mL, 500 μL) and partially reduced by DTT (3.25 eq) in 0.025 M sodium borate pH 8, 0.025 M NaCl, 1 mM EDTA for 2 h at 37 °C. The excess of DTT was purified from the partially reduced cargo by size exclusion (NAP-5). The concentration of cargo-cysteine thiols produced was determined by titrating with DTNB.

Method 2 - Limited disulfide reduction with TCEP

The cargo solution was diluted (2 mg/mL, 500 μL) and was partially reduced by TCEP (2.5 eq respectively) in 0.025 M sodium borate pH 8, 0.025 M NaCl, 1 mM EDTA for 2 h at 37 °C. No purification was needed. The concentration of cargo - cysteine thiols produced was determined by titrating with DTNB.

Method 3 - Full reduction followed by partial reoxidation

This reaction was performed with DTNB after total reduction with DTT. The cargo solution was diluted (2 mg/mL, 500 μL) and was totally reduced by DTT (150 eq) in 0.025 M sodium borate pH 8, 0.025 M NaCl, 1 mM EDTA for 2 h at 37 °C. The excess of DTT was purified from the partially reduced cargo by size exclusion (NAP-5). The fully reduced cargo was cooled to 0 °C and then treated with 2.0 equivalents of DTNB (0°C, 20 min).

Alkylation

The partially reduced cargo was alkylated with 1.1 molar equiv of BBB-shuttle/thiol. The alkylation reaction was performed at 0 °C for 30 min. Cysteine (1 mM final) was used to quench any unreacted, excess of BBB shuttle. The excess of peptide was removed from the partially reduced cargo by size exclusion (NAP-5, GE Healthcare following manufacturer's instructions). The cargo concentration was quantified using Nanodrop.

Antibody modification through lysines

Thiol-maleimide

The coupling of antibodies through lysine residues using thiol-maleimide chemistry was performed in solution according to the protocol described in *Hermanson. 2008* with some modifications.[359] 20 μL of 10 mg/mL 2-iminothiolane (50 eq) were added to 1 mL of 2 mg/mL Cx and reacted for 1 h at 20 °C in sodium phosphate buffer 50 mM at pH 8 (EDTA 1 mM). The crude was then purified

through a NAP-5 column equilibrated with the same buffer. 500 μL of the eluted solution (activated Cx at 1 mg/mL) was reacted with 25 eq of the maleimide-peptide.

CuAAC

The coupling of antibodies through lysine residues using copper-catalyzed azide-alkyne cycloaddition was performed in solution using the protocol described in van *Dongen. 2009* with some modifications.[375] Briefly, to 250 μL of cargo solution ($3.3 \cdot 10^{-9}$ mol) an aqueous solution of K_2CO_3 (10 μL, 2 mg/mL) was added along with 0.7 μL of $Cu_2SO_4 \cdot H_2O$ (1 mg/mL, 2.9 eq). After mixing, a solution of imidazole-1-sulfonyl azide hydrochloride in milliQ water was added (2.7 μL, 25 mg/mL, 100 eq) and the reaction was stirred overnight. The protein buffer was exchanged by NaPi 50 mM pH 8 using a PD10 G25 desalting column. 450 μL of the resulting solution, which should contain most of the derivatized cargo, was mixed with: 20 μL of stock hexynoic acid-peptide (5 mM); 12.5 μL $CuSO_4$ (20 mM) premixed with 25.0 μL of ligand THPTA (50 mM); 112.5 μL of aminoguanidine (100 mM); 112.5 μL of sodium ascorbate (100 mM) and 171.5 μL of NaPi 50 mM pH 8. The mixture was allowed to react 1 h at RT and finally the product was purified using a PD10 column.

Protein characterization

SDS-PAGE

SDS-PAGE electrophoresis was carried out using BioRad system (Miniprotean cell) 7.5 % Tris gel, 25 mM Tris, 192 mM glycine, 0.1% SDS running buffer). Protein molecular weights were approximated by comparison to a protein marker (Perfect Protein Markers 15–150 kDa from Novagen). Gels were visualised by coomassie staining (staining solution: 10 % AcOH, 0.25 g brilliant blue; discoloration solution: 20 % MeOH, 3 % AcOH glacial, in water). Densitometric analysis was performed using Fiji.

HPLC

HPLC chromatograms were obtained on a Waters Alliance 2695 with an automatic injector and a photodiode array detector 2998 Waters (Waters, Milford, MA) using a Sunfire C18 column (100 x 4.6 mm x 5 μm, 100 Å, Waters) for peptides or BioSuite C18 (150 x 2.1 mm x 3.5 μm, 300Å, Waters) for proteins. The software used was EmpowerPro 2. The flow rate was 1 mL/min using MeCN (0.036 % TFA) and H2O (0.045 % TFA). 8 or 25 min linear gradients (G) were used for peptide or protein analysis respectively.

Capillary electrophoresis

IgG Heterogeneity kit was used following manufacturer instructions (Beckman-Coulter manual). Between two successive runs, the capillary was rinsed with 0.1 M

NaOH, 0.1 M HCl, water, and SDS-gel buffer for 10, 5, 2 and 10 min, respectively. Both the capillary inlet and outlet were dipped twice into water to clean the viscous residual gel buffer before sample injection. Sample injection was performed at the anode of Agilent G1600AX 3D Capilary Electrophoresis System with reverse polarity using −5 kV for 20 s, then both ends of the capillary were dipped one more time to reduce sample carry over. Separation was then carried out at −15 kV for 40 min in the reverse polarity mode with 20 psi of pressure applied to both capillary ends during the electrophoretic run. A typical current of 29 μA was observed during separation. UV detection was conducted at 220 nm. Sample storage and cartridge temperatures were maintained at 25 °C.

All investigated antibodies were prepared in 100 μL of SDS sample buffer (100 mM Tris–HCl pH 9.0, 1 mM SDS) at a concentration of 1–2 mg/mL. Two microliters of the 10 kDa protein standard were systematically added before sample injection in the PA800 electrophoretic system. Molecular weight estimation was obtained from the plot of log (MW) versus the relative migration time (tm/tI.S.) where tm and tI.S. represent the migration times of a given fragment and the internal standard (10 kDa), respectively. A linear relationship was obtained with a determination coefficient higher than 0.98.

Edman sequencing

3 cycles of Edman degradation were performed with the sequencer cLC 492 Applied Biosystems with a UV detector 785A (Perkin Elmer) in the Preotemics Unit of the Barcelona Science Park.

LC-MS

Protein conjugates were characterized by HPLC-ESI MS using an LCT-Premier (Waters) with a cromatograph Acquity UPLC binary Sol MGR (Waters) and a column BioSuite pPhenyl 1000RPC 2.0 x 75 mm, 10 μm. Eluents were water (A) and acetonitrile (B), both with 0.1 % formic acid. The gradient used was 5 % to 80 % eluent B in 60 min and flow rate 100 μL/min. Mass spectra were deconvoluted using Waters MassLynx MaxEnt 1.

ELISA for Bv detection

9 μL of VEGF in PBS (0.1 mg/mL in PBS with 0.1 % BSA) was diluted 1:500 in ammonium bicarbonate buffer pH 9.6. 100 μL/well of this solution (0.2 μg/mL) were applied to a 96-well ELISA plate to coat the wells and shacked at RT for 2 h (100 rpm). Four 5-min-washings with 200 μL/well PBST (PBS + Tween 20 0.05 %) were performed to remove excess ligand. The plate was blcoked with 2 % BSA in PBST for 1 h (200 μL/well). After 4 washings, samples were incubated for 1 h. Then 6 washings were performed and an anti-human Fab linked to HRP (Sigma-Aldrich) was applied at 1:1200 dilution for 1 h (100 μL/well). Finally, it was washed 6 times

more and 100 μL/well of turbo TMB were applied followed by 1 M sulfuric acid (100 μL/well). Absorbance was measured at 405 nm. All measurements were performed in triplicate.

^{125}I protein labelling and quantification

Using Iodogen®

Iodination was carried out using Pierce Iodination beads or Iodogen® pre-coated iodination tubes using manufacter´s instructions. Briefly, proteins in reaction buffer (NaPi, 50 mM, pH 6.5) was added to a Iodogen® Pre-coated iodination tube. Carrier free Na^{125}I (approximately 1 mCi/mg) was added to the tube and allowed to react for 15 min. The crude was added to a solution of tyrosine (10 mg/mL) to stop iodination. Excess of reagents was eliminated by SEC purification (NAP-5, GE Healthcare, equilibrated with Ringer Hepes). Fractions of 250, 500, 250, 250 and 1000 μL were collected and radioactivity of 10 μL fractions was measured for 2 min using Packard Cobra II Gamma Counter. BCA was used to determine the protein concentration.

Using Iodobeads®

Two iodination beads were used for each antibody. Briefly, beads were washed with reaction buffer (NaPi, 50 mM, pH 6.5) and dried on filter paper. In a glass vial, beads were added to a solution of carrier free Na^{125}I (approximately 1 mCi/mg) and incubated for 5 min. Proteins were added to the activated solution and the reaction was allowed to proceed for 15 min with eventual mixing. The reaction was stopped by removing the solution from the reaction vessel and adding it to a NAP-5 column (GE Helathcare) equilibrated with Ringer Hepes. Fractions of 250, 500, 250, 250 and 1000 μL were collected and radioactivity of 10 μL fractions were measured for two min using Packard Cobra II Gamma Counter. BCA was used to determine the protein concentration.

NP modification and characterization

Quantum dot modification

Quantum dots were conjugated as previously described with some modifications.[289] Briefly: 1 μL of 0.4 M *N*-(γ-maleimidobutyryloxy)succinimide in DMF (400 nmol, 1000 eq) (Sigma-Aldrich) was diluted with 79 μL of 50 mM borate buffer pH 8. pH was readjusted to 8 with 0.1 M NaOH. This solution was mixed with 50 μL of 8 μM Amino PEG QDot 605 (0.4 nmol, 1 eq) (Life Technologies). The mixture was incubated for 1h at room temperature under gentle shaking and was then separated with a NAP-5 column (GE Healthcare) eluting in PBS.

A 0.4 M solution of 80 μL of 0.4 M *tris*(2-carboxyethyl)phosphine (TCEP) was prepared in 100 mM phosphate buffer pH 8. 4 μL of this TCEP solution (1.6 μmol, 4000 eq) was preincubated with 80 μL of 5 mM Cys-MiniAp-4 in water (400 nmol, 1000 eq) to minimize the presence and further formation of peptide dimers linked through a disulfide bond. This solution was mixed with the functionalized QDots and stirred for 1h at room temperature being gently shaken.

Most of the peptide was then removed through a NAP-5 column. To verify the abscence of free peptide, the derivatized QDots were buffer-exchanged by centrifugal filtration using a Vivaspin-500 MWCO 100000 (GE Healthcare) until no peptide could be detected by HPLC-UV. The amount of linked peptide was quantified by amino acid analysis after 3-day hydrolysis in 6 M HCl. The last washings were quantified using the same technique and no peptide could be detected.

Gold nanoparticles synthesis and modification

12 nm AuNPs were synthesized as reported elsewhere.[376] 50 mL of 1 mM $HAuCl_4$ (Sigma-Aldrich) in water solution was heated at 110ºC and refluxed for 10 min. 5 mL of 38.8 M sodium citrate was added and the mixture was refluxed for another 30 min. The solution was cooled to room temperature and pH was adjusted to 8.66 with 1M NaOH. Samples were filtered and characterized using a UV-spectrophotometer (Shimazu) and TEM. Buffer is exchanged through precipitation and resuspension for more diluted 2.2 mM citrate (Sigma-Aldrich). The conjugation was performed by ligand exchange using 8.6 nM AuNPs and 100 μM peptide for 3 h at room temperature under mild shaking. Unconjugated peptide was removed using a PD-10 column (GE Healthcare) and buffer exchange precipitation-resuspension until no peptide was detected by HPLC-UV in the supernatant. Conjugated NPs were again characterized by UV-spectrophotometry and TEM. The amount of conjugated peptide was obtained using amino acid analysis after washing with 1% TFA followed by a 3-day hydrolysis in 6 M HCl. The NPs were quantified spectrophotometrically ($\varepsilon = 5.7 \cdot 10^7\ M^{-1}cm^{-1}$)[291].

Characterization and quantification

Transmission electron microscopy

Electron micrographs were acquired using a Tecnai Spirit electron microscope, equipped for cryo and tomography or Jeol JEM 2010F, operating at 200 KV coupled to an electron energy loss spectrometer. TEM grid covered with Formvar were activated for 5 min under UV illumination and the sample was deposited and dryed in a desiccator.

Inductively coupled plasma – mass spectrometry

Inductively coupled plasma – mass spectrometry (ICP-MS) was used to quantify QDots and AuNPs in the cell-based BBB model transport assays. The instrument was an Agilent ICP-MS 7500 cx equipped with a collision chamber. Rhodium (200 ppb) was used as an internal standard.

Amino acid analysis

Amino acid analysis of the peptides coating NPs was performed as described in the *Peptide Synthesis* section but digestion with HCl 6 M was extended to 72 h.

Cell-based assays

Cell culture conditions

Cells for internalization and MTT experiments were cultured in DMEM complete medium (glucose 4.5 g/L and 2 mM glutamine) with 10 % FBS (both from Sigma). Medium was changed 3 times per week and cells were passaged using 0.05 % trypsin/EDTA when they reached 80-90 % confluence. For the BBB cell-based models special media were used as specified below.

Cytotoxicity - MTT

3500 HeLa cells or 7000 bEnd.3 cells were seeded in 96-well plates 24 h before starting the assay. After this period, peptides were incubated at 10, 50 and 500 μM in DMEM (1 mg/mL or 4.5 mg/mL glucose for HeLa and bEnd.3 respectively) supplemented with 10 % serum for 24 h. After 22 h, MTT reagent was added to a final concentration of 0.5 mg/mL. After a 2-h-incubation, the medium was discarded and the purple crystals of formazan were dissolved in 200 μL of DMSO. The plate was shaked for 30 min and absorbance was measured at 570 nm. Cell viability was calculated dividing the absorbance of wells treated with a given peptide by the absorbance of untreated wells. Measurements were performed in triplicate. As a positive control, cells were incubated with 1% SDS.

EGFR phosphorilation inhibition experiment

U87MG cells engineered to over-express EGFR were counted and seeded at equal densities in multi-well plates in complete media. Following an overnight incubation, adherent cells were washed with PBS and serum-free media was applied for 48 h. Cells were treated for 15 min at 37 ºC at 5 % CO_2 with 20 ng/ml of EGF o previously pre-incubated with 33 nM Cx or Cx conjugates. Cells were then harvested in RIPA buffer and cell lysates were quantified by BCA, resolved by SDS-PAGE, transferred to nitrocellulose membranes and blotted with the specific antibodies. Antibodies used were as follows: anti- phospho-tyrosine 4G10 for EGFR phosphorylation and anti-β-actin for loading control.

Internalization

200000 bEnd.3 cells/well were seeded in 12-well plates. After 2 days of growth, cells were treated with filipin III (10 μg/mL), chlorpromazine (10 μg/mL) or vehicle (Ringer HEPE) for 15 min. After this preincubation time, enough labelled peptide was added to reach a final concentration of 200 μM. After 30 min, cells were washed 5 times with Ringer HEPES at 4 ºC, detached with trypsin(0.05 %)/EDTA and kept in ice. Cells were immediately analized using an FC500-MPL flow cytometer with a 488 nm laser (Beckman Coulter).

Permeability assays

PAMPA

The PAMPA assay[3] was used to determine the effective or apparent permeability (P_{app}) of the compounds, which reflects their capacity to cross the BBB by passive diffusion. The buffer was prepared from the concentrated solution by pION following the manufacturer's instructions. The pH was adjusted to 7.4 using a 0.5 M NaOH solution. Each compound was dissolved in buffer solution to an initial concentration of 200 μM.

The PAMPA sandwich was separated and the donor well was filled with 195 μL of the compound solution and a stirring magnet was added. Then, the acceptor plate was placed into the donor plate. 4 μL of the 20 mg/mL phospholipid mixture (PBLEP) in dodecane was added to the filter of each well, 200 μL of buffer solution was added to each acceptor well and the plate was covered. Three replicates were performed for each compound. The PAMPA plate was incubated for 4 h at 20ºC and saturated atmosphere in the GUT-BOX™ apparatus under an agitation vigorous enough to reduce the unstirred water layer down to 25 μm. After the incubation, the sandwich was separated and an aliquot of each donor and acceptor well was analyzed by RP-HPLC.

The phosphorlipid mixture used was a porcine polar brain lipid extract, which is composed by: 12.6% phosphatidylcholine (PC), 33.1% phosphatidylethanolamine (PE), 18.5% phosphatidylserine (PS), 4.1% phosphatidylinositol (PI), 0.8% phosphatidic acid and 30.9% of other compounds.

Caco-2 Cell-Based Model Assay

A 96-well plate format of the CacoReady kit from Readycell was used to evaluate the permeability through a Caco-2 monolayer. The manufacturer's protocol was thoroughly followed. The MiniAp-1 was evaluated in triplicates at a concentration of 200 μM. Peptides were incubated for 2 h, after which the donor and acceptor wells were analyzed by HPLC-UV. Measurement of TEER was used to assess the integrity of individual monolayers in each well, and Lucifer yellow was used as an external standard to verify the correct performance of the assay.

BBB-RTU assay

This experiment was performed using the BBB-RTU 24 well kit by Cellial Technologies S.A. The kit contains the plates with and without cells as well as the mediums and buffers required for the assay. The protocol for cell culture and transport assay followed is summarized in the following lines.

The complete culture medium was defrosted the day of manipulation and pre-heated at 37ºC. As soon as the RTU plate was removed from -80ºC, BBB complete culture medium (CCM) was poured in the lower compartment without separating the plates and in each donor well. The cells were resuspended in each insert (donor well) and the plates were placed in a cell culture incubator (Binder BD 53) at 37 ºC, 5 % CO_2 and 95 % humidity during 4h. After that time, the medium from all compartments was removed gently using an aspiration system. The plate was washed once with BBB CCM and refilled with new BBB CCM. The plates were put into the cell culture incubator and the cells were allowed to grow for three days. At the 3rd day, BBB inducing medium (IM) was incorporated. The BBB CCM was replaced and the plate was placed in a cell culture incubator for 48h.

The day of the transport experiment, the stock solutions of test peptides were prepared in RH buffer in a 200 μM concentration containing Lucifer Yellow (LY) 20 μM. Transport plates (24-well Receiver Tray, Millipore ref. PSMW010R5) were filled by adding 800 μL of warm RH buffer and put into a cell culture incubator. The inserts containing cells and lower compartment were washed with RH buffer, which was removed after less than 5 minutes. At time zero, the insert plate was gently transferred to the 24-well plate containing RH buffer and 400 μL of the peptide stock solution were applied to each insert. After 2 h in the incubator the samples from both donor and acceptor wells were recovered and frozen until analysis.

LY fluorescence was measured using a 96-well plate in a Fluoroskan Ascent Microplate Fluoromoeter (Thermo Fisher Scientific). The samples were injected in an HPLC. Areas under the peaks were integrated and, considering that they are proportional to the concentration of the sample, they were used in equation 3 to obtain P_{app}. In addition, mass balances were also calculated to estimate the amount of peptide that is degraded or trapped in the cells or membranes. Samples were evaluated in triplicates.

Endothelial permeability: $$P_e \sim 1 \div \left(\frac{1}{P_{app}} - \frac{1}{P_f}\right)$$ ***Equation 4***

Total transport: $$T, \% = 100 \cdot \frac{Q_A(t)}{Q_D(t_0)}$$ ***Equation 5***

Membrane retention: $$M_r, \% = 100 \cdot \frac{Q_D(t) + Q_A(t)}{Q_D(t_0)}$$ ***Equation 6***

where P_{app} and P_e are obtained in cm/s, t is the length of the assay in seconds, P_f corresponds to P_{app} of inserts without cells, $Q_A(t)$ is the amount of compound at time t in the acceptor wells, $Q_D(t_0)$ is the amount of compound at the beginning of the experiment in the donor wells.

Bovine BBB Cell-Based Model Assay

This assay was performed in a model adapted from Gaillard and de Boer.[269] Briefly, astrocytes were extracted from 2-5 day Wistar rat pups and bovine brain microvascular endothelial cells (ECCAC BBMVEC B840-05) were subcultured up to passage 3 and frozen. The apical side of 24-well Transwell inserts (Corning) was coated with collagen type IV (Sigma-Aldrich). Then the filters were turned upside down and glial cells (45000 cells/insert) were seeded on the basolateral side of the membrane. Defrosted passage 4-5 bovine endothelial cells were then seeded on the apical side of the Transwell inserts (45000 cells/insert). The co-culture was maintained in EBM2 medium supplemented with bovine brain microvascular endothelial cell growth medium BulletKit (Lonza) and 125 μg/mL of heparin (Sigma-Aldrich); this medium was changed every 2 days. After 4 days, this medium was additionally supplemented with 8-(4-chlorophenylthio)-cAMP and RO-20-1724 (Sigma-Aldrich) and the assay was performed 24 h later. The TEER was measured to control the increasing tightness of the monolayer. Experiments were not initiated until all wells had TEER > 100 ohm·cm^2. It was determined using an ohmmeter Millicell ERS system (MERS 000 01, Millipore) and calculated using the following equation:

$$TEER = \left(TEER_{filter\ with\ cells} - TEER_{filter\ without\ cells}\right) \cdot A \qquad \textbf{Equation 7}$$

where A is the area of the filter in cm^2

All peptides were assayed at 200 μM in Ringer HEPES. 200 μL of the compound was placed in the apical compartment and 800 μL of plain Ringer HEPES were poured into the basolateral well. After 2 h, the solutions from each compartment were recovered and quantified by HPLC-UV. Lucifer Yellow lithium salt (20 μM) (Sigma-Aldrich) was used as a control (Papp < $17 \cdot 10^{-6}$ cm/s) and measured in a 96-well plate with a Fluoroskan Ascent Microplate Fluorometer (Thermo Fisher Scientific).

Human BBB Cell-Based Model Assay

This experiment was performed using the model recently developed in the laboratory of Prof. Cecchelli.[59] In brief: Endothelial cells and pericytes were defrosted in gelatin-coated Petri dishes (Corning). Pericytes were cultured in DMEM pH 6.8 while endothelial cells were cultured in supplemented endothelial cell growth medium (Sciencells). After 48 h, pericytes were plated in gelatin-coated 12-well plates (50000 cells/well) and endothelial cells were seeded (80000 cell/well) in 12-well Transwell inserts (Corning) previously coated with Matrigel (Corning). Medium was changed every 2-3 days. Assays were performed 7-8 days after seeding. Lucifer Yellow (50 μM) was used as a control (Papp < $17 \cdot 10^{-6}$ cm/s).

Analyte concentration in the assays was: 200 μM for peptides, 100 nM for ^{125}I labelled GFP constructs, 30 nM for QDot605 and 5 nM for AuNPs. 500 μL of the compound in Ringer HEPES was introduced in the apical compartment and 1500 μL of Ringer HEPES alone in the basolateral compartment. The plates were set on a shaker at 60 rpm (1.6 mm radius) and 37^{o}C. After 2h, the solutions from both compartments were recovered and analysed. Samples were quantified as follows: an HPLC-UV system for peptides, a gamma counter for ^{125}I labelled GFP and ICP-MS for QDot605 and AuNPs.

In vivo assays

FET

Five concentrations of each peptide were evaluated (4.6, 10, 22, 46 and 100 mg/L) in water with 0.1 % DMSO. Two control groups were used, one with the vehicle (0.1% DMSO in water) and another with 3,4-dichloroaniline. First, fertilized eggs that did not show any anomaly were chosen and transferred into 24-well plates with 2 mL of vehicle or control in each well. The plates were incubated at 26 ± 1 ºC during 24 and 48 h. After each period of incubation, eggs were examined and results were analysed according to lethal parameters (number of coagulated embryos, tail detachment, lack of heartbeat and lack of somite formation) and sublethal parameter (spontaneous movements, pigmentation, oedema formation, rickets, malformation, scoliosis and generalised delayed development).

Immunogenicity

The immunogenic response of the peptides was evaluated by AntibodyBCN. Briefly: Free peptides were inoculated to BALB/C mice (n = 4) each other week during 12 weeks. Doses were 50 μg for MiniAp-1 and MiniAp-4 and 25 μg for apamin. The first inoculation was performed using Freund's complete adjuvant, while the rest were performed with Freund's incomplete adjuvant. Bleedings from the retromandibular vein were carried out at the beginning (preinoculation) as well as one week after the 4th and the 7th inoculations. The titer of antibodies in each bleeding was quantified using an indirect ELISA. Plates were coated with BSA conjugated to each peptide in carbonate buffer (overnight at 4ºC) and subsequently blocked with powder milk (2 h at 37 1C). Serial dilutions (1/2) starting in 1/100 were incubated (1 h at 37ºC). Anti-mouse IgG-HRP (Acris) was used as a detection antibody (1/5000 dilution, 1 h at 37ºC). Colorimetric quantification was achieved adding TMB (100 μL, 30 min), which was stopped with 1 M HCl (100 μL), and reading the plate at 450 nm. An IC50 was calculated when absorbance saturation was reached under these conditions.

General considerations for other experiments on mice

5-week CD1 mice (*Mus musculus*) were obtained from Charles River. Animals were housed at the Barcelona Science Park or in the Hospital Clinic de Barcelona animal facility in a 12 h light/dark cycle according to the standard of holding facility and were fed ad libitum. All experiments were approved by the animal ethics committee of the Barcelona Science Park or the Hospital Clinic de Barcelona respectively.

Acute toxicity test on mice

Four groups (n = 6) of mice were used (20 ± 2 g). Each group was injected with 200 μL of one of the following solutions: 6 mM MiniAp-1 or MiniAp-4 solutions (1200 nmol), 0.25 mM apamin solution (200 nmol) or sterile water. Mice were observed during the first hour and after 2, 4, 8 and 24 h.

In vivo total animal fluorescence imaging

Cyanine5.5 conjugates were injected via the tail vein (4 nmol in 150 μL of sterile water) in 6- to 7-week-old CD1 mice (n = 4). Fluorescence was measured in an IVIS Spectrum Pre-clinical In Vivo Imaging System (IVIS-200) 0.5, 1, 2, 4, 8 and 24 h after injection. Filters were set to measure cyanine5.5 subtracting cyanine5.5 background (1-s exposure). The heads of the animals were shaved before the first measurement, and for each time-point mice were anesthetized with isofluorane for 3 min and kept under anaesthesia during image acquisition. Between measurements, mice were allowed to recover and were fed *ad libitum*. Three groups of mice (n = 4) were injected either with cyaniene5.5-MiniAp-4, cyanine5.5-cysteamine or vehicle (sterile water).

Ex vivo fluorescence imaging

Cyanine5.5 conjugates were injected via the tail vein (4 nmol in 150 μL of sterile water) in 6- to 7-week-old CD1 mice (n = 4). After 1 h, mice were deeply anesthetized, imaged in the IVIS chamber and perfused with PBS for 5 min. The organs were immediately excised and the fluorescence was quantified in the IVIS chamber.

Confocal microscopy of brain slices

Cyanine5.5 conjugates were injected via the tail vein (4 nmol in 150 μL of sterile water) in 6- to 7-week-old CD1 mice (n = 3). After 1h, animals were deeply anesthetized and perfused with PBS followed by PFA to fix the tissues and the molecules for microscopy. Brains were immerged in sucrose 30% until density was equalled inside the tissue and cryoprotected with OTC (Tissue-Tek/ Sakuram Ref 4583) before freezing. Tissues were cut in coronal 15 or 50 μm slices using a cryostat. Frozen sections were permeabilized with PBS bearing 0.3% Triton X-100 (PBSTri) and treated with blocking solution (PBS containing 5% goat serum in PBSTri). In 50 μm slices capillaries were stained by free-floating with lectin-rhodamine for 2 h (1:500, Vector Labs). In 15 μm slices neurons were stained overnight with rabbit anti-NeuN antibody (1:100; Abcam) and glial cells with rabbit anti-GFAP (1:200; Abcam). After washing with PBSTr, the secondary antibody used was goat anti-rabbit Alexa 488 (1:500; Abcam). Antifading fluorescence mounting medium (Dako) was used to mount the slides. Samples were visualized in a Leica TCS SP5 MP system (DMI 6000) inverted spectral confocal microscope. A 60x/1.3 glycerol and a 20x/0.75 objectives were used.

Product characterization

Peptides

Yields were calculated after purification and quantification by amino acid analysis. * = yield of the fluorophore-peptide conjugation step.

HPLC or UPLC chromatograms and MALDI-TOF or LC-ESI-Q mass spectra are shown for each synthesized peptide. All HPLC chromatograms here shown were recorded at 220 nm in an 8-min linear gradient from 0 to 100 % of MeCN with (0.036% TFA) in H_2O (0.045% TFA) unless otherwise specified. All UPLC chromatograms here shown were recorded at 220 nm in a 2-min linear gradient from 0 to 100 % of MeCN with (0.036% TFA) in H_2O (0.045% TFA). Values represented the chromatograms represent time in minutes and those on the mass spectra correspond to the observed $[M+H]^+$. UPLC t_R are shown in italics to distinguish them from HPLC t_R and LC-ESI-Q m/z are displayed followed by ** to differenciate them from those obtaiend using MALDI-TOF.

For the nomenclature of cyclic peptides we followed the abbreviation rules proposed by Spengler *et al.*[122]

Peptides	Calc Mw	FTMS Mw	$[M+H]^+$ MALDI-TOF MS	t_R HPLC, min	Purity, %	Yield, %	Sequence, cargoes and linkers
Apamin	2025.887	2025.882	2027.0	3.4	> 99	8	H-C(&[1])NC(&[2])KAPETALC(&[1])ARRC(&[2])QQH-NH_2
ApOO	1941.843	1941.841	1943.0	3.2	> 99	9	H-C(&[1])NC(&[2])KAPETALC(&[1])A[Orn][Orn]C(&[2])QQH-NH_2
MiniAp-1	1599.641	1599.640	1600.8	3.9	95	5	H-C(&[1])NC(&[2])KAPETALC(&[1])AAAC(&[2])H-NH_2
MiniAp-2	727.423	727.423	728.5	3.5	> 99	30	H-KAPETAL-NH2
MiniAp-3	931.426	931.427	932.5	*3.8*	> 99	10	H-C(&)KAPETALC(&)-NH2
MiniAp-4	910.487	910.487	911.5	3.7	99	12	H-[Dap](&)KAPETALD(&)-NH_2
Peptides with small cargoes							
MiniAp1-β_sheet_breaker-peptide	2276.971	2276.973	2277.1	5.0	> 99	5	H-C(&[1])NC(&[2])KAPETALC(&[1])AAAC(&[2])HLPFFD-NH_2
Carboxyfluorescein-MiniAp1	1957.689	1957.690	1959.0	4.9	92	2	carboxyfluorescein-C(&[1])NC(&[2])KAPETALC(&[1])AAAC(&[2])H-NH_2
Carboxylfuorescein-MiniAp4	1325.556	1325.561	1326.7	4.6	98	7	carboxyfluorescein-G[Dap](&)KAPETALD(&)-NH_2
Levodopa-MiniAp1	1778.700	1778.699	1780.1	3.9	> 99	1	levodopa-C(&[1])NC(&[2])KAPETALC(&[1])AAAC(&[2])H-NH_2
Levodopa-MiniAp4	1089.546		1090.7	3.7	> 99	6	levodopa-[Dap](&)KAPETALD(&)-NH2
SulforhodamineB-MiniAp1	2197.810	2197.821	2197.8	5.1	91	0.2	sulforhodamineB-C(&[1])NC(&[2])KAPETALC(&[1])AAAC(&[2])H-NH_2
cyanine5-Zyentia_peptide	1573.981		1574.2	*1.90*	> 99	29*	cyanine5-a(*N*Me)f-^{D}2[Nal]-vlkk-NH_2
cyanine5-Zyentia_peptide-MiniAp4	2466.442		2467.6	*1.83*	> 99	24*	cyanine5-a(*N*Me)f-^{D}2[Nal]-vlkk[Dap](&)KAPETALD(&)-NH_2
cyanine5-Zyentia_peptide-THR	3045.699		3046.9	*1.83*	93	35*	cyanine5-a(*N*Me)f-^{D}2[Nal]-vlkkTHRPPMWSPVWP-NH_2
cyanine5-Zyentia_peptide-THRre	3045.699		3046.9	*1.82*	97	44*	cyanine5-a(*N*Me)f-^{D}2[Nal]-vlkkPWVPSWMPPRHT-NH_2
cyanine5.5-Zyentia_peptide	1673.012		1674.1	*2.02*	99	43*	cyanine5.5-a(*N*Me)f-^{D}2[Nal]-vlkk-NH_2
cyanine5.5-Zyentia_peptide-MiniAp4	2566.433	2566.447	2567.7	*1.93*	98	19*	cyanine5.5-a(*N*Me)f-^{D}2[Nal]-vlkk[Dap](&)KAPETALD(&)-NH_2
cyanine5.5-Zyentia_peptide-THR	3144.738	3144.738	3146.0	*1.93*	98	56*	cyanine5.5-a(*N*Me)f-^{D}2[Nal]-vlkkTHRPPMWSPVWP-NH_2
cyanine5.5-Zyentia_peptide-THRre	3144.738		3146.2	*1.93*	> 99	17*	cyanine5.5-a(*N*Me)f-^{D}2[Nal]-vlkkPWVPSWMPPRHT-NH_2
cyanine5.5-cysteamine	781.403	781.405	-	*1.98*	> 99	51*	cyanine5.5-cysteamine
cyanine5.5-MiniAp4	1717.869	1717.877	1718.9	*1.88*	> 99	48*	cyanine5.5-[Dap](&)KAPETALD(&)-NH_2
cyanine5.5-THR	2297.134	2297.136	2297.3	*1.84*	98	24*	cyanine5.5-THRPPMWSPVWP-NH_2
cyanine5.5-THRre	2297.127	2297.132	2297.2	*1.84*	99	32*	cyanine5.5-PWVPSWMPPRHT-NH_2

Peptides with linkers and reactive groups	Calc Mw	FTMS Mw	[M+H]+ MALDI-TOF MS	tR HPLC, min	Purity, %	Yield, %	Sequence, cargoes and linkers
alkyne-MiniAp1	1693.683		1694.8	5.0	93	4	hexynoyl-C(&[1])NC(&[2])KAPETALC(&[1])AAAC(&[2])H-NH_2
alkyne-RVG	3457.630			4.5	91	3	hexynoyl-YTIWMPENPRPGTPCDIFTNSRGKRASNG-NH_2
alkyne-Zyentia_peptide	1008.616		1009.6	5.1	> 99	11	hexynoyl-a(*N*Me)f-^{D}2[Nal]-vlkk-NH_2
alkyne-Zyentia_peptide-MiniAp4	1902.077	1902.078	1903.3	4.9	98	1	hexynoyl-a(*N*Me)f-^{D}2[Nal]-vlkk[Dap](&)KAPETALD(&)-NH_2
alkyne-Zyentia_peptide-THR	2480.334	2480.337	2481.2	5.0	> 99	9	hexynoyl-a(*N*Me)f-^{D}2[Nal]-vlkkTHRPPMWSPVWP-NH_2
alkyne-Zyentia_peptide-THRre	2480.334		2481.6	5.0	> 99	10	hexynoyl-a(*N*Me)f-^{D}2[Nal]-vlkkPWVPSWMPPRHT-NH_2
THRre-aminooxy	1661.825		1662.8	6.2	80	0.5	H-GPWVPSWMPPRHT-aminooxyacetyl
aminooxy-THRre	1746.878		1747.9	4.4	95	10	H-GK(aminooxyacetyl)PWVPSWMPPRHT-NH_2
carboxyfluorescein-(aminooxy)THRre	2047.904		2049.1	4.3	97	4	carboxyfluorescein-K(aminooxyacetyl)PWVPSWMPPRHT-NH_2
rhodamineB-(aminooxy)THRre	2116.509		2117.7	5.3	96	6	Rhodamine_B-K(aminooxyacetyl)PWVPSWMPPRHT-NH_2
carboxyfluorescein-(aminooxy)Angiopep2	2859.257		2860.7	*1.51*	94	2	Rhodamine_B-K(aminooxyacetyl)TFFYGGSRGKRNNFKTEEY-NH_2
Cys-MiniAp4	1013.496	*1013.498*	1014.6	3.9	> 99	4	H-C[Dap](&)KAPETALD(&)-NH_2
Cys-THRre	1591.754		1592.8	4.9	> 99	8	H-CPWVPSWMPPRHT-NH_2
maleimide-Angiopep2	2493.171		2494.0	*1.44*	95	9	maleimidohexanoyl-TFFYGGSRGKRNNFKTEEY-NH_2
maleimide-ApoE(159-167)$_2$	2564.744		2565.6	*1.38*	97	7	maleimidohexanoyl-TFFYGGSRGKRNNFKTEEY-NH_2
maleimide-MiniAp4	1103.561	1103.560	1104.5	4.2	> 99	4	maleimidohexanoyl-[Dap](&)KAPETALD(&)-NH2
maleimide-RVG(Ser)	3441.652		3461*	*1.49*	91	1	maleimidohexanoyl-TFFYGGSRGKRNNFKTEEY-NH_2
maleimide-TAT	1531.940		1544*	*1.09*	97	18	maleimidohexanoyl-YGRKKRRQRRR-NH_2
maleimide-THRre	1681.819		1682.9	5.0	99	7	maleimidohexanoyl-PWVPSWMPPRHT-NH_2
maleimide-PEG-THRre	1984.987		1985.1	5.0	97	4	maleimidohexanoyl-YTIWMPENPRPGTPSDIFTNSRGKRASNG-NH_2
maleimide-THRre(scr)	1681.819		1682.8	*1.62*	98	13	maleimidohexanoyl-LRKLRKRLLLRKLRKRLL-NH_2
carboxyfluorescein-THRre(maleimide)	2167.962		2168.8	5.2	96	2	carboxyfluoresceine-K(maleimidohexanoyl)PWVPSWMPPRHT-NH_2
rhodamine B-THRre(maleimide)	2235.136		2236.0	5.3	95	3	rhodamine_B-K(carboxyfluoresceine)PWVPSWMPPRHT-NH_2

Apamin

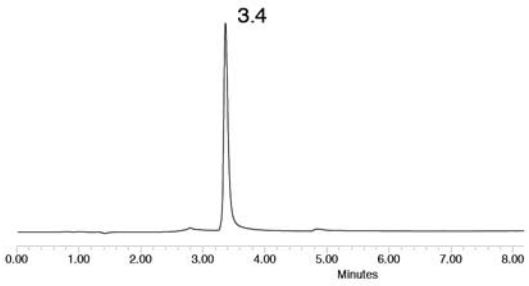

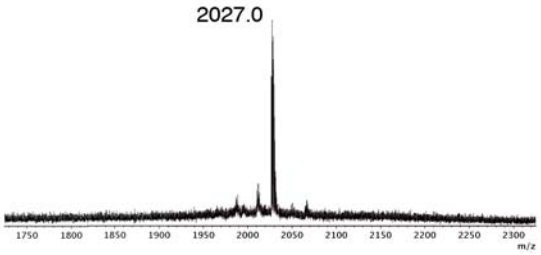

ApOO

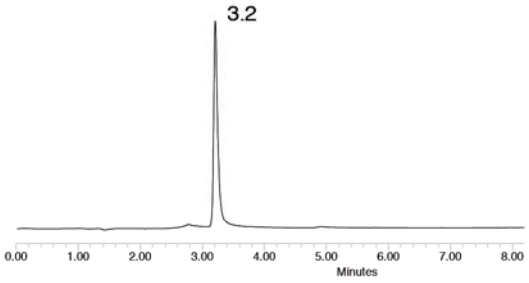

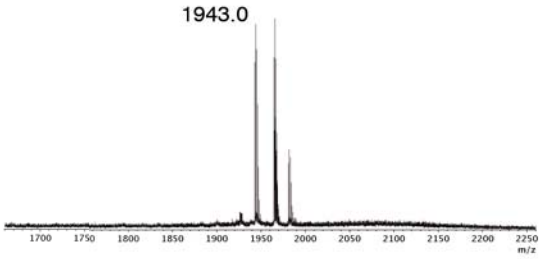

MiniAp-1

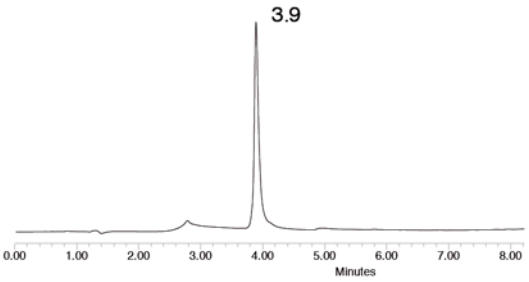

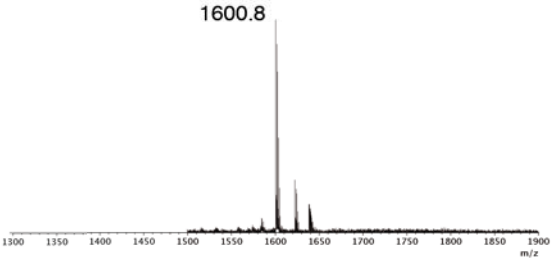

MiniAp-2

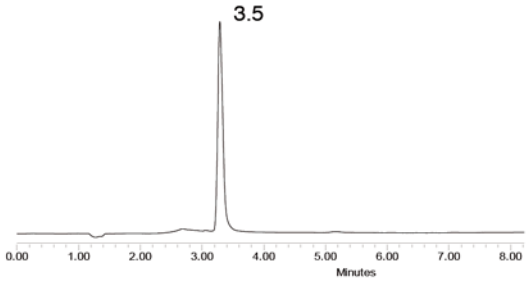

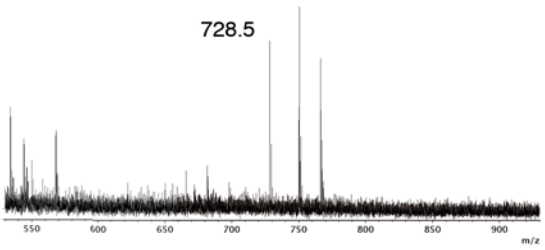

MiniAp-3

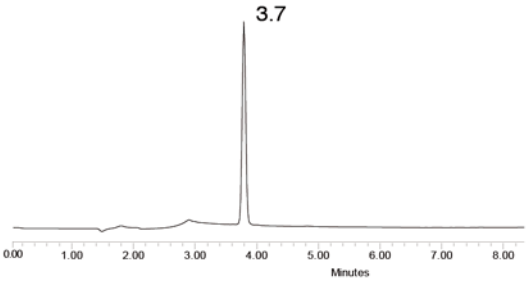

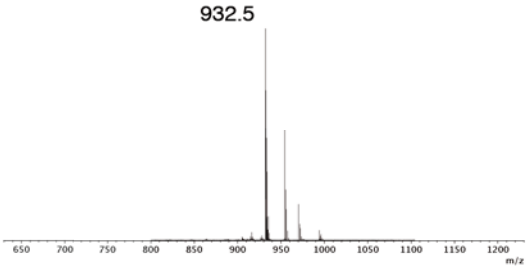

MiniAp-4

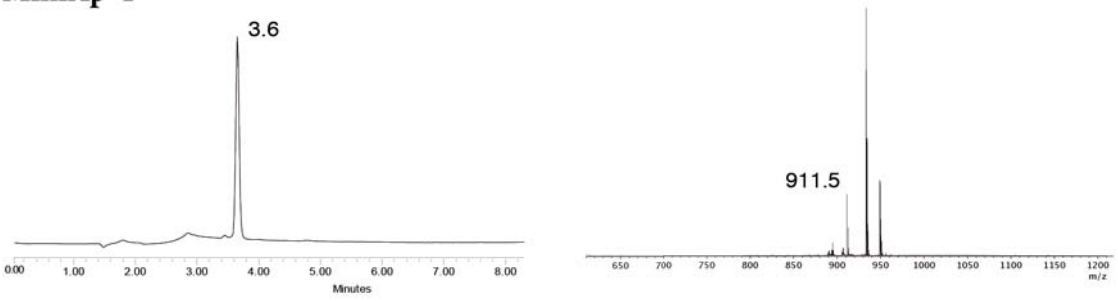

MiniAp1-β_sheet_breaker-peptide

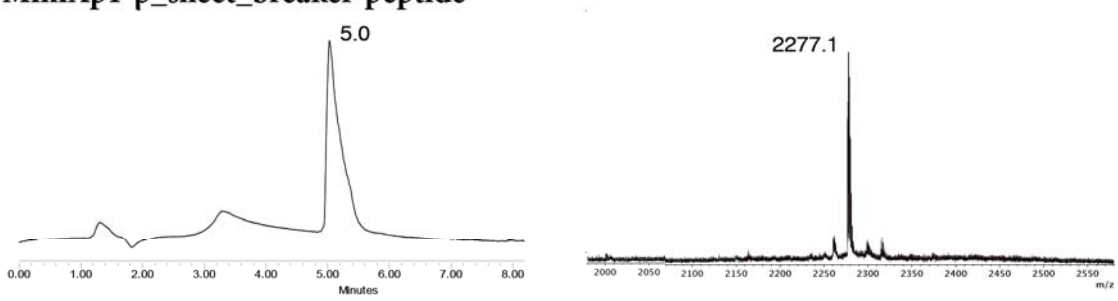

CFluorescein-MiniAp1

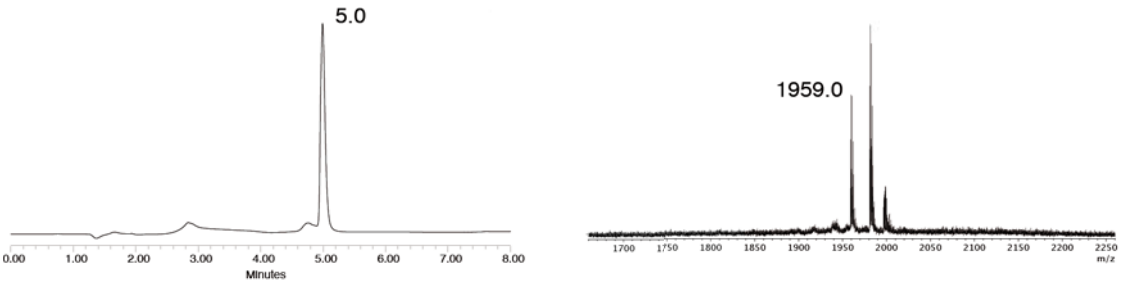

CFluorescein-MiniAp4

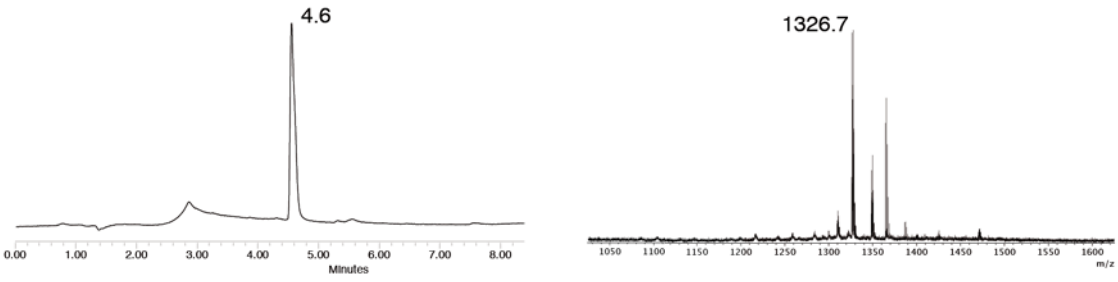

levodopa-MiniAp1

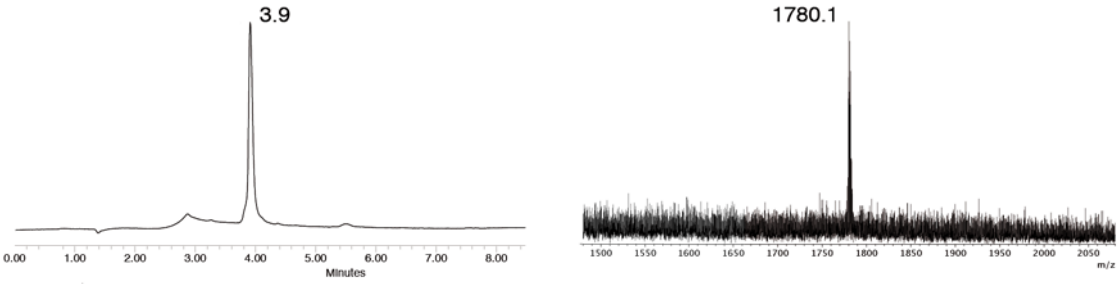

levodopa-MiniAp4

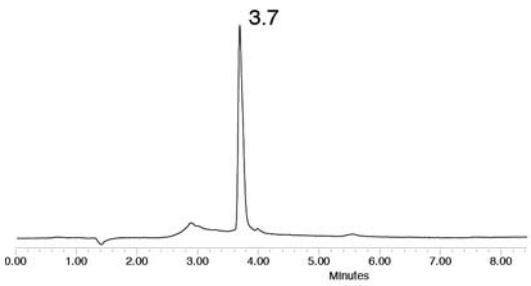

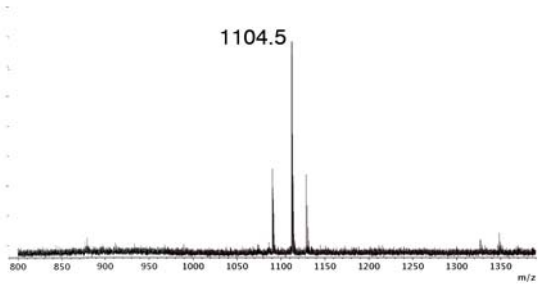

SRhodamine-MiniAp1

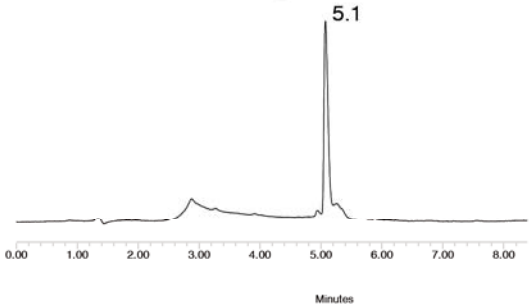

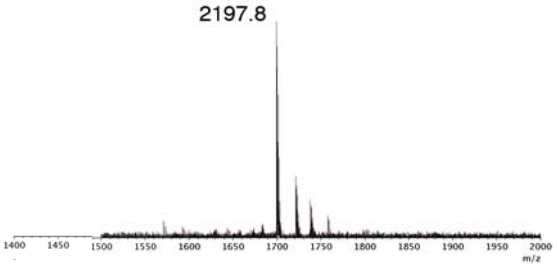

cyanine5-Zyentia_peptide

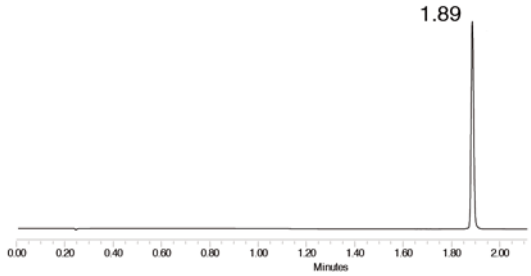

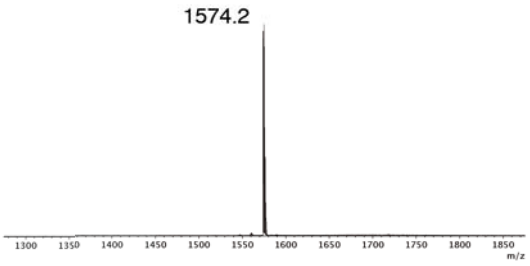

cyanine5-Zyentia_peptide-MiniAp4

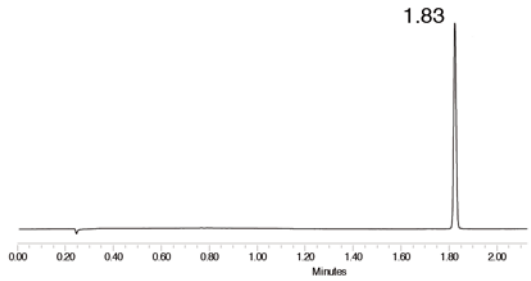

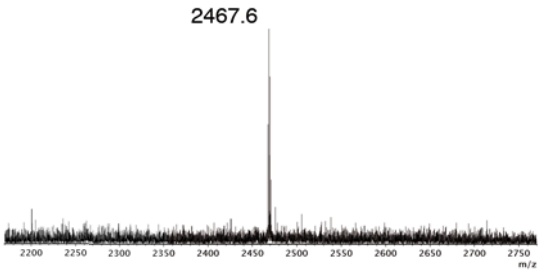

cyanine5-Zyentia_peptide-THR

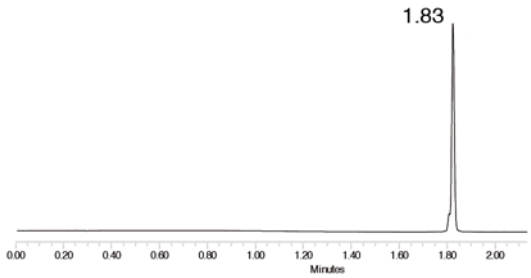

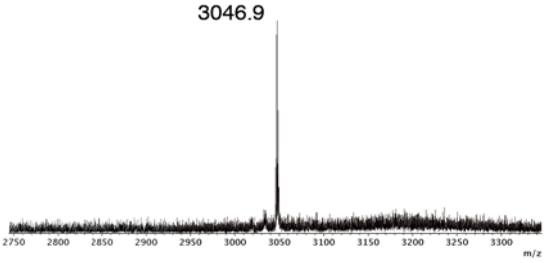

cyanine5-Zyentia_peptide-THRre

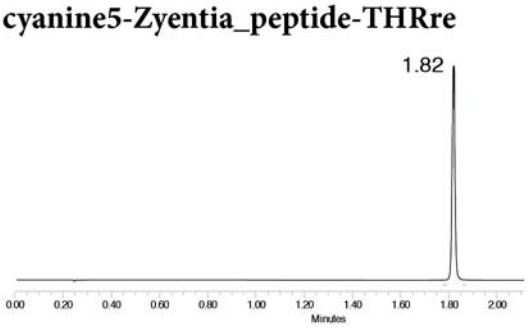

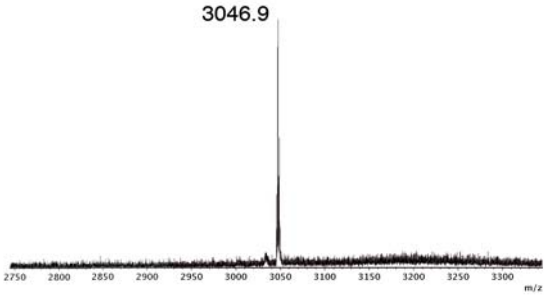

cyanine5.5-Zyentia_peptide

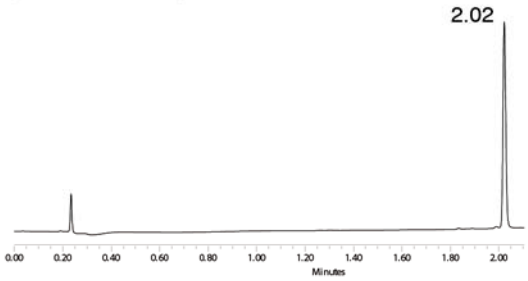

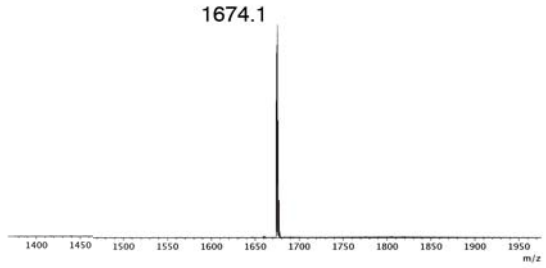

cyanine5.5-Zyentia_peptide-MiniAp4

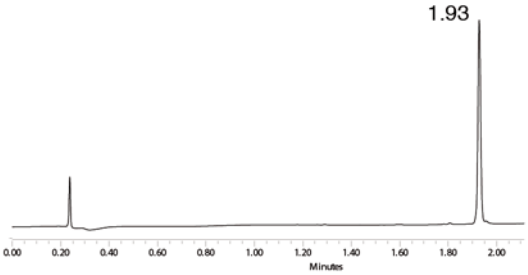

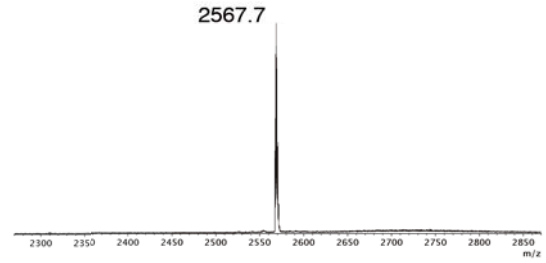

cyanine5.5-Zyentia_peptide-THR

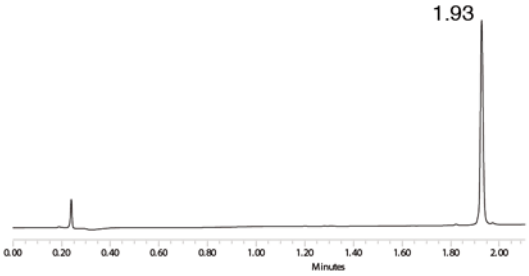

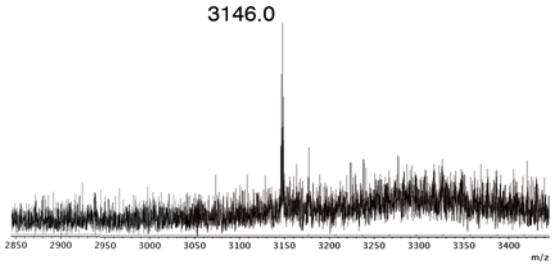

cyanine5.5-Zyentia_peptide-THRre

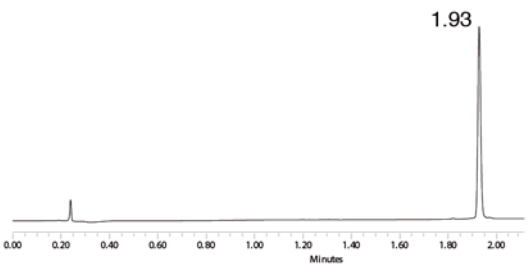

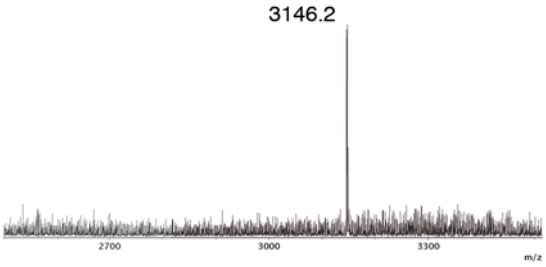

cyanine5.5-cysteamine

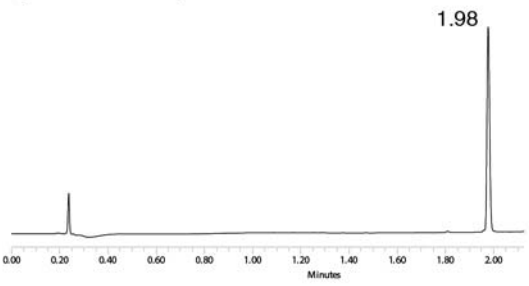

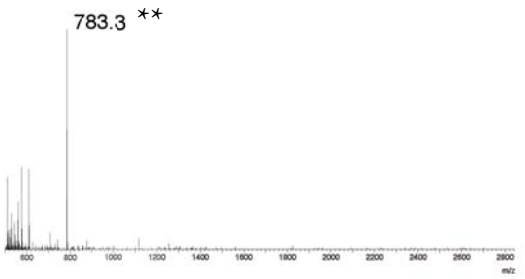

cyanine5.5-MiniAp4

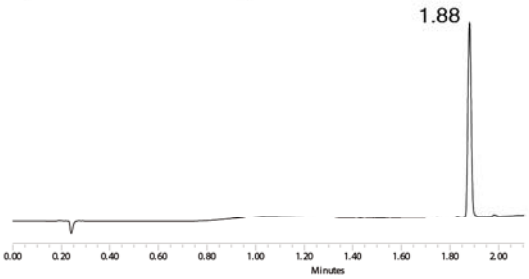

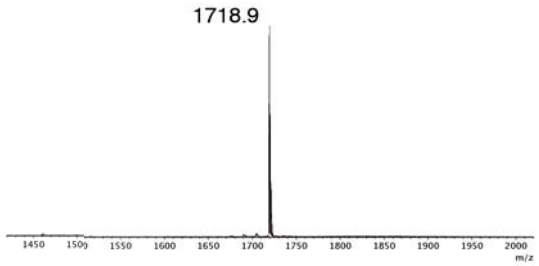

cyanine5.5-THR

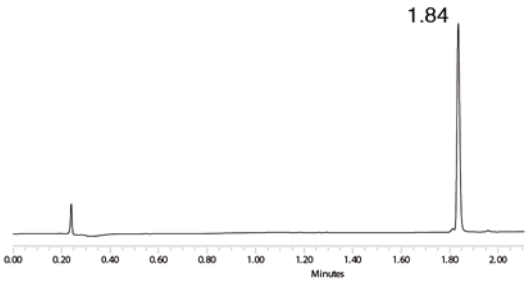

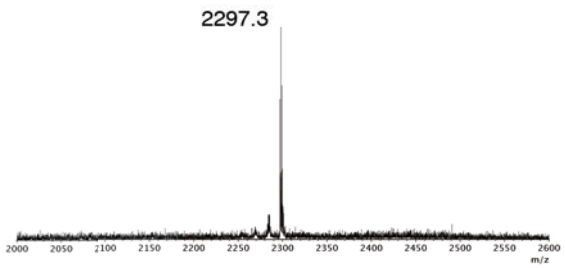

cyanine5.5-THRre

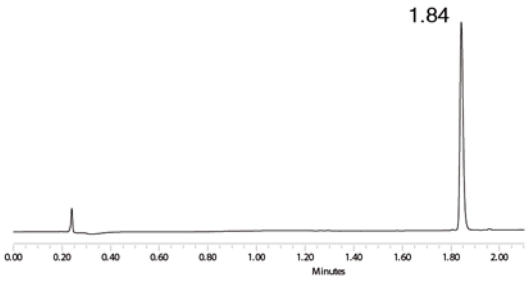

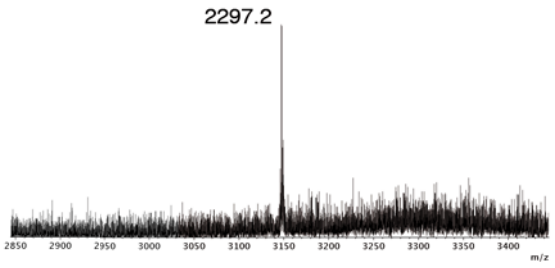

alkyne-MiniAp1

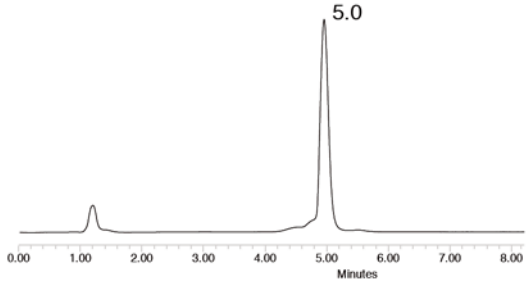

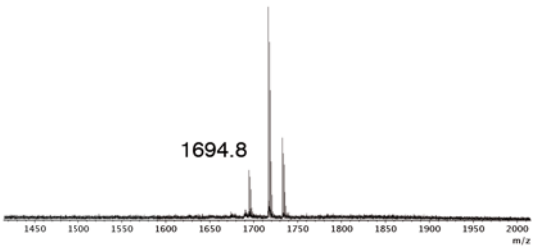

alkyne-RVG

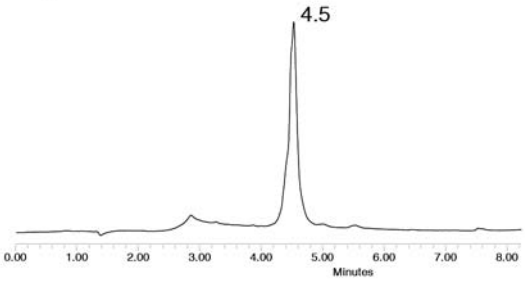

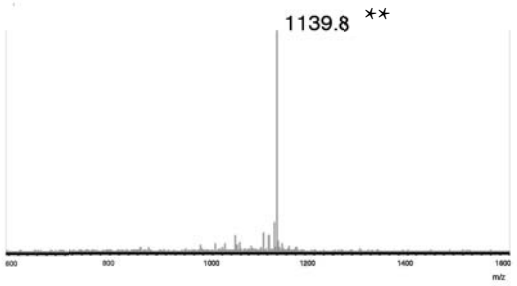

alkyne-Zyentia_peptide

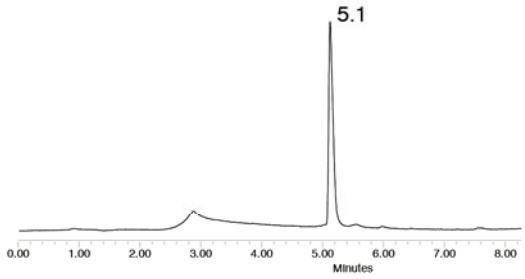

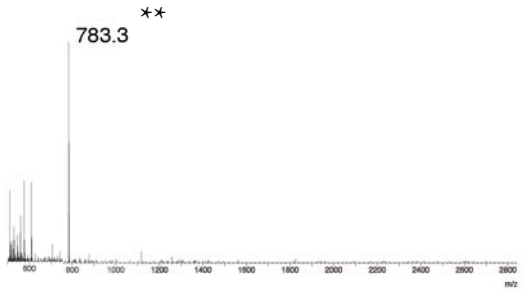

alkyne-Zyentia_peptide-MiniAp4

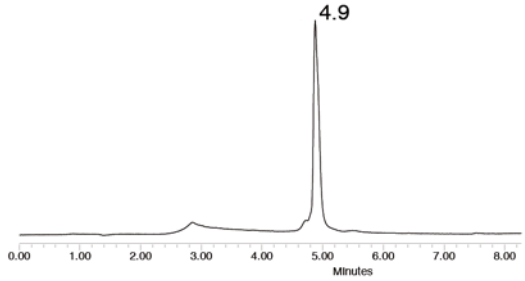

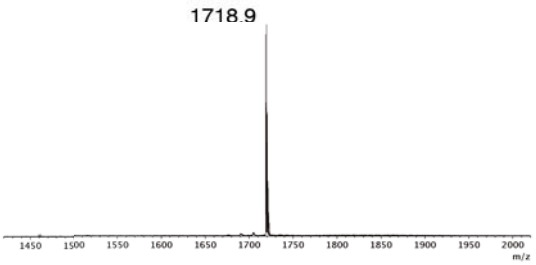

alkyne-Zyentia_peptide-THR

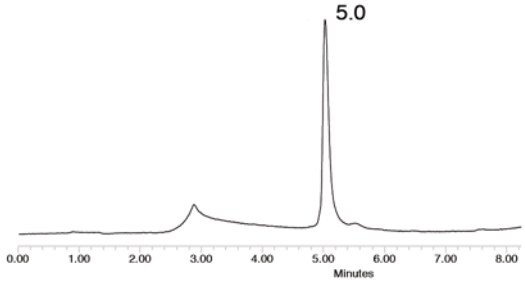

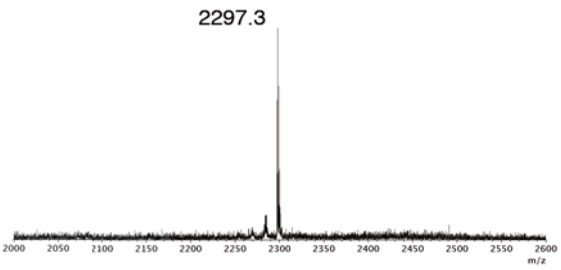

alkyne-Zyentia_peptide-THRre

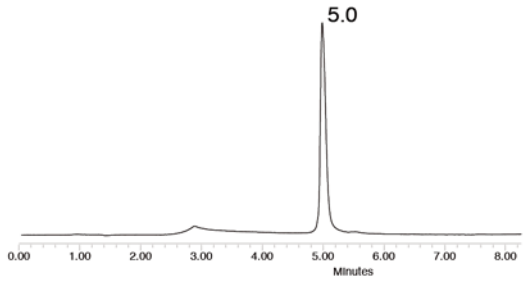

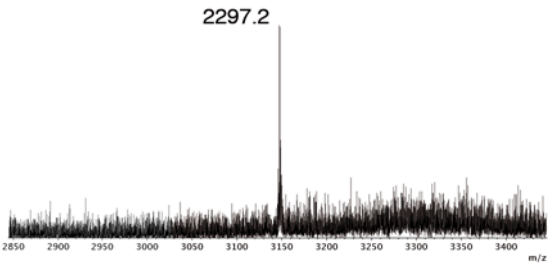

THRre-aminooxy

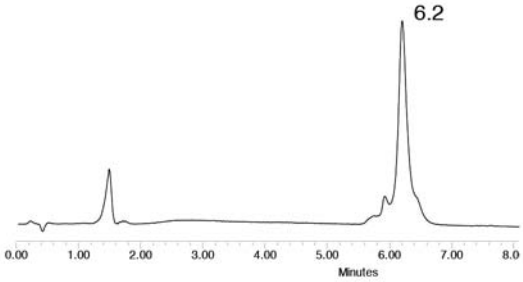

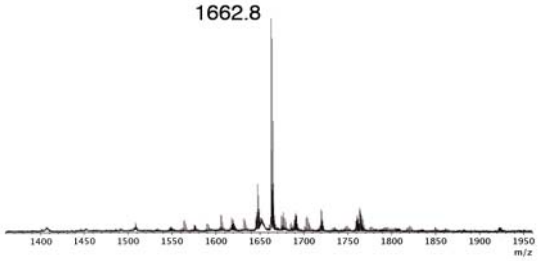

aminooxy-THRre

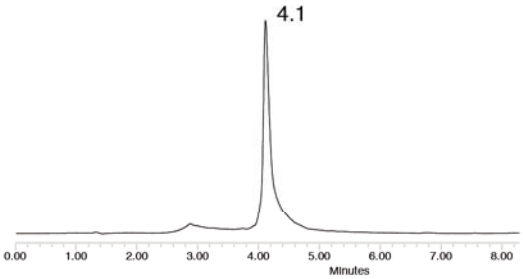

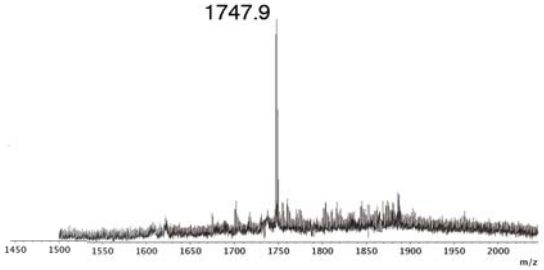

CFluorescein-THRre(aminooxy)

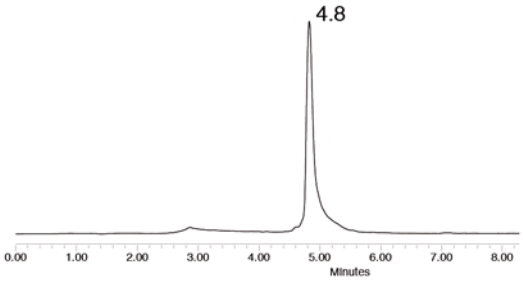

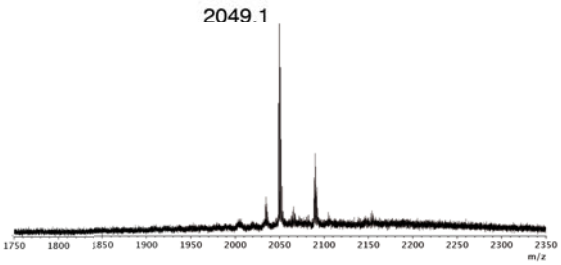

rhodamineB-THRre(aminooxy)

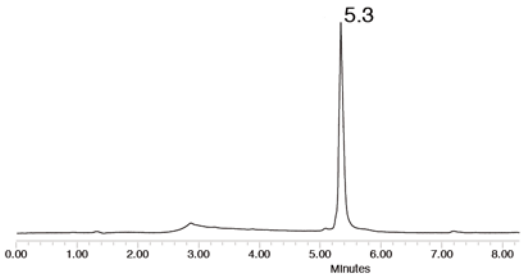

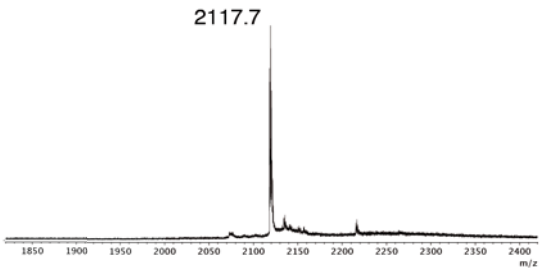

Cys-MiniAp4

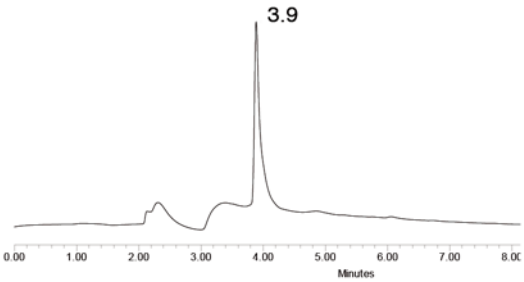

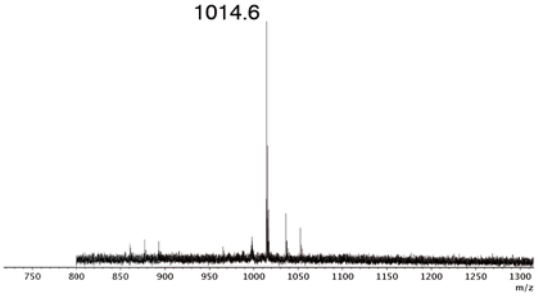

Cys-THRre

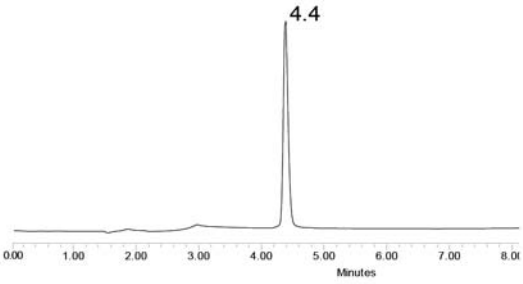

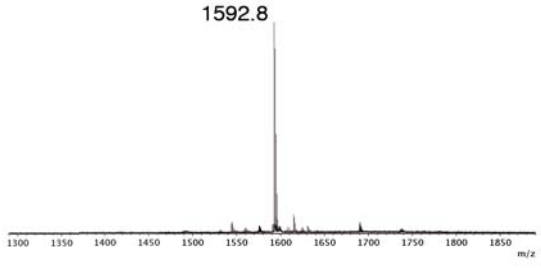

maleimide-Angiopep2

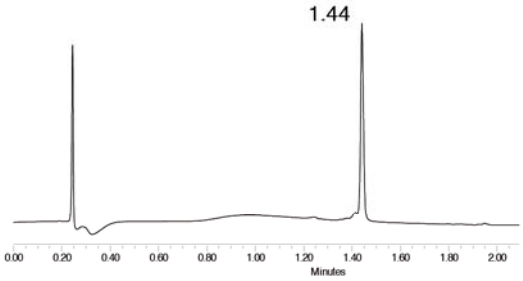

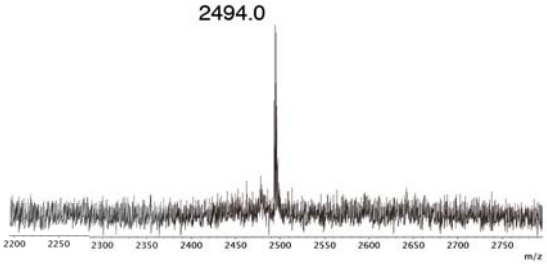

maleimide-ApoE(159-167)$_2$

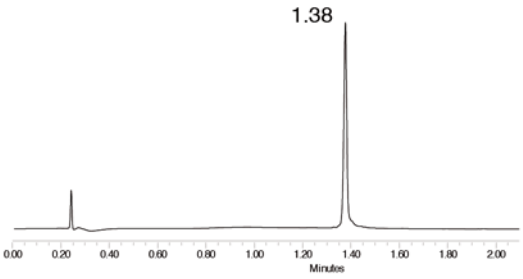

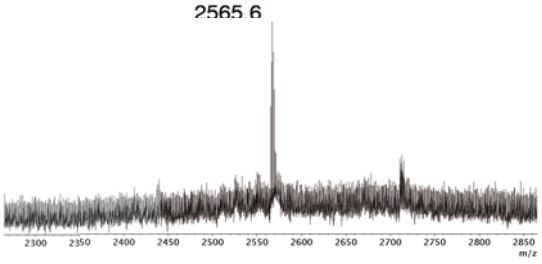

maleimide-MiniAp4

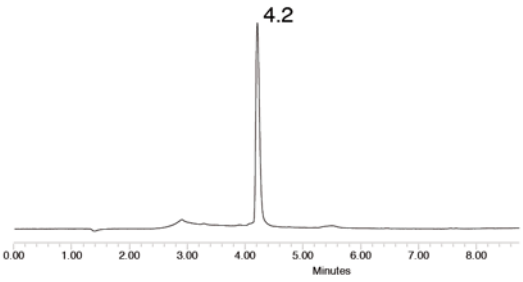

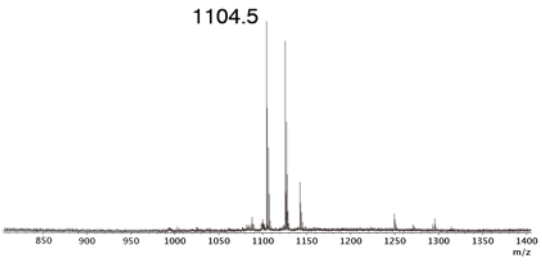

maleimide-RVG(Ser)

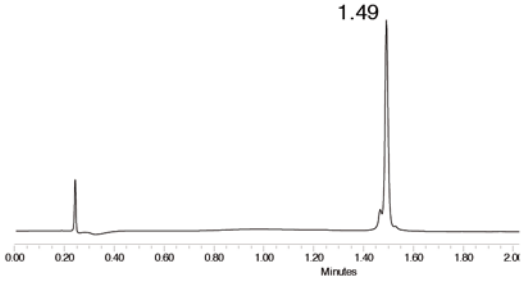

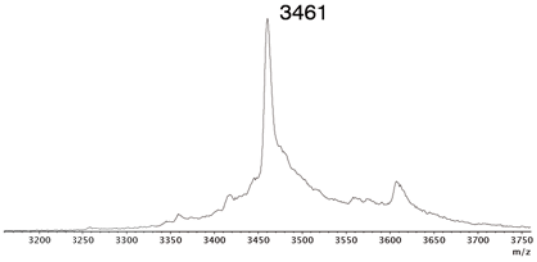

maleimide-TAT

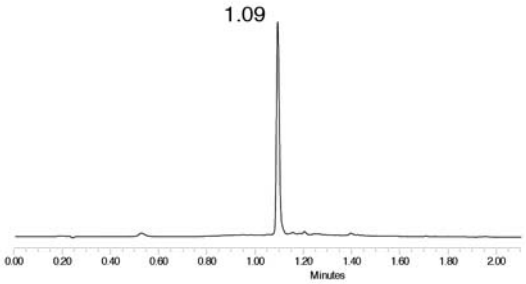

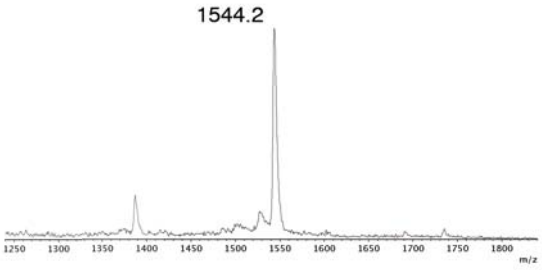

maleimide-THRre

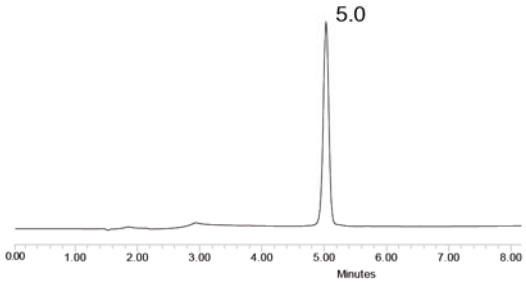

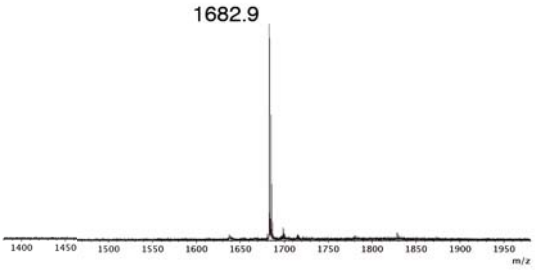

maleimide-PEG-THRre

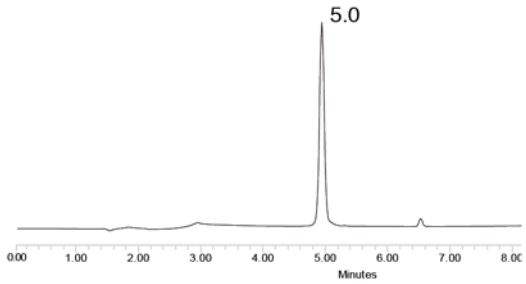

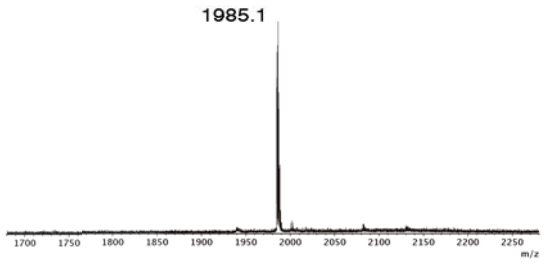

maleimide-THRre(scram)

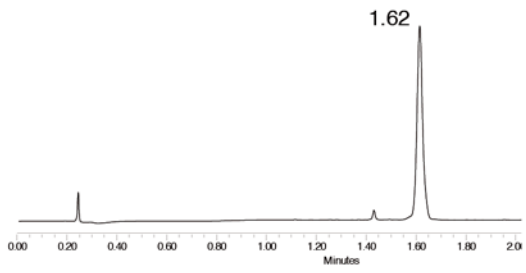

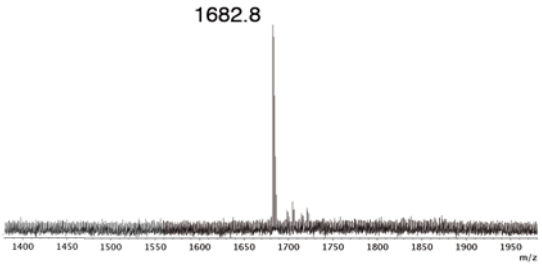

CFluorescein-THRre(maleimide)

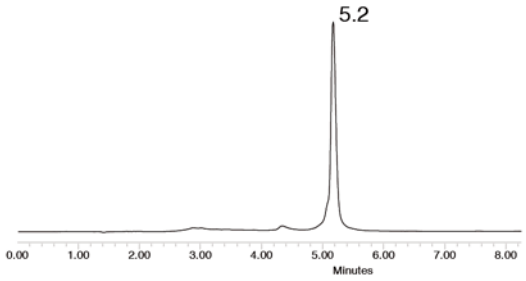

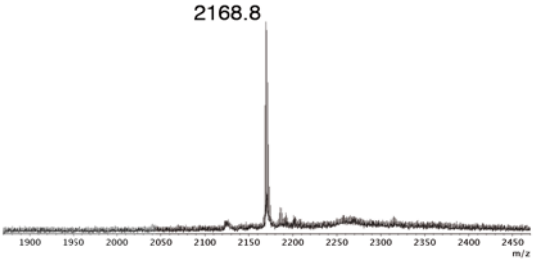

rhodamineB-THRre(maleimide)

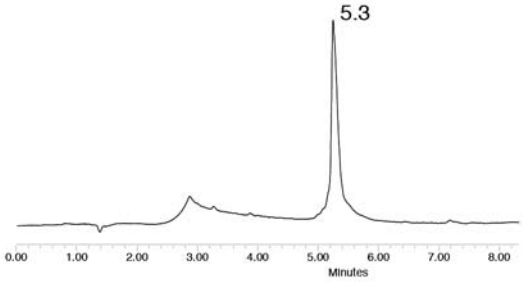

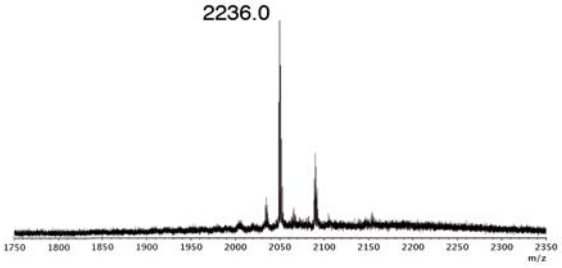

Proteins

In this section we include SDS-PAGE and mass spectra that have not been shown in the discussion. All spectra have been deconvoluted using MassLynx software.

GFP-MiniAp4

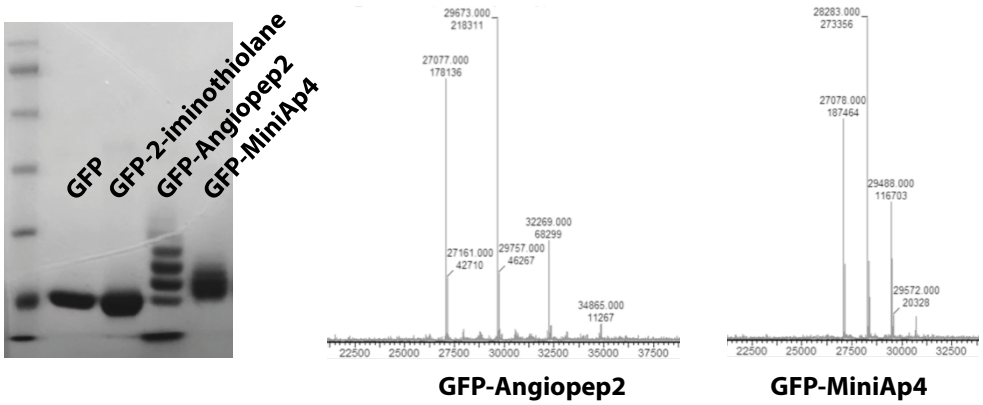

Table 6. *Species obtained upon conjugation of GFP.*

	Angiopep-2		**MiniAp-4**	
# peptides	Expected	Found	Expected	Found
1	29671	29673	28282	28283
2	32265	32269	29487	29488
3	34859	34865	30692	30694

Table 7. *Fragments found in the mass spectra of the Cx(Cys)-BBB-shuttle peptide conjugates by LC-MS.*

	L_{CH}-peptide		**L_{CH}-H_{CH}-(peptide)$_2$**	
	Expected	Observed	Expected	Observed
Angiopep-2	25760	25918	80988	81313
TAT	24798	24957	76000	76396
ApoE	25832	25988	78566	77964
THRre(scram)	24949	25105	79366	79698
THRre	24949	25107	79366	79691
PEG-THRre	25252	25408	79972	80293
MiniAp-4	24370	24527	78208	78530
RVG(Ser)	26709	26864	82886	n.d.

n.d. stands for not detected. L_{CH} stands for light chain and H_{CH} for heavy chain.

Bv(Nterm)-Angiopep-2

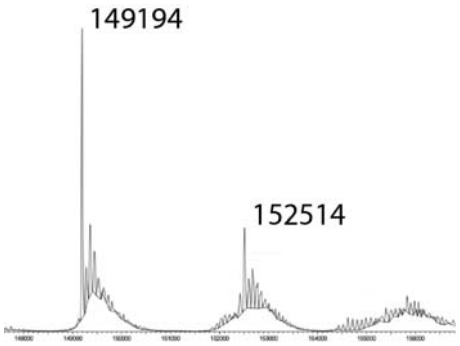

Bv(Lys)-CFluorescein (left) and RhodamineB (right)

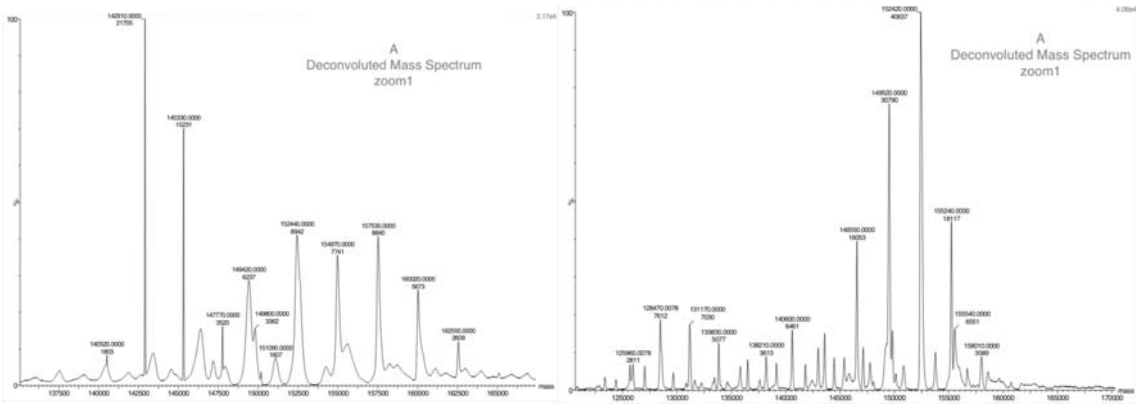

Cx

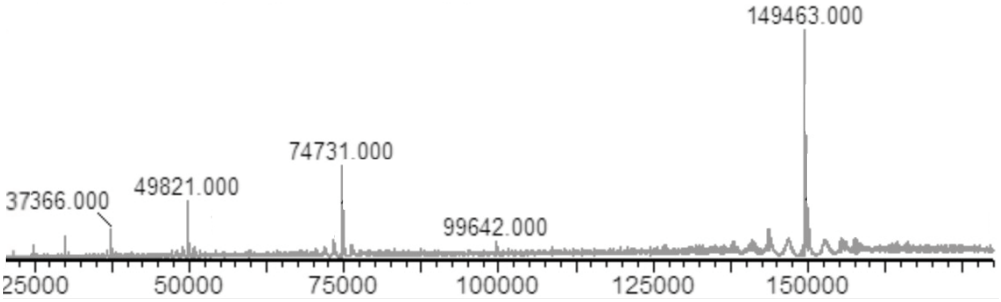

Cx(Cys)-Angiopep2

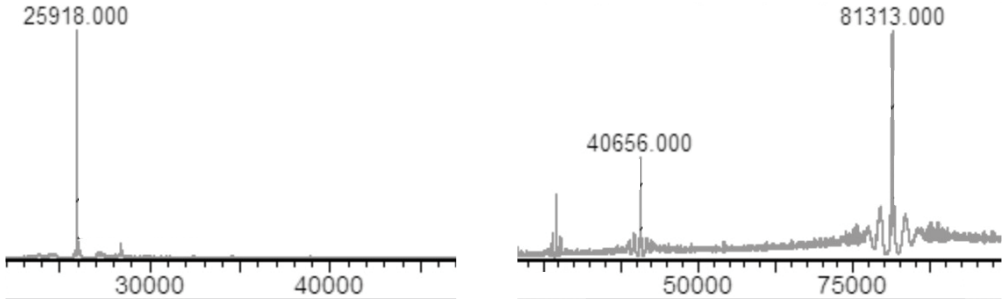

Cx(Cys)-ApoE

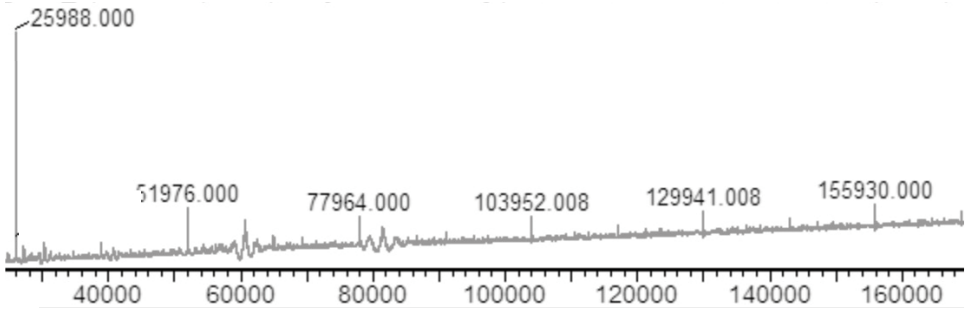

Cx(Cys)-MiniAp4

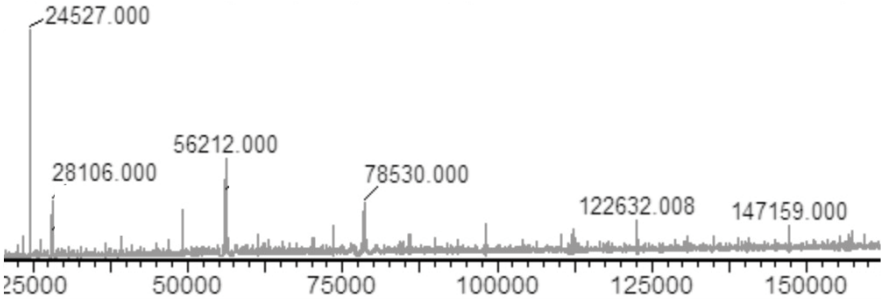

Cx(Cys)-RVG(Ser)

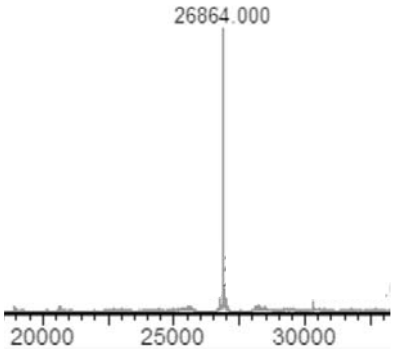

Cx(Cys)-TAT

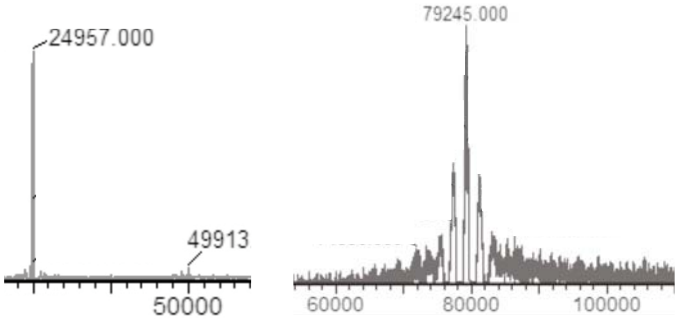

Cx(Cys)-THRre (deglycosylated)

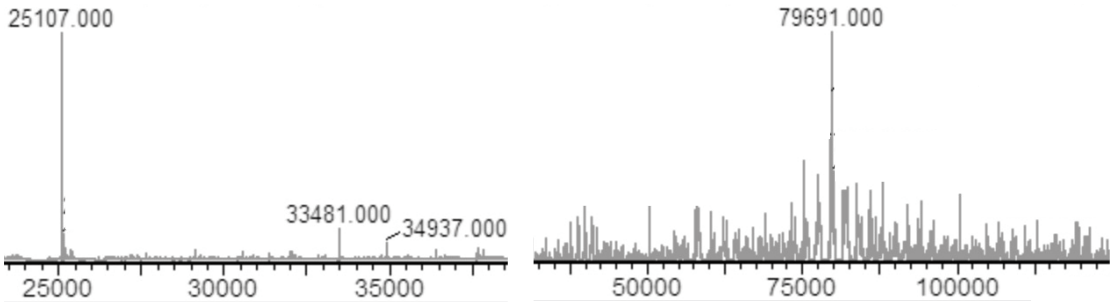

Cx(Cys)-PEG-THRre

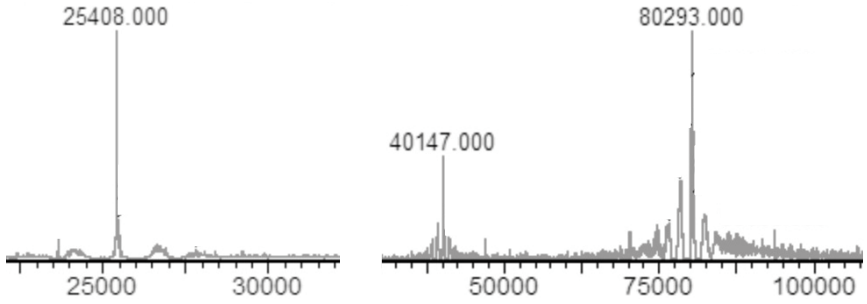

Cx(Cys)-PEG-THRre(scram)

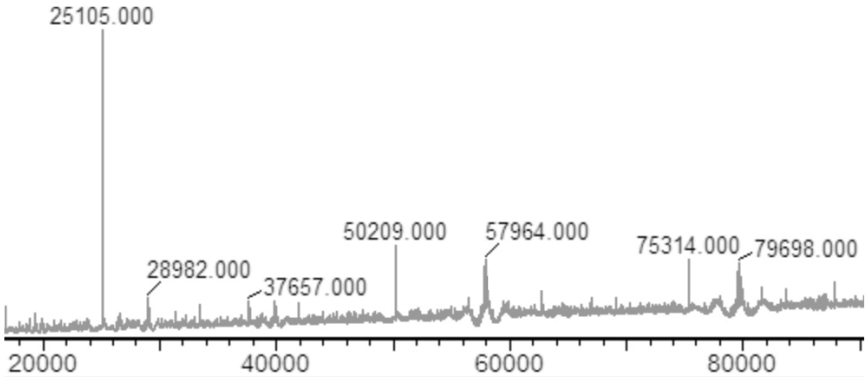

REFERENCES

1. Murray, C. J. L.; Vos, T.; Lozano, R.; Naghavi, M.; Flaxman, A. D.; Michaud, C.; Ezzati, M.; Shibuya, K.; Salomon, J. A.; Abdalla, S.; Aboyans, V.; Abraham, J.; Ackerman, I.; Aggarwal, R.; Ahn, S. Y. *et al.* Disability-adjusted life years (DALYs) for 291 diseases and injuries in 21 regions, 1990?2010: a systematic analysis for the Global Burden of Disease Study 2010. *Lancet* **2012**, *380*, 2197-2223.
2. Gustavsson, A.; Svensson, M.; Jacobi, F.; Allgulander, C.; Alonso, J.; Beghi, E.; Dodel, R.; Ekman, M.; Faravelli, C.; Fratiglioni, L.; Gannon, B.; Jones, D. H.; Jennum, P.; Jordanova, A.; Jönsson, L. *et al.* Cost of disorders of the brain in Europe 2010. *Eur. Neuropsychopharmacol.* **2011**, *21*, 718-779.
3. Pardridge, W. M. Drug transport across the blood-brain barrier. *J. Cereb. Blood Flow Metab.* **2012**, *32*, 1959-1972.
4. Pardridge, W. M. Drug and gene targeting to the brain with molecular Trojan horses. *Nat. Rev. Drug Discov.* **2002**, *1*, 131-139.
5. Dohrmann, G. J. The choroid plexus: a historical review. *Brain Res.* **1970**, *18*, 197-218.
6. Nagpal, K.; Singh, S. K.; Mishra, D. N. Drug targeting to brain: a systematic approach to study the factors, parameters and approaches for prediction of permeability of drugs across BBB. *Expert Opin. Drug Deliv.* **2013**, *10*, 927-955.
7. Abbott, N. J.; Patabendige, A. A.; Dolman, D. E.; Yusof, S. R.; Begley, D. J. Structure and function of the blood-brain barrier. *Neurobiol. Dis.* **2010**, *37*, 13-25.
8. Woodworth, G. F.; Dunn, G. P.; Nance, E. A.; Hanes, J.; Brem, H. Emerging insights into barriers to effective brain tumor therapeutics. *Front. Oncol.* **2014**, *4*, 126.
9. Wolak, D. J.; Thorne, R. G. Diffusion of macromolecules in the brain: implications for drug delivery. *Mol. Pharm.* **2013**, *10*, 1492-1504.
10. Prades, R.; Teixidó, M.; Giralt, E. In *Nanostructured Biomaterials for Overcoming Biological Barriers*; Alonso, M. J., Csaba, N. S., Eds.; Royal Soc Chemistry, Thomas Graham House, Science Park, Cambridge Cb4 4wf, Cambs, Uk: 2012, p 364-391.
11. Jain, K. K. *Drug Delviery in Central Nervous System Disorders - Technologies, Markets and Companies*, Jain PharmaBiotech, 2012.
12. Lu, C. T.; Zhao, Y. Z.; Wong, H. L.; Cai, J.; Peng, L.; Tian, X. Q. Current approaches to enhance CNS delivery of drugs across the brain barriers. *Int. J. Nanomedicine* **2014**, *9*, 2241-2257.
13. Chen, Y.; Liu, L. Modern methods for delivery of drugs across the blood-brain barrier. *Adv. Drug Deliv. Rev.* **2012**, *64*, 640-665.
14. Obermeier, B.; Daneman, R.; Ransohoff, R. M. Development, maintenance and disruption of the blood-brain barrier. *Nat. Med.* **2013**, *19*, 1584-1596.
15. Di, L.; Rong, H.; Feng, B. Demystifying brain penetration in central nervous system drug discovery. Miniperspective. *J. Med. Chem.* **2013**, *56*, 2-12.
16. Wager, T. T.; Villalobos, A.; Verhoest, P. R.; Hou, X.; Shaffer, C. L. Strategies to optimize the brain availability of central nervous system drug candidates. *Expert Opin. Drug Discov.* **2011**, *6*, 371-381.
17. Gaillard, P. J.; Appeldoorn, C. C.; Rip, J.; Dorland, R.; van der Pol, S. M.; Kooij, G.; de Vries, H. E.; Reijerkerk, A. Enhanced brain delivery of liposomal methylprednisolone improved therapeutic efficacy in a model of neuroinflammation. *J. Control. Release* **2012**, *164*, 364-369.

18. Prokai, L.; Prokai-Tatrai, K.; Bodor, N. Targeting drugs to the brain by redox chemical delivery systems. *Med. Res. Rev.* **2000**, *20*, 367-416.

19. Rautio, J.; Laine, K.; Gynther, M.; Savolainen, J. Prodrug approaches for CNS delivery. *AAPS J.* **2008**, *10*, 92-102.

20. Lentz, T. B.; Gray, S. J.; Samulski, R. J. Viral vectors for gene delivery to the central nervous system. *Neurobiol. Dis.* **2012**, *48*, 179-188.

21. Bourdenx, M.; Dutheil, N.; Bezard, E.; Dehay, B. Systemic gene delivery to the central nervous system using Adeno-associated virus. *Front. Mol. Neurosci.* **2014**, *7*, 1-8.

22. Batrakova, E. V.; Gendelman, H. E.; Kabanov, A. V. Cell-mediated drug delivery. *Expert Opin. Drug Deliv.* **2011**, *8*, 415-433.

23. Malakoutikhah, M.; Teixidó, M.; Giralt, E. Shuttle-mediated drug delivery to the brain. *Angew. Chem. Int. Ed. Engl.* **2011**, *50*, 7998-8014.

24. Mitragotri, S.; Burke, P. A.; Langer, R. Overcoming the challenges in administering biopharmaceuticals: formulation and delivery strategies. *Nat. Rev. Drug Discov.* **2014**, *13*, 655-672.

25. Niewoehner, J.; Bohrmann, B.; Collin, L.; Urich, E.; Sade, H.; Maier, P.; Rueger, P.; Stracke, J. O.; Lau, W.; Tissot, A. C.; Loetscher, H.; Ghosh, A.; Freskgård, P. O. Increased brain penetration and potency of a therapeutic antibody using a monovalent molecular shuttle. *Neuron* **2014**, *81*, 49-60.

26. Liu, H.; Zhang, W.; Ma, L.; Fan, L.; Gao, F.; Ni, J.; Wang, R. The improved blood-brain barrier permeability of endomorphin-1 using the cell-penetrating peptide synB3 with three different linkages. *Int. J. Pharm.* **2014**, *476*, 1-8.

27. Zhang, B.; Sun, X.; Mei, H.; Wang, Y.; Liao, Z.; Chen, J.; Zhang, Q.; Hu, Y.; Pang, Z.; Jiang, X. LDLR-mediated peptide-22-conjugated nanoparticles for dual-targeting therapy of brain glioma. *Biomaterials* **2013**, *34*, 9171-9182.

28. Guarnieri, D.; Falanga, A.; Muscetti, O.; Tarallo, R.; Fusco, S.; Galdiero, M.; Galdiero, S.; Netti, P. A. Shuttle-mediated nanoparticle delivery to the blood-brain barrier. *Small* **2013**, *9*, 853-862.

29. Xin, H.; Sha, X.; Jiang, X.; Chen, L.; Law, K.; Gu, J.; Chen, Y.; Wang, X.; Fang, X. The brain targeting mechanism of Angiopep-conjugated poly(ethylene glycol)-co-poly(epsilon-caprolactone) nanoparticles. *Biomaterials* **2012**, *33*, 1673-1681.

30. Malcor, J. D.; Payrot, N.; David, M.; Faucon, A.; Abouzid, K.; Jacquot, G.; Floquet, N.; Debarbieux, F.; Rougon, G.; Martinez, J.; Khrestchatisky, M.; Vlieghe, P.; Lisowski, V. Chemical optimization of new ligands of the low-density lipoprotein receptor as potential vectors for central nervous system targeting. *J. Med. Chem.* **2012**, *55*, 2227-2241.

31. Thomas, F. C.; Taskar, K.; Rudraraju, V.; Goda, S.; Thorsheim, H. R.; Gaasch, J. A.; Mittapalli, R. K.; Palmieri, D.; Steeg, P. S.; Lockman, P. R.; Smith, Q. R. Uptake of ANG1005, a novel paclitaxel derivative, through the blood-brain barrier into brain and experimental brain metastases of breast cancer. *Pharm. Res.* **2009**, *26*, 2486-2494.

32. Malakoutikhah, M.; Guixer, B.; Arranz-Gibert, P.; Teixidó, M.; Giralt, E. 'À la carte' peptide shuttles: tools to increase their passage across the blood-brain barrier. *ChemMedChem* **2014**, *9*, 1594-1601.

33. Malakoutikhah, M.; Prades, R.; Teixidó, M.; Giralt, E. N-methyl phenylalanine-rich peptides as highly versatile blood-brain barrier shuttles. *J. Med. Chem.* **2010**, *53*, 2354-2363.

34. Malakoutikhah, M.; Teixidó, M.; Giralt, E. Toward an optimal blood-brain barrier shuttle by synthesis and evaluation of peptide libraries. *J. Med. Chem.* **2008**, *51*, 4881-4889.

35. Teixidó, M.; Zurita, E.; Malakoutikhah, M.; Tarragó, T.; Giralt, E. Diketopiperazines as a tool for the study of transport across the blood-brain barrier (BBB) and their potential use as BBB-shuttles. *J. Am. Chem. Soc.* **2007**, *129*, 11802-11813.

36. Pardridge, W. M. Receptor-mediated peptide transport through the blood-brain barrier. *Endocr. Rev.* **1986**, *7*, 314-330.

37. Kumagai, A. K.; Eisenberg, J. B.; Pardridge, W. M. Absorptive-mediated endocytosis of cationized albumin and a beta-endorphin-cationized albumin chimeric peptide by isolated brain capillaries. Model system of blood-brain barrier transport. *J. Biol. Chem.* **1987**, *262*, 15214-15219.

38. Friden, P. M.; Walus, L. R.; Musso, G. F.; Taylor, M. A.; Malfroy, B.; Starzyk, R. M. Anti-transferrin receptor antibody and antibody-drug conjugates cross the blood-brain barrier. *Proc. Natl. Acad. Sci. U.S.A.* **1991**, *88*, 4771-4775.

39. Ohtsuki, S.; Terasaki, T. Contribution of carrier-mediated transport systems to the blood-brain barrier as a supporting and protecting interface for the brain; importance for CNS drug discovery and development. *Pharm. Res.* **2007**, *24*, 1745-1758.

40. Lichota, J.; Skjørringe, T.; Thomsen, L. B.; Moos, T. Macromolecular drug transport into the brain using targeted therapy. *J. Neurochem.* **2010**, *113*, 1-13.

41. Hervé, F.; Ghinea, N.; Scherrmann, J. M. CNS delivery via adsorptive transcytosis. *AAPS J.* **2008**, *10*, 455-472.

42. Jones, A. R.; Shusta, E. V. Blood-brain barrier transport of therapeutics via receptor-mediation. *Pharm. Res.* **2007**, *24*, 1759-1771.

43. Xiao, G.; Gan, L.-S. Receptor-mediated endocytosis and brain delivery of therapeutic biologics. *Int. J. Cell Biol.* **2013**, *2013*, 14.

44. Koffie, R. M.; Farrar, C. T.; Saidi, L.-J.; William, C. M.; Hyman, B. T.; Spires-Jones, T. L. Nanoparticles enhance brain delivery of blood–brain barrier-impermeable probes for in vivo optical and magnetic resonance imaging. *Proceedings of the National Academy of Sciences* **2011**, *108*, 18837-18842.

45. Yu, Y. J.; Zhang, Y.; Kenrick, M.; Hoyte, K.; Luk, W.; Lu, Y.; Atwal, J.; Elliott, J. M.; Prabhu, S.; Watts, R. J.; Dennis, M. S. Boosting brain uptake of a therapeutic antibody by reducing its affinity for a transcytosis target. *Sci. Transl. Med.* **2011**, *3*, 84ra44.

46. Yu, Y. J.; Atwal, J. K.; Zhang, Y.; Tong, R. K.; Wildsmith, K. R.; Tan, C.; Bien-Ly, N.; Hersom, M.; Maloney, J. A.; Meilandt, W. J.; Bumbaca, D.; Gadkar, K.; Hoyte, K.; Luk, W.; Lu, Y. *et al.* Therapeutic bispecific antibodies cross the blood-brain barrier in nonhuman primates. *Sci. Transl. Med.* **2014**, *6*, 261ra154.

47. Banks, W. A.; Broadwell, R. D. Blood to brain and brain to blood passage of native horseradish peroxidase, wheat germ agglutinin, and albumin: pharmacokinetic and morphological assessments. *J. Neurochem.* **1994**, *62*, 2404-2419.

48. Gaillard, P. J.; Visser, C. C.; de Boer, A. G. Targeted delivery across the blood-brain barrier. *Expert Opin. Drug Deliv.* **2005**, *2*, 299-309.

49. Uhlig, T.; Kyprianou, T.; Martinelli, F. G.; Oppici, C. A.; Heiligers, D.; Hills, D.; Calvo, X. R.; Verhaert, P. The emergence of peptides in the pharmaceutical business: From exploration to exploitation. *EuPA Open Proteomics* **2014**, *4*, 58-69.

50. Uchida, Y.; Ohtsuki, S.; Katsukura, Y.; Ikeda, C.; Suzuki, T.; Kamiie, J.; Terasaki, T. Quantitative targeted absolute proteomics of human blood-brain barrier transporters and receptors. *J. Neurochem.* **2011**, *117*, 333-345.

51. Deo, A. K.; Theil, F. P.; Nicolas, J. M. Confounding parameters in preclinical assessment of blood-brain barrier permeation: an overview with emphasis on species differences and effect of disease states. *Mol. Pharm.* **2013**, *10*, 1581-1595.

52. Mensch, J.; Oyarzabal, J.; Mackie, C.; Augustijns, P. In vivo, in vitro and in silico methods for small molecule transfer across the BBB. *J. Pharm. Sci.* **2009**, *98*, 4429-4468.

53. Wilhelm, I.; Krizbai, I. A. In vitro models of the blood-brain barrier for the study of drug delivery to the brain. *Mol. Pharm.* **2014**, *11*, 1949-1963.

54. Bicker, J.; Alves, G.; Fortuna, A.; Falcão, A. Blood-brain barrier models and their relevance for a successful development of CNS drug delivery systems: a review. *Eur. J. Pharm. Biopharm.* **2014**, *87*, 409-432.

55. Terasaki, T.; Ohtsuki, S.; Hori, S.; Takanaga, H.; Nakashima, E.; Hosoya, K. New approaches to in vitro models of blood-brain barrier drug transport. *Drug Discov. Today* **2003**, *8*, 944-954.

56. Calabria, A. R.; Shusta, E. V. A genomic comparison of in vivo and in vitro brain microvascular endothelial cells. *J. Cereb. Blood Flow Metab.* **2008**, *28*, 135-148.

57. Ohtsuki, S.; Ikeda, C.; Uchida, Y.; Sakamoto, Y.; Miller, F.; Glacial, F.; Decleves, X.; Scherrmann, J. M.; Couraud, P. O.; Kubo, Y.; Tachikawa, M.; Terasaki, T. Quantitative targeted absolute proteomic analysis of transporters, receptors and junction proteins for validation of human cerebral microvascular endothelial cell line hCMEC/D3 as a human blood-brain barrier model. *Mol. Pharm.* **2013**, *10*, 289-296.

58. Lippmann, E. S.; Al-Ahmad, A.; Azarin, S. M.; Palecek, S. P.; Shusta, E. V. A retinoic acid-enhanced, multicellular human blood-brain barrier model derived from stem cell sources. *Sci. Rep.* **2014**, *4*, 4160.

59. Cecchelli, R.; Aday, S.; Sevin, E.; Almeida, C.; Culot, M.; Dehouck, L.; Coisne, C.; Engelhardt, B.; Dehouck, M. P.; Ferreira, L. A stable and reproducible human blood-brain barrier model derived from hematopoietic stem cells. *PLoS ONE* **2014**, *9*, e99733.

60. Cecchelli, R.; Berezowski, V.; Lundquist, S.; Culot, M.; Renftel, M.; Dehouck, M. P.; Fenart, L. Modelling of the blood-brain barrier in drug discovery and development. *Nat. Rev. Drug Discov.* **2007**, *6*, 650-661.

61. Böckenhoff, A.; Cramer, S.; Wölte, P.; Knieling, S.; Wohlenberg, C.; Gieselmann, V.; Galla, H. J.; Matzner, U. Comparison of five peptide vectors for improved brain delivery of the lysosomal enzyme arylsulfatase A. *J. Neurosci.* **2014**, *34*, 3122-3129.

62. Sharma, G.; Modgil, A.; Zhong, T.; Sun, C.; Singh, J. Influence of short-chain cell-penetrating peptides on transport of Doxorubicin encapsulating receptor-targeted liposomes across brain endothelial barrier. *Pharm. Res.* **2014**, *31*, 1194-1209.

63. Prades, R.; Guerrero, S.; Araya, E.; Molina, C.; Salas, E.; Zurita, E.; Selva, J.; Egea, G.; López-Iglesias, C.; Teixidó, M.; Kogan, M. J.; Giralt, E. Delivery of gold nanoparticles to the brain by conjugation with a peptide that recognizes the transferrin receptor. *Biomaterials* **2012**, *33*, 7194-7205.

64. Demeule, M.; Régina, A.; Ché, C.; Poirier, J.; Nguyen, T.; Gabathuler, R.; Castaigne, J. P.; Béliveau, R. Identification and design of peptides as a new drug delivery system for the brain. *J. Pharmacol. Exp. Ther.* **2008**, *324*, 1064-1072.

65. Wang, D.; El-Amouri, S. S.; Dai, M.; Kuan, C. Y.; Hui, D. Y.; Brady, R. O.; Pan, D. Engineering a lysosomal enzyme with a derivative of receptor-binding domain of apoE enables delivery across the blood-brain barrier. *Proc. Natl. Acad. Sci. U. S. A.* **2013**, *110*, 2999-3004.

66. Markoutsa, E.; Papadia, K.; Giannou, A. D.; Spella, M.; Cagnotto, A.; Salmona, M.; Stathopoulos, G. T.; Antimisiaris, S. G. Mono and dually decorated nanoliposomes for brain targeting, in vitro and in vivo studies. *Pharm. Res.* **2014**, *31*, 1275-1289.

67. Lee, J. H.; Engler, J. A.; Collawn, J. F.; Moore, B. A. Receptor mediated uptake of peptides that bind the human transferrin receptor. *Eur. J. Biochem.* **2001**, *268*, 2004-2012.

68. Hammarlund-Udenaes, M.; Fridén, M.; Syvänen, S.; Gupta, A. On the rate and extent of drug delivery to the brain. *Pharm. Res.* **2008**, *25*, 1737-1750.

69. Mariappan, T. T.; Mandlekar, S.; Marathe, P. Insight into tissue unbound concentration: utility in drug discovery and development. *Curr. Drug Metab.* **2013**, *14*, 324-340.

70. Geldenhuys, W. J.; Allen, D. D.; Bloomquist, J. R. Novel models for assessing blood-brain barrier drug permeation. *Expert Opin. Drug Metab. Toxicol.* **2012**, *8*, 647-653.

71. Turner, P. V.; Brabb, T.; Pekow, C.; Vasbinder, M. A. Administration of substances to laboratory animals: routes of administration and factors to consider. *Journal of the American Association for Laboratory Animal Science : JAALAS* **2011**, *50*, 600-613.

72. Kuhnline Sloan, C. D.; Nandi, P.; Linz, T. H.; Aldrich, J. V.; Audus, K. L.; Lunte, S. M. Analytical and biological methods for probing the blood-brain barrier. *Annu. Rev. Anal. Chem. (Palo Alto Calif.)* **2012**, *5*, 505-531.

73. Uhl, P.; Fricker, G.; Haberkorn, U.; Mier, W. Radionuclides in drug development. *Drug Discov. Today* **2015**, *20*, 198-208.

74. Bickel, U.; Yoshikawa, T.; Pardridge, W. M. Delivery of peptides and proteins through the blood–brain barrier. *Adv. Drug Deliv. Rev.* **2001**, *46*, 247-279.

75. Birngruber, T.; Raml, R.; Gladdines, W.; Gatschelhofer, C.; Gander, E.; Ghosh, A.; Kroath, T.; Gaillard, P. J.; Pieber, T. R.; Sinner, F. Enhanced doxorubicin delivery to the brain administered through glutathione PEGylated liposomal doxorubicin (2B3-101) as compared with generic Caelyx,(®)/Doxil(®)--a cerebral open flow microperfusion pilot study. *J. Pharm. Sci.* **2014**, *103*, 1945-1948.

76. Kumar, P.; Wu, H.; McBride, J. L.; Jung, K. E.; Kim, M. H.; Davidson, B. L.; Lee, S. K.; Shankar, P.; Manjunath, N. Transvascular delivery of small interfering RNA to the central nervous system. *Nature* **2007**, *448*, 39-43.

77. Wu, J.; Jiang, H.; Bi, Q.; Luo, Q.; Li, J.; Zhang, Y.; Chen, Z.; Li, C. Apamin-mediated actively targeted drug delivery for treatment of spinal cord injury: more than just a concept. *Mol. Pharm.* **2014**, *11*, 3210-3222.

78. Kim, J. Y.; Choi, W. I.; Kim, Y. H.; Tae, G. Brain-targeted delivery of protein using chitosan- and RVG peptide-conjugated, pluronic-based nano-carrier. *Biomaterials* **2013**, *34*, 1170-1178.

79. Fu, A.; Zhang, M.; Gao, F.; Xu, X.; Chen, Z. A novel peptide delivers plasmids across blood-brain barrier into neuronal cells as a single-component transfer vector. *PLoS ONE* **2013**, *8*, e59642.

80. Fu, A.; Wang, Y.; Zhan, L.; Zhou, R. Targeted delivery of proteins into the central nervous system mediated by rabies virus glycoprotein-derived peptide. *Pharm. Res.* **2012**, *29*, 1562-1569.

81. Xiang, L.; Zhou, R.; Fu, A.; Xu, X.; Huang, Y.; Hu, C. Targeted delivery of large fusion protein into hippocampal neurons by systemic administration. *J. Drug Target.* **2011**, *19*, 632-636.

82. Sarkar, G.; Curran, G. L.; Mahlum, E.; Decklever, T.; Wengenack, T. M.; Blahnik, A.; Hoesley, B.; Lowe, V. J.; Poduslo, J. F.; Jenkins, R. B. A carrier for non-covalent delivery of functional beta-galactosidase and antibodies against amyloid plaques and IgM to the brain. *PLoS ONE* **2011**, *6*, e28881.

83. Shi, N.; Zhang, Y.; Zhu, C.; Boado, R. J.; Pardridge, W. M. Brain-specific expression of an exogenous gene after i.v. administration. *Proceedings of the National Academy of Sciences* **2001**, *98*, 12754-12759.

84. Sorrentino, N. C.; D'Orsi, L.; Sambri, I.; Nusco, E.; Monaco, C.; Spampanato, C.; Polishchuk, E.; Saccone, P.; De Leonibus, E.; Ballabio, A.; Fraldi, A. A highly secreted sulphamidase engineered to cross the blood-brain barrier corrects brain lesions of mice with mucopolysaccharidoses type IIIA. *EMBO Mol. Med.* **2013**, *5*, 675-690.

85. Youn, P.; Chen, Y.; Furgeson, D. Y. A myristoylated cell-penetrating peptide bearing a transferrin receptor-targeting sequence for neuro-targeted siRNA delivery. *Mol. Pharm.* **2014**, *11*, 486-495.

86. Gong, C.; Li, X.; Xu, L.; Zhang, Y. H. Target delivery of a gene into the brain using the RVG29-oligoarginine peptide. *Biomaterials* **2012**, *33*, 3456-3463.

87. Liu, Y.; Li, J.; Shao, K.; Huang, R.; Ye, L.; Lou, J.; Jiang, C. A leptin derived 30-amino-acid peptide modified pegylated poly-L-lysine dendrigraft for brain targeted gene delivery. *Biomaterials* **2010**, *31*, 5246-5257.

88. Schwarze, S. R.; Ho, A.; Vocero-Akbani, A.; Dowdy, S. F. In vivo protein transduction: delivery of a biologically active protein into the mouse. *Science* **1999**, *285*, 1569-1572.

89. Pham, W.; Zhao, B. Q.; Lo, E. H.; Medarova, Z.; Rosen, B.; Moore, A. Crossing the blood-brain barrier: a potential application of myristoylated polyarginine for in vivo neuroimaging. *Neuroimage* **2005**, *28*, 287-292.

90. Bertrand, Y.; Currie, J. C.; Demeule, M.; Régina, A.; Ché, C.; Abulrob, A.; Fatehi, D.; Sartelet, H.; Gabathuler, R.; Castaigne, J. P.; Stanimirovic, D.; Béliveau, R. Transport characteristics of a novel peptide platform for CNS therapeutics. *J. Cell. Mol. Med.* **2010**, *14*, 2827-2839.

91. Li, J.; Zhang, Q.; Pang, Z.; Wang, Y.; Liu, Q.; Guo, L.; Jiang, X. Identification of peptide sequences that target to the brain using in vivo phage display. *Amino Acids* **2012**, *42*, 2373-2381.

92. Spencer, B. J.; Verma, I. M. Targeted delivery of proteins across the blood–brain barrier. *Proceedings of the National Academy of Sciences* **2007**, *104*, 7594-7599.

93. Zhang, C.; Wan, X.; Zheng, X.; Shao, X.; Liu, Q.; Zhang, Q.; Qian, Y. Dual-functional nanoparticles targeting amyloid plaques in the brains of Alzheimer's disease mice. *Biomaterials* **2014**, *35*, 456-465.

94. Gaillard, P. J.; Appeldoorn, C. C.; Dorland, R.; van Kregten, J.; Manca, F.; Vugts, D. J.; Windhorst, B.; van Dongen, G. A.; de Vries, H. E.; Maussang, D.; van Tellingen, O. Pharmacokinetics, brain delivery, and efficacy in brain tumor-bearing mice of glutathione pegylated liposomal doxorubicin (2B3-101). *PLoS ONE* **2014**, *9*, e82331.

95. Rip, J.; Chen, L.; Hartman, R.; van den Heuvel, A.; Reijerkerk, A.; van Kregten, J.; van der Boom, B.; Appeldoorn, C.; de Boer, M.; Maussang, D.; de Lange, E. C.; Gaillard, P. J.

Glutathione PEGylated liposomes: pharmacokinetics and delivery of cargo across the blood-brain barrier in rats. *J. Drug Target.* **2014**, *22*, 460-467.

96. Ying, X.; Wang, Y.; Liang, J.; Yue, J.; Xu, C.; Lu, L.; Xu, Z.; Gao, J.; Du, Y.; Chen, Z. Angiopep-conjugated electro-responsive hydrogel nanoparticles: therapeutic potential for epilepsy. *Angew. Chem. Int. Ed. Engl.* **2014**, *53*, 12436-12440.

97. Cheng, Y.; Dai, Q.; Morshed, R. A.; Fan, X.; Wegscheid, M. L.; Wainwright, D. A.; Han, Y.; Zhang, L.; Auffinger, B.; Tobias, A. L.; Rincón, E.; Thaci, B.; Ahmed, A. U.; Warnke, P. C.; He, C. *et al.* Blood-brain barrier permeable gold nanoparticles: an efficient delivery platform for enhanced malignant glioma therapy and imaging. *Small* **2014**, *29*, 5137-5150.

98. Lindqvist, A.; Rip, J.; Gaillard, P. J.; Björkman, S.; Hammarlund-Udenaes, M. Enhanced brain delivery of the opioid peptide DAMGO in glutathione pegylated liposomes: a microdialysis study. *Mol. Pharm.* **2013**, *10*, 1533-1541.

99. Leblond, F.; Davis, S. C.; Valdés, P. A.; Pogue, B. W. Pre-clinical whole-body fluorescence imaging: Review of instruments, methods and applications. *J. Photochem. Photobiol. B* **2010**, *98*, 77-94.

100. Kuang, Y.; An, S.; Guo, Y.; Huang, S.; Shao, K.; Liu, Y.; Li, J.; Ma, H.; Jiang, C. T7 peptide-functionalized nanoparticles utilizing RNA interference for glioma dual targeting. *Int. J. Pharm.* **2013**, *454*, 11-20.

101. Staquicini, F. I.; Ozawa, M. G.; Moya, C. A.; Driessen, W. H.; Barbu, E. M.; Nishimori, H.; Soghomonyan, S.; Flores, L. G., 2nd; Liang, X.; Paolillo, V.; Alauddin, M. M.; Basilion, J. P.; Furnari, F. B.; Bogler, O.; Lang, F. F. *et al.* Systemic combinatorial peptide selection yields a non-canonical iron-mimicry mechanism for targeting tumors in a mouse model of human glioblastoma. *J. Clin. Invest.* **2011**, *121*, 161-173.

102. Frigell, J.; García, I.; Gómez-Vallejo, V.; Llop, J.; Penadés, S. 68Ga-labeled gold glyconanoparticles for exploring blood-brain barrier permeability: preparation, biodistribution studies, and improved brain uptake via neuropeptide conjugation. *J. Am. Chem. Soc.* **2014**, *136*, 449-457.

103. Qiao, R.; Jia, Q.; Hüwel, S.; Xia, R.; Liu, T.; Gao, F.; Galla, H. J.; Gao, M. Receptor-mediated delivery of magnetic nanoparticles across the blood-brain barrier. *ACS Nano* **2012**, *6*, 3304-3310.

104. Yan, H.; Wang, L.; Wang, J.; Weng, X.; Lei, H.; Wang, X.; Jiang, L.; Zhu, J.; Lu, W.; Wei, X.; Li, C. Two-order targeted brain tumor imaging by using an optical/paramagnetic nanoprobe across the blood brain barrier. *ACS Nano* **2012**, *6*, 410-420.

105. Yan, H.; Wang, J.; Yi, P.; Lei, H.; Zhan, C.; Xie, C.; Feng, L.; Qian, J.; Zhu, J.; Lu, W.; Li, C. Imaging brain tumor by dendrimer-based optical/paramagnetic nanoprobe across the blood-brain barrier. *Chem. Commun. (Camb.)* **2011**, *47*, 8130-8132.

106. Han, L.; Li, J.; Huang, S.; Huang, R.; Liu, S.; Hu, X.; Yi, P.; Shan, D.; Wang, X.; Lei, H.; Jiang, C. Peptide-conjugated polyamidoamine dendrimer as a nanoscale tumor-targeted T1 magnetic resonance imaging contrast agent. *Biomaterials* **2011**, *32*, 2989-2998.

107. Gabathuler, R. In *Drug Delivery to the Central Nervous System*; Jain, K. K., Ed.; Humana Press: 2010; Vol. 45, p 249-260.

108. Veiseh, O.; Sun, C.; Fang, C.; Bhattarai, N.; Gunn, J.; Kievit, F.; Du, K.; Pullar, B.; Lee, D.; Ellenbogen, R. G.; Olson, J.; Zhang, M. Specific targeting of brain tumors with an optical/magnetic resonance imaging nanoprobe across the blood-brain barrier. *Cancer Res.* **2009**, *69*, 6200-6207.

109. Boado, R. J.; Hui, E. K. W.; Lu, J. Z.; Sumbria, R. K.; Pardridge, W. M. Blood-brain barrier molecular trojan horse enables imaging of brain uptake of radioiodinated recombinant protein in the rhesus monkey. *Bioconjug. Chem.* **2013**, *24*, 1741-1749.

110. Shen, J.; Zhan, C.; Xie, C.; Meng, Q.; Gu, B.; Li, C.; Zhang, Y.; Lu, W. Poly(ethylene glycol)-block-poly(D,L-lactide acid) micelles anchored with angiopep-2 for brain-targeting delivery. *J. Drug Target.* **2011**, *19*, 197-203.

111. Bickel, U. How to measure drug transport across the blood-brain barrier. *NeuroRx* **2005**, *2*, 15-26.

112. Sumbria, R. K.; Zhou, Q. H.; Hui, E. K.; Lu, J. Z.; Boado, R. J.; Pardridge, W. M. Pharmacokinetics and brain uptake of an IgG-TNF decoy receptor fusion protein following intravenous, intraperitoneal, and subcutaneous administration in mice. *Mol. Pharm.* **2013**, *10*, 1425-1431.

113. Ché, C.; Yang, G.; Thiot, C.; Lacoste, M. C.; Currie, J. C.; Demeule, M.; Régina, A.; Béliveau, R.; Castaigne, J. P. New Angiopep-modified doxorubicin (ANG1007) and etoposide (ANG1009) chemotherapeutics with increased brain penetration. *J. Med. Chem.* **2010**, *53*, 2814-2824.

114. Villegas, J. C.; Broadwell, R. D. Transcytosis of protein through the mammalian cerebral epithelium and endothelium. II. Adsorptive transcytosis of WGA-HRP and the blood-brain and brain-blood barriers. *J. Neurocytol.* **1993**, *22*, 67-80.

115. Wiley, D. T.; Webster, P.; Gale, A.; Davis, M. E. Transcytosis and brain uptake of transferrin-containing nanoparticles by tuning avidity to transferrin receptor. *Proceedings of the National Academy of Sciences* **2013**, *110*, 8662-8667.

116. Revelo, N. H.; Kamin, D.; Truckenbrodt, S.; Wong, A. B.; Reuter-Jessen, K.; Reisinger, E.; Moser, T.; Rizzoli, S. O. A new probe for super-resolution imaging of membranes elucidates trafficking pathways. *J. Cell Biol.* **2014**, *205*, 591-606.

117. Jeon, H.; Blacklow, S. C. Structure and physiologic function of the low-density lipoprotein receptor. *Annu. Rev. Biochem.* **2005**, *74*, 535-562.

118. Chung, N. S.; Wasan, K. M. Potential role of the low-density lipoprotein receptor family as mediators of cellular drug uptake. *Adv. Drug Deliv. Rev.* **2004**, *56*, 1315-1334.

119. Dehouck, B.; Fenart, L.; Dehouck, M. P.; Pierce, A.; Torpier, G.; Cecchelli, R. A new function for the LDL receptor: transcytosis of LDL across the blood-brain barrier. *J. Cell Biol.* **1997**, *138*, 877-889.

120. Sagare, A. P.; Deane, R.; Zlokovic, B. V. Low-density lipoprotein receptor-related protein 1: a physiological Abeta homeostatic mechanism with multiple therapeutic opportunities. *Pharmacol. Ther.* **2012**, *136*, 94-105.

121. Notarnicola, M.; Linsalata, M.; Caruso, M.; Cavallini, A.; Di Leo, A. Low density lipoprotein receptors and polyamine levels in human colorectal adenocarcinoma. *J. Gastroenterol.* **1995**, *30*, 705-709.

122. Spengler, J.; Jiménez, J. C.; Burger, K.; Giralt, E.; Albericio, F. Abbreviated nomenclature for cyclic and branched homo- and hetero-detic peptides. *J. Pept. Res.* **2005**, *65*, 550-555.

123. Kurzrock, R.; Gabrail, N.; Chandhasin, C.; Moulder, S.; Smith, C.; Brenner, A.; Sankhala, K.; Mita, A.; Elian, K.; Bouchard, D.; Sarantopoulos, J. Safety, pharmacokinetics, and activity of GRN1005, a novel conjugate of angiopep-2, a peptide facilitating brain penetration, and paclitaxel, in patients with advanced solid tumors. *Mol. Cancer Ther.* **2012**, *11*, 308-316.

124. Drappatz, J.; Brenner, A.; Wong, E. T.; Eichler, A.; Schiff, D.; Groves, M. D.; Mikkelsen, T.; Rosenfeld, S.; Sarantopoulos, J.; Meyers, C. A.; Fielding, R. M.; Elian, K.; Wang, X.; Lawrence, B.; Shing, M. *et al.* Phase I study of GRN1005 in recurrent malignant glioma. *Clin. Cancer Res.* **2013**, *19*, 1567-1576.

125. Demeule, M.; Beaudet, N.; Reégina, A.; Besserer-Offroy, É.; Murza, A.; Tétreault, P.; Belleville, K.; Ché, C.; Larocque, A.; Thiot, C.; Béliveau, R.; Longpré, J. M.; Marsault, É.; Leduc, R.; Lachowicz, J. E. *et al.* Conjugation of a brain-penetrant peptide with neurotensin provides antinociceptive properties. *J. Clin. Invest.* **2014**, *124*, 1199-1213.

126. Regina, A.; Demeule, M.; Tripathy, S.; Lord-Dufour, S.; Currie, J. C.; Iddir, M.; Annabi, B.; Castaigne, J. P.; Lachowicz, J. E. ANG4043, a novel brain-penetrant peptide-mAb conjugate, is efficacious against HER2-positive intracranial tumors in mice. *Mol. Cancer Ther.* **2015**, *14*, 129-140.

127. Sun, X.; Pang, Z.; Ye, H.; Qiu, B.; Guo, L.; Li, J.; Ren, J.; Qian, Y.; Zhang, Q.; Chen, J.; Jiang, X. Co-delivery of pEGFP-hTRAIL and paclitaxel to brain glioma mediated by an angiopep-conjugated liposome. *Biomaterials* **2012**, *33*, 916-924.

128. Yang, Z. Z.; Li, J. Q.; Wang, Z. Z.; Dong, D. W.; Qi, X. R. Tumor-targeting dual peptides-modified cationic liposomes for delivery of siRNA and docetaxel to gliomas. *Biomaterials* **2014**, *35*, 5226-5239.

129. Ren, J.; Shen, S.; Wang, D.; Xi, Z.; Guo, L.; Pang, Z.; Qian, Y.; Sun, X.; Jiang, X. The targeted delivery of anticancer drugs to brain glioma by PEGylated oxidized multi-walled carbon nanotubes modified with angiopep-2. *Biomaterials* **2012**, *33*, 3324-3333.

130. Xin, H.; Jiang, X.; Gu, J.; Sha, X.; Chen, L.; Law, K.; Chen, Y.; Wang, X.; Jiang, Y.; Fang, X. Angiopep-conjugated poly(ethylene glycol)-co-poly(epsilon-caprolactone) nanoparticles as dual-targeting drug delivery system for brain glioma. *Biomaterials* **2011**, *32*, 4293-4305.

131. Xin, H.; Sha, X.; Jiang, X.; Zhang, W.; Chen, L.; Fang, X. Anti-glioblastoma efficacy and safety of paclitaxel-loading Angiopep-conjugated dual targeting PEG-PCL nanoparticles. *Biomaterials* **2012**, *33*, 8167-8176.

132. Huile, G.; Shuaiqi, P.; Zhi, Y.; Shijie, C.; Chen, C.; Xinguo, J.; Shun, S.; Zhiqing, P.; Yu, H. A cascade targeting strategy for brain neuroglial cells employing nanoparticles modified with angiopep-2 peptide and EGFP-EGF1 protein. *Biomaterials* **2011**, *32*, 8669-8675.

133. Gao, X.; Qian, J.; Zheng, S.; Xiong, Y.; Man, J.; Cao, B.; Wang, L.; Ju, S.; Li, C. Up-regulating blood brain barrier permeability of nanoparticles via multivalent effect. *Pharm. Res.* **2013**, *30*, 2538-2548.

134. Huang, S.; Li, J.; Han, L.; Liu, S.; Ma, H.; Huang, R.; Jiang, C. Dual targeting effect of Angiopep-2-modified, DNA-loaded nanoparticles for glioma. *Biomaterials* **2011**, *32*, 6832-6838.

135. Ke, W.; Shao, K.; Huang, R.; Han, L.; Liu, Y.; Li, J.; Kuang, Y.; Ye, L.; Lou, J.; Jiang, C. Gene delivery targeted to the brain using an Angiopep-conjugated polyethyleneglycol-modified polyamidoamine dendrimer. *Biomaterials* **2009**, *30*, 6976-6985.

136. Huang, R.; Ma, H.; Guo, Y.; Liu, S.; Kuang, Y.; Shao, K.; Li, J.; Liu, Y.; Han, L.; Huang, S.; An, S.; Ye, L.; Lou, J.; Jiang, C. Angiopep-conjugated nanoparticles for targeted long-term gene therapy of Parkinson's disease. *Pharm. Res.* **2013**, *30*, 2549-2559.

137. Ruan, S.; Yuan, M.; Zhang, L.; Hu, G.; Chen, J.; Cun, X.; Zhang, Q.; Yang, Y.; He, Q.; Gao, H. Tumor microenvironment sensitive doxorubicin delivery and release to glioma using angiopep-2 decorated gold nanoparticles. *Biomaterials* **2015**, *37*, 425-435.

138. Ni, D.; Zhang, J.; Bu, W.; Xing, H.; Han, F.; Xiao, Q.; Yao, Z.; Chen, F.; He, Q.; Liu, J.; Zhang, S.; Fan, W.; Zhou, L.; Peng, W.; Shi, J. Dual-targeting upconversion nanoprobes across the blood-brain barrier for magnetic resonance/fluorescence imaging of intracranial glioblastoma. *ACS Nano* **2014**, *8*, 1231-1242.

139. Gao, H.; Zhang, S.; Cao, S.; Yang, Z.; Pang, Z.; Jiang, X. Angiopep-2 and activatable cell-penetrating peptide dual-functionalized nanoparticles for systemic glioma-targeting delivery. *Mol. Pharm.* **2014**, *11*, 2755-2763.

140. Shao, K.; Huang, R.; Li, J.; Han, L.; Ye, L.; Lou, J.; Jiang, C. Angiopep-2 modified PE-PEG based polymeric micelles for amphotericin B delivery targeted to the brain. *J. Control. Release* **2010**, *147*, 118-126.

141. Shao, K.; Wu, J.; Chen, Z.; Huang, S.; Li, J.; Ye, L.; Lou, J.; Zhu, L.; Jiang, C. A brain-vectored angiopep-2 based polymeric micelles for the treatment of intracranial fungal infection. *Biomaterials* **2012**, *33*, 6898-6907.

142. Wei, X.; Zhan, C.; Chen, X.; Hou, J.; Xie, C.; Lu, W. Retro-inverso isomer of Angiopep-2: a stable d-peptide ligand inspires brain-targeted drug delivery. *Mol. Pharm.* **2014**, *11*, 3261-3268.

143. Dintzis, H. M.; Symer, D. E.; Dintzis, R. Z.; Zawadzke, L. E.; Berg, J. M. A comparison of the immunogenicity of a pair of enantiomeric proteins. *Proteins* **1993**, *16*, 306-308.

144. Wagner, S.; Zensi, A.; Wien, S. L.; Tschickardt, S. E.; Maier, W.; Vogel, T.; Worek, F.; Pietrzik, C. U.; Kreuter, J.; von Briesen, H. Uptake mechanism of ApoE-modified nanoparticles on brain capillary endothelial cells as a blood-brain barrier model. *PLoS ONE* **2012**, *7*, e32568.

145. Kreuter, J.; Hekmatara, T.; Dreis, S.; Vogel, T.; Gelperina, S.; Langer, K. Covalent attachment of apolipoprotein A-I and apolipoprotein B-100 to albumin nanoparticles enables drug transport into the brain. *J. Control. Release* **2007**, *118*, 54-58.

146. Dyer, C. A.; Cistola, D. P.; Parry, G. C.; Curtiss, L. K. Structural features of synthetic peptides of apolipoprotein E that bind the LDL receptor. *J. Lipid Res.* **1995**, *36*, 80-88.

147. Clayton, D.; Brereton, I. M.; Kroon, P. A.; Smith, R. NMR studies of the low-density lipoprotein receptor-binding peptide of apolipoprotein E bound to dodecylphosphocholine micelles. *Protein Sci.* **1999**, *8*, 1797-1805.

148. Wang, X.; Ciraolo, G.; Morris, R.; Gruenstein, E. Identification of a neuronal endocytic pathway activated by an apolipoprotein E (apoE) receptor binding peptide. *Brain Res.* **1997**, *778*, 6-15.

149. Re, F.; Cambianica, I.; Zona, C.; Sesana, S.; Gregori, M.; Rigolio, R.; La Ferla, B.; Nicotra, F.; Forloni, G.; Cagnotto, A.; Salmona, M.; Masserini, M.; Sancini, G. Functionalization of liposomes with ApoE-derived peptides at different density affects cellular uptake and drug transport across a blood-brain barrier model. *Nanomedicine* **2011**, *7*, 551-559.

150. Meng, Y.; Sohar, I.; Sleat, D. E.; Richardson, J. R.; Reuhl, K. R.; Jenkins, R. B.; Sarkar, G.; Lobel, P. Effective intravenous therapy for neurodegenerative disease with a therapeutic enzyme and a peptide that mediates delivery to the brain. *Mol. Ther.* **2014**, *22*, 547-553.

151. Qian, Z. M.; Li, H.; Sun, H.; Ho, K. Targeted drug delivery via the transferrin receptor-mediated endocytosis pathway. *Pharmacol. Rev.* **2002**, *54*, 561-587.

152. Daneman, R.; Zhou, L.; Agalliu, D.; Cahoy, J. D.; Kaushal, A.; Barres, B. A. The mouse blood-brain barrier transcriptome: a new resource for understanding the development and function of brain endothelial cells. *PLoS ONE* **2010**, *5*, e13741.

153. Uchida, Y.; Tachikawa, M.; Obuchi, W.; Hoshi, Y.; Tomioka, Y.; Ohtsuki, S.; Terasaki, T. A study protocol for quantitative targeted absolute proteomics (QTAP) by LC-MS/MS: application for inter-strain differences in protein expression levels of transporters, receptors, claudin-5, and marker proteins at the blood–brain barrier in ddY, FVB, and C57BL/6J mice. *Fluids Barriers CNS* **2013**, *10*, 21.

154. Xia, H.; Anderson, B.; Mao, Q.; Davidson, B. L. Recombinant human adenovirus: targeting to the human transferrin receptor improves gene transfer to brain microcapillary endothelium. *J. Virol.* **2000**, *74*, 11359-11366.

155. Liu, Z.; Gao, X.; Kang, T.; Jiang, M.; Miao, D.; Gu, G.; Hu, Q.; Song, Q.; Yao, L.; Tu, Y.; Chen, H.; Jiang, X.; Chen, J. B6 peptide-modified PEG-PLA nanoparticles for enhanced brain delivery of neuroprotective peptide. *Bioconjug. Chem.* **2013**, *24*, 997-1007.

156. Prades, R.; Oller-Salvia, B.; Schwarzmaier, S. M.; Selva, J.; Moros, M.; Balbi, M.; Grazú, V.; de La Fuente, J. M.; Egea, G.; Plesnila, N.; Teixidó, M.; Giralt, E. Applying the Retro-Enantio Approach to Obtain a Peptide Capable of Overcoming the Blood–Brain Barrier. *Angew. Chem. Int. Ed.* **2015**, *54*, 3967-3972.

157. Liu, S.; Guo, Y.; Huang, R.; Li, J.; Huang, S.; Kuang, Y.; Han, L.; Jiang, C. Gene and doxorubicin co-delivery system for targeting therapy of glioma. *Biomaterials* **2012**, *33*, 4907-4916.

158. Brammer, L. A.; Bolduc, B.; Kass, J. L.; Felice, K. M.; Noren, C. J.; Hall, M. F. A target-unrelated peptide in an M13 phage display library traced to an advantageous mutation in the gene II ribosome-binding site. *Anal. Biochem.* **2008**, *373*, 88-98.

159. Wu, J.; Lukas, R. J. Naturally-expressed nicotinic acetylcholine receptor subtypes. *Biochem. Pharmacol.* **2011**, *82*, 800-807.

160. Gotti, C.; Clementi, F. Neuronal nicotinic receptors: from structure to pathology. *Prog. Neurobiol.* **2004**, *74*, 363-396.

161. Kim, S. S.; Ye, C.; Kumar, P.; Chiu, I.; Subramanya, S.; Wu, H.; Shankar, P.; Manjunath, N. Targeted delivery of siRNA to macrophages for anti-inflammatory treatment. *Mol. Ther.* **2010**, *18*, 993-1001.

162. Zadran, S.; Akopian, G.; Zadran, H.; Walsh, J.; Baudry, M. RVG-mediated calpain2 gene silencing in the brain impairs learning and memory. *Neuromolecular Med.* **2013**, *15*, 74-81.

163. Liu, Y.; Hu, Y.; Guo, Y.; Ma, H.; Li, J.; Jiang, C. Targeted imaging of activated caspase-3 in the central nervous system by a dual functional nano-device. *J. Control. Release* **2012**, *163*, 203-210.

164. Hwang do, W.; Son, S.; Jang, J.; Youn, H.; Lee, S.; Lee, D.; Lee, Y. S.; Jeong, J. M.; Kim, W. J.; Lee, D. S. A brain-targeted rabies virus glycoprotein-disulfide linked PEI nanocarrier for delivery of neurogenic microRNA. *Biomaterials* **2011**, *32*, 4968-4975.

165. Son, S.; Hwang do, W.; Singha, K.; Jeong, J. H.; Park, T. G.; Lee, D. S.; Kim, W. J. RVG peptide tethered bioreducible polyethylenimine for gene delivery to brain. *J. Control. Release* **2011**, *155*, 18-25.

166. Huo, H.; Gao, Y.; Wang, Y.; Zhang, J.; Wang, Z. Y.; Jiang, T.; Wang, S. Polyion complex micelles composed of pegylated polyasparthydrazide derivatives for siRNA delivery to the brain. *J. Colloid Interface Sci.* **2015**, *447*, 8-15.

167. Liu, Y.; Huang, R.; Han, L.; Ke, W.; Shao, K.; Ye, L.; Lou, J.; Jiang, C. Brain-targeting gene delivery and cellular internalization mechanisms for modified rabies virus glycoprotein RVG29 nanoparticles. *Biomaterials* **2009**, *30*, 4195-4202.

168. Liu, Y.; Guo, Y.; An, S.; Kuang, Y.; He, X.; Ma, H.; Li, J.; Lu, J.; Zhang, N.; Jiang, C. Targeting caspase-3 as dual therapeutic benefits by RNAi facilitating brain-targeted nanoparticles in a rat model of Parkinson's disease. *PLoS ONE* **2013**, *8*, e62905.

169. Alvarez-Erviti, L.; Seow, Y.; Yin, H.; Betts, C.; Lakhal, S.; Wood, M. J. A. Delivery of siRNA to the mouse brain by systemic injection of targeted exosomes. *Nat. Biotechnol.* **2011**, *29*, 341-345.

170. Zhan, C.; Yan, Z.; Xie, C.; Lu, W. Loop 2 of Ophiophagus hannah toxin b binds with neuronal nicotinic acetylcholine receptors and enhances intracranial drug delivery. *Mol. Pharm.* **2010**, *7*, 1940-1947.

171. Zhan, C.; Li, B.; Hu, L.; Wei, X.; Feng, L.; Fu, W.; Lu, W. Micelle-based brain-targeted drug delivery enabled by a nicotine acetylcholine receptor ligand. *Angew. Chem. Int. Ed. Engl.* **2011**, *50*, 5482-5485.

172. Wei, X.; Zhan, C.; Shen, Q.; Fu, W.; Xie, C.; Gao, J.; Peng, C.; Zheng, P.; Lu, W. A d-Peptide ligand of nicotine acetylcholine receptors for brain-targeted drug delivery. *Angew. Chem. Int. Ed. Engl.* **2015**, *54*, 3023-3027.

173. Tu, H.; Pan, W.; Feucht, L.; Kastin, A. J. Convergent trafficking pattern of leptin after endocytosis mediated by ObRa-ObRd. *J. Cell. Physiol.* **2007**, *212*, 215-222.

174. Barrett, G. L.; Trieu, J.; Naim, T. The identification of leptin-derived peptides that are taken up by the brain. *Regul. Pept.* **2009**, *155*, 55-61.

175. Lee, D. H.; Rötger, C.; Appeldoorn, C. C.; Reijerkerk, A.; Gladdines, W.; Gaillard, P. J.; Linker, R. A. Glutathione PEGylated liposomal methylprednisolone (2B3-201) attenuates CNS inflammation and degeneration in murine myelin oligodendrocyte glycoprotein induced experimental autoimmune encephalomyelitis. *J. Neuroimmunol.* **2014**, *274*, 96-101.

176. Mdzinarishvili, A.; Sutariya, V.; Talasila, P. K.; Geldenhuys, W. J.; Sadana, P. Engineering triiodothyronine (T3) nanoparticle for use in ischemic brain stroke. *Drug Deliv. Transl. Res.* **2013**, *3*, 309-317.

177. Geldenhuys, W.; Mbimba, T.; Bui, T.; Harrison, K.; Sutariya, V. Brain-targeted delivery of paclitaxel using glutathione-coated nanoparticles for brain cancers. *J. Drug Target.* **2011**, *19*, 837-845.

178. Rotman, M.; Welling, M. M.; Bunschoten, A.; de Backer, M. E.; Rip, J.; Nabuurs, R. J.; Gaillard, P. J.; van Buchem, M. A.; van der Maarel, S. M.; van der Weerd, L. Enhanced glutathione PEGylated liposomal brain delivery of an anti-amyloid single domain antibody fragment in a mouse model for Alzheimer's disease. *J. Control. Release* **2015**, *203*, 40-50.

179. More, S. S.; Vince, R. Design, synthesis and biological evaluation of glutathione peptidomimetics as components of anti-Parkinson prodrugs. *J. Med. Chem.* **2008**, *51*, 4581-4588.

180. Bachhawat, A. K.; Thakur, A.; Kaur, J.; Zulkifli, M. Glutathione transporters. *Biochim. Biophys. Acta* **2013**, *1830*, 3154-3164.

181. Sugahara, K. N.; Teesalu, T.; Karmali, P. P.; Kotamraju, V. R.; Agemy, L.; Greenwald, D. R.; Ruoslahti, E. Coadministration of a tumor-penetrating peptide enhances the efficacy of cancer drugs. *Science* **2010**, *328*, 1031-1035.

182. Wang, K.; Zhang, X.; Liu, Y.; Liu, C.; Jiang, B.; Jiang, Y. Tumor penetrability and anti-angiogenesis using iRGD-mediated delivery of doxorubicin-polymer conjugates. *Biomaterials* **2014**, *35*, 8735-8747.

183. Lei, Y.; Wang, J.; Xie, C.; Wagner, E.; Lu, W.; Li, Y.; Wei, X.; Dong, J.; Liu, M. Glutathione-sensitive RGD-poly(ethylene glycol)-SS-polyethylenimine for intracranial glioblastoma targeted gene delivery. *J. Gene Med.* **2013**, *15*, 291-305.

184. Wang, H.; Su, W.; Wang, S.; Wang, X.; Liao, Z.; Kang, C.; Han, L.; Chang, J.; Wang, G.; Pu, P. Smart multifunctional core-shell nanospheres with drug and gene co-loaded for enhancing the therapeutic effect in a rat intracranial tumor model. *Nanoscale* **2012**, *4*, 6501-6508.

185. Liu, Y.; Ran, R.; Chen, J.; Kuang, Q.; Tang, J.; Mei, L.; Zhang, Q.; Gao, H.; Zhang, Z.; He, Q. Paclitaxel loaded liposomes decorated with a multifunctional tandem peptide for glioma targeting. *Biomaterials* **2014**, *35*, 4835-4847.

186. Zhan, C.; Wei, X.; Qian, J.; Feng, L.; Zhu, J.; Lu, W. Co-delivery of TRAIL gene enhances the anti-glioblastoma effect of paclitaxel in vitro and in vivo. *J. Control. Release* **2012**, *160*, 630-636.

187. Miura, Y.; Takenaka, T.; Toh, K.; Wu, S.; Nishihara, H.; Kano, M. R.; Ino, Y.; Nomoto, T.; Matsumoto, Y.; Koyama, H.; Cabral, H.; Nishiyama, N.; Kataoka, K. Cyclic RGD-linked polymeric micelles for targeted delivery of platinum anticancer drugs to glioblastoma through the blood-brain tumor barrier. *ACS Nano* **2013**, *7*, 8583-8592.

188. Jain, S.; Mishra, V.; Singh, P.; Dubey, P. K.; Saraf, D. K.; Vyas, S. P. RGD-anchored magnetic liposomes for monocytes/neutrophils-mediated brain targeting. *Int. J. Pharm.* **2003**, *261*, 43-55.

189. Qin, J.; Chen, D.; Hu, H.; Qiao, M.; Zhao, X.; Chen, B. Body distributioin of RGD-mediated liposome in brain-targeting drug delivery. *Yakugaku Zasshi* **2007**, *127*, 1497-1501.

190. Qin, J.; Yang, X.; Zhang, R.-X.; Luo, Y.-X.; Li, J.-L.; Hou, J.; Zhang, C.; Li, Y.-J.; Shi, J.; Lu, L.; Wang, J.-X.; Zhu, W.-L. Monocyte mediated brain targeting delivery of macromolecular drug for the therapy of depression. *Nanomedicine* **2015**, *11*, 391-400.

191. Tettamanti, G.; Bassi, R.; Viani, P.; Riboni, L. Salvage pathways in glycosphingolipid metabolism. *Biochimie* **2003**, *85*, 423-437.

192. Daniotti, J. L.; Iglesias-Bartolomé, R. Metabolic pathways and intracellular trafficking of gangliosides. *IUBMB life* **2011**, *63*, 513-520.

193. Saslowsky, D. E.; te Welscher, Y. M.; Chinnapen, D. J.; Wagner, J. S.; Wan, J.; Kern, E.; Lencer, W. I. Ganglioside GM1-mediated transcytosis of cholera toxin bypasses the retrograde pathway and depends on the structure of the ceramide domain. *J. Biol. Chem.* **2013**, *288*, 25804-25809.

194. Lencer, W. I.; Moe, S.; Rufo, P. A.; Madara, J. L. Transcytosis of cholera toxin subunits across model human intestinal epithelia. *Proc. Natl. Acad. Sci. U. S. A.* **1995**, *92*, 10094-10098.

195. Liu, J. K.; Teng, Q.; Garrity-Moses, M.; Federici, T.; Tanase, D.; Imperiale, M. J.; Boulis, N. M. A novel peptide defined through phage display for therapeutic protein and vector neuronal targeting. *Neurobiol. Dis.* **2005**, *19*, 407-418.

196. Georgieva, J. V.; Brinkhuis, R. P.; Stojanov, K.; Weijers, C. A.; Zuilhof, H.; Rutjes, F. P.; Hoekstra, D.; van Hest, J. C.; Zuhorn, I. S. Peptide-mediated blood-brain barrier transport of polymersomes. *Angew. Chem. Int. Ed. Engl.* **2012**, *51*, 8339-8342.

197. Egleton, R. D.; Witt, K. A.; Davis, T. P. In *Handbook of Biologically Active Peptides*; Kastin, A. J., Ed.; Academic Press: Burlington, 2006, p 1429-1434.

198. Costantino, L.; Gandolfi, F.; Tosi, G.; Rivasi, F.; Vandelli, M. A.; Forni, F. Peptide-derivatized biodegradable nanoparticles able to cross the blood-brain barrier. *J. Control. Release* **2005**, *108*, 84-96.

199. Tosi, G.; Bortot, B.; Ruozi, B.; Dolcetta, D.; Vandelli, M. A.; Forni, F.; Severini, G. M. Potential use of polymeric nanoparticles for drug delivery across the blood-brain barrier. *Curr. Med. Chem.* **2013**, *20*, 2212-2225.

200. Tosi, G.; Bondioli, L.; Ruozi, B.; Badiali, L.; Severini, G. M.; Biffi, S.; De Vita, A.; Bortot, B.; Dolcetta, D.; Forni, F.; Vandelli, M. A. NIR-labeled nanoparticles engineered for brain targeting: in vivo optical imaging application and fluorescent microscopy evidences. *J. Neural Transm.* **2011**, *118*, 145-153.

201. Vergoni, A. V.; Tosi, G.; Tacchi, R.; Vandelli, M. A.; Bertolini, A.; Costantino, L. Nanoparticles as drug delivery agents specific for CNS: in vivo biodistribution. *Nanomedicine* **2009**, *5*, 369-377.

202. Tosi, G.; Vilella, A.; Chhabra, R.; Schmeisser, M. J.; Boeckers, T. M.; Ruozi, B.; Vandelli, M. A.; Forni, F.; Zoli, M.; Grabrucker, A. M. Insight on the fate of CNS-targeted nanoparticles. Part II: Intercellular neuronal cell-to-cell transport. *J. Control. Release* **2014**, *177*, 96-107.

203. Vilella, A.; Tosi, G.; Grabrucker, A. M.; Ruozi, B.; Belletti, D.; Vandelli, M. A.; Boeckers, T. M.; Forni, F.; Zoli, M. Insight on the fate of CNS-targeted nanoparticles. Part I: Rab5-dependent cell-specific uptake and distribution. *J. Control. Release* **2014**, *174*, 195-201.

204. Li, J.; Feng, L.; Fan, L.; Zha, Y.; Guo, L.; Zhang, Q.; Chen, J.; Pang, Z.; Wang, Y.; Jiang, X.; Yang, V. C.; Wen, L. Targeting the brain with PEG-PLGA nanoparticles modified with phage-displayed peptides. *Biomaterials* **2011**, *32*, 4943-4950.

205. Gao, H.; Qian, J.; Cao, S.; Yang, Z.; Pang, Z.; Pan, S.; Fan, L.; Xi, Z.; Jiang, X.; Zhang, Q. Precise glioma targeting of and penetration by aptamer and peptide dual-functioned nanoparticles. *Biomaterials* **2012**, *33*, 5115-5123.

206. Li, J.; Zhang, C.; Li, J.; Fan, L.; Jiang, X.; Chen, J.; Pang, Z.; Zhang, Q. Brain delivery of NAP with PEG-PLGA nanoparticles modified with phage display peptides. *Pharm. Res.* **2013**, *30*, 1813-1823.

207. Smith, M. W.; Al-Jayyoussi, G.; Gumbleton, M. Peptide sequences mediating tropism to intact blood-brain barrier: an in vivo biodistribution study using phage display. *Peptides* **2012**, *38*, 172-180.

208. van Rooy, I.; Cakir-Tascioglu, S.; Couraud, P. O.; Romero, I. A.; Weksler, B.; Storm, G.; Hennink, W. E.; Schiffelers, R. M.; Mastrobattista, E. Identification of peptide ligands for targeting to the blood-brain barrier. *Pharm. Res.* **2010**, *27*, 673-682.

209. van Rooy, I.; Hennink, W. E.; Storm, G.; Schiffelers, R. M.; Mastrobattista, E. Attaching the phage display-selected GLA peptide to liposomes: factors influencing target binding. *Eur. J. Pharm. Sci.* **2012**, *45*, 330-335.

210. Martín, I.; Teixidó, M.; Giralt, E. Intracellular fate of peptide-mediated delivered cargoes. *Curr. Pharm. Des.* **2013**, *19*, 2924-2942.

211. Madani, F.; Lindberg, S.; Langel, Ü.; Futaki, S.; Gräslund, A. Mechanisms of cellular uptake of cell-penetrating peptides. *J. Biophys.* **2011**, *2011*.

212. Frankel, A. D.; Pabo, C. O. Cellular uptake of the tat protein from human immunodeficiency virus. *Cell* **1988**, *55*, 1189-1193.

213. Vasconcelos, L.; Pärn, K.; Langel, U. Therapeutic potential of cell-penetrating peptides. *Ther. Deliv.* **2013**, *4*, 573-591.

214. Kim, M. J.; Kim, D. W.; Jeong, H. J.; Sohn, E. J.; Shin, M. J.; Ahn, E. H.; Kwon, S. W.; Kim, Y. N.; Kim, D. S.; Park, J.; Eum, W. S.; Hwang, H. S.; Choi, S. Y. Tat-Frataxin protects dopaminergic neuronal cells against MPTP-induced toxicity in a mouse model of Parkinson's disease. *Biochimie* **2012**, *94*, 2448-2456.

215. Kilic, E.; Dietz, G. P.; Hermann, D. M.; Bähr, M. Intravenous TAT-Bcl-Xl is protective after middle cerebral artery occlusion in mice. *Ann. Neurol.* **2002**, *52*, 617-622.

216. Elliger, S. S.; Elliger, C. A.; Lang, C.; Watson, G. L. Enhanced secretion and uptake of beta-glucuronidase improves adeno-associated viral-mediated gene therapy of mucopolysaccharidosis type VII mice. *Mol. Ther.* **2002**, *5*, 617-626.

217. Kilic, E.; Kilic, U.; Hermann, D. M. TAT-GDNF in neurodegeneration and ischemic stroke. *CNS Drug Rev.* **2005**, *11*, 369-378.

218. Aarts, M.; Liu, Y.; Liu, L.; Besshoh, S.; Arundine, M.; Gurd, J. W.; Wang, Y. T.; Salter, M. W.; Tymianski, M. Treatment of ischemic brain damage by perturbing NMDA receptor-PSD-95 protein interactions. *Science* **2002**, *298*, 846-850.

219. Cao, G.; Pei, W.; Ge, H.; Liang, Q.; Luo, Y.; Sharp, F. R.; Lu, A.; Ran, R.; Graham, S. H.; Chen, J. In vivo delivery of a Bcl-xL fusion protein containing the TAT protein transduction domain protects against ischemic brain injury and neuronal apoptosis. *J. Neurosci.* **2002**, *22*, 5423-5431.

220. Rao, K. S.; Reddy, M. K.; Horning, J. L.; Labhasetwar, V. TAT-conjugated nanoparticles for the CNS delivery of anti-HIV drugs. *Biomaterials* **2008**, *29*, 4429-4438.

221. Santra, S.; Yang, H.; Stanley, J. T.; Holloway, P. H.; Moudgil, B. M.; Walter, G.; Mericle, R. A. Rapid and effective labeling of brain tissue using TAT-conjugated CdS:Mn/ZnS quantum dots. *Chem. Commun. (Camb.)* **2005**, 3144-3146.

222. Qin, Y.; Chen, H.; Yuan, W.; Kuai, R.; Zhang, Q.; Xie, F.; Zhang, L.; Zhang, Z.; Liu, J.; He, Q. Liposome formulated with TAT-modified cholesterol for enhancing the brain delivery. *Int. J. Pharm.* **2011**, *419*, 85-95.

223. Wang, H.; Xu, K.; Liu, L.; Tan, J. P.; Chen, Y.; Li, Y.; Fan, W.; Wei, Z.; Sheng, J.; Yang, Y. Y.; Li, L. The efficacy of self-assembled cationic antimicrobial peptide nanoparticles against Cryptococcus neoformans for the treatment of meningitis. *Biomaterials* **2010**, *31*, 2874-2881.

224. Liu, L.; Venkatraman, S. S.; Yang, Y. Y.; Guo, K.; Lu, J.; He, B.; Moochhala, S.; Kan, L. Polymeric micelles anchored with TAT for delivery of antibiotics across the blood-brain barrier. *Biopolymers* **2008**, *90*, 617-623.

225. Tian, X.-H.; Wang, Z.-G.; Meng, H.; Wang, Y.-H.; Feng, W.; Wei, F.; Huang, Z.-C.; Lin, X.-N.; Ren, L. Tat peptide-decorated gelatin-siloxane nanoparticles for delivery of CGRP transgene in treatment of cerebral vasospasm. *Int. J. Nanomedicine* **2013**, *8*, 865-876.

226. Qin, Y.; Chen, H.; Zhang, Q.; Wang, X.; Yuan, W.; Kuai, R.; Tang, J.; Zhang, L.; Zhang, Z.; Zhang, Q.; Liu, J.; He, Q. Liposome formulated with TAT-modified cholesterol for improving brain delivery and therapeutic efficacy on brain glioma in animals. *Int. J. Pharm.* **2011**, *420*, 304-312.

227. Drin, G.; Cottin, S.; Blanc, E.; Rees, A. R.; Temsamani, J. Studies on the internalization mechanism of cationic cell-penetrating peptides. *J. Biol. Chem.* **2003**, *278*, 31192-31201.

228. Rousselle, C.; Clair, P.; Lefauconnier, J. M.; Kaczorek, M.; Scherrmann, J. M.; Temsamani, J. New advances in the transport of doxorubicin through the blood-brain barrier by a peptide vector-mediated strategy. *Mol. Pharmacol.* **2000**, *57*, 679-686.

229. Rousselle, C.; Smirnova, M.; Clair, P.; Lefauconnier, J. M.; Chavanieu, A.; Calas, B.; Scherrmann, J. M.; Temsamani, J. Enhanced delivery of doxorubicin into the brain via a peptide-vector-mediated strategy: saturation kinetics and specificity. *J. Pharmacol. Exp. Ther.* **2001**, *296*, 124-131.

230. Rousselle, C.; Clair, P.; Smirnova, M.; Kolesnikov, Y.; Pasternak, G. W.; Gac-Breton, S.; Rees, A. R.; Scherrmann, J. M.; Temsamani, J. Improved brain uptake and pharmacological activity of dalargin using a peptide-vector-mediated strategy. *J. Pharmacol. Exp. Ther.* **2003**, *306*, 371-376.

231. Temsamani, J.; Bonnafous, C.; Rousselle, C.; Fraisse, Y.; Clair, P.; Granier, L. A.; Rees, A. R.; Kaczorek, M.; Scherrmann, J. M. Improved brain uptake and pharmacological activity profile of morphine-6-glucuronide using a peptide vector-mediated strategy. *J. Pharmacol. Exp. Ther.* **2005**, *313*, 712-719.

232. Tian, X.-h.; Wei, F.; Wang, T.-x.; Wang, D.; Wang, J.; Lin, X.-n.; Wang, P.; Ren, L. Blood–brain barrier transport of Tat peptide and polyethylene glycol decorated gelatin–siloxane nanoparticle. *Mater. Lett.* **2012**, *68*, 94-96.

233. Caillé, I.; Allinquant, B.; Dupont, E.; Bouillot, C.; Langer, A.; Müller, U.; Prochiantz, A. Soluble form of amyloid precursor protein regulates proliferation of progenitors in the adult subventricular zone. *Development* **2004**, *131*, 2173-2181.

234. Du, L.; Kayali, R.; Bertoni, C.; Fike, F.; Hu, H.; Iversen, P. L.; Gatti, R. A. Arginine-rich cell-penetrating peptide dramatically enhances AMO-mediated ATM aberrant splicing correction and enables delivery to brain and cerebellum. *Hum. Mol. Genet.* **2011**, *20*, 3151-3160.

235. Xia, H.; Gao, X.; Gu, G.; Liu, Z.; Hu, Q.; Tu, Y.; Song, Q.; Yao, L.; Pang, Z.; Jiang, X.; Chen, J.; Chen, H. Penetratin-functionalized PEG-PLA nanoparticles for brain drug delivery. *Int. J. Pharm.* **2012**, *436*, 840-850.

236. Zong, T.; Mei, L.; Gao, H.; Cai, W.; Zhu, P.; Shi, K.; Chen, J.; Wang, Y.; Gao, F.; He, Q. Synergistic dual-ligand doxorubicin liposomes improve targeting and therapeutic efficacy of brain glioma in animals. *Mol. Pharm.* **2014**, *11*, 2346-2357.

237. Chikhale, E. G.; Ng, K. Y.; Burton, P. S.; Borchardt, R. T. Hydrogen bonding potential as a determinant of the in vitro and in situ blood-brain barrier permeability of peptides. *Pharm. Res.* **1994**, *11*, 412-419.

238. Teixidó, M.; Zurita, E.; Mendieta, L.; Oller-Salvia, B.; Prades, R.; Tarragó, T.; Giralt, E. Dual system for the central nervous system targeting and blood-brain barrier transport of a selective prolyl oligopeptidase inhibitor. *Biopolymers* **2013**, *100*, 662-674.

239. King, G. F. Venoms as a platform for human drugs: translating toxins into therapeutics. *Expert Opin. Biol. Ther.* **2011**, *11*, 1469-1484.

240. Osipov, A.; Utkin, Y. Effects of snake venom polypeptides on central nervous system. *Cent. Nerv. Syst. Agents Med. Chem.* **2012**, *12*, 315-328.

241. King, G. F.; Gentz, M. C.; Escoubas, P.; Nicholson, G. M. A rational nomenclature for naming peptide toxins from spiders and other venomous animals. *Toxicon* **2008**, *52*, 264-276.

242. Mamelak, A. N.; Jacoby, D. B. Targeted delivery of antitumoral therapy to glioma and other malignancies with synthetic chlorotoxin (TM-601). *Expert Opin. Drug Deliv.* **2007**, *4*, 175-186.

243. Vincent, J. P.; Schweitz, H.; Lazdunski, M. Structure-function relationships and site of action of apamin, a neurotoxic polypeptide of bee venom with an action on the central nervous system. *Biochemistry* **1975**, *14*, 2521-2525.

244. Xiang, Y.; Wu, Q.; Liang, L.; Wang, X.; Wang, J.; Zhang, X.; Pu, X.; Zhang, Q. Chlorotoxin-modified stealth liposomes encapsulating levodopa for the targeting delivery against Parkinson's disease in the MPTP-induced mice model. *J. Drug Target.* **2012**, *20*, 67-75.

245. Habermann, E. Bee and wasp venoms. *Science* **1972**, *177*, 314-322.

246. Wulff, H.; Kolski-Andreaco, A.; Sankaranarayanan, A.; Sabatier, J. M.; Shakkottai, V. Modulators of small- and intermediate-conductance calcium-activated potassium channels and their therapeutic indications. *Curr. Med. Chem.* **2007**, *14*, 1437-1457.

247. Habermann, E. Apamin. *Pharmacol. Ther.* **1984**, *25*, 255-270.

248. Alvarez-Fischer, D.; Noelker, C.; Vulinović, F.; Grünewald, A.; Chevarin, C.; Klein, C.; Oertel, W. H.; Hirsch, E. C.; Michel, P. P.; Hartmann, A. Bee venom and its component apamin as neuroprotective agents in a Parkinson disease mouse model. *PLoS ONE* **2013**, *8*, e61700.

249. Cosand, W. L.; Merrifield, R. B. Concept of internal structural controls for evaluation of inactive synthetic peptide analogs: synthesis of [Orn13,14]apamin and its guanidination to an apamin derivative with full neurotoxic activity. *Proc. Natl. Acad. Sci. U. S. A.* **1977**, *74*, 2771-2775.

250. Labbé-Jullié, C.; Granier, C.; Albericio, F.; Defendini, M. L.; Ceard, B.; Rochat, H.; van Rietschoten, J. Binding and toxicity of apamin. Characterization of the active site. *European Journal of Biochemistry* **1991**, *196*, 639-645.

251. Chau, M. H.; Nelson, J. W. Cooperative disulfide bond formation in apamin. *Biochemistry* **1992**, *31*, 4445-4450.

252. Huyghues-Despointes, B. M.; Nelson, J. W. Stabilities of disulfide bond intermediates in the folding of apamin. *Biochemistry* **1992**, *31*, 1476-1483.

253. Ramalingam, K.; Snyder, G. H. Selective disulfide formation in truncated apamin and sarafotoxin. *Biochemistry* **1993**, *32*, 11155-11161.

254. Dempsey, C. E.; Sessions, R. B.; Lamble, N. V.; Campbell, S. J. The asparagine-stabilized beta-turn of apamin: contribution to structural stability from dynamics simulation and amide hydrogen exchange analysis. *Biochemistry* **2000**, *39*, 15944-15952.

255. Fiori, S.; Pegoraro, S.; Rudolph-Böhner, S.; Cramer, J.; Moroder, L. Synthesis and conformational analysis of apamin analogues with natural and non-natural cystine/selenocystine connectivities. *Biopolymers* **2000**, *53*, 550-564.

256. Schroll, A. L.; Hondal, R. J.; Flemer, S., Jr. 2,2'-Dithiobis(5-nitropyridine) (DTNP) as an effective and gentle deprotectant for common cysteine protecting groups. *J. Pept. Sci.* **2012**, *18*, 1-9.

257. Wemmer, D.; Kallenbach, N. R. Structure of apamin in solution: a two-dimensional nuclear magnetic resonance study. *Biochemistry* **1983**, *22*, 1901-1906.

258. Pease, J. H.; Wemmer, D. E. Solution structure of apamin determined by nuclear magnetic resonance and distance geometry. *Biochemistry* **1988**, *27*, 8491-8498.

259. Glushka, J.; Lee, M.; Coffin, S.; Cowburn, D. Nitrogen-15 chemical shifts of backbone amides in bovine pancreatic trypsin inhibitor and apamin. *J. Am. Chem. Soc.* **1989**, *111*, 7716-7722.

260. Giralt, E.; Albericio, F.; Pedroso, E.; Granier, C.; van Rietschoten, J. Convergent solid phase peptide synthesis. II. Synthesis of the 1–6 apamin protected segment on a NBB-resin. Synthesis of apamin. *Tetrahedron* **1982**, *38*, 1193-1201.

261. Albericio, F.; Granier, C.; Labbé-Jullié, C.; Seagar, M.; Couraud, F.; van Rietschoten, J. Solid phase synthesis and hplc purification of the protected 1-12 sequence of apamin for rapid synthesis of apamin analogues differing in the c-terminal region. *Tetrahedron* **1984**, *40*, 4313-4326.

262. Brazil, B. T.; Cleland, J. L.; McDowell, R. S.; Skelton, N. J.; Paris, K.; Horowitz, P. M. Model peptide studies demonstrate that amphipathic secondary structures can be recognized by the chaperonin GroEL (cpn60). *J. Biol. Chem.* **1997**, *272*, 5105-5111.

263. Weston, C. J.; Cureton, C. H.; Calvert, M. J.; Smart, O. S.; Allemann, R. K. A stable miniature protein with oxaloacetate decarboxylase activity. *Chembiochem* **2004**, *5*, 1075-1080.

264. Li, C.; Pazgier, M.; Liu, M.; Lu, W. Y.; Lu, W. Apamin as a template for structure-based rational design of potent peptide activators of p53. *Angew. Chem. Int. Ed.* **2009**, *48*, 8712-8715.

265. Oller-Salvia, B.; Teixidó, M.; Giralt, E. From venoms to BBB shuttles: Synthesis and blood-brain barrier transport assessment of apamin and a nontoxic analog. *Biopolymers* **2013**, *100*, 675-686.

266. Defendini, M. L.; Pierres, M.; Regnier-Vigouroux, A.; Rochat, H.; Granier, C. Epitope mapping of apamin by means of monoclonal antibodies raised against free or carrier-coupled peptide. *Mol. Immunol.* **1990**, *27*, 551-558.

267. Defendini, M. L.; el-Ayeb, M.; Regnier-Vigouroux, A.; Granier, C.; Pierres, M. H-2A-linked control of T-cell and antibody responses to apamin. *Immunogenetics* **1988**, *28*, 139-141.

268. Culot, M.; Lundquist, S.; Vanuxeem, D.; Nion, S.; Landry, C.; Delplace, Y.; Dehouck, M. P.; Berezowski, V.; Fenart, L.; Cecchelli, R. An in vitro blood-brain barrier model for high throughput (HTS) toxicological screening. *Toxicol. In Vitro* **2008**, *22*, 799-811.

269. Gaillard, P. J.; de Boer, A. G. 2B-Trans technology: targeted drug delivery across the blood-brain barrier. *Methods Mol. Biol.* **2008**, *437*, 161-175.

270. Cecchelli, R.; Dehouck, B.; Descamps, L.; Fenart, L.; Buée-Scherrer, V. V.; Duhem, C.; Lundquist, S.; Rentfel, M.; Torpier, G.; Dehouck, M. P. In vitro model for evaluating drug transport across the blood-brain barrier. *Adv. Drug Deliv. Rev.* **1999**, *36*, 165-178.

271. Yang, Y.; Sweeney, W. V.; Schneider, K.; Chait, B. T.; Tam, J. P. Two-step selective formation of three disulfide bridges in the synthesis of the C-terminal epidermal growth factor-like domain in human blood coagulation factor IX. *Protein Sci* **1994**, *3*, 1267-1275.

272. Beliveau, R.; Demeule, M.; Google Patents: 2004.

273. Akan, M.; Ata, B.; Olsen, T. Congestion-based lead-time quotation for heterogenous customers with convex-concave delay costs: optimality of a cost-balancing policy based on convex hull functions. *Oper. Res.* **2012**, *60*, 1505-1519.

274. Garcia, A. E.; Tai, K. P.; Puttamadappa, S. S.; Shekhtman, A.; Ouellette, A. J.; Camarero, J. A. Biosynthesis and antimicrobial evaluation of backbone-cyclized α-defensins. *Biochemistry* **2011**, *50*, 10508-10519.

275. Strong, N. E. H. Receptor-mediated endocytosis of apamin by liver cells. *European Journal of Biochemistry* **1987**, *163*, 267-273.

276. Hopp, T. P.; Woods, K. R. Prediction of protein antigenic determinants from amino acid sequences. *Proceedings of the National Academy of Sciences* **1981**, *78*, 3824-3828.

277. Soto, C.; Sigurdsson, E. M.; Morelli, L.; Kumar, R. A.; Castaño, E. M.; Frangione, B. Beta-sheet breaker peptides inhibit fibrillogenesis in a rat brain model of amyloidosis: implications for Alzheimer's therapy. *Nat. Med.* **1998**, *4*, 822-826.

278. Raldúa, D.; Piña, B. In vivo zebrafish assays for analyzing drug toxicity. *Expert Opin. Drug Metab. Toxicol.* **2014**, *10*, 685-697.

279. Scholz, S.; Ortmann, J.; Klüver, N.; Léonard, M. Extensive review of fish embryo acute toxicities for the prediction of GHS acute systemic toxicity categories. *Regul. Toxicol. Pharmacol.* **2014**, *69*, 572-579.

280. Parng, C.; Seng, W. L.; Semino, C.; McGrath, P. Zebrafish: a preclinical model for drug screening. *Assay Drug Dev. Technol.* **2002**, *1*, 41-48.

281. Ali, S.; Mil, H. G. J. v.; Richardson, M. K. Large-scale assessment of the zebrafish embryo as a possible predictive model in toxicity testing. *PLoS ONE* **2011**, *6*, e21076.

282. Lammer, E.; Carr, G. J.; Wendler, K.; Rawlings, J. M.; Belanger, S. E.; Braunbeck, T. Is the fish embryo toxicity test (FET) with the zebrafish (Danio rerio) a potential alternative for the fish acute toxicity test? *Comp. Biochem. Physiol. C Toxicol. Pharmacol.* **2009**, *149*, 196-209.

283. Saint-Amant, L.; Drapeau, P. Synchronization of an embryonic network of identified spinal interneurons solely by electrical coupling. *Neuron* **2001**, *31*, 1035-1046.

284. OECD *Test No. 236: Fish Embryo Acute Toxicity (FET) Test*; OECD Publishing, 2013.

285. Le-Nguyen, D.; Chiche, L.; Hoh, F.; Martin-Eauclaire, M. F.; Dumas, C.; Nishi, Y.; Kobayashi, Y.; Aumelas, A. Role of Asn2 and Glu7 residues in the oxidative folding and on the conformation of the N-terminal loop of apamin. *Biopolymers* **2007**, *86*, 447-462.

286. Stoddart, M. J. Cell viability assays: introduction. *Methods Mol. Biol.* **2011**, *740*, 1-6.

287. Tuma, P.; Hubbard, A. L. Transcytosis: crossing cellular barriers. *Physiol. Rev.* **2003**, *83*, 871-932.

288. Doherty, G. J.; McMahon, H. T. Mechanisms of endocytosis. *Annu. Rev. Biochem.* **2009**, *78*, 857-902.

289. Cai, W.; Chen, X. Preparation of peptide-conjugated quantum dots for tumor vasculature-targeted imaging. *Nat. Protoc.* **2008**, *3*, 89-96.

290. Hermanson, G. T. In *Bioconjugate Techniques (Second Edition)*; Hermanson, G. T., Ed.; Academic Press: New York, 2008, p 169-212.

291. Olmedo, I.; Araya, E.; Sanz, F.; Medina, E.; Arbiol, J.; Toledo, P.; Álvarez-Lueje, A.; Giralt, E.; Kogan, M. J. How changes in the sequence of the peptide CLPFFD-NH2 can modify the conjugation and stability of gold nanoparticles and their affinity for beta-amyloid fibrils. *Bioconjug. Chem.* **2008**, *19*, 1154-1163.

292. May, T. W.; Wiedmeyer, R. H. A table of polyatomic interferences in ICP-MS. *At. Spectrosc.* **1998**, *19*, 150-155.

293. Phan, T. G.; Bullen, A. Practical intravital two-photon microscopy for immunological research: faster, brighter, deeper. *Immunol. Cell Biol.* **2010**, *88*, 438-444.

294. Hilderbrand, S. A.; Weissleder, R. Near-infrared fluorescence: application to in vivo molecular imaging. *Curr. Opin. Chem. Biol.* **2010**, *14*, 71-79.

295. Abulrob, A.; Brunette, E.; Slinn, J.; Baumann, E.; Stanimirovic, D. Dynamic analysis of the blood-brain barrier disruption in experimental stroke using time domain in vivo fluorescence imaging. *Mol. Imaging* **2008**, *7*, 248-262.

296. Zurdo, J.; Fowler, S.; Stallwood, Y.; Giralt, E.; Teixidó, M.; Carulla, N.; Zyentia Limited, UK . 2008, p 50pp.

297. Hou, J.; Liu, X.; Shen, J.; Zhao, G.; Wang, P. G. The impact of click chemistry in medicinal chemistry. *Expert Opin. Drug Discov.* **2012**, *7*, 489-501.

298. Shen, B. Q.; Xu, K.; Liu, L.; Raab, H.; Bhakta, S.; Kenrick, M.; Parsons-Reponte, K. L.; Tien, J.; Yu, S. F.; Mai, E.; Li, D.; Tibbitts, J.; Baudys, J.; Saad, O. M.; Scales, S. J. *et al.* Conjugation site modulates the in vivo stability and therapeutic activity of antibody-drug conjugates. *Nat. Biotechnol.* **2012**, *30*, 184-189.

299. Moellering, Raymond E.; Cravatt, Benjamin F. How chemoproteomics can enable drug discovery and development. *Chem. Biol.* **2012**, *19*, 11-22.

300. Nelson, A. L.; Dhimolea, E.; Reichert, J. M. Development trends for human monoclonal antibody therapeutics. *Nature Reviews Drug Discovery* **2010**, *9*, 767-774.

301. Jones, A. R.; Shusta, E. V. In *Therapeutic Monoclonal Antibodies*; John Wiley & Sons, Inc.: 2009, p 483-502.

302. Cooper, P. R.; Ciambrone, G. J.; Kliwinski, C. M.; Maze, E.; Johnson, L.; Li, Q.; Feng, Y.; Hornby, P. J. Efflux of monoclonal antibodies from rat brain by neonatal Fc receptor, FcRn. *Brain Res.* **2013**, *1534*, 13-21.

303. Lampson, L. A. Monoclonal antibodies in neuro-oncology: Getting past the blood-brain barrier. *MAbs* **2011**, *3*, 153-160.

304. Dolecek, T. A.; Propp, J. M.; Stroup, N. E.; Kruchko, C. CBTRUS statistical report: primary brain and central nervous system tumors diagnosed in the United States in 2005-2009. *Neuro-oncology* **2012**, *14 Suppl 5*, v1-49.

305. Jovčevska, I.; Kočevar, N.; Komel, R. Glioma and glioblastoma - how much do we (not) know? *Mol. Clin. Oncol.* **2013**, *1*, 935-941.

306. Chacko, A. M.; Li, C.; Pryma, D. A.; Brem, S.; Coukos, G.; Muzykantov, V. Targeted delivery of antibody-based therapeutic and imaging agents to CNS tumors: crossing the blood-brain barrier divide. *Expert Opin. Drug Deliv.* **2013**, *10*, 907-926.

307. Wolburg, H.; Noell, S.; Fallier-Becker, P.; Mack, A. F.; Wolburg-Buchholz, K. The disturbed blood-brain barrier in human glioblastoma. *Mol. Aspects Med.* **2012**, *33*, 579-589.

308. Serwer, L. P.; James, C. D. Challenges in drug delivery to tumors of the central nervous system: an overview of pharmacological and surgical considerations. *Adv. Drug Deliv. Rev.* **2012**, *64*, 590-597.

309. Le Rhun, E.; Taillibert, S.; Chamberlain, M. C. The future of high-grade glioma: Where we are and where are we going. *Surg. Neurol. Int.* **2015**, *6*, 9-44.

310. Wang, Y.; Fei, D.; Vanderlaan, M.; Song, A. Biological activity of bevacizumab, a humanized anti-VEGF antibody in vitro. *Angiogenesis* **2004**, *7*, 335-345.

311. Sliwkowski, M. X.; Mellman, I. Antibody Therapeutics in Cancer. *Science* **2013**, *341*, 1192-1198.

312. Zahonero, C.; Sánchez-Gómez, P. EGFR-dependent mechanisms in glioblastoma: towards a better therapeutic strategy. *Cell. Mol. Life Sci.* **2014**, *71*, 3465-3488.

313. Janjigian, Y. Y.; Ku, G. Y.; Campbell, J. C.; Shah, M. A.; Capanu, M.; Kelsen, D. P.; Ilson, D. H. Phase II trial of cetuximab plus cisplatin and irinotecan in patients with cisplatin and irinotecan-refractory metastatic esophagogastric cancer. *Am. J. Clin. Oncol.* **2014**, *37*, 126-130.

314. Alexander, B. M.; Lee, E. Q.; Reardon, D. A.; Wen, P. Y. Current and future directions for Phase II trials in high-grade glioma. *Expert Rev. Neurother.* **2013**, *13*, 369-387.

315. Perez, H. L.; Cardarelli, P. M.; Deshpande, S.; Gangwar, S.; Schroeder, G. M.; Vite, G. D.; Borzilleri, R. M. Antibody-drug conjugates: current status and future directions. *Drug Discov. Today* **2014**, *19*, 869-881.

316. Chari, R. V. J.; Miller, M. L.; Widdison, W. C. Antibody-drug conjugates: an emerging concept in cancer therapy. *Angew. Chem. Int. Ed.* **2014**, *53*, 3796-3827.

317. Mullard, A. Maturing antibody-drug conjugate pipeline hits 30. *Nat. Rev. Drug Discov.* **2013**, *12*, 329-332.

318. Bouchard, H.; Viskov, C.; Garcia-Echeverria, C. Antibody–drug conjugates—a new wave of cancer drugs. *Bioorg. Med. Chem. Lett.* **2014**, *24*, 5357-5363.

319. Arnold, J. N.; Wormald, M. R.; Sim, R. B.; Rudd, P. M.; Dwek, R. A. The impact of glycosylation on the biological function and structure of human immunoglobulins. *Annu. Rev. Immunol.* **2007**, *25*, 21-50.

320. Gautier, V.; Boumeester, A. J.; Lössl, P.; Heck, A. J. R. Lysine conjugation properties in human IgGs studied by integrating high-resolution native mass spectrometry and bottom-up proteomics. *Proteomics* **2015**, n/a-n/a.

321. Feng, Y.; Zhu, Z.; Chen, W.; Prabakaran, P.; Lin, K.; Dimitrov, D. Conjugates of small molecule drugs with antibodies and other proteins. *Biomedicines* **2014**, *2*, 1-13.

322. Behrens, C. R.; Liu, B. Methods for site-specific drug conjugation to antibodies. *MAbs* **2014**, *6*, 46-53.

323. Agarwal, P.; Bertozzi, C. R. Site-specific antibody–drug conjugates: the nexus of bioorthogonal chemistry, protein engineering, and drug development. *Bioconjug. Chem.* **2015**, *26*, 176-192.

324. Hamblett, K. J.; Senter, P. D.; Chace, D. F.; Sun, M. M.; Lenox, J.; Cerveny, C. G.; Kissler, K. M.; Bernhardt, S. X.; Kopcha, A. K.; Zabinski, R. F.; Meyer, D. L.; Francisco, J. A. Effects of drug loading on the antitumor activity of a monoclonal antibody drug conjugate. *Clin. Cancer Res.* **2004**, *10*, 7063-7070.

325. Sun, M. M.; Beam, K. S.; Cerveny, C. G.; Hamblett, K. J.; Blackmore, R. S.; Torgov, M. Y.; Handley, F. G.; Ihle, N. C.; Senter, P. D.; Alley, S. C. Reduction-alkylation strategies for the modification of specific monoclonal antibody disulfides. *Bioconjug. Chem.* **2005**, *16*, 1282-1290.

326. Vidarsson, G.; Dekkers, G.; Rispens, T. IgG subclasses and allotypes: from structure to effector functions. *Front. Immunol.* **2014**, *5*, 520.

327. Junttila, T. T.; Li, G.; Parsons, K.; Phillips, G. L.; Sliwkowski, M. X. Trastuzumab-DM1 (T-DM1) retains all the mechanisms of action of trastuzumab and efficiently inhibits growth of lapatinib insensitive breast cancer. *Breast Cancer Res. Treat.* **2011**, *128*, 347-356.

328. McDonagh, C. F.; Kim, K. M.; Turcott, E.; Brown, L. L.; Westendorf, L.; Feist, T.; Sussman, D.; Stone, I.; Anderson, M.; Miyamoto, J.; Lyon, R.; Alley, S. C.; Gerber, H. P.; Carter, P. J. Engineered anti-CD70 antibody-drug conjugate with increased therapeutic index. *Mol. Cancer Ther.* **2008**, *7*, 2913-2923.

329. Carter, P. Improving the efficacy of antibody-based cancer therapies. *Nat. Rev. Cancer* **2001**, *1*, 118-129.

330. McDonagh, C. F.; Turcott, E.; Westendorf, L.; Webster, J. B.; Alley, S. C.; Kim, K.; Andreyka, J.; Stone, I.; Hamblett, K. J.; Francisco, J. A.; Carter, P. Engineered antibody-drug conjugates with defined sites and stoichiometries of drug attachment. *Protein Eng. Des. Sel.* **2006**, *19*, 299-307.

331. Junutula, J. R.; Raab, H.; Clark, S.; Bhakta, S.; Leipold, D. D.; Weir, S.; Chen, Y.; Simpson, M.; Tsai, S. P.; Dennis, M. S.; Lu, Y.; Meng, Y. G.; Ng, C.; Yang, J.; Lee, C. C. *et al.* Site-specific conjugation of a cytotoxic drug to an antibody improves the therapeutic index. *Nat Biotech* **2008**, *26*, 925-932.

332. Xiao, H.; Chatterjee, A.; Choi, S.-h.; Bajjuri, K. M.; Sinha, S. C.; Schultz, P. G. Genetic incorporation of multiple unnatural amino acids into proteins in mammalian cells. *Angew. Chem. Int. Ed.* **2013**, *52*, 14080-14083.

333. Hofer, T.; Skeffington, L. R.; Chapman, C. M.; Rader, C. Molecularly defined antibody conjugation through a selenocysteine interface. *Biochemistry* **2009**, *48*, 12047-12057.

334. Carrico, I. S.; Carlson, B. L.; Bertozzi, C. R. Introducing genetically encoded aldehydes into proteins. *Nat. Chem. Biol.* **2007**, *3*, 321-322.

335. Agarwal, P.; Kudirka, R.; Albers, A. E.; Barfield, R. M.; de Hart, G. W.; Drake, P. M.; Jones, L. C.; Rabuka, D. Hydrazino-Pictet-Spengler ligation as a biocompatible method for the generation of stable protein conjugates. *Bioconjug. Chem.* **2013**, *24*, 846-851.

336. Lin, C.-W.; Ting, A. Y. Transglutaminase-catalyzed site-specific conjugation of small-molecule probes to proteins in vitro and on the surface of living cells. *J. Am. Chem. Soc.* **2006**, *128*, 4542-4543.

337. Jeger, S.; Zimmermann, K.; Blanc, A.; Grünberg, J.; Honer, M.; Hunziker, P.; Struthers, H.; Schibli, R. Site-Specific and Stoichiometric Modification of Antibodies by Bacterial Transglutaminase. *Angew. Chem. Int. Ed.* **2010**, *49*, 9995-9997.

338. Mao, H.; Hart, S. A.; Schink, A.; Pollok, B. A. Sortase-mediated protein ligation: a new method for protein engineering. *J. Am. Chem. Soc.* **2004**, *126*, 2670-2671.

339. Swee, L. K.; Guimaraes, C. P.; Sehrawat, S.; Spooner, E.; Barrasa, M. I.; Ploegh, H. L. Sortase-mediated modification of alphaDEC205 affords optimization of antigen presentation and immunization against a set of viral epitopes. *Proc. Natl. Acad. Sci. U. S. A.* **2013**, *110*, 1428-1433.

340. Möhlmann, S.; Bringmann, P.; Greven, S.; Harrenga, A. Site-specific modification of ED-B-targeting antibody using intein-fusion technology. *BMC Biotechnol.* **2011**, *11*, 76.

341. Witus, L. S.; Francis, M. Site-specific protein bioconjugation via a pyridoxal 5'-phosphate-mediated N-terminal transamination reaction. *Curr. Protoc. Chem. Biol.* **2010**, *2*, 125-134.

342. Scheck, R. A.; Francis, M. B. Regioselective labeling of antibodies through N-terminal transamination. *ACS Chem. Biol.* **2007**, *2*, 247-251.

343. Snell, E. E. The vitamin B6 group. V. The reversible interconversion of pyridoxal and pyridoxamine by transamination reactions. *J. Am. Chem. Soc.* **1945**, *67*, 194-197.

344. Cennamo, C. Metal ion independent non-enzimatic transamination bertween pyridoxal and amino acid esters. . *Biochim. Biophys. Acta* **1964**, *93*, 323-332.

345. Dixon, H. B. F. N-terminal modification of proteins—a review. *J. Protein Chem.* **1984**, *3*, 99-108.

346. Gilmore, J. M.; Scheck, R. A.; Esser-Kahn, A. P.; Joshi, N. S.; Francis, M. B. N-terminal protein modification through a biomimetic transamination reaction. *Angew. Chem. Int. Ed. Engl.* **2006**, *45*, 5307-5311.

347. Ducry, L.; Stump, B. Antibody–drug conjugates: linking cytotoxic payloads to monoclonal antibodies. *Bioconjug. Chem.* **2010**, *21*, 5-13.

348. Forget, D.; Renaudet, O.; Defrancq, E.; Dumy, P. Efficient preparation of carbohydrate–oligonucleotide conjugates (COCs) using oxime bond formation. *Tetrahedron Lett.* **2001**, *42*, 7829-7832.

349. Hong, L.; Lei, J. Scaling law for the radius of gyration of proteins and its dependence on hydrophobicity. *Journal of Polymer Science Part B: Polymer Physics* **2009**, *47*, 207-214.

350. Dill, K. A.; Ghosh, K.; Schmit, J. D. Physical limits of cells and proteomes. *Proc. Natl. Acad. Sci. U.S.A.* **2011**, *108*, 17876-17882.

351. Kumaresan, P. R.; Luo, J.; Song, A.; Marik, J.; Lam, K. S. Evaluation of ketone-oxime method for developing therapeutic on-demand cleavable immunoconjugates. *Bioconjug. Chem.* **2008**, *19*, 1313-1318.

352. Ohta, M.; Iwasaki, M.; Kouno, K.; Ueda, Y. Mechanism of the Molisch reaction. *Chem. Pharm. Bull.* **1985**, *33*, 2862-2865.

353. Dirksen, A.; Hackeng, T. M.; Dawson, P. E. Nucleophilic catalysis of oxime ligation. *Angew. Chem. Int. Ed.* **2006**, *45*, 7581-7584.

354. Zuberbühler, K.; Casi, G.; Bernardes, G. J. L.; Neri, D. Fucose-specific conjugation of hydrazide derivatives to a vascular-targeting monoclonal antibody in IgG format. *Chem. Commun.* **2012**, *48*, 7100-7102.

355. Anthony, R. M.; Wermeling, F.; Ravetch, J. V. Novel roles for the IgG Fc glycan. *Ann. N. Y. Acad. Sci.* **2012**, *1253*, 170-180.

356. Zhou, Q.; Stefano, J. E.; Manning, C.; Kyazike, J.; Chen, B.; Gianolio, D. A.; Park, A.; Busch, M.; Bird, J.; Zheng, X.; Simonds-Mannes, H.; Kim, J.; Gregory, R. C.; Miller, R. J.; Brondyk, W. H. *et al.* Site-specific antibody-drug conjugation through glycoengineering. *Bioconjug. Chem.* **2014**, *25*, 510-520.

357. Ayoub, D.; Jabs, W.; Resemann, A.; Evers, W.; Evans, C.; Main, L.; Baessmann, C.; Wagner-Rousset, E.; Suckau, D.; Beck, A. Correct primary structure assessment and extensive glyco-profiling of cetuximab by a combination of intact, middle-up, middle-down and bottom-up ESI and MALDI mass spectrometry techniques. *MAbs* **2013**, *5*, 699-710.

358. Wakankar, A.; Chen, Y.; Gokarn, Y.; Jacobson, F. S. Analytical methods for physicochemical characterization of antibody drug conjugates. *MAbs* **2011**, *3*, 161-172.

359. Hermanson, G. T. In *Bioconjugate Techniques (Second Edition)*; Hermanson, G. T., Ed.; Academic Press: New York, 2008, p 783-823.

360. Devey, M. E. In *The Human IgG Subclasses: molecular analysis of structure, function and regulation*; Shakib, F., Ed.; Pergamon Press: Amsterdam, 1990, p 185-194.

361. Sinapis, C. I.; Routsias, J. G.; Sinapis, A. I.; Sinapis, D. I.; Agrogiannis, G. D.; Pantopoulou, A.; Theocharis, S. E.; Baltatzis, S.; Patsouris, E.; Perrea, D. Pharmacokinetics of intravitreal bevacizumab (Avastin®) in rabbits. *Clin. Ophthalmol.* **2011**, *5*, 697-704.

362. Bergsland, E.; Dickler, M. N. Maximizing the potential of bevacizumab in cancer treatment. *Oncologist* **2004**, *9*, 36-42.

363. Kozak, K. R.; Tsai, S. P.; Fourie-O'Donohue, A.; dela Cruz Chuh, J.; Roth, L.; Cook, R.; Chan, E.; Chan, P.; Darwish, M.; Ohri, R.; Raab, H.; Zhang, C.; Lin, K.; Wong, W. L. Total antibody quantification for MMAE-conjugated antibody-drug conjugates: impact of assay format and reagents. *Bioconjug. Chem.* **2013**, *24*, 772-779.

364. Hermanson, G. T. In *Bioconjugate Techniques (Second Edition)*; Hermanson, G. T., Ed.; Academic Press: New York, 2008, p 546-561.

365. Lappin, G. In *Radiotraces in drug development*; Lappin, G., Temple, S., Eds.; Boca Raton: CRC/Taylor & Francis: 2006, p 41-54.

366. Kaiser, E.; Colescott, R. L.; Bossinger, C. D.; Cook, P. I. Color test for detection of free terminal amino groups in the solid-phase synthesis of peptides. *Anal. Biochem.* **1970**, *34*, 595-598.

367. Triola, G.; Gerauer, M.; Görmer, K.; Brunsveld, L.; Waldmann, H. Solid-phase synthesis of lipidated Ras peptides employing the Ellman sulfonamide linker. *Chemistry* **2010**, *16*, 9585-9591.

368. Hwang, T.-L.; Shaka, A. J. Water suppression that works. Excitation sculpting using arbitrary waveforms and pulsed field gradients. *J. Magn. Reson., Ser. A* **1995**, *112*, 275-279.

369. Bax, A.; Davis, D. G. MLEV-17-based two-dimensional homonuclear magnetization transfer spectroscopy. *J. Magn. Reson.* **1985**, *65*, 355-360.

370. Bax, A.; Freeman, R. Investigation of complex networks of spin-spin coupling by two-dimensional NMR. *J. Magn. Reson.* **1981**, *44*, 542-561.

371. Jeener, J.; Meier, B. H.; Bachmann, P.; Ernst, R. R. Investigation of exchange processes by two-dimensional NMR spectroscopy. *J. Chem. Phys.* **1979**, *71*, 4546-4553.

372. Brünger, A. T.; Adams, P. D.; Clore, G. M.; DeLano, W. L.; Gros, P.; Grosse-Kunstleve, R. W.; Jiang, J. S.; Kuszewski, J.; Nilges, M.; Pannu, N. S.; Read, R. J.; Rice, L. M.; Simonson, T.; Warren, G. L. Crystallography & NMR system: A new software suite for macromolecular structure determination. *Acta Crystallogr. D Biol. Crystallogr.* **1998**, *54*, 905-921.

373. Berjanskii, M. V.; Neal, S.; Wishart, D. S. PREDITOR: a web server for predicting protein torsion angle restraints. *Nucleic Acids Res.* **2006**, *34*, W63-69.

374. Laskowski, R. A.; MacArthur, M. W.; Moss, D. S.; Thornton, J. M. PROCHECK: a program to check the stereochemical quality of protein structures. *J. Appl. Crystallogr.* **1993**, *26*, 283-291.

375. van Dongen, S. F. M.; Teeuwen, R. L. M.; Nallani, M.; van Berkel, S. S.; Cornelissen, J. J. L. M.; Nolte, R. J. M.; van Hest, J. C. M. Single-step azide introduction in proteins via an aqueous diazo transfer. *Bioconjug. Chem.* **2009**, *20*, 20-23.

376. Guerrero, S.; Araya, E.; Fiedler, J. L.; Arias, J. I.; Adura, C.; Albericio, F.; Giralt, E.; Arias, J. L.; Fernández, M. S.; Kogan, M. J. Improving the brain delivery of gold nanoparticles by conjugation with an amphipathic peptide. *Nanomedicine (Lond.)* **2010**, *5*, 897-913.

SUMMARY
IN CATALAN

Introducció – Llançadores per creuar la barrera hematoencefàlica: un paradigma emergent per l'administració de fàrmacs al cervell

L'augment de la incidència de les malalties neurodegeneratives, donat l'envelliment de la població, i la creixent prevalença dels tumors cerebrals fan que l'administració de fàrmacs al cervell sigui un repte cabdal en el desenvolupament de fàrmacs. Actualment, per moltes malalties que afecten el sistema nerviós central no existeixen tractaments eficients i, a més, els costos directes i indirectes d'aquestes patologies a Europa ja representen un quart de la despesa mèdica. Així doncs, incrementar l'eficiència dels tractaments no només milloraria el benestar d'una part important de la població, sinó que, a més, reduiria considerablement els costos derivats de les malalties associades al cervell. Malauradament, avui dia la majoria de compostos dissenyats per tractar aquestes afeccions no poden arribar a interaccionar amb les seves dianes en quantitats terapèuticament rellevants perquè no són capaces de creuar la barrera hematoencefàlica (BHE).

Juntament amb la barrera sang-líquid cefaloraquidi i l'epèndima, la BHE protegeix el cervell limitant l'accés de substàncies nocives i agents patògens, però també impedeix la penetració de fàrmacs i compostos per diagnosi. Al mateix temps, la BHE és la principal ruta d'entrada de nutrients al cervell i la màxima distància entre cèl·lules i capil·lars és inferior a 20 μm. Així doncs, superar aquesta barrera seria la manera més eficient d'administrar fàrmacs a qualsevol part del cervell.

La BHE es una barrera física, metabòlica i de transport. Està formada principalment per les cèl·lules endotelials que constitueixen les parets dels capil·lars del cervell, les quals es diferencien de la resta perquè estan unides mitjançant unions estretes. Aquestes unions consisteixen en intricades xarxes de proteïnes transmembrana i proteïnes citoplasmàtiques unides al citoesquelet que restringeixen la difusió paracel·lular. A més, l'endoteli cerebral forma una capa contínua sense porus, expressa una quantitat elevada d'enzims citosòlics i extracel·lulars i té un transport vesicular 100 vegades inferior al dels vasos d'altres teixits. Aquestes cèl·lules contenen bombes d'eflux, les quals retornen a la sang principalment molècules hidrofòbiques que són capaces de penetrar la cèl·lula per transport passiu. La regulació del transport a través de la BHE és complexa i està influïda per totes les cèl·lules que formen la unitat neurovascular, incloent astròcits, perícits, micròglia i neurones.

Per tal de permetre l'accés de nutrients al parènquima cerebral, existeixen diversos mecanismes d'entrada. Certes molècules petites hidrofòbiques com els lípids poden difondre a través de les membranes, mentre que algunes d'hidrofíliques com la glucosa penetren mitjançant transportadors. Diverses molècules més grans

necessàries per mantenir l'homeòstasi del cervell, com la insulina, la transferrina, la leptina o les proteïnes de baixa densitat, penetren la BHE mitjançant transcitosi per receptor. En canvi d'altres molècules ho fan a través de transcitosi per adsorció, la qual inclou tots aquells mecanismes de transport vesiculars que no requereixen un receptor i principalment es desencadena per la interacció de molècules catiòniques.

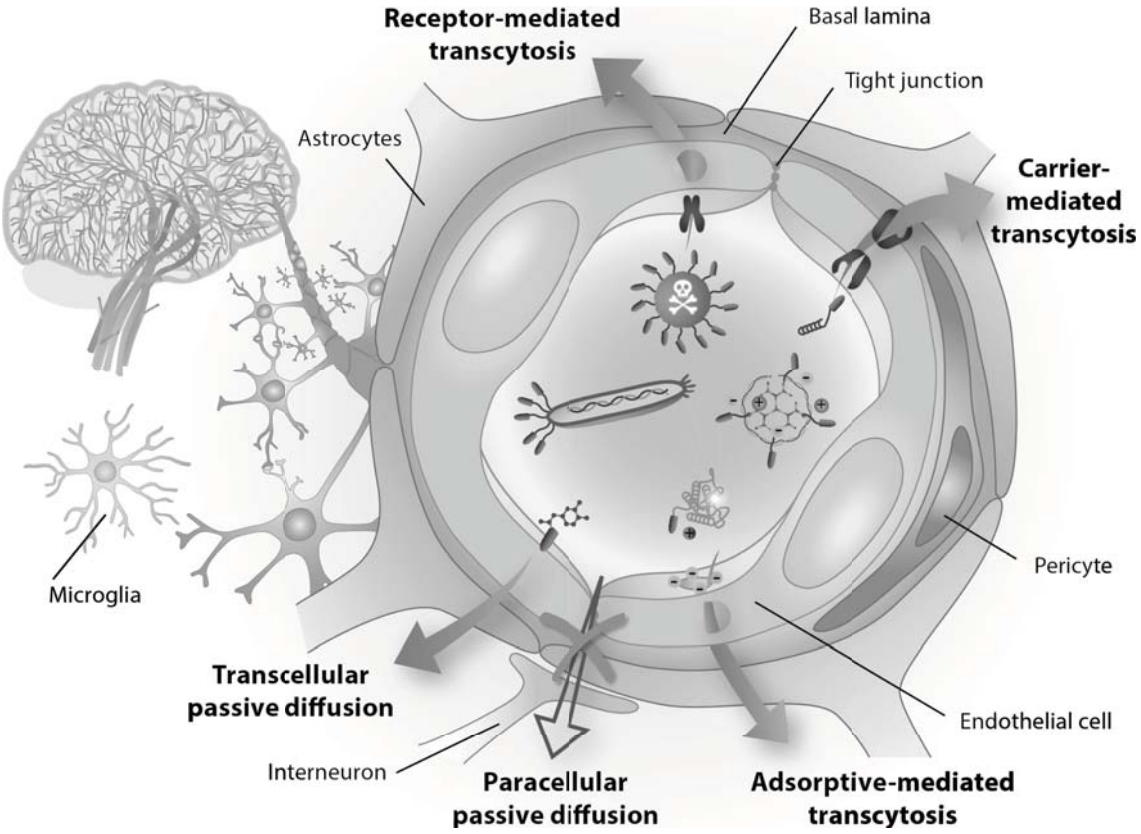

Figura i. *Transcitosi a través de la BHE de conjugats cargo-llançadora. (Disseny: Benjamí Oller Salvia. Realització: Iris Joval)*

Com que creuar la BHE encara suposa un gran repte, els mètodes més eficients que s'empren actualment per administrar fàrmacs al cervell són locals i molt invasius, de manera que comporten un risc important i requereixen un dispositiu complex. Darrerament s'està explorant l'opció de evitar la BHE mitjançant l'administració nasal, però aquesta tècnica permet emprar volums relativament petits i només és efectiva en zones determinades del cervell. Una estratègia que permet una major distribució dels fàrmacs injectats per via intravenosa és la disrupció temporal de la BHE. Per aquest propòsit s'han estudiat mètodes físics com l'aplicació d'ultrasons i molècules que afecten la regulació de les unions estretes. Tanmateix, afectar aquestes unions implica permetre l'entrada al parènquima cerebral de totes les substàncies de la sang que poden causar neuroinflamació, disfunció neuronal i neurodegeneració.

Donats els riscs associats als mètodes invasius i a la alteració de la BHE, s'ha consagrat molts esforços en modificar les molècules per augmentar la seva

permeabilitat a través d'aquesta barrera, de manera passiva o activa. Actualment, es coneix que els paràmetres principals que regeixen la difusió de molècules petites (< 500 Da) a través de la BHE són la lipofília, el pKa, el pes molecular, l'àrea de superfície topològica polar i el nombre de donadors i d'acceptors de ponts d'hidrogen. Emprant aquests paràmetres, existeixen algoritmes que permeten millorar la permeabilitat de molts compostos. Tot i això, la predicció de l'efecte de les bombes d'eflux encara no està completament resolta i un augment de la hidrofobicitat pot resultar en el millor reconeixement del fàrmac per part d'aquests transportadors. A més, augmentar la hidrofobicitat de la molècula sol comportar un increment inespecífic de la permeabilitat en tots els teixits i no només al cervell. En certs casos, com el de la levodopa, és possible modificar la molècula perquè esdevingui substrat d'un transportador que facilita la seva entrada al parènquima.

Malgrat la gran varietat de modificacions que s'han emprat per millorar el transport de molècules petites, cap té una aplicabilitat general. A més, tampoc no es poden extrapolar a compostos més grans com les proteïnes. La permeabilitat d'aquestes darreres es pot incrementar augmentant la seva càrrega positiva, però aquesta també origina l'adsorció inespecífica a d'altres teixits i n'augmenta la toxicitat.

L'única estratègia per creuar la BHE que és aplicable a qualsevol compost o, si més no, a famílies de compostos, és l'ús de vectors. Tot i que vectors biològics com virus i cèl·lules s'han emprat per administrar material genètic i fins i tot proteïnes, aquests comporten riscos elevats i l'eficiència i la selectivitat són limitades si la BHE està íntegra. En canvi, els vectors moleculars, els quals anomenarem "llançadores", en general ofereixen major versatilitat, selectivitat i seguretat. Les llançadores es poden definir com molècules que poden transportar càrregues a través de la BHE sense pertorbar la integritat de les unions estretes. Aquestes càrregues poden ser des de molècules orgàniques petites fins a nanopartícules, passant per proteïnes i material genètic. Algunes llançadores s'han dissenyat per augmentar el transport passiu, però la majoria tenen com a objectiu mecanismes actius com transportadors en el cas de càrregues petites o transcitosi via receptor o adsorció per les més grans.

Tot i que la transcitosi via adsorció permet un transport més elevat, la majoria d'esforços s'han centrat en els receptors sobreexpressats en l'endoteli cerebral donat que permeten major selectivitat i, per tant, menors efectes secundaris. Els pioners en aquest camp van ser Frieden i Pardridge, els quals van desenvolupar anticossos contra els receptors de transferrina i insulina. Recentment científics de Genentech i Hoffman-La Roche han optimitzat aquests anticossos disminuint-ne l'afinitat i fer-los més eficients. També, s'han emprat una gran varietat de proteïnes endògenes o molècules que interaccionen amb aquestes (com el polisorbat 80), però tenen l'inconvenient que han de competir amb les que estan a la sang. Fins i tot s'han

trobat altres proteïnes exògenes que són capaces d'interaccionar amb certs receptors com la toxina de la diftèria, però no han tingut un gran seguiment donada la seva modesta eficiència.

Tanmateix, produir i caracteritzar agents terapèutics biològics, així com reduir-ne la immunogenicitat, és molt costós. És per aquesta raó que els pèptids han emergit durant la darrera dècada com una alternativa que combina el menor cost de les molècules petites i la selectivitat dels "biològics". A més, la seva síntesi química permet introduir modificacions no naturals i una gran varietat de grups funcionals per incorporar-los a nanopartícules o proteïnes. Tot i que generalment han estat subestimats en química farmacèutica per la seva labilitat a proteases, actualment existeixen diversos mètodes per millorar-ne les propietats, com l'ús d'aminoàcids no naturals, la *N*-metilació i la ciclació.

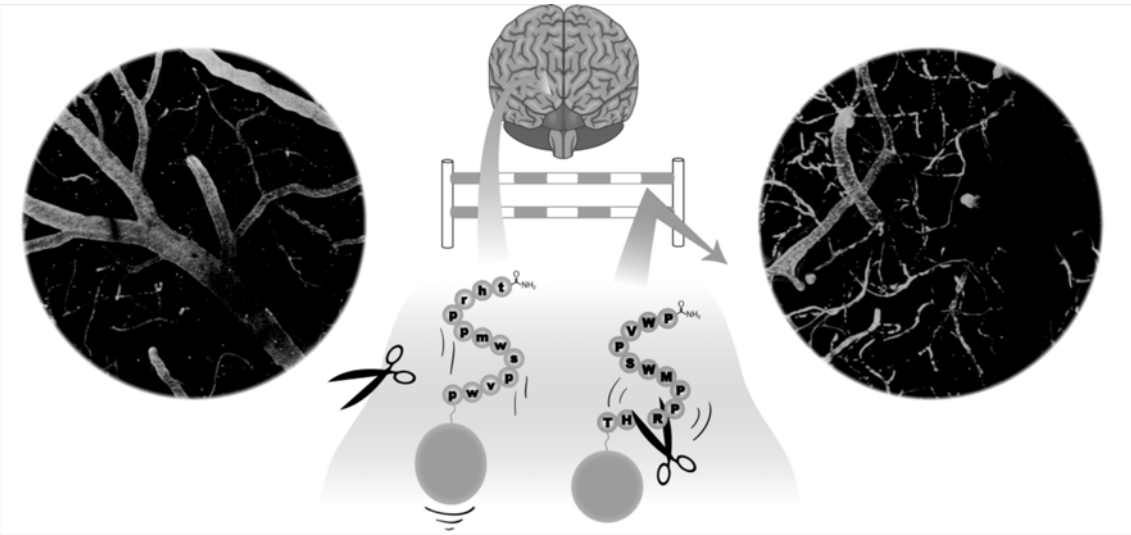

Figura ii. *El pèptid resistent a proteases THRre és capaç de transportar quantum dots dins del parènquima cerebral. (Dibuixat per Benjamí Oller-Salvia per l'abstract de Prades et al 2015)*

A dia d'avui existeixen una gran varietat de llançadores peptídiques capaces de transportar compostos a través de la BHE mitjançant diversos mecanismes. Alguns empren receptors pels quals el mecanisme de transcitosi està força acceptat com el de transferrina (THR, CRT, B6), el de proteïnes de baixa densitat (Angiopep-2, pèptids derivats de les apolipoproteïnes B i E, pèptid-22) o el de leptina (pèptids derivats de la leptina). Per d'altres llançadores hi ha indicis que suggereixen que interaccionen amb receptors pels quals el mecanisme de transport és desconegut com el de acetilcolina (pèptids derivats de la glicoproteïna del virus de la ràbia, com el RVG29), el de glutatió o els gangliòsids (G-23). En alguns casos com el del pèptid g7 o el TGN només es coneix que el mecanisme de transport és actiu i saturable. Pel que fa a les llançadores que no empren receptor, s'agrupen principalment en la transcitosi per adsorció (TAT, penetratina) i difusió passiva (*N*MePhe i dicetopiperazines).

El fet que dues llançadores hagin arribat a fases clíniques en els darrers anys, l'Angiopep-2 i el glutatió, indiquen que aquesta estratègia és prometedora. Tanmateix, l'eficiència de transport i la selectivitat són punts a millorar. Per incrementar la primera, el nostre laboratori, entre d'altres, ha demostrat que un camí és augmentar la resistència a proteases. Pel que fa a la selectivitat pel cervell, es pot incrementar buscant noves seqüències capaces d'interaccionar amb receptors coneguts o encara per descobrir mitjançant tècniques com el *phage display* o en productes naturals. Una de les fonts naturals més riques en molècules que afecten el sistema nerviós central són els verins. A més, aquests contenen una gran varietat de pèptids molts dels quals són resistents a proteases. L'objectiu principal d'aquesta tesi era desenvolupar una nova llançadora a partir d'un pèptid que tingués aquesta resistència intrínseca i fos capaç de transportar molècules grans com proteïnes i nanopartícules.

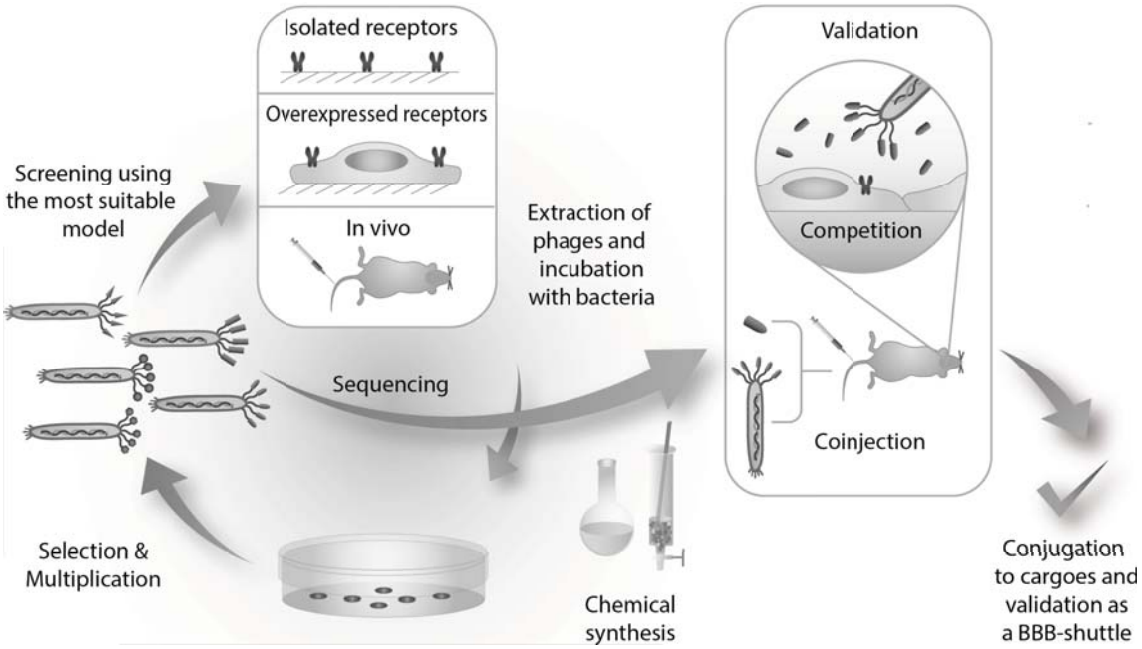

Figura iii. *Tècnica de phage display aplicada al descobriment de noves llançadores. (Disseny: Benjamí Oller-Salvia. Realització: Iris Joval)*

Fins ara, la major part d'estudis s'han centrat principalment en el transport de nanopartícules carregades amb molècules petites i material genètic. Tanmateix, hi ha una necessitat creixent de millorar la permeabilitat de proteïnes com els anticossos pel tractament de tumors cerebrals; adreçar aquest repte és el segon objectiu d'aquesta tesi.

Capítol 1. Mini-apamines com a noves llançadores per creuar la BHE

L'apamina és una toxina del verí de l'abella que actua bloquejant certs canals de potassi mediats per calci en el sistema nerviós central. Tot i que no se'n coneixia l'estabilitat a proteases, aquest pèptid presentava una estructura bicíclica molt ben definida gràcies a dos ponts disulfur que unien una α-hèlix amb un gir β. Aquesta estructura compacta apuntava a una elevada resistència a la proteòlisi. A més, es coneixia que els residus implicats en la toxicitat eren dues arginines i una glutamina situats cap a l'extrem *C*-terminal.

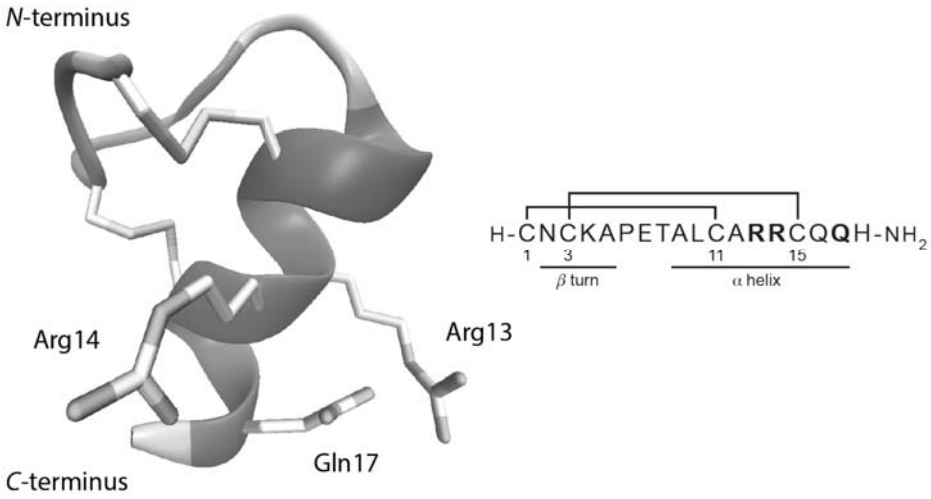

Figura iv. *Representació de l'apamina, enfatitzatn els residus Arg13, Arg14 i Gln17, i la seva seqüència. Aquest model es basa en les coordenades del PDB amb ID: 3IUX corresponent a un anàleg estrucutral de l'apamina.*

Per tal d'estudiar-ne el transport, primerament es va sintetitzar el pèptid emprant química Fmoc/*t*Bu seguida de ciclació en solució. Es va corroborar que el regioisòmer format tenia l'estructura globular desitjada mitjançant RMN i per coelució amb un patró del pèptid natural. Seguidament es va sintetitzar un anàleg prèviament descrit en el qual s'havien intercanviat les arginines per ornitines provocant una disminució dràstica de la toxicitat (ApOO). Per tal d'assegurar la connectivitat del ponts disulfur, aquest anàleg el vam sintetitzar amb dues cisteïnes protegides amb el grup acetamidometil i el vam ciclar en dos passos.

Seguidament, amb l'objectiu d'esbrinar si la manca de toxicitat provenia d'una menor afinitat pel canal de potassi o un menor transport a través de la BHE, vam assajar l'apamina i l'ApOO en un model cel·lular de BHE. Aquest model consistia en una monocapa de cèl·lules endotelials sembrades sobre un filtre tipus Transwell®, polaritzades i amb una permeabilitat paracel·lular reduïda gràcies a l'ús de medi condicionat per astròcits. L'assaig de transport en aquest model va revelar que la permeabilitat dels dos pèptids era pràcticament idèntica, indicant que els residus implicats en la toxicitat no eren necessaris pel transport. A més, la permeabilitat

d'aquests pèptids era semblant a d'altres llançadores que s'havien emprat per transportar diversos compostos i, fins i tot, nanopartícules. El balanç de matèria va mostrar que pràcticament no quedaven retinguts a les cèl·lules o als filtres i tampoc es degradaven durant l'assaig. D'altra banda, el fet de no arribar a detectar la permeabilitat de l'apamina i l'ApOO en un model de difusió passiva, indicava que el principal mecanisme de transport era actiu. A més, el reduït transport en un model de Caco-2, apuntava al fet que el mecanisme podia ser selectiu per certs tipus de cèl·lules; aquesta observació era consistent amb l'existència d'un receptor com s'havia suggerit en un estudi previ de la internalització d'apamina en cèl·lules hepàtiques.

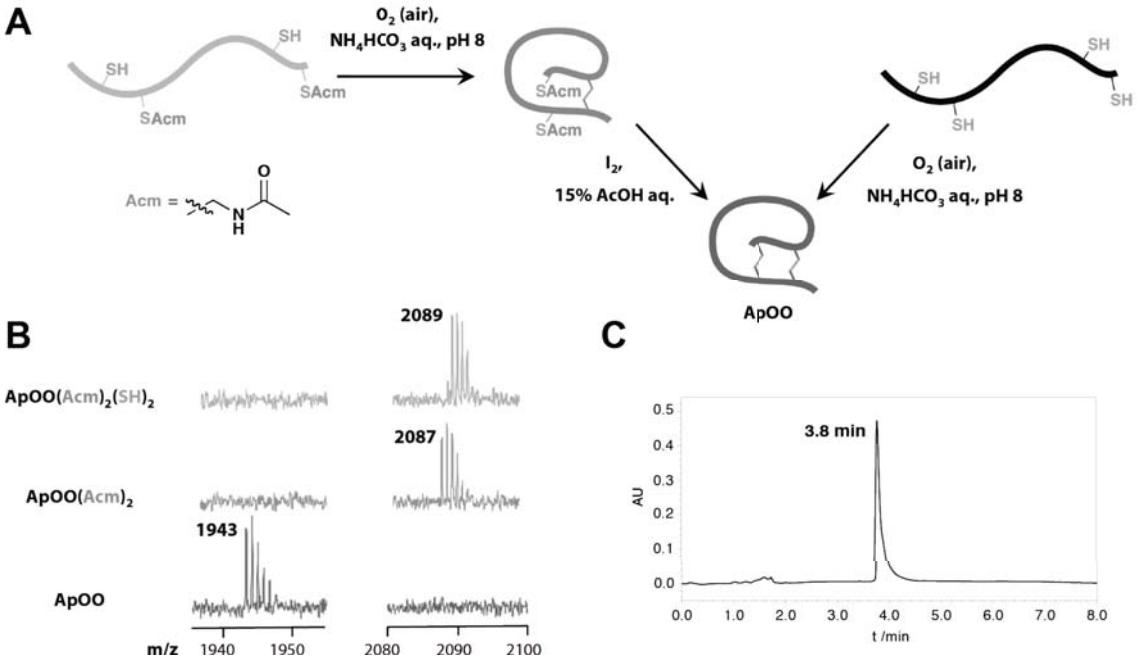

Figura v. *Síntesi de ApOO A) Esquema de la formació de disulfurs regioselectiva vs ciclació simultània en solució. B) Monitorització mitjançant espectrometeria de masses de MALDI-TOF. C) Coelució dels pèptids sintetitzats mitjançant les dues síntesis. El cromatograma es va obtenir en un gradient lineal de 8 min de 5 a 20 % d'acetonitrol amb (0.036 % TFA) en aigua (0.045 % TFA).*

Els dos pèptids estudiats van mostrar una resistència a les proteases del sèrum sorprenentment elevada fins i tot per seqüències riques en cisteïnes, amb un temps de semivida superior a 24 h. Aquesta característica, juntament amb la capacitat de creuar les cèl·lules endotelials mitjançant transport actiu, feien dels derivats no-tòxics d'apamina excel·lents candidats a llançadores.

Per tal d'obtenir derivats menys tòxics, menys immunogènics i més fàcils de sintetitzar, vam procedir a dissecar l'estructura de l'apamina per obtenir el que a partir d'ara anomenarem mini-apamines (MiniAps). Vam començar eliminant les glutamines, situades a fora de l'estructura bicíclica i bescanviant les arginines per alanines per tal de mantenir l'estructura de α-hèlix, donant lloc a la MiniAp-1. Sorprenentment, aquest anàleg va mostrar un transport 60 % superior a l'apamina.

El transport de la MiniAp-1 es devia, si més no en part, a un mecanisme actiu donat que s'inhibia parcialment amb azida sòdica i disminuint la temperatura. Com el pèptid natural, la MiniAp-1 tenia una permeabilitat indetectable en el model de difusió passiva PAMPA i en Caco-2, indicant que l'augment de transport no era atribuïble a la major hidrofobicitat. Així doncs, aquest augment es podria explicar pel fet que aquest anàleg no seria capaç d'interaccionar amb el canal de potassi, però sí amb el receptor que suposadament permet la seva transcitosi i, per tant, la concentració disponible per ser transportada seria major. A continuació, vam demostrar que la conjugació de diverses molècules als extrems *N*- o *C*-terminals d'aquest pèptid no afectaven el seu transport.

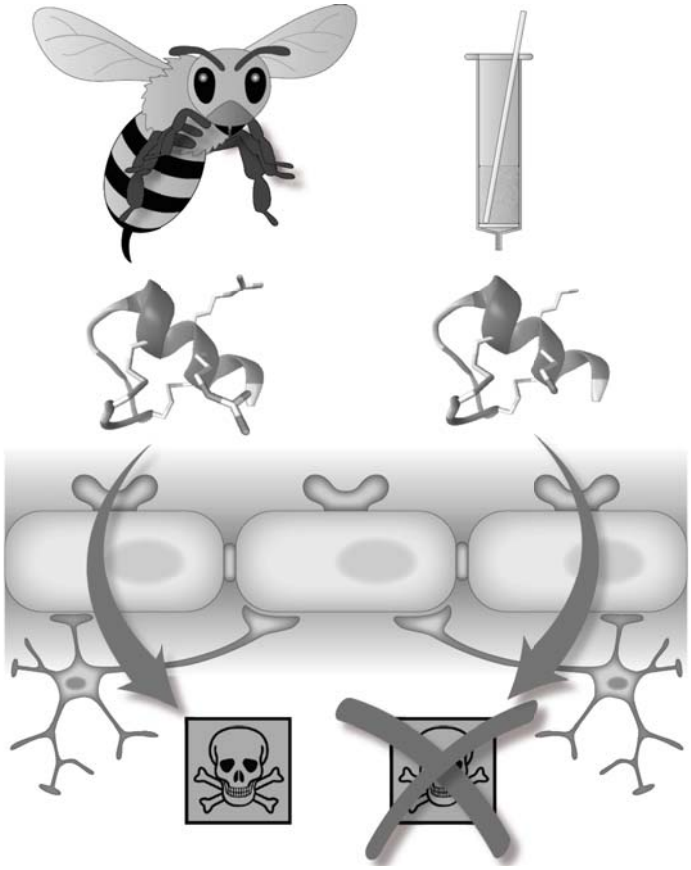

Figura vi. *La disminució de la toxicitat en l'apamina no ve donada per un menor transport a través de la BHE (Imatge seleccionada com a portada de la revista Biopolymers – Peptide Science.* ***2013****, 100)*

Per tal d'obtenir anàlegs més senzills, vam centrar-nos en la part de l'apamina més allunyada dels residus implicats en la toxicitat. Vam sintetitzar una versió lineal (MiniAp-2) i dues tancant artificialment el gir entre els residus 3 i 11 mitjançant un pont disulfur (MiniAp-3) o un enllaç amida (MiniAp-4).

La versió lineal tenia una permeabilitat semblant a l'apamina, mentre que l'anàleg ciclat mitjançant ponts disulfur mostrava el mateix transport que MiniAp-1. Sorprenentment, el derivat lactama, MiniAp-4, tenia una permeabilitat 3 vegades més elevada que l'apamina. Per tal de tractar d'explicar les diferències en

permeabilitat vam dur a terme un estudi conformacional mitjançant RMN i dicroisme circular i també vam estudiar l'estabilitat d'aquests pèptids en front de proteases del sèrum.

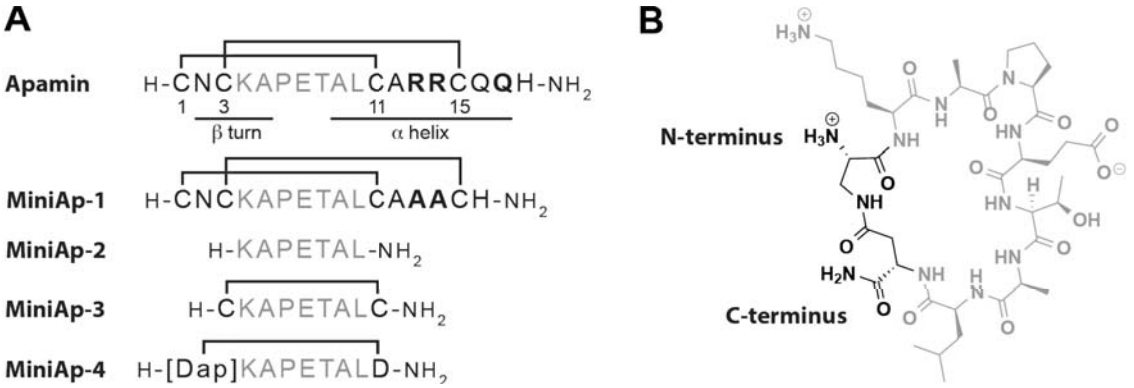

Figura vii. *Comparació de les mini-apamines candidates a llançadora. A) Seqüències de les mini-apamines. B) Estructura molecular de MiniAp.4.*

L'estudi estructural va confirmar que MiniAp-1 tenia una disposició molt semblant a l'apamina. També va revelar que els anàlegs monocíclics tenien una proporció *cis*/*trans* del rotàmer de l'enllaç Ala^{5}-Pro^{6} 1:1, mentre que en la mini-apamina bicíclica (MiniAp-1) i en la lineal (MiniAp-2) la proporció era 1:9. Aquesta observació podria estar relacionada amb una certa preorganització necessària per interaccionar amb el suposat transportador d'apamina.

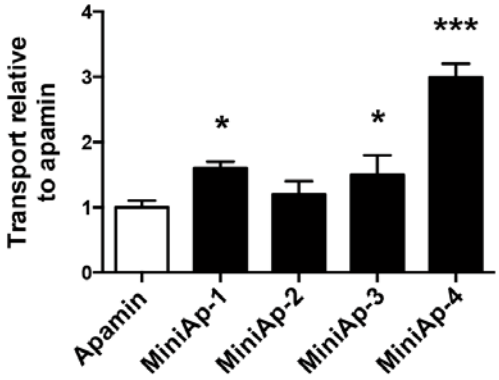

Figura viii. *Transport de les mini-apamines en el model cel·lular boví de BHE relatiu a l'apamina. Les dades representen la mitja ± desviació estàndard (n = 3). * P < 0.05, ***P < 0.001 (t-test).*

La diferència entre la permeabilitat dels dos anàlegs monocíclics, es podria explicar per la gran estabilitat de l'anàleg lactama respecte el disulfur envers les proteases. El temps de semivida de la MiniAp-4 era superior a les 24 h, comparable a la dels derivats bicíclics, mentre que per la mini-apamina amb el pont disulfur (MiniAp-3) només era de 2.8 h. El que també vam poder concloure és que la resistència provenia de la ciclació donat que el temps de semivida del derivat lineal era inferior a 10 min.

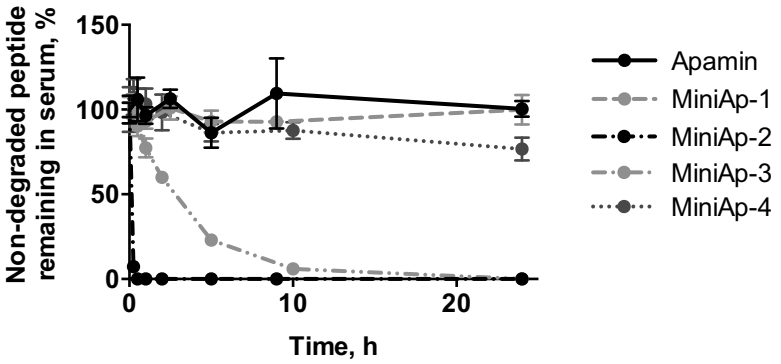

Figura ix. *Estabilitat dels pèptids en sèrum humà a 37 ºC. Les dades representen la mitja ± desviació estàndard (n = 3).*

Els dos anàlegs més prometedors en termes de permeabilitat i estabilitat en sèrum, MiniAp-1 i MiniAp-4, no van mostrar toxicitat aguda en ratolins a una dosi 20 vegades superior al LD50 de l'apamina. Com que també s'havia descrit que aquesta toxina era altament immunogènica, es van testar aquests candidats en un assaig d'immunogenicitat de 12 setmanes. Tot i que MiniAp-1 va generar una quantitat d'anticossos 6 vegades inferior que apamina, va seguir mostrant una virulència important. En canvi, MiniAp-4 pràcticament no va generar resposta immunitària. Així, doncs aquest darrer pèptid es va considerar com a llançadora cap de sèrie.

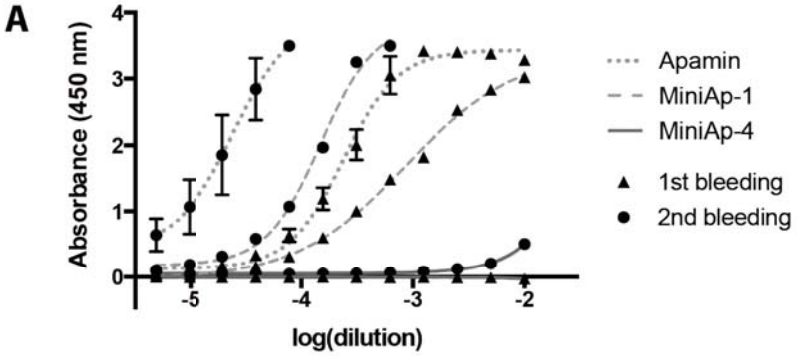

B

	Apamin	MiniAp-1	MiniAp-4
1st bleeding	4200	1200	<< 100
2nd bleeding	41000	6700	< 100

Figura x. *Quantificacio dels anicossos després del 1r sagnat (4 dosis, triangles) i del 2n sagnat (7 dosis, punts). n = 4 per apamina i n = 2 per MiniAp-1. La variabilitat està les barres d'error representen la desviació estàndard. A) Absorbància obtinguda en el ELISA front al logaritme de la dilució del sèrum. Les dades representen la mitja ± desviació estàndard (n = 4 per apamina i MiniAp-4, n = 2 per MiniAp-1). B) Invers de la dilució del sèrum a la meitat de resposta del ELISA.*

Després de comprovar que el transport de MiniAp-4 no s'alterava dràsticament en conjugar-hi molècules petites com fluoresceïna o levodopa, vam conjugar aquest pèptid a compostos més grans. Tots es van assajar en un model cel·lular humà de

BHE per tal d'obtenir dades de permeabilitat més rellevants. En primer lloc vam posar a punt un mètode de modificació de quàntum dots estables en condicions fisiològiques. La unió la vam realitzar mitjançant química tiol-maleimida, d'una manera semblant a com vam modificar posteriorment GFP amb el mateix pèptid. També vam preparar nanopartícules d'or i les vam recobrir amb MiniAp-4 derivatitzada amb una cisteïna. Tots aquests conjugats van resultar significativament més permeables que les mateixes entitats sense modificar, fet que confirmava la capacitat de MiniAp-4 com a llançadora.

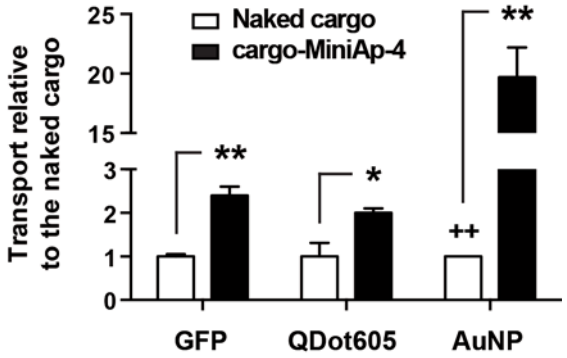

Figura xi. *Augment en el transport dels cargos en el model humà de BHE. ++ representa el límit de quantificació d'aquest analit per l'ICP-MS. Les dades representen la mitja ± error estàndard (n = 3). * P < 0.05, **P < 0.01 (t-test).*

Per tal d'explorar la capacitat de MiniAp-4 *in vivo*, es va conjugar primer a un pèptid que evita la formació de fibres β-amiloide dissenyat en una col·laboració entre el laboratori del Prof. Giralt i l'empresa Zyentia. Per tal d'estudiar l'acumulació dels pèptids en el cervell en temps real, es van conjugar a la cianina 5.5, la qual va permetre la seva visualització mitjançant fluorescència de l'animal complet. També es van emprar llançadores més establertes com el THR i el THRre com a control. El resultat d'aquest experiment mostrava que aquest pèptid ja presentava una acusada acumulació en el cervell per sí sol i que cap de les llançadores era capaç d'augmentar-la.

Així doncs, es va conjugar els mateixos pèptids a la cianina 5.5 sola com a compost a transportar. En aquest cas, el THR no va incrementar-ne el transport, però sí el THRre, confirmant la major capacitat de transport d'aquest pèptid resistent a proteases. Sorprenentment, l'augment de permeabilitat produït per MiniAp-4 va ser molt superior, fins a 7.6 vegades la del fluoròfor sol, analitzant el cervell després de perfusió i necròpsia. A més, la selectivat d'aquest pèptid pel cervell va resultar ser molt significativa respecte a d'altres òrgans. Finalment, es va verificar mitjançant microscòpia confocal i immunohistoquímica que part del conjugat cyanina5.5-MiniAp4 es trobava fora dels capil·lars, en el parènquima cerebral. La major part d'aquest compost que havia creuat la BHE semblava internalitzat en forma de vesícules o agregats en neurones.

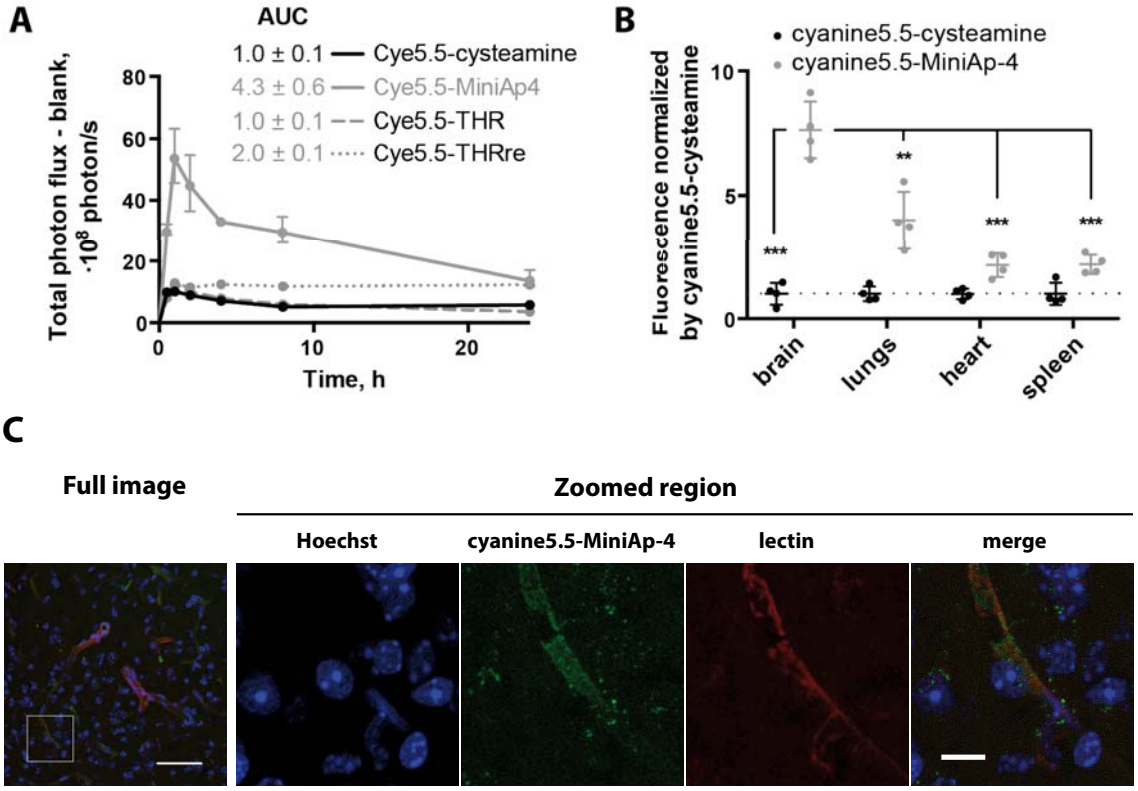

Figura xii. *Avaluació del conjugat de cianina5.5-MiniAp4 en ratolins. A) Fluorescència mesurada a l'àrea del cervell in vivo. B) Intensitat de fluorescènica relativa de diversos òrgans ex vivo, després de perfusió. C) Imatges representtaives de microscòpia confocal mostrant el conjugat dins del parènquima cerebral. Les dades representen la mitja ± error estàndard (n = 4). **P < 0.01, ***P < 0.001 (t-test).*

Capítol 2. Envers el transport d'anticossos a través de la BHE

Els anticossos monoclonals presenten una gran afinitat per les seves dianes terapèutiques o un llarg temps de semivida en sang i han trobat una gran aplicabilitat en el tractament de diversos tipus de càncer. Tanmateix, també presenten inconvenients com la seva complexa producció o la incapacitat de creuar barreres biològiques com la BHE. Tot i que el bevacizumab (Bv, Avastin®), un anticòs monoclonal contra el factor de creixement endotelial, està aprovat per tractar el càncer cerebral més maligne, el glioblastoma multiforme, la seva eficiència està en entredit i la mitjana de supervivència incloent el tractament és d'uns 15 mesos. Altres anticossos com el cetuximab (Cx, Erbitux®), el qual bloqueja el receptor del factor de creixement epidèrmic, han mostrat una gran eficiència *in vitro* i en estudis preclínics, però en fases clíniques no han demostrat ser més eficients que els tractaments vigents. Aquesta baixa eficiència s'atribueix principalment a la reduïda permeabilitat d'aquestes macromolècules a través de la BHE. Així doncs, vam proposar-nos conjugar diverses llançadores als dos anticossos més estudiats per tractar el glioblastoma per tal de tractar d'augmentar-ne el transport i l'eficiència. En aquesta línia, molt recentment s'ha demostrat que Angiopep-2 és capaç d'augmentar el transport al cervell de l'anticòs trastuzumab per tractar metàstasis al cervell de tumors que sobreexpressen HER2.

Vam posar a punt diversos mètodes de conjugació dels pèptids llançadora als anticossos per tal de seleccionar els més eficients i els que permetessin un major increment de transport basant-nos en els anomenats "conjugats anticòs-fàrmac". Cal destacar que aquests conjugats són conceptualment l'invers dels constructes anticòs-llançadora que tractem en aquesta tesi, doncs en els primers és l'anticòs el responsable de dirigir la toxina enllaçada i en el segon és el pèptid que fa de vector de l'anticòs. Aquest camp s'ha popularitzat durant els darrers 5-10 anys, oferint una gran varietat de tècniques de modificació. Tot i això, moltes d'elles es basen la introducció d'aminoàcids o seqüències durant la expressió i en aquest projecte no era possible fer-ne ús perquè volíem emprar anticossos comercials. D'altra banda, alguns mètodes de modificació enzimàtica s'han aplicat a aquest tipus de proteïnes molt recentment, de manera que no es van tenir en compte a l'hora de plantejar aquest projecte. Per tal de posar a punt les conjugacions es va fer servir l'anticòs del qual es disposava a l'inici, el Bv, tot i que més endavant es va emprar el Cx perquè la seva manca d'eficàcia és més clarament atribuïble a la presència de la BHE. Com a la llançadora, es va emprar la que estava més desenvolupada en el laboratori en començar aquesta tesi, el THRre.

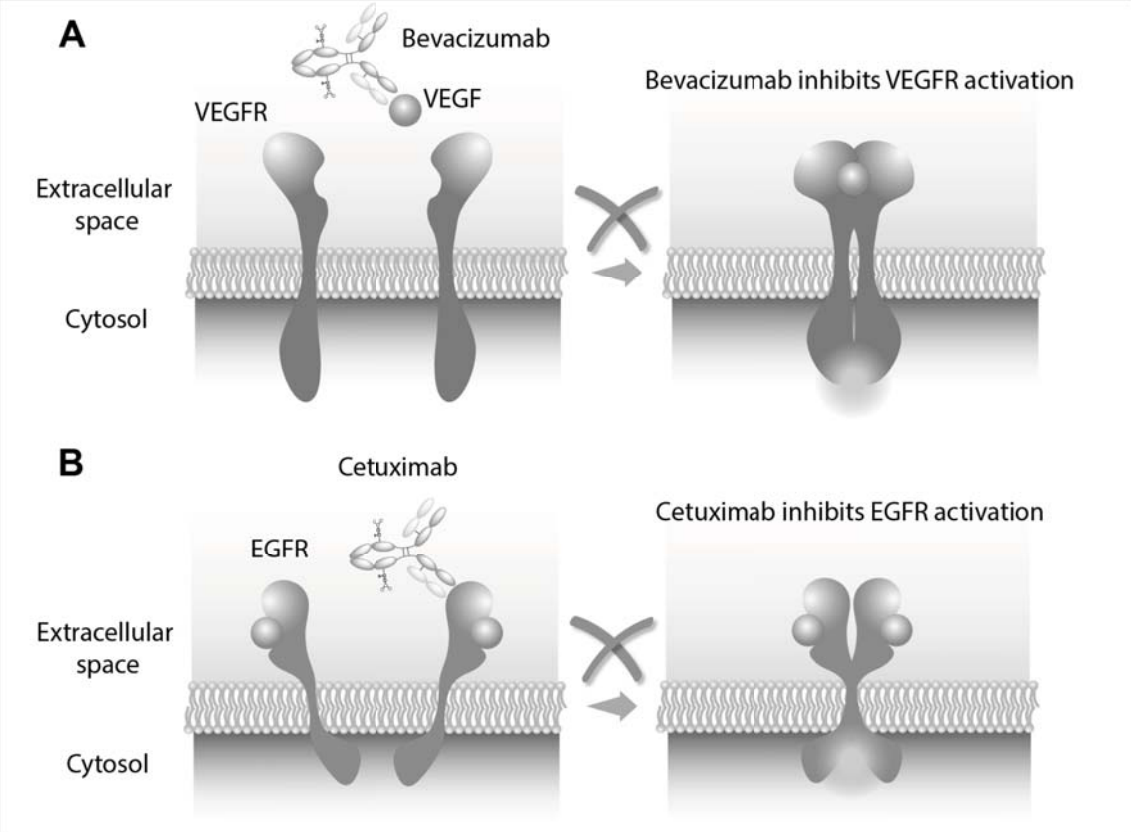

Figura xiii. *Representació del mode d'acció dels anticossos sel·leccionats A) Bv B) Cx*

Inicialment vam emprar la conjugació dels extrems *N*-terminals de l'anticòs donat que és una de les que permet major selectivitat sense necessitat de modificar-ne la seqüència. La reacció consisteix en la transaminació del darrer aminoàcid mitjançant fosfat de piridoxal, seguida de la conjugació del carboni generat amb un grup aminooxi incorporat a la llançadora. En primer lloc es va posar a punt la reacció amb la mioglobina perquè era més senzilla d'analitzar per espectrometria de masses. La reacció es va dur a terme primerament amb molècules petites que contenien grups hidrazina o aminooxi i després amb el THRre, determinant que l'ús d'anilina com a catalitzador en les condicions emprades era essencial. Posteriorment aquesta tècnica es va aplicar als anticossos, pels quals l'anàlisi per MALDI-TOF no oferia prou resolució i l'ús de l'electroforesi en gel i la cromatografia líquida acoblada a ionització per electrosprai en aparells d'alta resolució era necessària. També es va comprovar que per obtenir rendiments raonables amb els anticossos emprats es requeria temps de transaminació molt llargs (48 h).

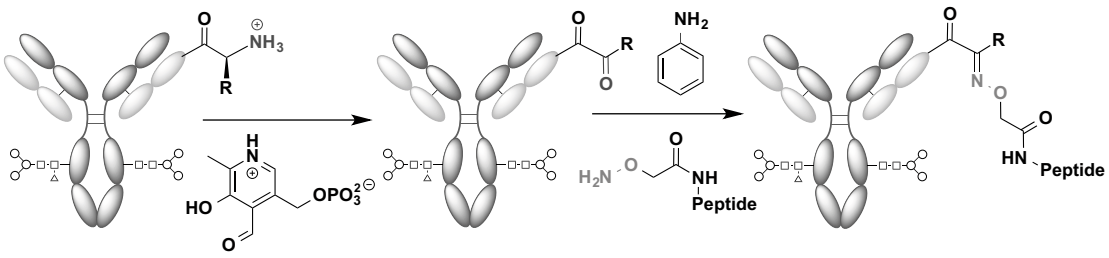

Figura xiv. *Modificació dels extrems N-terminals de l'anticòs transaminats.*

En el cas de Bv vam aconseguir conjugar vora una molècula de pèptid per anticòs, essent la glutamina al *N*-terminal de la cadena gran més reactiva que l'aspartat de la cadena petita. En pèptids està descrit que aquests dos residus tenen una reactivitat molt semblant, però estudiant l'estructura tridimensional de l'anticòs sembla que efectivament la glutamina està més exposada que l'aspartat. Tanmateix, en Cx, aquesta conjugació només va rendir 0.3 molècules de pèptid per anticòs donat que un dels extrems contenia una lisina, la qual forma un adducte estable amb el fosfat de piridoxal. Així doncs, aquesta reacció es va descartar per aquest anticòs és el que posteriorment s'estudiaria en els assajos de transport.

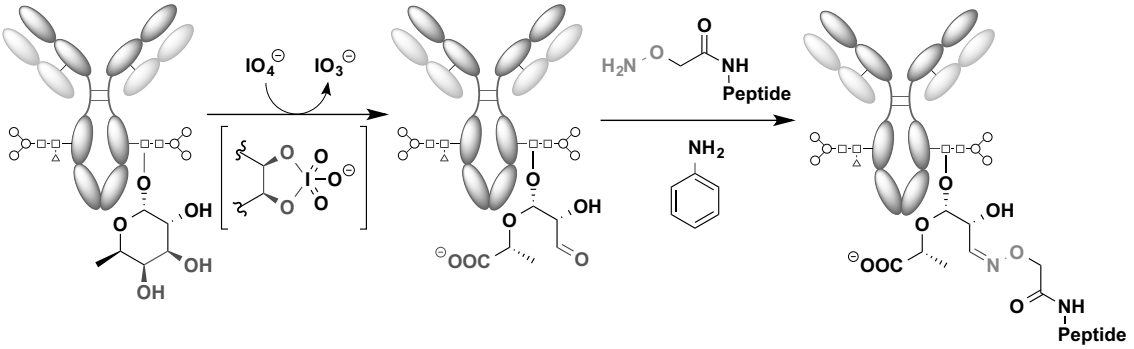

Figura xv. *Conjugació de l'anticòs mitjançant l'oxidació de les cadenes glicosídiques.*

A continuació vam posar a punt un mètode de modificació de les cadenes glicosídiques de Bv. Aquesta conjugació es basava en l'ús descrit d'una quantitat reduïda de periodat sòdic a baixa temperatura i tampó àcid per tal de modificar principalment la fucosa i introduir només 2 molècules de pèptid per anticòs. Tot i que aquesta reacció va funcionar amb Bv, no es va aplicar a Cx perquè el seu patró de glicosilació era força més complex. A més, en els darrers anys s'havia observat que la modificació de les cadenes glicosídiques generalment desencadenen respostes immunitàries citotòxiques.

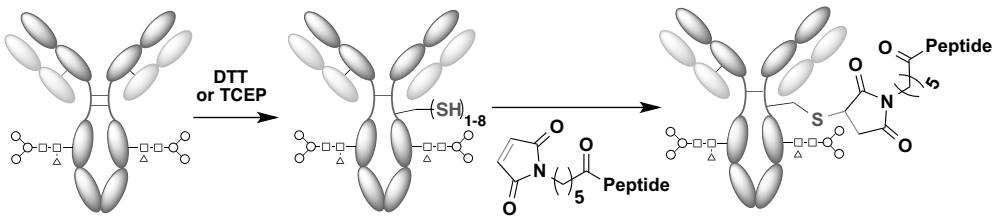

Figura xvi. *Conjugació de les cisteínes resultants de la reducció parcial de l'anticòs.*

Com que les conjugacions anteriors eren selectives però depenien de les característiques de cada anticòs, com a tercera opció es va optar per una tècnica d'aplicació més general: la reducció parcial dels ponts disulfur que uneixen les cadenes de l'anticòs. Aquest mètode és un dels més emprats en la producció de conjugats anticòs-fàrmac i és el que s'aplica per generar un dels dos conjugats comercials (Adcetris®). Després d'emprar diverses proporcions de DTT i TCEP, a les nostres mans, 3 equivalents de DTT donaven lloc a la formació de 3.5-4 tiols lliures

en Cx d'una manera molt reproduïble. Aquest nombre està considerat l'òptim per diversos conjugats d'anticossos per tal de minimitzar l'impacte de la molècula conjugada en les propietats farmacocinètiques de la immunoglobulina. Emprant aquesta tècnica es va conjugar 7 llançadores o derivats a Cx i es van caracteritzar mitjançant electroforesi en gel i espectrometria de masses. En la majoria de conjugats es va detectar la cadena petita modificada amb un pèptid i la meitat de l'anticòs modificada amb dos.

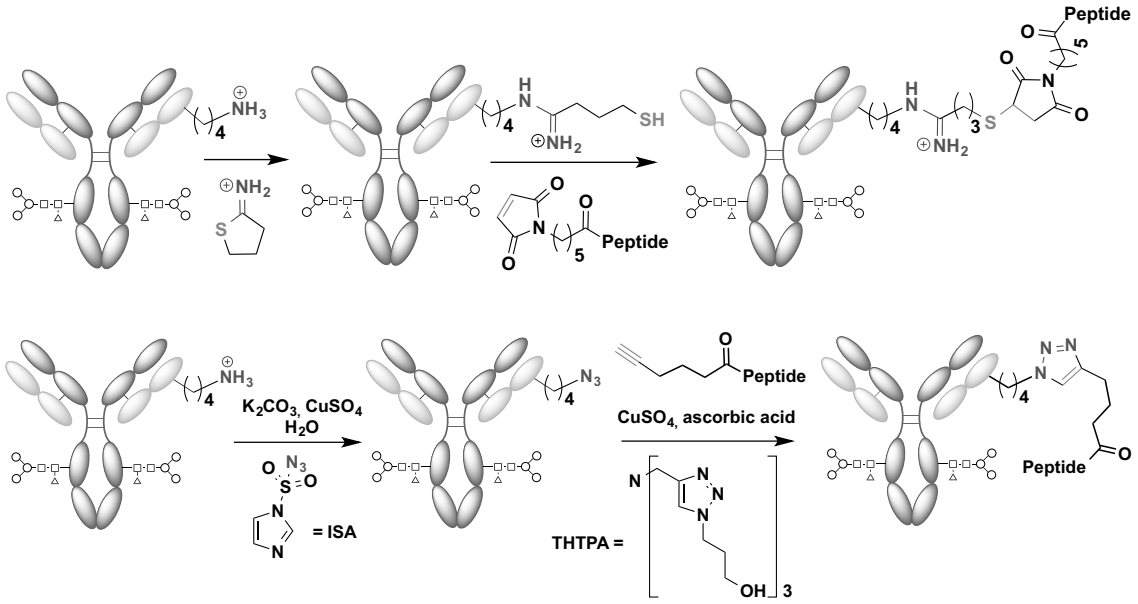

Figura xvii. *Conjugació de les llançadores peptídiques a les lisines de l'anticòs derivatitzant-lo amb 2-iminotiolà (a dalt) o amb azida (a baix).*

Per tal d'emprar la menor quantitat possible de pèptid, es va derivatitzar l'anticòs amb 2-iminotiolà generant tiols o bé amb imidazol-1-sulfonil azida per derivatitzar amb una azides. Amb el primer mètode es va enllaçar el THRre que contenia un grup maleimido i amb el segon es van conjugar el RVG i la MiniAp-1. En les modificacions de les lisines, el nombre de pèptids inserits va ser difícil de determinar amb exactitud perquè la gran diversitat d'espècies feia que no es poguessin distingir bé per electroforesi, sobretot en el cas de la cadena gran. Tanmateix, es va estimar que la proporció pèptid/anticòs oscil·lava entre 4 i 8.

Taula 1. *Resum de les conjugacions posades a punt amb THRre i Angiopep-2.*

		THRre		**Angiopep-2**	
Conjugation site	**Abbreviation**	**Bv**	**Cx**	**Bv**	**Cx**
N-termini	(Nterm)	1	0.3	-	-
Glycan	(Glyc)	2	-	2	-
Int. cysteines	(Cys)	4	4	4	4
Lysines	(Lys)	4-7	4-7	6-8	6-8

Tot i que l'enllaç tioèter entre un tiol i una maleimida és molt estable *in vitro*, científics de Genentech han demostrat que *in vivo* el tiol es pot intercanviar en certes condicions. L'albúmina, la cisteïna lliure o el glutatió presents a la sang poden desplaçar la molècula enllaçada a la maleimida en menys de 24 h si aquesta està molt exposada i no s'hidrolitza formant l'àcid. És per això que vam comprovar l'estabilitat d'aquest enllaç en els conjugats amb els pèptids llançadora. Vam conjugar pèptids amb carboxifluoresceina a les lisines o les cisteïnes dels anticossos i en vam seguir l'estabilitat mitjançant gels d'electroforesi. La intensitat de la fluorescència dels conjugats es va mantenir gairebé estable durant tot el temps de l'assaig, especialment en el cas de la modificació de les cisteïnes.

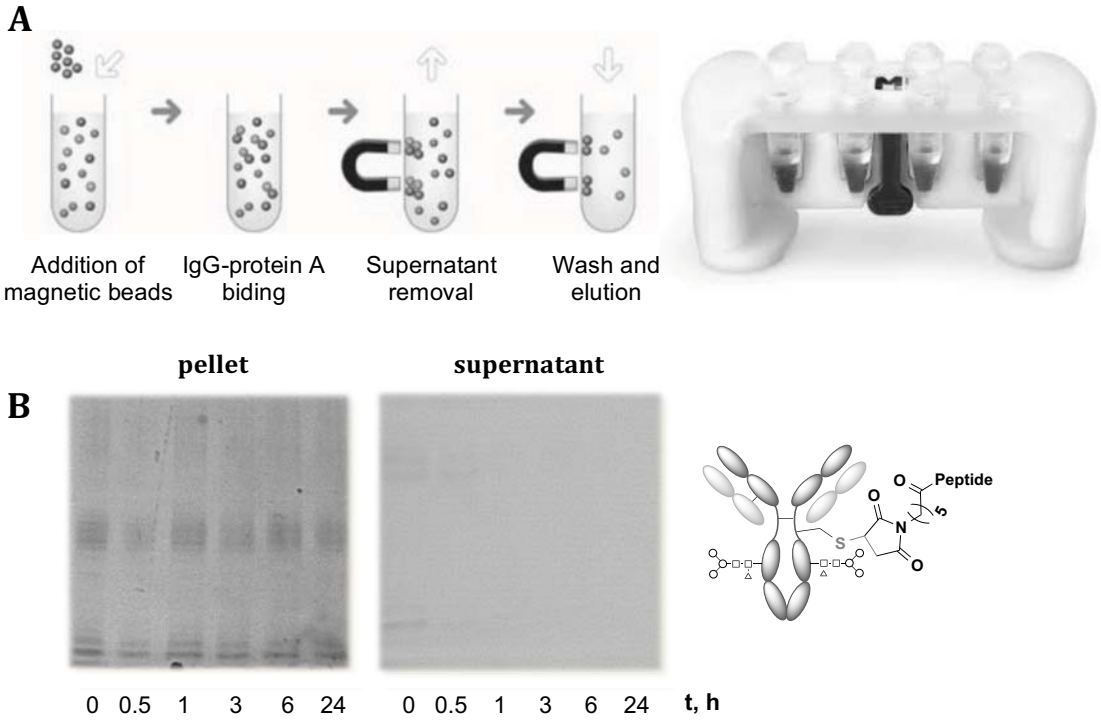

***Figura xviii**. Monitorització de l'estabilitat en sèrum de l'enllaç tioèter format entre les cisteïnes resultants de la reducció parcial de l'anticòs i la maleimida incorporada als pèptids llançadora. A) Esquema del procés de purificació. B) Gel d'electroforesi (fluorescènica) en el precipitat (t_0-t_{24h}) i en el sobrenedant (s_0-s_{24h}) del Cx modificat a través de les cisteïnes.*

A continuació vam estudiar quin era l'impacte de la conjugació dels pèptids llançadora en l'afinitat dels anticossos, tan per impediment estèric com per alteració de l'estructura de l'anticòs durant la conjugació. En el cas de Bv es va estimar l'afinitat relativa mitjançant un assaig tipus ELISA i en el de Cx l'estudi es va realitzar amb un assaig cel·lular funcional donat que no es va poder establir un ELISA prou assequible. L'assaig funcional consistia en mesurar la inhibició de la fosforilació del receptor del factor de creixement epidèrmic. En cap cas es va veure una disminució dràstica de l'afinitat, tot i que pel Bv la modificació del *N*-terminal semblava afectar en una major proporció que la resta, disminuint l'afinitat global entre un 20 i un 30%.

Finalment, es van assajar els conjugats en el model cel·lular boví de BHE. Inicialment es va emprar una concentració semblant a la que es troba a la sang quan s'administren dosis terapèutiques d'anticòs. Tanmateix, en aquestes condicions es va obtenir una gran variabilitat i un increment molt modest de la permeabilitat en els conjugats només en el cas d'Angiopep-2 via cadenes glicosídiques i lisines. Aquest reduït increment mesurat podria indicar que les llançadores no eren prou efectives, que el nombre no era suficient o que els mètodes de conjugació no eren adients. Tanmateix, també es podria explicar per un reconeixement inferior dels conjugats amb més pèptids a l'assaig ELISA com s'ha descrit recentment. Una altra hipòtesi seria la saturació dels receptors per l'excés de conjugat.

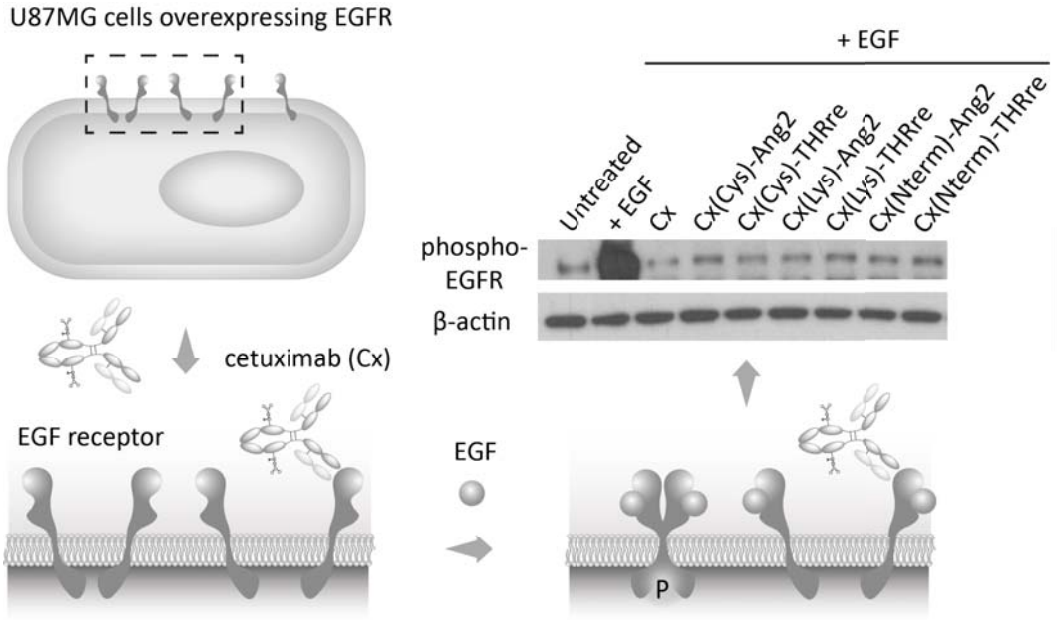

Figura xix. *Assaig funcional per avaluar la capacitat d'inhibició del Cx i Western blot mostrant la fosforilació del receptor del factor de creixement epidèrmic amb els conjugats Cx-llanádora. La β-actina es mostra com a control de la càrrega de proteïna.*

Tenint en compte la hipòtesi de la saturació i també per canviar el mètode de detecció, vam optar per disminuir la concentració dels conjugats i marcar-los amb el radioisòtop ^{125}I. En aquestes condicions, vam obtenir un increment significatiu i reproduïble dels conjugats amb THRre. A més, el valor de permeabilitat de l'anticòs sol era comparable al que havien obtingut els nostres col·laboradors que havien posat a punt el model. Realitzant el marcatge amb iode no radioactiu i també mesurant les fraccions eluïdes de les columnes de purificació vam comprovar que l'augment de permeabilitat que no provingués del iode romanent de la reacció o de la tirosina marcada (emprada per capturar les restes de iode).

Amb aquest experiment vam demostrar que les llançadores podien augmentar la permeabilitat de l'anticòs monoclonal Cx en el model cel·lular humà de BHE. Principalment vam assajar conjugats enllaçats a través de les cisteïnes, però també

vam incloure constructes modificats a través de les lisines mitjançant cicloaddició alquí-azida catalitzada per coure CuAAC en el cas dels pèptids que contenien cisteïnes i no era convenient sintetitzar-los amb un grup maleimida. Tot i que els pèptids emprats en tots dos mètodes de conjugació no eren idèntics, es va observar que els pèptids modificats via lisina-alquí tenien una permeabilitat superior als modificats via tioèter-cisteïna. Aquesta diferència es podria atribuir a la major accessibilitat de les llançadores conjugades a les lisines perquè estan més exposades. Tanmateix, sols la posició del pèptid no podia explicar l'augment de permeabilitat, doncs el THRre enllaçat via lisines mitjançant derivatització amb 2-iminotiolà era menys eficient que el mateix pèptid conjugat a les cisteïnes. Així doncs, semblava que l'espaiador amb el triazol podria tenir un rol important en la orientació del pèptid. Una altra possibilitat seria que les traces de coure romanents de la reacció afectessin el transport, però la integritat de la monocapa no s'havia vista afectada segons el patró intern (*Lucifer yellow*). Una explicació alternativa seria que l'excés de transferència d'azida augmentés la hidrofobicitat dels anticossos i n'afectés el transport. En qualsevol cas, per aclarir la contribució del tipus de conjugació, els mateixos pèptids es conjugaran mitjançant els diversos mètodes. També es prepararà un conjugat control amb només 3-azidopropanamina per estudiar l'efecte de l'enllaç d'una molècula petita mitjançant aquest mètode que no hauria de fer de llançadora.

L'assaig de transport va revelar que les dues mini-apamins assajades (MiniAp-1 i MiniAp-4) eren capaces d'augmentar la permeabilitat dels anticossos. Tanmateix, l'increment observat no seguia la mateixa tendència observada pels pèptids sols. MiniAp-1 unida a través de lisines mitjançant CuAAC va incrementar la permeabilitat de Cx unes 7 vegades, mentre que per MiniAp-4 l'augment va ser de 1.7 vegades. Per tal de confirmar si aquesta diferència es deu a l'espaiador, hem preparat la MiniAp-4 unida també mitjançant CuAAC a les lisines per assajar-la en el model cel·lular de BHE.

També vam observar que el THRre augmentava el transport de Cx unes 3 vegades. Aquest increment era significativament superior que el que proporcionava un pèptid que contenia els mateixos aminoàcids però ordenats aleatòriament (THRre(scram)), el qual havia estat descrit anteriorment que no interaccionava amb el receptor de transferrina. Tot i això aquest pèptid desordenat també va ser capaç d'augmentar el transport Cx, indicant que la transcitosi del THRre no és només mitjançant receptor, sinó segurament també adsorció. Potser en part per aquesta raó, la incorporació d'un espaiador de polietilenglicol per millorar l'accessibilitat del THRre no va donar lloc a un increment de transport addicional.

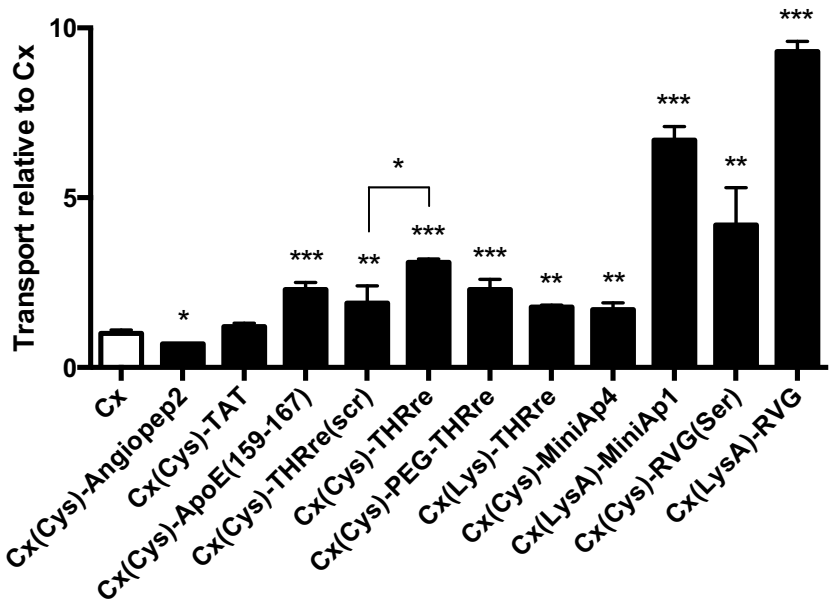

Figura xx. *Permeabilitat dels conjugats llançadora-Cx en el model humà de BHE. * = enllaç realitzat mitjançant CuAAC. Les dades representen la mitja ± error estàndard. * P < 0.05, **P < 0.01, ***P < 0.001 (t-test).*

RVG29 unit a les lisines de l'anticòs va proporcionar el major augment de permeabilitat, seguit del mateix pèptid modificat per poder-lo a enllaçar a les cisteïnes mitjançant química tiol-maleimida. Una altra llançadora de referència, el pèptid ApoE(159-167)$_2$, també va incrementar significativament el transport de Cx. Aquest pèptid està descrit que interacciona amb el receptor de proteïnes de baixa densitat. Tanmateix, en un assaig d'internalització-alliberament emprant el model cel·lular de BHE, es va comprovar que aquesta llançadora, que té una gran càrrega positiva, queda retinguda en gran mesura dins les cèl·lules endotelials. Aquest fet indicava que segurament en la transcitosi també hi intervé un mecanisme d'adsorció.

En canvi, el TAT no va augmentar la permeabilitat de Cx. Segurament la seva naturalesa catiònica afavoreix principalment l'endocitosi però no la transcitosi. El conjugat d'Angiopep-2 tampoc va augmentar el transport de Cx. Assajant aquest pèptid llançadora sense conjugar vam observar que es degradava durant l'assaig en el model cel·lular humà de BHE. Així doncs, segurament el residu a través del quals s'uneix aquesta llançadora a l'anticòs és cabdal per evitar la degradació. Aquest punt no està especificat en la recent publicació del conjugat d'Angiopep-2 i trastuzumab. Tot i això, la incapacitat d'aquest pèptid per augmentar la permeabilitat de Cx també podria atribuir-se a la diferent naturalesa dels dos anticossos.

Conclusions

Les conclusions respecte al primer objectiu, trobar noves llançadores per la BHE resistents a proteases, són les següents:

1. L'apamina, un pèptid del verí de l'abella, i anàlegs menys tòxics poden creuar una monocapa de cèl·lules endotelials a través d'un mecanisme actiu amb una permeabilitat semblant. Així doncs, els residus implicats en la toxicitat no són necessaris pel transport a través de la BHE, fent dels derivats d'apamina sense aquests residus candidats a llançadores més segurs.
2. El pèptid original i els seus derivats bicíclics tenen una elevada resistència a les proteases del sèrum, la qual es preserva parcialment en els anàlegs monocíclics i es perd completament a la versió lineal. L'enllaç amida emprat per ciclar MiniAp-4 és clau per a la seva elevada resistència a proteases, amb un temps de semivida de més de 24 h, i també per al seu elevat transport, 3 vegades el de l'apamina.
3. S'ha confirmat que l'apamina és altament immunogènica. L'eliminació de les arginines i les glutamines a MiniAp-1 va comportar una disminució de la immunogenicitat, mentre que la supressió completa de l'estructura helicoïdal en MiniAp-4 va donar lloc a una llançadora que pràcticament no desencadena resposta immunitària, generant 400 vegades menys d'anticossos que apamina. A més, cap dels dos derivats va mostrar símptomes d'enverinament a una dosi 24 vegades superior al LD50 del pèptid original (1.2 μmol/kg).
4. MiniAp-4 incrementa significativament el transport de la proteïna verda fluorescent, quàntum dots u nanopartícules d'or en un model humà de BHE, demostrant així *in vitro* la seva vàlua com a llançadora.
5. MiniAp-4 incrementa la concentració en cervell de la cianina-5.5, amb un pic d'acumulació després d'una hora, mostrant un increment de 8 vegades respecte el mateix fluoròfor conjugat a cisteamina després de perfusió. A més, aquesta llançadora mostra una selectivitat remarcable pel cervell perquè l'augment en altres òrgans és de 2 a 4 vegades. Igualment remarcable és el fet que aquest constructe es detecti més enllà de l'endoteli, majoritàriament en neurones, mitjançant microscòpia de fluorescència, demostrant la seva capacitat de creuar la BHE.

Les conclusions respecte al segon objectiu, augmentar el transport d'anticossos a través de la BHE, són les següents:

1. S'han posat a punt quatre tècniques de conjugació per enllaçar les llançadores anticossos per tractar el glioblastoma emprant THRre i Bevacizumab. Tanmateix, per cetuximab, la modificació dels *N*-terminals té molt baixa eficiència i el complex patró de glicosilació d'aquest anticòs fa que la conjugació a les cadenes

glicosídiques no sigui pràctica. La modificació de les lisines i les cisteïnes s'han aplicat amb èxit a ambdós anticossos. Tanmateix, la darrera genera espècies més definides que la primera, fent-la més adient per generar diversos conjugats de cetuximab amb diverses llançadores.

2. L'enllaç tioèter format mitjançant la unió tiol-maleimida entre el THRre i l'Angiopep-2 i les cisteïnes del cetuximab es estable durant més de 24 h en sèrum humà.

3. Els únics conjugats de Bevacizumab que va mostrar una afinitat significativament inferior pel factor de creixement endotelial vascular respecte l'anticòs sense modificar van ser els que contenien llançadores als extrems *N*-terminals. Pel que fa els conjugats de cetuximab, tots van inhibir la fosforilació del receptor del factor de creixement epidèrmic en cèl·lules que sobreexpressàven aquest receptor i que van ser estimulades amb el factor de creixement enpidèrmic.

4. Els conjugats de cetuximab MiniAp-1, MiniAp-4, THRre, ApoE, RVG(Ser) i RVG tenen una permeabilitat significativament més elevada que l'anticòs sense modificar en un model cel·lular humà de BHE. Per contra, Angiopep-2 i TAT no n'augmenten el transport en les condicions assajades. Els conjugats amb llançadores enllaçades a les lisines mitjançant cicloaddició alquí-azida catalitzada per coure són més permeables que els modificats a través de les cisteïnes. Tot i que aquesta observació es podria explicar per una major accessibilitat de les llançadores per poder interaccionar amb el seu receptor, més experiments serien necessaris per aclarir aquest punt.

APPENDIX

- Study of cell uptake and receptor binding of BBB-shuttle peptides.

This work was performed in my research stage at Prof. Kai Johnsson's laboratory at EPFL (Lausanne, Switzerland), from the 5th January to the 5th April 2015, with the financial support of a Boehringer Ingelheim Fonds travel grant.

Objective of the research stage

The central goal of this stage was to study the binding and internalization of three BBB-shuttle peptides expected to interact with membrane receptors, exploiting mainly the fluorogenicity of silicon rhodamine (SiR) and also using superresolution microscopy.[1]

The BBB-shuttle peptides of study were THR and THRre, which have been described to interact with TfR, and MiniAp-4, which is internalized by an active mechanism, probably receptor-mediated.

Because the only STED depletion beam available at EPFL is adapted for fluorophores emitting in the green part of the spectrum, we also prepared conjugates with rhodamine 110 (Rho110) and Abberior STAR 440SXP (Abberior 440).

[1] In my stage at EPFL I also worked on the synthesis of a new fluorophore based on SiR. However, only the work related to the peptides used in the thesis has been included in this appendix.

Peptide conjugates

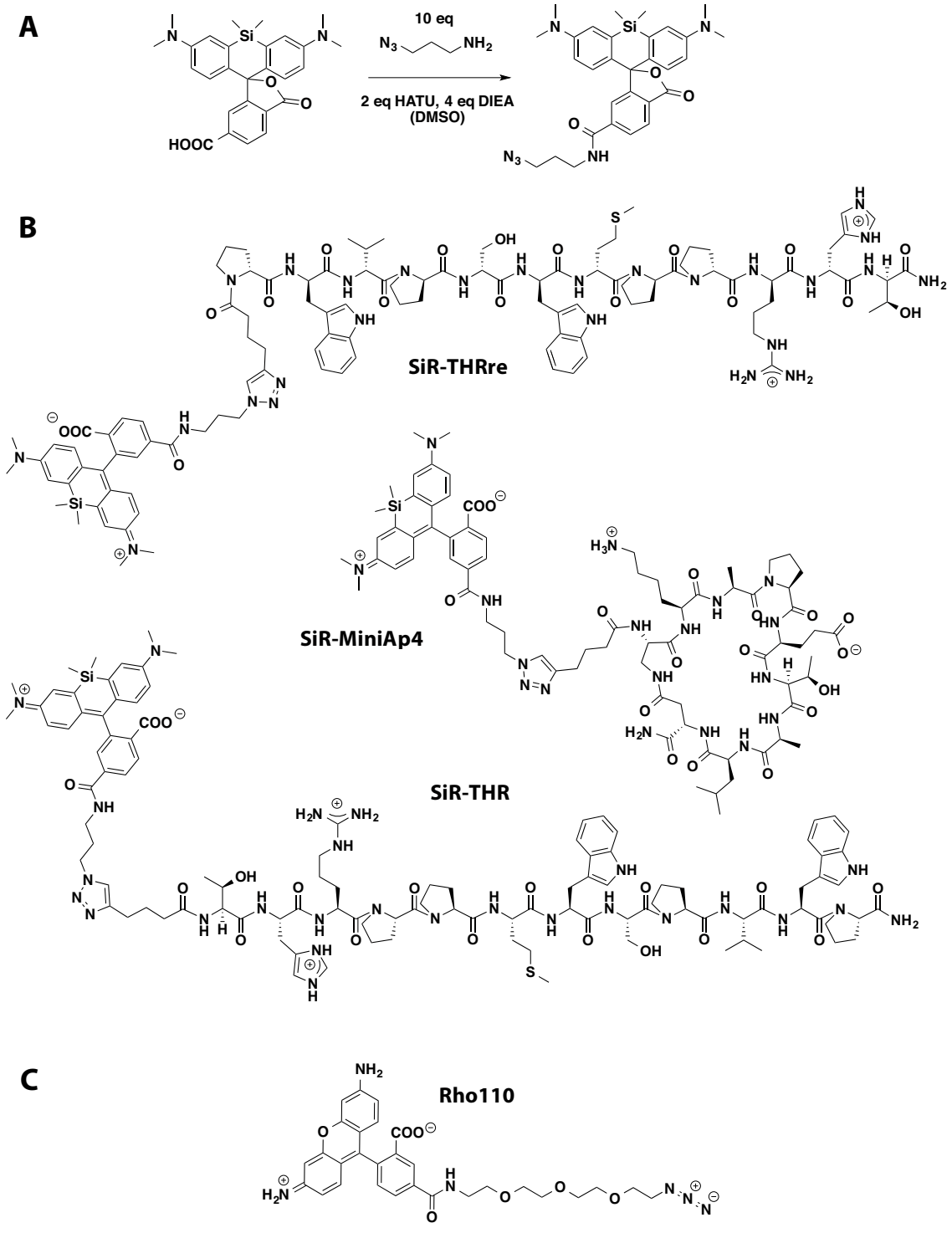

Figure I. *SiR-labeled peptides. A) Modification of SiR with a bifunctional linker containing an azide. B) Structures of the peptides. C) Structure of Rho110 with the PEG spacer used.*

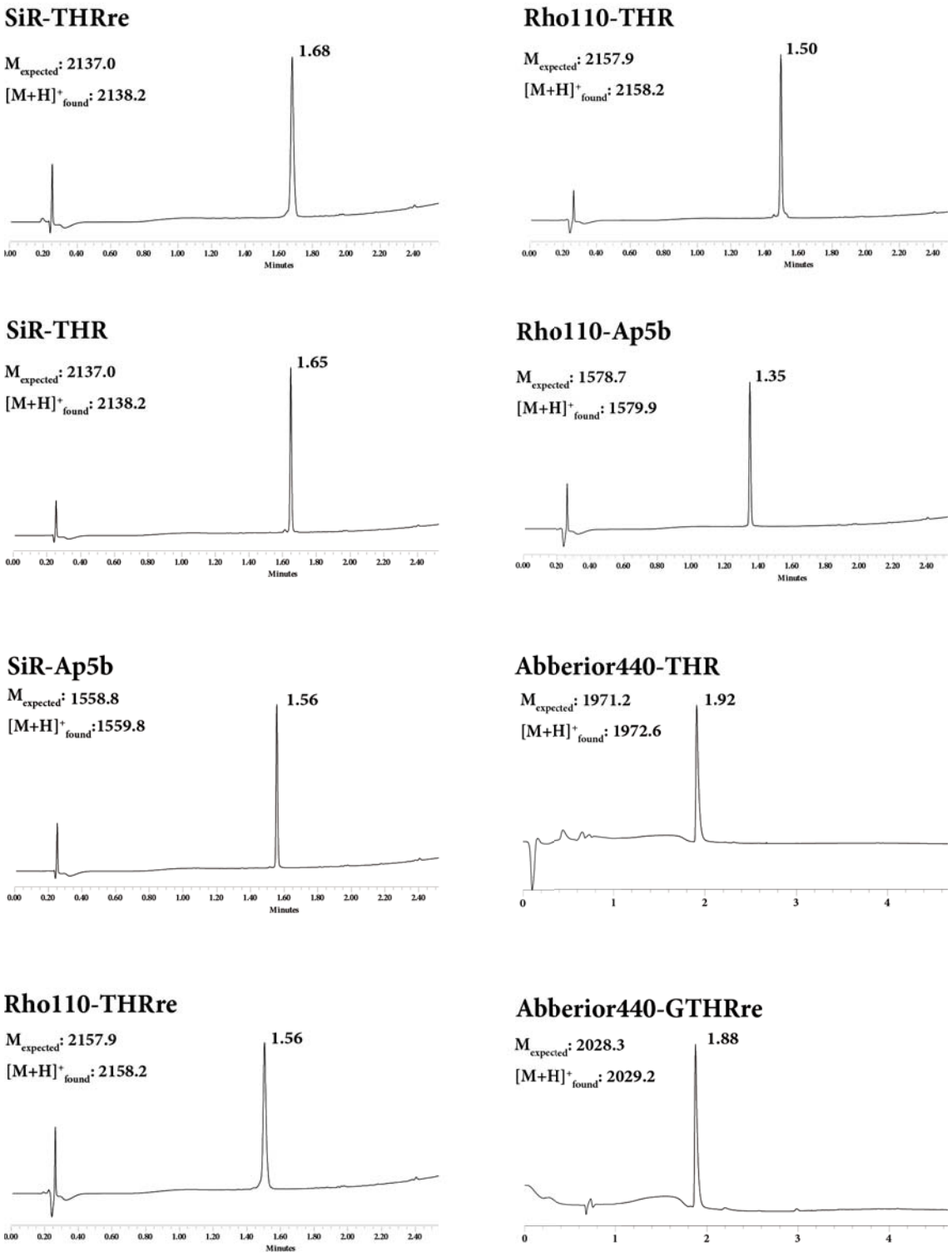

Figure II. *Chromatograms and masses calculated and obtained by MALDI-TOF MS. All UPLC chromatograms here shown were recorded at 220 nm in a 2-min linear gradient from 0 to 100 % of MeCN with (0.036% TFA) in H_2O (0.045% TFA), except for Abberior conjugates in which the gradient was of 4 min. Retention times are shown in min.*

Fluorogenicity of peptide-fluorophore conjugates

In order to know if the conjugates were fluorogenic we measured the ratio of the fluorescence in the presence or absence of a surfactant (SDS) (*Figure III*). Abberior conjugates did not display any degree of fluorogenicity due to their high hidrophilicity and Rho110 showed 2-4-fold increases, which are average values with respect to other hydrophobic fluorophores. However, SiR linked to the same peptides provided a higher enhancement of fluorescence for THR (6-fold) and especially in the case of THRre (10-fold). These increases were quite remarkable taking into account the hydrohpilicity of the peptide shuttles, which hampers aggregation of the fluorophore and thus fluorescence quenching. Moreover, one order of magnitude enhancement could already be useful for non-wash imaging or to study receptor interaction.

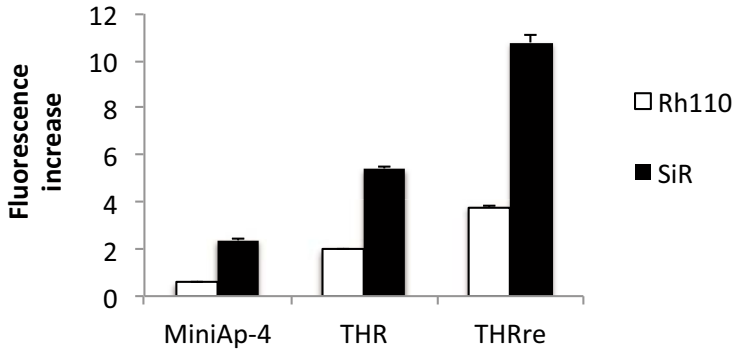

Figure III. *Fluorescence increase upon incubation with SDS.*

Aiming to assess the relationship between fluorogenicity and hydrophilicity, we estimated the logD (pH 7.5) of the peptide conjugates using MarvinSketch 15.1.5.0 software (VG logP method, 0.15 mM Cl^- and Na^+ concentration, no tautomerization/resonance considered). However, the calculated values were extremely low (*Table 1*), which was unreasonable for conjugates bearing such a hydrophobic fluorophore. This result was due to the algorithm not being adequate for large molecules such as our peptides. Hence, we determined them experimentally.

After incubating peptide conjugates with 1:1 mixtures PBS/octanol, we measured the amount of compound present in each phase. Quantification in the aqueous phase could be easily achieved by measuring absorbance at the excitation maximum, for which the extinction coefficient is known. However, absorbance in octanol at the excitation wavelength is extremely low for most fluorophores. Thus, we calculated extinction coefficients at 280 nm in octanol for each peptide.

Surprisingly, THR and THRre, which contain the same residues, apparently have 10-fold different solubility in octanol. Although there is no correlation between the

logD and the fluorogenicity of the two most hydrophobic peptides, MiniAp-4 is the least fluorogenic and also the most hydrophillic one.

Table 1. *Molar extinction coefficients in octanol and logD (PBS) of SiR-peptide conjugates.*

	SiR-MiniAp4	**SiR-THR**	**SiR-THRre**
Measured ε in octanol at 650 nm, $M^{-1}\cdot cm^{-1}$	$2.4\cdot10^4$	$3.4\cdot10^4$	$3.8\cdot10^4$
Calculated logD (pH 7.5) Not considering resonance	-8.7	-5.8	-5.8
Calculated logD (pH 7.5) Considering resonance	-11.9	-5.3	-5.3
Experimental logD (pH 7.4)	0,0	2,8	1,9
Fluorescence increase	2	6	11

In order to verify that the logD determination procedure provided values similar to the ones predicted for smaller molecules, we determined the logD of three unconjugated fluorophores. In this case, calculations were remarkably more accurate (*Table 2*). These results validated to some extent the method we were using for logD determination.

Table 2*. Molar extinction coefficients in octanol and logD (PBS) of some fluorophores.*

	TMR*	**CPY**	**SiR700**
Measured ε in octanol at absorption maximum, $M^{-1}\cdot cm^{-1}$	$5.2\cdot10^4$	$1.5\cdot10^4$	$1.7\cdot10^4$
Calculated logD (pH 7.5) Not considering resonance	0.1	1.9	1.3
Calculated logD (pH 7.5) Considering resonance	0.6	2.3	2.0
Experimental logD (pH 7.4)	0.0	1.0	2.5

*TMR: tetramethylrhodamine, *CPY: carbopyronine

Internalization

Receptor expression

Before studying the internalization of peptides, we analysed the receptor expression in the cell-lines we were going to use. For this purpose, firstly, we compared two antibodies against TfR by western blot using soluble TfR (sTfR). sTfR (80 kDa) is present in blood at 2-5 μg/mL and comes from proteolitic cleavage of membrane TfR. Antibody A (Life Technologies A11130) clearly gave a higher signal than antibody B (Sigma-Aldrich SAB4200398) (*Figure IV*). Gels were performed under non-reducing conditions because no receptor could be detected when β-mercaptoethanol and high temperature (95 ºC) were applied.

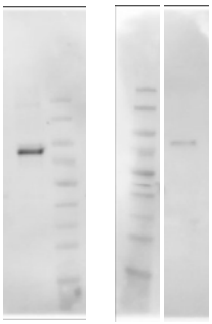

Figure IV. *Western blot comparing the detection of soluble TfR with two antibodies (Left: A and Right: B)*

The antibody that provided a higher signal (A) in the test with sTfR, stained a band above the highest one in the protein ladder (180 kDa). This band should correspond to the non-reduced membrane TfR (170 kDa). Conversely, antibody B displayed a band between 40 and 55 kDa that curiously overlapped the one stained by the antibody against actin.

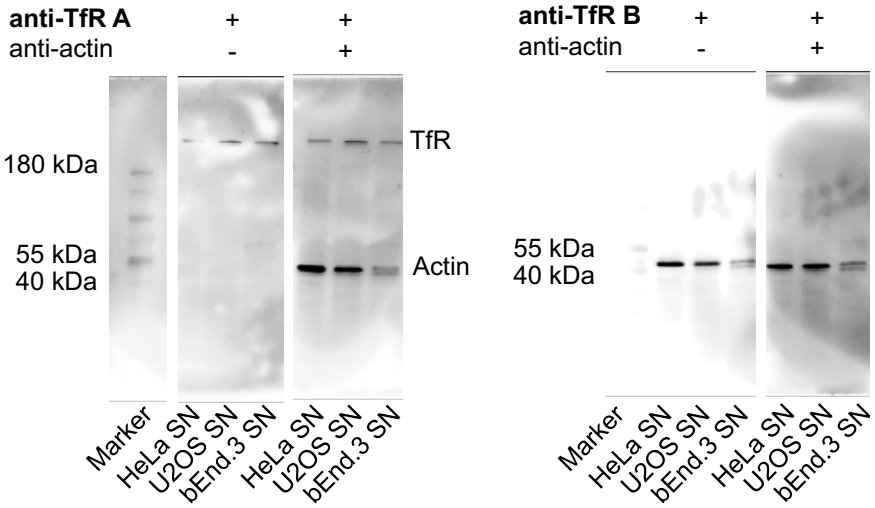

Figure V. *Western blot showing the xpression levels of transferrin receptor and the amount of actin in HeLa, U2-OS and bEnd.3 cell-lines.*

Although an equal amount of protein measured by BCA was loaded in each lain, we observed a lower intensity of the actin band in bEnd.3. Although this structural protein is usually used as a control for loading, it should be taken into account that, in this case, lysates belong to different cell-lines that may express different amounts of actin. Moreover, the analysis was repeated with a new batch of cells obtaining a similar result. From this determination we concluded that the amount of TfR in the three cell-lines studied (HeLa, U2OS and bEnd.3, the latter at passage 17) was comparable. Therefore, expression levels of this receptor could not be the cause of potential internalization differences in THR and THRre.

Visualization of BBB-shuttle internalization in bEnd.3

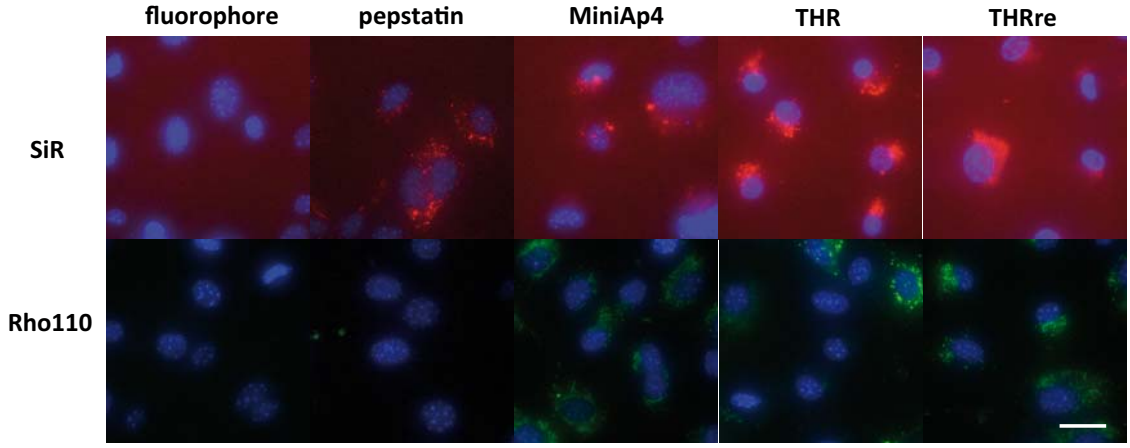

Figure VI. *Uptake of Rh110- (green) and SiR-peptides (red) by bEnd.3 cells. Hoechst, blue. Scalebar, 30 μm.*

We started studying the internalization of peptides in bEnd.3 cells in a wide-field fluorescence microscope. We first realized that high concentrations were required (10-20 μM) to appreciate internalization, as a first test at 1 μM did not stain cells visibly. The high amount of peptide present in the medium counterbalanced fluorogenicity, thus imaging without washing was not possible. After washing with medium, we could observe that both Rh110 and SiR conjugates displayed a vesicular pattern; considering their asymmetric accumulation near the nucleus they probably accumulate in the endoplasmatic reticulum. These observations are consistent with an endocytoic uptake mechanism, which could eventually lead to transcytosis if the cells were on a permeable support.

MiniAp-4 showed remarkably lower uptake with both fluorophores than the other two peptides. Conversely, THR showed the highest uptake. The internalization of this shuttle being more efficient than that of THRre could be explained by a higher affinity for the TfR. This result is not incompatible with the higher transcytosis reported for the *retro-enantio* version, as the L-peptide could enter cells more efficiently but then would be degraded.

The assay was repeated with a similar result (*Figure VI*). In this second experiment negative and positive controls were added. Non-conjugated fluorophores were used as negative controls, namely SiR-COOH and Rh110-PEG-N_3; both displayed very low uptake and did not appear to be contained in vesicles. Pepstatin (a peptidic aspartyl-protease inhibitor) linked to either SiR or BODIPY was intended to be a positive control; however, the vesicular pattern was only clear for the SiR conjugate.

Study of differences between cell-lines

Next, we studied the internalization behaviour in three cell-lines: U2-OS, an epithelial cell-line derived from human osteosarcoma, HeLa, another epithelial cell-line coming from human adenocarcinoma, and bEnd.3.

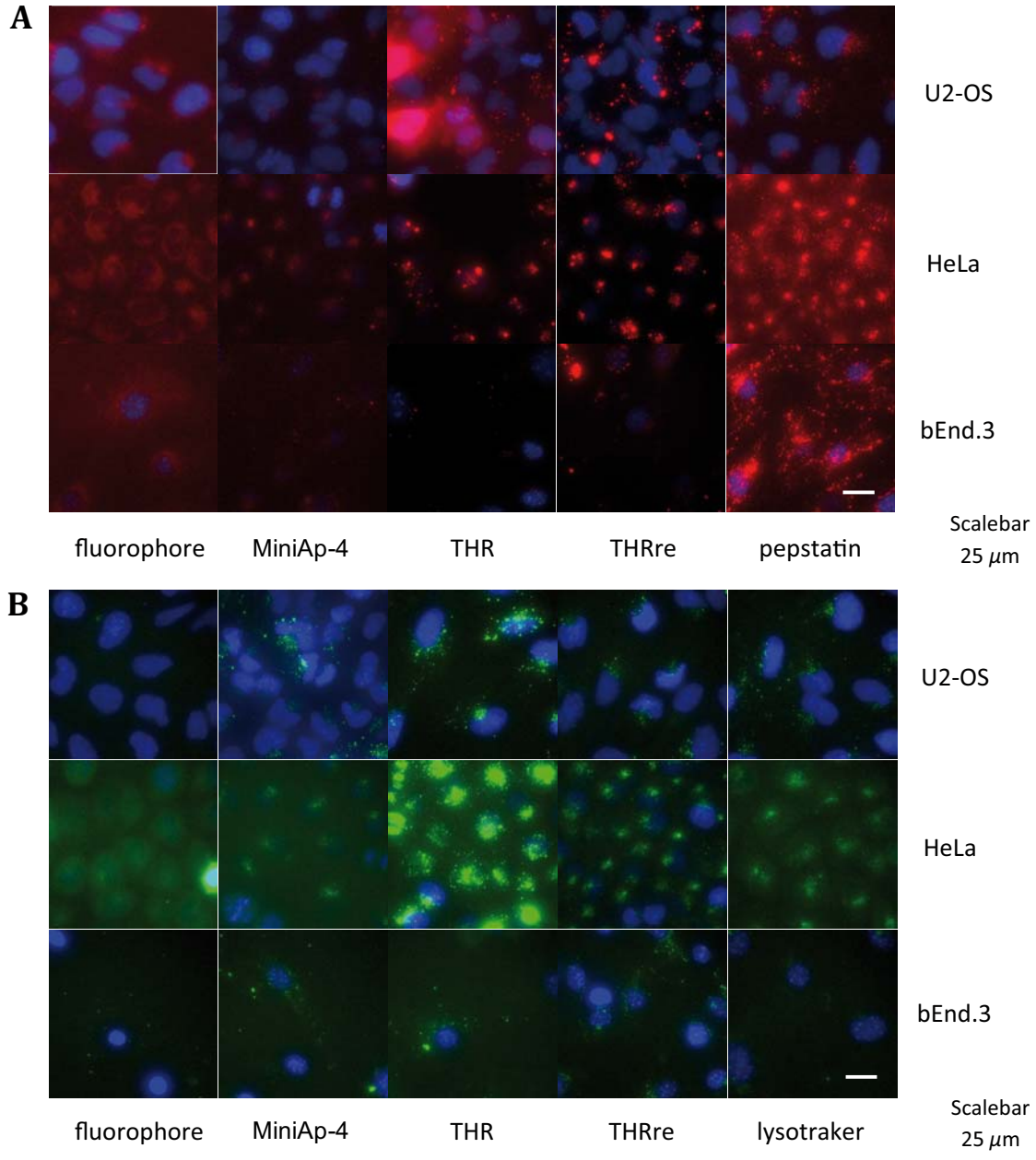

Figure VII. *A) Uptake of SiR-peptides (red) by U2-OS, HeLa and bEnd.3 cells. Hoechst, blue. B) Uptake of Rh110-peptides (green) by U2-OS, HeLa and bEnd.3 cells. Hoechst, blue.*

Although, the positive control pepstatin showed a clear vesicular pattern in bEnd.3, the peptides of study displayed very low uptake compared to other cell-lines. Conversely, in HeLa, internalization was highest for BBB-shuttle peptides, especially for Rh110-THR, and showed a more similar distribution to pepstatin. However, vesicles were most clearly resolved in U2-OS, especially in the Rh110 conjugates.

Regarding peptides, THR was the best internalised among the Rh110 conjugates but THRre performed better with SiR. In U2-OS, SiR-THR stained whole cells, which could be explained by the degradation of the peptide and subsequent diffusion through the cytosol. This result would be in agreement with the higher lability of THR to proteases with respect to the other peptides. However, Rh110-THR did not display this behaviour.

Visualization of internalization with STED microscopy

Aiming to get an insight into the endocytotic uptake of these peptides, we selected the two cell-lines in which vesicles were more defined (U2-OS and bEnd.3) and visualized them using STED super-resolution microscopy. In this experiment we confirmed that the peptides were prominently inside vesicles (*Figure VIII*). Surprisingly, in this experiment, the peptide showing highest uptake was THRre and not THR. Setting up the STED system resulted into a longer chase time after the 2.5 h pulse incubation (2-5 h instead of 10 min to 2 h), which might have affected the results. Thus, by the time of observation, the THR peptide could have been completely degraded.

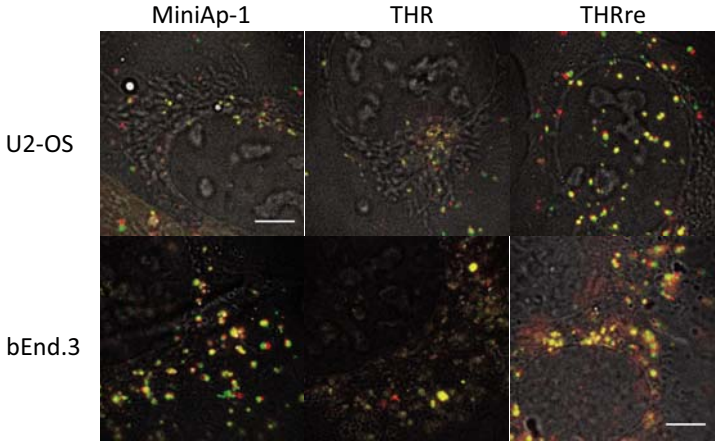

Figure VIII. *Visualization of Rh110-peptide uptake by U2-OS and bEnd.3 cells using STED (red) and the same confocal system without depletion beam (green). Scalebar, 5 µm.*

It should be noted that we could not see any increase in resolution using the STED system. We verified that the STED system was working properly by measuring the increase in resolution with respect to the same microscope without applying the

depletion beam. For this purpose we stained microtubules and centrosomes in bEnd.3 and U2-OS cells and measured the diameter under both conditions. We also applied deconvolution to obtain sharper images.

The resolution increase for the control samples was in the expected range (*Figure IX*); hence, the negligible difference in vesicle size between regular confocal and STED systems was due to vesicle diameter being near the diffraction limit (150-300 nm). Consequently, for subsequent experiments we focussed on confocal and wide-field microscopy.

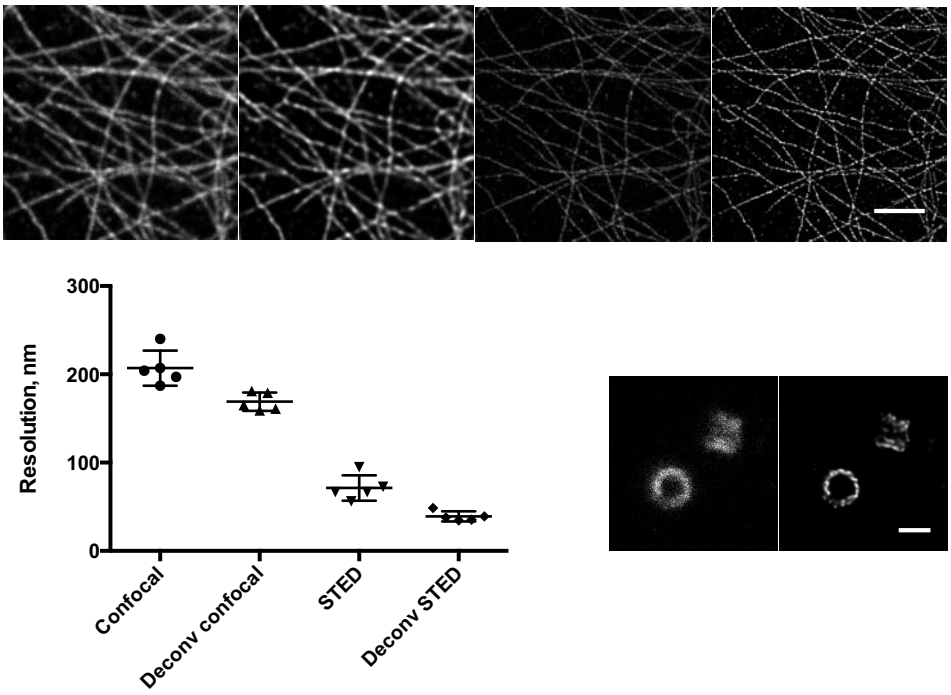

Figure IX. *Increase in resolution provided by STED and deconvolution. Error bars reprsent SD. Representattive images of microtubules and centrosomes of U2-OS cells are shown. Scalebars, 5 μm.*

Study of BBB-shuttle colocalization with lysosomes and endosomes

The goal of this experiment was to study the colocalization of peptides with endocytic vesicles in different stages of intracellular sorting after a 2-h-pulse incubation. Although initially we intended to label Rab4 and Rab11 proteins in recycling endosomes, no commercial transduction kit was available. Therefore we focussed on transducing a construct formed by red-fluorescein protein (RFP) and proteins present in lysosomes (Lamp1), early endosomes (Rab5) or late endosomes (Rab7). Because a high 3D resolution is required for an accurate colocalization, imaging was performed using a confocal SP8 Leica microscope with simultaneous acquisition of the green and red (or far-red) channels using argon and white lasers, respectively.

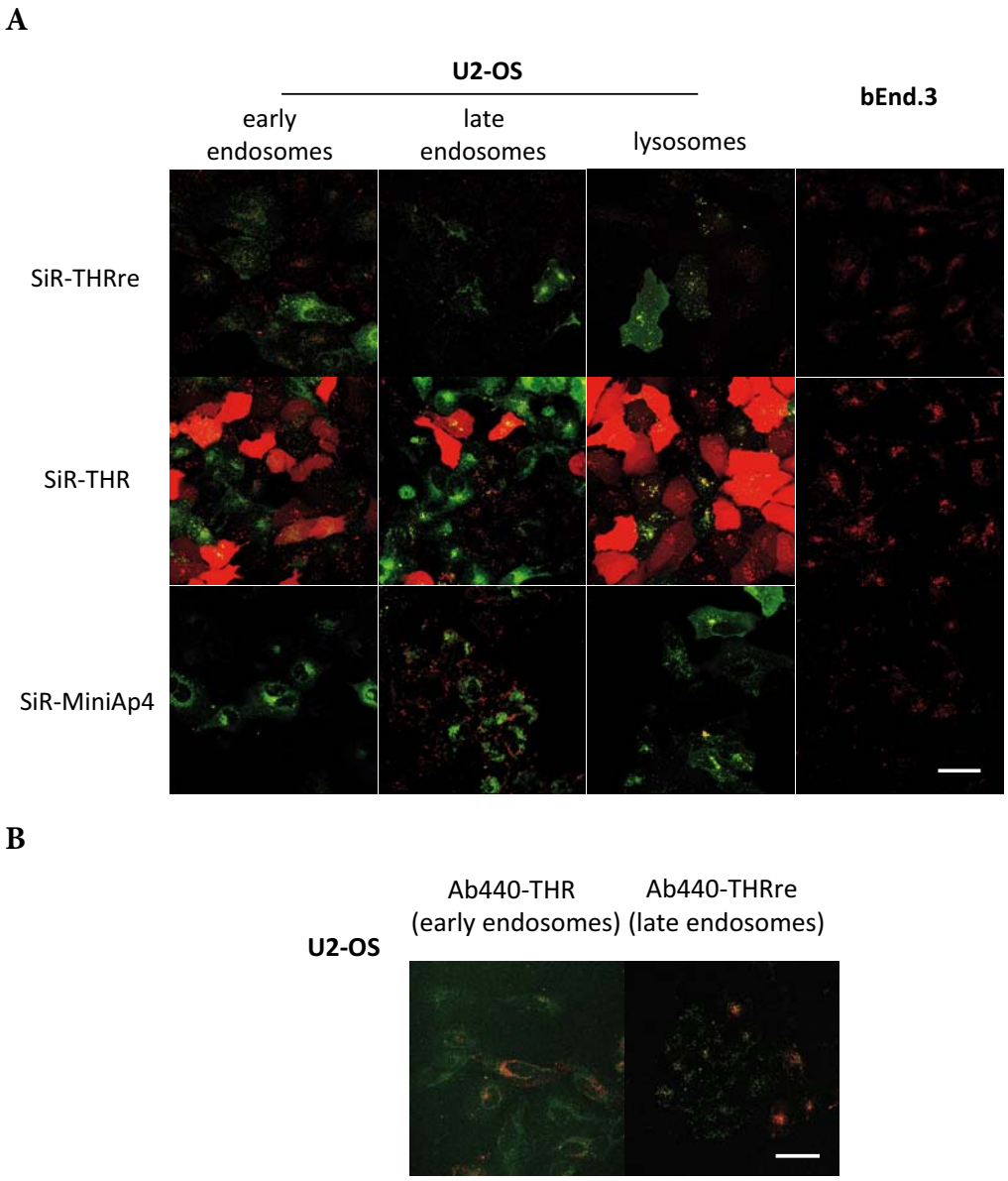

Figure X. *Internalization of peptides in cells transduced with RFP constructs.* ***A****) SiR-peptides (red) and RFP (green).* ***B****) Rh110-peptides (green) and RFP (red). Scale bar is 50 μm.*

Surprisingly, no expression of RFP in endosomes or lysosomes was observed in bEnd.3 (*Figure X*). Regarding U2-OS cells, they showed low levels of expression and RFP was very dispersed in the cytosol in many cells, which did not allow quantitative colocalization. In spite of this, all shuttles showed some degree of colocalization with the lysosomes and none with early or late endosomes. This observation indicated that after a 2-h pulse incubation followed by a 1-3h chase all peptides remaining inside the cell had been sorted toward degradation and there was no recycling. Consequently, either there is no recycling or the exocytosis only takes place in an earlier stage.

Table 3. *Summary of qualitative internalization levels.*

	bEnd.3	**U2-OS**
SD	medium	low (LE, L) medium (EE)
SL	high	high (red cytosol)
SA	low (LE, L) medium (EE)	very low (EE, L) high (LE)
AbL	-	high
AbD	-	low

In agreement with previous experiments, in both cell-lines THR was better internalized than THRre and uptake of this peptide was in turn higher than that of MiniAp-4. We also confirmed the vesicular distribution of peptides and the cytosolic staining by THR in U2-OS. It was also curious to observe that expression of some of the fusion proteins apparently affected peptide uptake. In this experiment we also saw that Abberior440-THRre conjugate had a higher uptake than the SiR derivative, while for THR, distribution appeared to be in both cases more cytoplasmatic.

Uptake kinetics

In the last internalization experiments we intended to follow uptake kinetics of SiR conjugates. In spite of the remarkable fluorogenicity of SiR-THR and -THRre, noise was very high due to the high concentration of peptide in the medium. While, in U2-OS cells, for THRre large aggregates started to appear after 30 min, for THR smaller dots that could correspond to vesicles were visible after 1 h. This time is remarkably longer than that observed for transferrin, which is internalized in observable amounts in less than 10 min.[2] For MiniAp-4 or any of the peptides in bEnd.3 no change was visible even after 2.5 h.

[2] Nevola, L.; Martin-Quiros, A.; Eckelt, K.; Camarero, N.; Tosi, S.; Llobet, A.; Giralt, E.; Gorostiza, P. Light-regulated stapled peptides to inhibit protein-protein interactions involved in clathrin-mediated endocytosis. *Angew. Chem. Int. Ed. Engl.* **2013**, *52*, 7704-7708.

Binding

Fluorogenicity assay

Although the fluorogenicity of SiR-THR and SiR-THRre was not enough to image uptake without washing, we attempted to exploit this property to study the interaction of these peptides with TfR. We expected that the K_d would be higher than the one reported for holotransferrin (8.3 nM) and probably also than the one reported for apotransferrin (160 nM).[3] Therefore we chose a low peptide concentration that could still provide a good signal-to-noise ratio, namely 25 nM. We then titrated the receptor from substoichiometric concentrations (11 nM) to one near the stock solution of receptor (3 μM).

After several unsuccessful attempts to perform the measurement with an old batch of TfR (which had been unduly frozen) with TBS or ammonium bicarbonate buffer, we attempted the same experiment with newly purchased receptor. In this case, despite the high variability, we obtained a significantly different response of TfR with respect to the control protein (BSA) (*Figure XI*).

$$A = A_f + (A_b - A_f) \times \frac{(L_T + K_d + R_T) - \sqrt{(L_T - K_d - R_T)^2 - 4L_TR_T}}{2L_T} \quad (\textit{Equation} \text{ I})$$

$$A = A_f + \left[(A_b - A_f) \times \frac{R_T}{K_d + R_T}\right] \quad (\textit{Equation} \text{ II})$$

where A_f is fluorescence intensity (FI) or polarization (FP) of free ligand, Ab is FI or FP of bound ligand, R_T is total receptor concentration, L_T is total ligand concentration and K_d is dissociation constant. Eq 2 is derived from eq I assuming no receptor depletion. (Kenakin (1993). Pharmacologic analysis of drug-receptor interaction. New York:Raven. p. 483.)

Data was fitted using equations I and II giving very similar K_ds for THR: 180 ± 110 nM and 210 ± 100 nM (mean ± SEM), respectively. Thus, the affinity of THR seems comparable to that of apotransferrin. With regard to THRre, the large variability at the highest concentration resulted into a higher error in the calculation of the a K_d, which was in the range of 1.7-16 μM, between 10 to 100 fold higher than that of THR. Very similar values were obtained when the experiment was repeated. The higher variability for THRre was also observed in the replicate, which suggests that it might be due to aggregation.

[3] Graziadei, I.; Kaserbacher, R.; Braunsteiner, H.; Vogel, W. The hepatic acute-phase proteins alpha 1-antitrypsin and alpha 2-macroglobulin inhibit binding of transferrin to its receptor. *Biochem. J.* **1993**, *290*, 109-113.

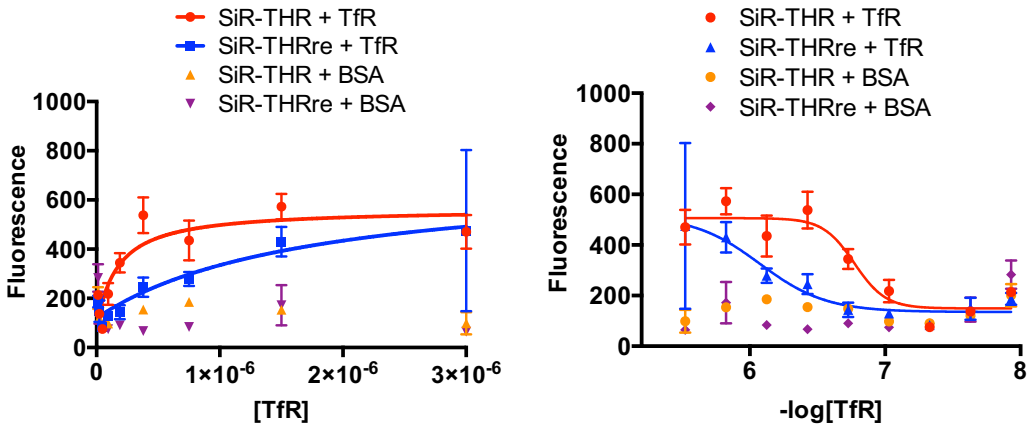

Figure XI. *FI from the titration of SiR-peptides with soluble TfR. Overlapped fittings of equations 1 and 2 (left) and sigmoidal fitting to emphasize the change in fluorescence (right). Data represent mean ± SEM (n = 3).*

Fluorescence anisotropy

Rh110-THR and SiR-THRre provided similar results for TfR and BSA. Conversely, SiR-labelled THR displayed a significant difference (*Figure XII*). The K_d for this conjugate, obtained using equation II, was of the same order of magnitude than the one estimated from the fluorogenicity assay: 500 ± 170 nM (mean ± SEM). It should be taken into account that, as shown in the fluorogenicity section, the SiR labelled peptides are aggregated in solution making more difficult to observe a specific change in polarization. This assay should be repeated with Abberior440 conjugates.

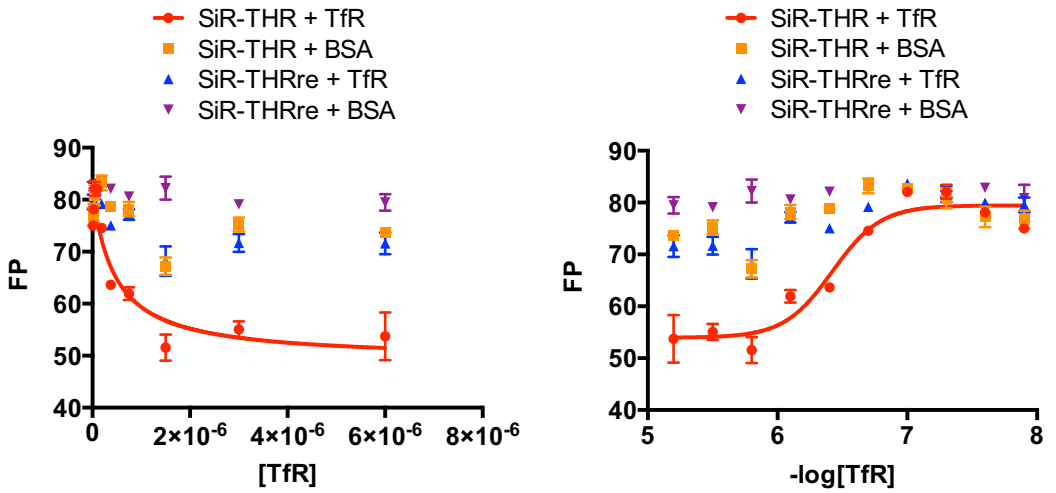

Figure XII. *Fluorescence polarization from the titration of SiR-peptides with soluble TfR. Overlapped fittings of equations 1 and 2 (left) and sigmoidal fitting to emphasize the change in fluorescence (right). Data represent mean ± SEM (n = 3).*

Thermal shift assay

Although thermal stabilization is stronger in ligands binding deep pockets in their receptors, we attempted to verify the interaction we had observed in the fluorogenicity assay. However, no increase was visible neither for unlabelled THR or THRre (*Figure XIII*) nor for the SiR-labelled versions. Probably this interaction is too superficial to stabilize TfR, which apparently is already highly stable on its own. Surprisingly apotransferrin that was intended to be the positive control, cross-reacted with the antibody anti-TfR, overlapping with the signal from TfR.

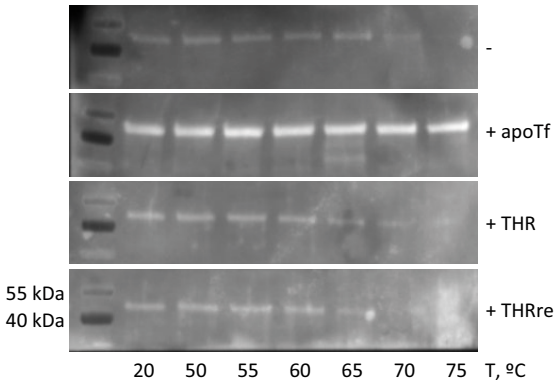

Figure XIII. *Thermal shift assay with unlabelled peptides.*

Conclusions of the research stage

1. MiniAp-4, THR and THRre are taken up by bEnd.3, U2-OS ad HeLa cells through a vesicular mechanism as shown by fluorescence microscopy, in agreement wit the suggested receptor-mediated endocytosis.
2. Binding of THR to TfR is in the high nanomolar range according to the fluorogenicity (210 ± 100 nM) and the fluorescent polarization (500 ± 170 nM) experiments. This affinity is comparable to that of apotransferrin, and 10- to 100-fold higher than its retro-enantio version, THRre.
3. Internalization efficiency in all the studied cell-lines is highest for THR, followed by THRre and MiniAp-4.
4. THR stains the whole cytoplasm only in the U2-OS cell-line, suggesting that the peptide conjugate is degraded releasing the fluorophore into the cytosol. Lower or no intracellular degradation, in addition to the reported protease-resistance in serum, could explain why THRre is a more efficient BBB-shuttle than THR despite its lower receptor binding and cell internalization.

Materials and methods

Fluorogenicity (SDS)

1 μM of each compound was incubated in TBS buffer (50 mM Tri·HCl pH 7.4, 150 mM NaCl) with or without 0.2 % SDS for 1 h. Final solutions contained 0.1% DMSO. Samples were prepared in triplicate in a 96-well plate and measured in a TECAN Infinite M1000 microplate reader.

ε determination

10 mM stock solutions of peptides in DMSO were diluted to 1 μM in octanol and absorbance at 280 nm was measured using a quartz cuvette (optical path of 1 cm) in a UV-1800 Shimadzu spectrophotometer. Molar extinction coefficient was calculated according to Lambert and Beer's law:

$$A_\lambda = \varepsilon_\lambda \cdot l \cdot C \qquad (\textit{Equation III})$$

where A_λ is absorbance at a certain wavelength (λ), ε_λ is the extinction coefficient at this wavelength, l is the optical path and C is the concentration.

LogD determinations

Octanol/PBS partition coefficients were measured following the protocol described by Leo *et al.*[4] Octanol used for this assay was presaturated in water and vice versa. Peptides were dissolved in 1 mL of water at 10 μM concentration. 1 mL of octanol was added and the mixture was placed in an end over end tube rotator for 5 min (20 rpm). After this time, the mixture was centrifuged 5 min at 6000 rpm. Each phase was diluted 2 times with the same solvent. Octanol phase was quantified directly and water phase was incubated with 0.2 % SDS and measured after 1 h. Absorbance was measured at 280 nm in octanol and at 650 nm in water using a quartz cuvette (optical path of 1 cm) in a UV-1800 Shimadzu spectrophotometer.

Cell lysis

A confluent p75 plate was scrapped and cells were collected using HBSS buffer. The cell suspension was centrifuged at 1000 rpm for 4 min. The pellet was vortexed and lysed with 0.5 mL of RIPA buffer containing a protease-inhibitor cocktail (cOmplete mini from Roche) for 30 min in ice. After that, the lysate was centrifuged at 20000 x*g* for 30 min at 4 ºC. The supernatant (SN) was then separated from the pellet. Finally, the latter was mixed with 0.5 mL of RIPA buffer and sonicated for another 10 min.

[4] Leo, A.; Hansch, C.; Elkins, D. Partition coefficients and their uses. *Chem. Rev.* **1971**, *71*, 525-616.

Western Blotting

Total protein concentration was determined using Bradford assay. Briefly, 5 μL of standards or samples were mixed with 200 μL of Bradford reagent (Coomassie brilliant blue G-250) and absorption was determined after 5 min at 595 nm. After adding Laemmli buffer without reducing reagents and heating to 50 ^{o}C, 17 μg of SN lysate was loaded or 7 μg of pellet was loaded in each lain. Transfer into polyvinyldene difluoride (PVDF) membranes was performed using semi-wet western blotting. We used transfer buffer from Novex and ECL trans blocking agent (2.5 % in PBS) from GE Healthcare. Primary antibodies were incubated for 1h at RT. Antibody A was from Life Technologies A11130 (mouse) or antibody B was Sigma-Aldrich SAB4200398 (rabbit). Depending on the primary antibody used, an anti-mouse or an anti-rabbit secondary antibody conjugated to HRP (Cell Signalling Technologies) were incubated for 45 min. 3 x 30 s washings and 2 x 5 min washings were performed after blocking and incubation steps. After that, development was achieved adding the HRP substrate (ECL Select^{TM} western blotting detection reagent, GE Healthcare) and captured with an Azure Biosystems c600 gel reader. In order to have a control for loading, actin was also stained using a primary goat antibody for actin (Santa Cruz Biotechnology), which was detected with a secondary anti-goat antibody (Cell Signalling Technologies).

Cell culture

Cells were cultured in DMEM complete medium (glucose 4.5 g/L and 2 mM glutamate) with 10 % FBS (both from Gibco). Medium was changed 2 times per week and cells were passaged when they reached confluence using 0.05 % trypsin/EDTA.

Internalization experiments

Internalization experiments were performed after a 2-3 h incubation with 10-20 μM peptide and 600 nM Hoechst in the same medium used for culture. They were then washed 5 times with medium and bEnd.3 cell-line (ATCC) was used between passages 7 and 18.

Imaging

Cells were seeded either in 3-cm petri dishes or 12-well plates with glass-coverslip bottom coated with poly-D-lysine and imaged before reaching confluence. Cells were imaged at 20 ^{o}C to slow down vesicular traffic.

Systems used: Leica LAS AF 6000 wide-field microscope. Leica SP8 FLIM microscope (63x 1.4 NA oil immersion objective). Leica SP5-white laser microscope with a STED system (100x 1.4 NA oil immersion objective).

Images acquired in the STED system were deconvoluted using the Huysgens Essentials package.

Staining of centrosomes and microtubules

Cell medium was aspirated and methanol at -20 ºC was immediately added and was kept overnight at -20 ºC. After that, cells were washed 5 times with PBS at room temperature and blocked for 1 h with 1 % BSA in PBS. Primary antibody was incubated for 16 h. CEP 152 (Sigma) was used to centrosomes, while DM1A (Sigma) was used for α-tubulin, both at 1:1000 dilution. Chromeo 488 or Alexa 488 secondary antibodies were incubated for 2 h at 1:1000 dilution.

Fluorogenicity (TfR binding)

The fluorogenicity assay was performed using 25 nM constant peptide concentration and increasing concentrations of TfR or BSA form 47 nM to 3 μM in a 384-well plate (triplicates). After a 1-h incubation fluorescence was measured in a TECAN Infinite M1000 microplate reader.

Fluorescence polarization

Fluorescence polarizaiton assay was performed using the same concentrations of peptides as for the fluorogenicity assay. After a 1-h incubation fluorescence anisotropy was measured in an EnVision 2103 multilabel plate reader (Perkin Elmer). FITC filters were used for the rhodamine 110-labelled peptides and Cy5 filters for the ones containing SiR.

Thermal shift assay

25 nM receptor was incubated with 1 μM apotransferrin or 10 μM peptides (peptides were in 1 mM stock solution in DMSO) for 4 h in 50 mM HEPES buffer pH 7.4 and 150 mM NaCl. Each sample was split into seven 50 μL-aliquots and each was heated at one of the following temperatures: 20, 50, 55, 60, 65, 70 and 75 ºC for 3 min, followed by a 3 min cooling period in a Verity thermocylcer from Applied Biosystems. Samples were centrifuged for 20 min at 4 ºC and 16.1 x*g* and supernatant was mixed with reducing Laemmli buffer and denatured at 95 ºC. 20 μL of each sample was loaded in a polyacrylamide gel and after western blotting was performed as previously described.